Evaluation of Mitigative Techniques for Non-Contact Lap Splices in Concrete Block Construction

A Thesis Submitted to the College of

Graduate Studies and Research

In Partial Fulfillment of the Requirements

For the Degree of Master of Science

In the Department of Civil and Geological Engineering

University of Saskatchewan

Saskatoon

By

ALEKSANDAR KISIN

PERMISSION TO USE

In presenting this thesis in partial fulfillment of the requirements for a Postgraduate degree from the University of Saskatchewan, I agree that the Libraries of this University may make it freely available for inspection. I further agree that permission for copying of this thesis in any manner, in whole or in part, for scholarly purposes may be granted by the professor or professors who supervised my thesis work or, in their absence, by the Head of the Department or the Dean of the College in which my thesis work was done. It is understood that any copying or publication or use of this thesis or parts thereof for financial gain shall not be allowed without my written permission. It is also understood that due recognition shall be given to me and to the University of Saskatchewan in any scholarly use which may be made of any material in my thesis.

Requests for permission to copy or to make other use of material in this thesis in whole or in part should be addressed to:

Head of the Department of Civil and Geological Engineering

University of Saskatchewan

Engineering Building

57 Campus Drive

Saskatoon, Saskatchewan, S7N 5A9

Canada

ABSTRACT

A previously completed study in the field of concrete block construction by Ahmed and Feldman (2012) indicated that, on average, the reinforcing bars in non-contact lap splices, where the lapped bars are located in adjacent cells, only develop 71% of the tensile resistance of spliced bars which are in contact. An experimental program was therefore initiated to design and evaluate remedial measures which can potentially increase the tensile resistance of non-contact lap splices to that of contact lap splice of the same lap length. Implementation of the proposed measures in various field situations was also analyzed. Six unique remedial splice details, along with standard contact and unaltered non-contact lap splices were evaluated and compared. The mitigative details included providing additional confinement, installing knock-out webs, placing splice reinforcement between the lapped bars, and combinations of these aforementioned details. Three replicates of each splice detail were constructed for a total of 24 wall splice specimens.

Each wall splice specimen was reinforced with No. 15 Grade 400 deformed steel reinforcing bars with 200 mm lap splice lengths at located the midspan. The specimens were tested in a horizontal position under a monotonic, four-point loading geometry. Load and deflection data were collected throughout testing and were subsequently used in an iterative moment-curvature analysis to calculate the maximum tensile resistance of the spliced reinforcement. This was then used to compare the structural performance of each remedial splice detail to the standard contact and non-contact lap splices.

The wall splice specimens which contained non-contact lap splices with knock-out webs, s-shaped, and transverse reinforcement in the splice region achieved similar tensile capacities as the wall splice specimens with standard contact lap splices. Industry professionals have indicated that the installation of the remedial measures evaluated in this study would not affect the constructability of masonry assemblages in field situations. The splice detail with knock-out webs confined within the lap splice length was determined to be the most viable procedure as it can be installed to increase the resistance of non-contact lap splices in almost all construction situations. This remedial procedure was able to improve the tensile resistance of the lapped reinforcement by 63% compared to the wall splice specimens with standard non-contact lap splices.

CO-AUTHORSHIP

All of the experimental and analytical work presented in this thesis was performed by Aleksandar Kisin and reviewed by Dr. Lisa R. Feldman. The test results from Phase 1 of the experimental program were published in the proceedings of the 12th Canadian Masonry Symposium, Vancouver, B.C., 2013. The results from Phases 1 and 2 of the experimental program were accepted for publication in the proceedings of the 9th International Masonry Conference, Guimarães, Portugal, 2014. A working draft summarizing the results of this investigation has been submitted to the American Concrete Institute's Structural Journal.

ACKNOWLEDGEMENTS

The author wishes to extend his utmost gratitude to Dr. Lisa Feldman for her continuous guidance, support, and commitment in the preparation of this thesis. The valuable input and advice from his committee members, Dr. Bruce Sparling, and Dr. Leon Wegner, is also gratefully acknowledged by the author.

A special thank-you is extended to the Structural Laboratory Technicians, Brennan Pokoyoway, and Dale Pavier, for their technical assistance and patience in the laboratory. The author also gratefully acknowledges the manual labour during the construction process provided by fellow grad students.

The author wishes to extend a thank-you to Bob Afseth, Kathy Beznoska, and the Saskatchewan Masonry Institute Members for accommodating him to complete the industry experience requirement of his scholarship, and supplying construction materials and an experienced mason. The author thanks Roy Nicolas, Gracom Masonry, for constructing the masonry specimens used in this investigation and Albert Pilon, Gracom Masonry, for accommodating the labour and equipment requirements of masonry construction.

The author gratefully recognizes the financial support provided by the Canada Masonry Design Centre, Natural Science and Engineering Research Council of Canada, the Saskatchewan Masonry Institute, and the scholarships provided by the University of Saskatchewan.

Finally, the author sincerely thanks his family and friends for their immeasurable amount of support and encouragement they continue to provide.

TABLE OF CONTENTS

LIST OF TABLES

LIST OF FIGURES

LIST OF SYMBOLS

A_s	Cross-sectional area of reinforcing steel
b	Width of a wall splice specimen
B_r	Bearing force
B_{rl}	Longitudinal component of bearing force
B_{rt}	Transverse component of bearing force
C	Total compressive force in the masonry assemblage
c	Depth to the neutral axis from the compression face
C_i	Compressive force in i^{th} strip
C_{tot}	Total compressive force developed in the compressive zone for the sectional analysis
COV	Coefficient of variation
d	Effective depth to the reinforcing steel from the compression face
d_b	Bar diameter
d_{eff}	Effective depth to the reinforcing steel from the compressive face
d_j	Distance from the neutral axis to the centroid of the j^{th} layer
E'_m	Modulus of elasticity for masonry
E_s	Modulus of elasticity of the reinforcing steel
E_{sh}	Slope at the initiation of strain hardening of the reinforcing steel
$f_m(\varepsilon_m)$	Compressive stress in the masonry assemblage at any given strain
f'_m	Compressive strength of the masonry
f_{mi}	Compressive strength of masonry in i^{th} strip

f_s	Tensile stress in the reinforcing steel
$f_s(\varepsilon_s)$	Tensile stress in the steel reinforcement at any given strain
F_{splice}	Correction factor for remediated non-contact lap splices
f_u	Ultimate stress of the reinforcing steel
f_y	Yield stress of the steel reinforcement
f_{yh}	Yield strength of the confinement steel in the masonry prism
I_{cr}	Moment of inertia for the cracked wall splice specimen cross-section
I_e	Effective moment of inertia of a wall splice specimen
I_g	Gross moment of inertia of a wall splice specimen
K	Strength enhancement factor
l.a.	Lever arm
L_d	Development length
L_{tot}	Length of wall splice specimen
M_a	Moment resulting from applied load
M_{cr}	Cracking moment
M_{ext}	Moment caused by the separation of the spliced bars in non-contact lap splices
M_{tot}	Total cross-sectional moment
n_{splice}	Percent difference between the mean tensile capacity of the non-contact lap splice specimens with remedial the control contact lap splices
P	Applied load
P_{cr}	Cracking load
T	Tensile force in reinforcing steel

u	Average bond stress
y_i	Distance from the centre of each strip to the neutral axis
ε_c	Strain at the extreme compression fibre
ε_{ex}	Strain at the extreme compressive fibre
ε_m	Compressive strain of the masonry prism
ε_j	Strain at the j^{th} layer
ε_s	Strain in the reinforcing steel
ε_{sh}	Strain at the initiation of strain hardening of the reinforcing steel
ε_u	Strain in the reinforcing steel at the ultimate stress
ε_y	Strain at the initiation of yield of the steel reinforcement
ρ_s	Volumetric ratio for the confining steel
ϕ	Curvature
ϕ_{eff}	Effective curvature
ϕ_{cr}	Curvature of the cracked section
ϕ_g	Curvature of the gross (un-cracked) section
ϕ_{uc}	Curvature of the wall splice specimen prior to cracking
σ_s	Stress in the reinforcing steel

CHAPTER 1: INTRODUCTION

1.1 Background

Masonry has been used as a means to construct countless structures since antiquity, many of which still stand to this day. The building method has evolved through time to improve its cost efficiency and allow it to be used in a wider variety of structural applications so it can remain competitive with structural steel and reinforced concrete construction. Steel reinforcement was first introduced into masonry construction in the 20th century to help improve its structural response (Hamid, 2004) and so allowed for higher slenderness ratios, larger openings, and improved response to dynamic loading. The steel reinforcement carries the tensile stresses that develop in the cross-section of masonry assemblages when they are subjected to out-of-plane flexure. These steel reinforcing bars are typically not continuous in order to accommodate openings and connect different structural elements. It also allows for the construction of reinforced assemblages which require longer reinforcing bars than the standard six meter length that is commonly available from the supplier. Instead, shorter lengths of reinforcing steel are overlapped, or "spliced", with another bar. The tensile force carried by the steel reinforcement must be effectively transferred between the spliced bars through bond development between the encapsulating grout within the splice region. An adequate splice length must be provided based on the reinforcing bar size used, the wall geometry, and loading scenarios. Failure to do so will result in a brittle failure, which is sudden in nature, within the splice region. This type of bond failure occurs at a lower load level than what would occur if the reinforcement was continuous and yielding was the assumed failure mode; therefore, the specification of adequate splice lengths is critical in reinforced masonry design.

Ideally, the spliced bars are in contact with one another; however, there are situations that arise where this is not feasible. Non-contact lap splices are frequently provided intentionally, adjacent to wall openings, and unintentionally, due to alignment errors, in masonry construction. A significant challenge arises when dowels are improperly placed in a concrete grade beam and fail to align with the intended reinforced cells in a masonry wall that is to be constructed above. The lap splices in these cases are governed by the length of the dowel extending above the grade beam. The conventional resolution in such situations results in the installation of non-contact lap

splices, where the lapped bars are located in adjacent cells of the masonry blocks with no increase in the lap length.

Bond research in reinforced concrete has been conducted since the early 1900's, while investigations focusing on bond in reinforced masonry were not initiated until the second half of the 20th century. This has resulted in the current Canadian masonry design code, CSA S304.1-04 - "Design of Masonry Structures" (CSA, 2004e), to have identical provisions for the development and lap splice length as the Canadian design code for reinforced concrete, CSA A23.3-04 – "Design of Concrete Structures" (CSA, 2004d), (Drysdale & Hamid, 2005). Reinforced masonry construction features numerous differences compared to reinforced concrete which have a negative effect on the bond strength of the embedded steel reinforcement in masonry assemblages. These include weak mortar joints which cause large cracks to form in concentrated areas and a reduced lever arm, which results in a higher compressive stress in the masonry assemblage for a given applied load.

Non-contact lap splices are permitted by CSA S304.1-04 (CSA, 2004e) without any adjustment to the lap splice length compared to contact lap splices. The masonry design code allows for the lapped reinforcing bars of these non-contact lap splices to be placed in adjacent cells. In these cases, the interaction between the reinforcing bars and the surrounding grout, block, and mortar of the masonry assemblage is required to effectively transfer the tensile force between the spliced reinforcement. This makes the tensile capacity of non-contact lap splices in masonry construction sensitive to the properties of the surrounding cementitious materials and their bond strength with one another. A review of the available literature indicated that studies which investigated non-contact lap splices prior to the publication of the current Canadian masonry design code, CSA S304.1-04 (CSA, 2004e) exclusively used reinforced concrete specimens. These types of specimens cannot model the interaction between the grout, masonry blocks, and mortar which comprise masonry assemblages and the effect that they have on the tensile resistance of spliced reinforcement, especially when the lapped bars are located in adjacent cells. Further research is therefore required to provide a better understanding of bond and splice performance in reinforced masonry construction.

A recently completed investigation by Ahmed and Feldman (2012) compared the tensile resistance of contact and non-contact lap splices, where the lapped bars were located in adjacent

cells, using a single bar size and lap splice length. The results of their research program indicated that the tensile resistance of non-contact lap splices was noticeably lower than the contact lap splices. Ahmed & Feldman (2012) therefore recommended a 50% increase in the required effective splice length for non-contact lap splices, where the lapped bars are located in adjacent cells, compared to contact lap splices, unless other approaches of enhancing the tensile resistance of non-contact lap splices are implemented.

A review of the available literature has shown that research programs which investigated novel methods of improving the tensile resistance of non-contact lap splices in reinforced masonry construction do not exist. Technical and practical means of solving such cases are necessary to maintain the viability of structural masonry construction in situations where non-contact lap splices cannot be avoided. An investigation was therefore initiated to design and test remedial splice details which could improve the structural performance of the lapped reinforcing bars in non-contact lap splices to that of contact lap splices with the same lap length. The ease of implementing each remedial splice detail in the field was qualitatively evaluated in an effort to ensure the viability of each design.

1.2 Research Objectives

The principal objective of this research program is the qualitative and quantitative comparison of the effect that various structural remediation measures applied to non-contact lap splices, where the lapped reinforcement is centred in adjacent cells, have on their tensile resistance.

The following are the specific objectives of this investigation:

1. To determine if any of the remedial measures used in conjunction with non-contact lap splices can achieve the same tensile resistance as that of contact lap splices of the same lap splice length;
2. To formulate multiplication factors to represent the available tensile resistance of non-contact lap splices with structural remedial measures based on the analyzed quantitative test data. Un-remediated non-contact lap splices and contact lap splices are used as the reference points.

3. To determine if any of the structural remedial measures applied to non-contact lap splices can attain the same deflection profile as that of contact lap splices of the same lap splice length;
4. To determine if the same failure mode can be achieved for the non–contact lap splices with structural remedial measures as the contact lap splices; and
5. To validate the ease of implementation for the various structural remedial measures.

1.3 Methodology and Scope

Twenty-four wall splice specimens were constructed and tested over two phases to investigate the maximum tensile resistance of each lap splice detail. Six different remedial techniques were evaluated. Two control splice details, one with unaltered contact and the other with non-contact lap splices, were also constructed to provide a reference for splice behaviour at the ideal and un-remediated conditions, respectively. Three replicate specimens were constructed in an effort to establish the average structural performance parameters for each lap splice detail. An effort was made to keep the properties of the individual materials used to construct a masonry assemblage as constant as practically feasible for all of the wall splice specimens. Testing of companion specimens was completed to determine the properties of each material in the masonry assemblage.

The wall splice specimens were tested in a horizontal position under monotonic, four–point loading with the lap splices located in the constant moment region. A numerical moment-curvature analysis was then performed using the applied load and deflection data from each wall splice specimen test and the material properties acquired for the companion specimen testing. This analysis was used to determine the maximum tensile resistance of the spliced reinforcement. The effectiveness of each remedial method was then determined by comparing visual observations of the resulting distress and analyzed quantifiable data of each lap splice detail to that of the two control details. The ease of implementing each remedial splice detail in the field was determined by consulting with industry professionals, taking the geometry of the remediation scheme into consideration, and reviewing qualitative data gathered during the construction of the specimens.

1.4 Thesis Outline

Chapter 1 – This chapter provided a brief background of bond research, established the need for further investigation of non-contact lap splices in masonry construction, stated the objectives of the current research study, and described the methodology used to complete the stated objectives.

Chapter 2 – This chapter presents the basic mechanics of bond in reinforced masonry, reviews the different specimens previously used in masonry research, and summarizes the results of relevant previous investigations which examined non-contact lap splices in flexural members. The results of the literature review were the basis for the current investigation.

Chapter 3 – The geometry, construction, and testing of the wall splice and companion specimens are detailed in this chapter.

Chapter 4 – The experimental results from the wall splice specimens and associated companion specimens are presented in this chapter. Visual observations of external and internal crack patterns are presented and compared for the different lap splice details. A finite difference model was used to determine the theoretical moment-curvature for each wall splice specimen. This was then used to calculate the midspan deflection and the tensile resistance capacity of the spliced reinforcement. The practical implications and viability of each structural remediation measure are then discussed.

Chapter 5 – An overview of the results from the experimental program and conclusions are presented to address the stated objectives. Recommendations for future relevant research are also discussed.

CHAPTER 2: LITERATURE REVIEW

2.1 Introduction

Reinforced masonry is a composite construction material. Structural members constructed with reinforced masonry are commonly subjected to flexural effects that cause internal forces to develop. These internal forces are comprised of a tensile force that is carried by the steel reinforcement and a compressive force that is resisted by the grout, mortar, and masonry blocks (ie. the cementitious materials). These forces must be transferred between the reinforcement and cementitious materials to effectively develop a flexural resisting system. Mechanical interaction between the reinforcing bars and the surrounding grout, commonly referred to as bond, is therefore required to accomplish this phenomenon.

The reinforcing bars in masonry assemblages are not typically continuous to accommodate openings within walls, connecting adjacent structural elements together, and to increase constructability, as explained in Section 1.1; thus, splices are required. The lap splice needs to be of sufficient length to allow the tensile force to be effectively transferred between the spliced reinforcing bars. Providing relevant data to continue to optimize the splice length in a variety of different situations and publish these findings in masonry design standards is the objective of the scientific community specializing in this field of study.

Bond research in reinforced concrete dates back to the early 20^{th} century; however, investigations focusing on bond in reinforced masonry assemblages were not initiated for another half century. In addition, the majority of bond research in reinforced masonry has focused on splice situations where the lapped bars are in contact. Section 1.1 described numerous situations that result in splices where the lapped bars are not in contact and may even be located in adjacent cells within a reinforced masonry assemblage. Only recently have researchers examined such splice situations in reinforced masonry construction. The results indicated that further investigations are required to provide recommended design practices for non-contact lap splices which can be used by industry professionals.

This chapter introduces the basic mechanics of bond in reinforced masonry, reviews the different specimens used in masonry bond research, and summarizes the results of relevant previous investigations examining non-contact lap splices in flexural members.

2.2 Mechanics of Bond

A sufficient length of reinforcing bar must be provided to transfer the tensile force, T, between the steel reinforcement and the surrounding grout in a composite system such as reinforced masonry. Figure 2.1 illustrates the concept of average bond stress with the application of a tensile force to a plain reinforcing bar that is concentrically embedded in a grouted masonry cell. The average bond stress, u, is assumed to be uniformly distributed over the development length, L_d. The following relationship must be satisfied to achieve equilibrium between the forces in the two materials:

$$T = A_s f_s = u\pi d_b L_d \qquad [2\text{-}1]$$

where A_s is the cross-sectional area of the reinforcing bar, f_s is equal to the tensile stress in the steel reinforcement, and d_b is the diameter of the reinforcing bar. Recognizing that πd_b is equal to the circumference of the reinforcing bar and A_s is equal to $\frac{\pi}{4} d_b^2$ enables equation 2-1 to be rearranged, resulting in the following relationship for the required development length:

$$L_d = \frac{d_b}{4u} f_s \qquad [2\text{-}2]$$

Equation 2-2 provides a simplified relationship to calculate the development length; however, it assumes that the bond stress is uniform. Abrams (1913), Soric & Tulin (1989), Cheema & Klingner (1985), and (Feldman & Bartlett, 2007) showed that the uniform stress assumption does not apply to plain or deformed reinforcing bars in reinforced concrete and masonry construction.

Soric & Tulin (1989) and Cheema & Klingner (1985) have shown that the concept of average bond stress is an oversimplification of the actual bond distribution along the development length of deformed reinforcing bars that are commonly used in masonry construction. Their experimental investigations have shown that the distribution of bond stresses along the development length of the reinforcing bar is non-linear and localized areas of high bond stress occur. These localized areas of high stress are typically located near the loaded ends of the reinforcement and shift along the length of the bar to the unloaded end as the tensile force in the bar is increased (Feldman & Bartlett, 2007). This phenomenon is not represented in the average bond stress model. As a result, the Canadian masonry design code, CSA S304.1, has discontinued publishing specified allowable values for bond stress, u, since the 1977 edition, CSA S304-77

(CSA, 1977); it now provides empirical equations to determine the required development based on the findings of these investigations.

Deformed reinforcing bars are predominantly used in modern reinforced masonry construction which can sustain higher bond stresses due to the mechanical interlock between the deformities and the surrounding cementitious material. Bond stress of deformed reinforcing bars depends on the rib pattern, the magnitude of the applied load, and the development length. Figure 2.2 (a) shows the bond mechanics between a deformed reinforcing bar and a grouted masonry cell. The ribs of the deformed reinforcing bar bear against the surrounding cementitious material to form inclined compressive struts. The horizontal, or axial, component of the struts transfers the tensile forces in the reinforcement to surrounding cementitious material through bearing while the radial component creates a circumferential tensile force surrounding cementitious material. Some of the force is also transferred between the two materials through the adhesion of the bar and the grout between the ribs of the deformed bar; however, the majority of the force transfer occurs at these deformations. Bond failure between the reinforcement and the grout between the ribs of the reinforcing bar is one possible mode of failure. It occurs when the shear strength of the surrounding grout is overcome by the combined magnitude of horizontal component of the diagonal compressive struts and the shear between the ribs. Bar pullout is another failure mode associated with reinforced concrete and masonry elements. It occurs when the radial component of the bond force overcomes the tensile capacity of the cementitious material and the confinement provided by a fully-grouted cell in a masonry assemblage. Splitting of the surrounding grout and masonry block is another failure mode associated with reinforced concrete and masonry elements. Figure 2.2 (b) shows the additional lateral tensile force that is produced in the plane of the adjacent reinforcing bars when they move relative to each other. This movement causes the ribs of the bars to ride over one another and induces tensile stresses in the surrounding grout and masonry block (Schuller et al., 1993) which ultimately leads to splitting of the surrounding masonry assemblage.

The following sections examine previous investigations of bond in reinforced masonry and concrete. Research related to reinforced concrete is included in this review to supplement the limited number of research studies conducted on non-contact lap splices in reinforced masonry. Investigations related to the behaviour of contact lap splices are also briefly examined to focus on

the different types of specimens in bond research. The advantages and shortcomings of each specimen type are discussed and compared to provide a rationale for the type of specimen selected for this investigation. Several research programs that have examined non-contact lap splices in reinforced masonry and concrete are then reviewed to highlight the need for this investigation.

2.3 Evaluation of Contact Lap Splices

The majority of investigations in the field of masonry bond research have focused on lap splices where the spliced bars are in contact with each other. The types of specimens used in these investigations have evolved throughout the years in an effort to more accurately model the stress state of a masonry wall in field conditions. The following sub-sections examine this evolution.

2.3.1 Pullout Specimens

Pullout specimens have been used by numerous researchers [Baynit, (1980); Cheema & Klingner, (1985); Soric & Tulin, (1989); Schuller et. al., (1993); NMCA, (1999); and Ahmed & Feldman, (2012)] to investigate bond and anchorage in reinforced masonry. The popularity of pullout specimens is due to their low construction costs, simplicity of fabrication, small storage footprint, and simple test setup. This allowed researchers to cost effectively construct and test a larger number of replicates and so provide enough data for statistical analyses. The disadvantage of pullout specimens is that they were tested in direct tension and not in flexure. Therefore, tensile stress was induced only in the reinforcement while the surrounding grout was subjected to compression or no stress at all. This affected the overall behaviour of the spliced reinforcement and resulted in an inability to compare the tensile resistance of lap splices in laboratory prepared pullout specimens directly to those in masonry walls constructed in the field. Ahmed (2011) reported the evolution of pullout specimens and noted that their advancement did result in minor improvements in modelling the stress state of masonry. Ahmed and Feldman (2012) concluded that pullout specimens can be used for bond testing, particularly for the evaluation of contact lap splices in members subjected to axial loads only. However, they produce different results than those of wall splice specimens, which are tested in flexure, due to the differing internal stress state.

2.3.2 Beam Specimens

Beam specimens are tested in flexure and therefore better represent the loading conditions that a masonry wall will experience in the field compared to pullout specimens. Beam specimens have been used for several previous masonry investigations to study bond [Baynit, (1980); and Matsumara, (1997)]. Figure 2.3 shows the beam specimens used in Baynit's (1980) investigation of development lengths in reinforced masonry. Lintel blocks were used to construct the beam specimens and the reinforcement was placed near the bottom of the cross-section. Sections of the reinforcing bar were de-bonded to control the location of the development length. The specimens were tested under four-point loading and the displacement and load data were recorded. Baynit (1980) observed that the average bond stress was 1.2 to 1.7 times lower in the beam specimens as compared to the pullout specimens that were tested in the same investigation. Similar behaviour was observed by Matsumura et al. (1997). The higher bond stresses in the pullout tests were the result of the high compressive reaction that developed adjacent to the support located at the base of the pullout specimen. This stress was not present in the beam specimens due to their loading geometry. Baynit (1980) concluded that pullout tests can provide an indication of the general bond behaviour but should not be used when a quantitative analysis of bond capacity is required. However, the specimens in Baynit's (1980) investigation did not include lap splices which are more sensitive to the internal stress state of the masonry assemblage in the splice region.

Beam specimens provide a more reasonable representation of the internal stress state of a masonry wall compared to pullout specimens. However, numerous differences exist between the geometry of beam and wall splice specimens that affect the stress state within the masonry assemblage and affect the bond behaviour. One example of how the cross-sectional geometry differs between the two specimens is that the reinforcement in wall specimens is typically centered in the cross-section while it is placed near the bottom of a beam cross-section. As a result, beam specimens typically have a larger moment arm between the internal force resultants as compared to wall specimens. Beam specimens are also typically constructed in a stack bond pattern while masonry walls are typically constructed in running bond. The geometry of the stack bond allows for a larger uninterrupted area of grout since the cells of the masonry blocks are slightly staggered when they are placed in running bond. The larger uninterrupted area of grout reduces the proportional area of the mortar joints in the cross-section of the specimen. This

increases the flexural capacity of beam specimens since the mortar joints are typically weaker in compression than the grout. Another difference between the two specimen types is the type of masonry blocks used in their construction. Beam specimens are constructed using lintel blocks which have an open cross section and do not have the same confining effect as the regular masonry blocks used in masonry walls, which have a closed cross-section. Beam specimens are therefore not suitable for investigating the splice capacity of reinforcement in masonry walls.

2.3.3 Wall Splice Specimens

Wall splice specimens tested in flexure most accurately model the stress state found in masonry walls constructed in the field compared to pullout and beam specimens. The geometry of wall splice specimens eliminates the shortcomings of the beam specimens listed in the previous section. Wall splice specimens have been used by numerous researchers [Uniat, (1983); Suter & Fenton, (1985); Ahmadi, (2001); Ahmed & Feldman, (2012); Sanchez & Feldman, (2013)] to test contact lap splices in reinforced masonry. Wall splice specimens are not as popular as pullout specimens due to their higher construction costs, large storage requirements in the laboratory, and the more complex test setup required to adequately accommodate their larger size and mass. All of these factors have resulted in a limited number of research studies where full-scale masonry wall splice specimens were used to investigate the splice strength or development length of reinforcement in masonry construction.

Recent investigations completed at the University of Saskatchewan by Ahmed & Feldman (2012) and Sanchez & Feldman (2013) used wall splice and pullout specimens to compare the capacity of spliced reinforcement. Figure 2.4 (a) and (b) shows the double pullout and wall splice specimens with contact lap splices used in Ahmed and Feldman's (2012) investigation, respectively. Eight specimens of each type were constructed and all specimens were reinforced with No. 15 deformed reinforcement which had a 300 mm lap splice length. The reinforcing bars in the pullout specimens were de-bonded outside of the lap splice length. This ensured that no additional resistance was obtained from the section of bar beyond the lap splice region. Ahmed and Feldman (2012) observed that the mean tensile capacity of the contact lap splices in the double pullout specimens was 8.47% less than those in the wall splice specimens with an identical splice arrangement. This represented a statistically significant difference at the 95%

confidence level. These results indicate that pullout specimens do not generate the same results as wall splice specimens when investigating the bond of spliced reinforcement in masonry walls.

2.4 Evaluation of Non-Contact Lap Splices

Chapter 1 discussed situations where non-contact lap splices are required, both intentionally and unintentionally, in field situations to accommodate the geometry and structural requirements of a masonry assemblage. The current edition of the Canadian masonry design code, CSA S304.1-04 (CSA, 2004e), permits the use of non-contact lap splices in reinforced masonry construction without any adjustments to the lap splice length. However, the lack of research related to non-contact lap splices in masonry has resulted in design codes which may not adequately take into account the effects of higher transverse spacings or the lapped bars being located in adjacent cells. Several studies related to the use of non-contact lap splices in reinforced concrete members have been completed; however, few research projects have investigated this splice geometry in masonry construction. The added complexity of the various materials used in masonry construction (grout, mortar, and concrete blocks) cannot be modelled in reinforced concrete specimens. Ahmed and Feldman (2012) have shown that the interfaces between these three materials are areas of poor bond and reduce the tensile capacity of the spliced bars if they are located in adjacent cells. Despite this, there have not been any known investigations in the field of masonry research that included the design and testing of remedial measures to improve the structural performance of these splices. The following sections summarize the previous investigations of non-contact lap splices in reinforced concrete and masonry design, and explain how the tensile forces are transferred between the lapped bars in a non-contact lap splice.

2.4.1 Reinforced Concrete Studies

Two relevant investigations relating to non-contact lap splices in reinforced concrete specimens are described in the following sections due to the lack of similar research in masonry and because the Canadian design codes for the two construction methods have similar clauses regarding this splice geometry. The review of the studies shows how tensile forces are transferred between bars that are not in contact as well as highlight the limitations of using the results from reinforced concrete investigations to predict the behaviour of non-contact lap splices in reinforced masonry construction.

Sagan et al.'s (1991) Concrete Double Pullout Specimens

The purpose of Sagan et. al.'s (1991) investigation was to provide results-based recommendations for the design of non-contact lap splices in reinforced concrete elements. Figure 2.5 shows the geometry of the concrete double pullout specimens used in this investigation. Forty-seven specimens were tested, each having two identical symmetrically arranged splices. The concrete specimens varied from 34.5 to 42 in. (877 mm to 1067 mm) in length and 10 to 46 in. (254 mm to 1168 mm) in width. Two different imperial longitudinal reinforcing bar sizes and two lap splice lengths were tested: No. 20 bars with a 22.5 in. (572 mm) lap splice length, and No. 25 bars with a 30 in. (762 mm) lap splice length. The transverse spacing between the spliced reinforcement also ranged from 3 to 9 in. (76 mm to 229 mm).The effect that the transverse reinforcement and its spacing had on the tensile capacity of the spliced bars was studied. The specimens were tested in direct tension and were loaded either monotonically or dynamically, where the load was cycled to the theoretical yield load until failure was achieved.

The results showed that the ultimate tensile force carried by the monotonically loaded spliced reinforcement was independent of the transverse spacing provided that the spacing did not exceed $6d_b$, where d_b is the diameter of the longitudinal reinforcement. However, the number of repeated load cycles until failure began to decrease as the transverse spacing between the spliced bars was increased beyond four bar diameters. The results also showed that the transverse reinforcement had a noticeable effect on the tensile capacity of non-contact lap splices. The specimens without transverse reinforcement showed a 30 to 40% reduction in the tensile capacity of the lapped bars as compared to specimens with transverse reinforcement. Sagan et. al. (1991) found that it was conservative to ignore the effects of transverse spacing of the spliced reinforcement and design the splice as a contact lap splice if the transverse spacing provided was less than 12 in. (305 mm) for monotonically loaded members and 8 in. (203 mm) for dynamically loaded members.

Sagan et. al. (1991) also showed that the force transfer between lapped bars in non-contact lap splices can be modelled by a planar truss. This model can also be applied to non-contact lap splices in reinforced masonry construction. Figure 2.6 shows the planer truss model within a reinforced masonry assemblage. The longitudinal force along the bar resists the tension in the reinforcement while the diagonal compressive struts, which are similar to the diagonal webs of a

plane truss, transfer the forces through the cementitious material separating the two bars. Figure 2.6 also shows that the separation of the bars results in a lever arm, l.a., between the tensile forces carried by the spliced reinforcement, T. This creates an external moment, M_{ext}, which must be resisted by an internal moment couple that forms between the lapped bars. The capacity of the internal moment couple is predominantly dependent on the confinement provided by the in-plane stiffness of the surrounding cementitious material's geometry. The relatively small scale of the specimens used in Sagan et. al.'s (1991) investigation limited the available lateral confinement. Splitting of the specimens therefore resulted before pullout failure could be achieved. In masonry construction, most of the walls built in the field are continuous, and extend beyond the cells where the lap splice is located. The stiffness of the surrounding masonry assemblage counteracts the in-plane moment caused by the separation of the spliced bars. This increases the overall tensile resistance of the lap splice.

Hamid & Mansour's (1996) Reinforced Concrete Slab Specimens

Hamid and Mansour (1996) investigated the performance of non-contact lap splices in reinforced concrete slabs subjected to flexure. The purpose of their investigation was to provide a more complete understanding on the effect that transverse spacing between spliced bars had on their tensile resistance. Figure 2.7 shows the geometry of the reinforced concrete slab specimens. Each specimen contained three pairs of spliced bars of the same splice length. A 300 mm lap splice length was used in the specimens that were reinforced with 14 mm and 16 mm diameter deformed reinforcing bars, and 350 mm lap splice length was used in the specimens reinforced with 20 mm reinforcement. The transverse spacing between the spliced bars ranged from 0 to 150 mm. All of the specimens were designed so that bond failure would occur prior to yielding of the reinforcement. Information regarding the end anchorage for the longitudinal reinforcement was not provided in this paper. Transverse reinforcement was not provided in Hamid and Mansour's (1996) slab specimens as it was in the double pullout specimens used in Sagan et. al's (1991) investigation.

The slab specimens were tested under four-point loading with the lap splices located in the constant moment region. Bond failure was observed in of all the slab specimens as noted by the presence of longitudinal splitting and diagonal surface cracks in the constant moment region. The tensile capacity of the splices was improved by 10% compared to the contact lap splices when the

transverse spacing was less than 30% of the lap splice length. The tensile capacity then began to decrease once the transverse spacing exceeded 30% of the lap splice length. Hamid and Mansour (1996) advised that a transverse spacing equal to 20% and 30% of the lap splice length was optimal for the bars with a 14 mm and 16-20 mm diameter, respectively, based on the results of their test program. However, the reinforcement was cast near the bottom of the slab specimens which allowed for a larger moment arm compared to masonry reinforced masonry walls where the reinforcement is located at the centre of the assemblage. This resulted in a lower compressive stress state in the cementitious material in the slab specimens at a given load level compared to masonry wall with the same thickness. Interfaces between different cementitious materials, which may have a negative effect on the flexural resistance of a structural member, are also not present in reinforced concrete construction. For these reasons, the results from the two investigations discussed in this section are not suitable for predicting the tensile capacity of non-contact lap splices in masonry construction, where the lapped bars are located in adjacent cells.

2.4.2 Reinforced Masonry Studies

Two relevant investigations relating to non-contact lap splices in reinforced masonry specimens will be examined in the following section. A review of these studies will show the effect of non-contact lap splices on the tensile resistance of the lapped reinforcement in masonry assemblages and highlight the limited body of research on the subject.

Sanchez & Feldman's (2013) Reinforced Wall Splice Specimens

Sanchez & Feldman (2013) investigated the tensile resistance of non-contact lap splices where the lapped bars were located in the same cell. Figure 2.8 shows the elevation and cross section of the wall splice specimens that were tested. Each specimen was 13 courses tall by 2.5 blocks-wide and was reinforced with No. 15 Grade 400 deformed bars. The lap splice length and transverse spacing between the lapped bars were varied to measure their effect on the tensile resistance of the spliced reinforcement. Three different lap splice lengths were tested (150 mm, 200 mm, and 250 mm) in conjunction with three difference transverse spacings: 0 mm, 25 mm, and 50 mm. Three replicates of each lap splice geometry were constructed, for a total of 27 wall splice specimens.

The specimens were tested in a horizontal position, under four-point monotonic loading, with the load and deflection data recorded throughout testing. All of the specimens failed by pullout of the reinforcing bars, although it was less evident in the specimens with a 150 mm lap splice length or a 50 mm transverse spacing. The largest cracks were located in the bed joints adjacent to the ends of the lap splice length. Sanchez & Feldman (2013) observed that the tensile force was highest for spliced reinforcement in contact. The higher force in the reinforcement for this splice geometry was likely the result of the lugs of the bars riding over each other as the slip of the two bars increased. The results of a regression analysis indicated that the tensile resistance of the non-contact lap splices was insensitive to the magnitude of the transverse spacing between the lapped bars for the arrangements tested in the investigation. Sanchez & Feldman (2013) also noted that the poor bond at the grout-block interface and the lower compressive strength of the mortar joints compared to that of the grout and concrete blocks likely has a negative effect on the flexural capacity of reinforced masonry walls.

Ahmed & Feldman's (2012) Investigation of Non-Contact Lap Splices in Pullout and Wall Splice Specimens

Ahmed & Feldman (2012) also tested 16 pullout and wall splice specimens (eight of each specimen type) with non-contact lap splices, where the lapped bars were located in adjacent cells, to compare the tensile resistance to the contact lap splice specimens discussed in Section 2.3.3 and shown in Figure 2.4. A review of the available literature suggests that Ahmed & Feldman's (2012) investigation is the sole work which examined the bond behaviour of non-contact lap splices in masonry walls, where the lapped bars were located in adjacent cells.

Figure 2.9 shows the geometry of both specimen types with non-contact lap splices. The double pullout (Figure 2.9 (a)) and the wall splice specimens (Figure 2.9 (b)) were both reinforced with No. 15 Grade 400 deformed bars with a 300 mm lap splice length. The reinforcing bars in the double pullout specimens with non-contact lap splices were also de-bonded outside of the lap splice region for the same reason as the pullout specimens with contact lap splices discussed in Section 2.3.3. All of the reinforcing bars in the specimens with non-contact lap splices were centred in the adjacent cells. This was done to simulate typical construction practices in the field despite the requirement in Clause 12.5.2.2 of CSA S304.1-04 (CSA, 2004e) specifying that the transverse spacing of the lapped bars not exceed $1/5^{th}$ of the required lap length or 150 mm.

Reinforcement is typically centred in the cells of masonry walls constructed in the field since it is easier to place in this manner and it maximizes the clear spacing around all sides of the bar to allow for better consolidation of the grout by a mechanical vibrator.

The performance of the double pullout specimens with non-contact lap splices was noticeably different than those with contact lap splices, as reported in Section 2.3.3. The mean tensile resistance of the double pullout specimens with contact and non-contact lap splices was 89.7 kN (COV 2.37%) and 40.7 kN (COV 7.75%), respectively; this difference is a product of the different resulting failure modes. A sudden splitting failure was observed in the specimens with non-contact lap splices while bar pullout and yielding of the reinforcement was observed in the specimens with contact lap splices.

The face shell of select pullout specimens with non-contact lap splices was removed following testing to observe the internal distresses within the splice region. Ahmed and Feldman (2012) noted that the diagonal cracks between the lapped bars only extend to the adjacent web of the concrete block. The cracks then changed orientation such that they propagated along the grout-block interface. These observations suggest that a poor bond existed at this interface. This poor bond was due to shrinkage cracks that formed at the grout-block interface. The formation of shrinkage cracks, similar to those shown in Figure 2.10, is a result of the high water content in the grout used in typical masonry construction to ensure adequate consolidation. Bischoff and Moxon (2005) also noted that excessive shrinkage in the grout used to fill masonry cells led to restrained shrinkage cracking which decreased the overall flexural capacity of masonry specimens. The poor bond at the grout-block interface interrupted the formation of the vertical, or shear component, of the diagonal compressive struts, shown in Figure 2.6, since shear cannot be effectively transferred through a cracked medium. This reduced the tensile resistance capacity of the lapped reinforcement. This interaction between the materials in a masonry assemblage cannot be simulated in reinforced concrete specimens; therefore, studies such as Sagan et. al.'s (1991) and Hamid and Mansour's (1996) investigations cannot be used to predict the performance of non-contact lap splices in masonry construction where the lapped bars are located in adjacent cells.

The placement of the spliced longitudinal bars in the outermost cell of the non-contact lap splice specimens limited the available confinement and stiffness of the masonry assemblage to form the

resisting internal moment couple and so counteract the external moment caused by the transverse separation of the spliced bars. This likely further decreased the tensile resistance of the non-contact lap splice. Ahmed & Feldman (2012) therefore hypothesized that the tensile resistance of non-contact lap splices placed in the non-exterior of larger masonry assemblages would likely be higher than those tested in the 2.5 block wide specimens.

The performance of the wall splice specimens with non-contact lap splices was also noticeably lower than those with contact lap splices. The mean tensile resistance of the wall splice specimens with contact and non-contact lap splices was 98 kN (COV 3.19%) and 68.2 kN (COV 11.4%), respectively. This difference in the mean tensile resistance represented a statistically significant result at the 95% confidence level. Internal crack patterns showed that the diagonal cracks between the lapped bars in the wall splice specimens with non-contact lap splices also changed orientation at the grout-block interface, similar to what was observed in the double pullout specimens. The noted internal damage identified for the wall splice specimens with contact lap splices included crushing of the grout keys, which is indicative of a pullout failure, and flexural cracking at the bed joints.

The coefficients of variation for the double pullout and wall splice specimens with contact lap splices was furthermore noticeably lower compared to respective specimens with non-contact lap splices. Ahmed & Feldman (2012) deduced that this was attributed to the failure mode of the specimens with non-contact lap splices, which involved splitting due to the poor bond at the grout-block interface, compared to the reinforcement pullout in the specimens with contact lap splices. Failures which involve pullout of the reinforcing bars typically have lower coefficients of variation since this failure mode is predominantly dependent on the length of the lap splice and the properties of the reinforcement, while splitting failure is dependent on the highly variable tensile properties of cementitious materials.

Ahmed & Feldman (2012) concluded that a correction factor of 1.5 was reasonable, for the range of parameters investigated, in the calculation of the effective splice length when the lapped are placed in adjacent cells unless remedial methods which enhance the tensile resistance of these splices are implemented.

2.5 Summary

A review of the existing literature showed that the majority of bond research conducted for reinforced masonry was completed using pullout specimens and contact lap splices. Pullout specimens are tested in a different stress state than what is typically induced in reinforced masonry walls in the field. This affects the performance of the splice reinforcement; therefore, pullout specimen tests are not appropriate for modeling lap splices in reinforced masonry. A select number of investigations using wall splice specimens exist, but the majority of these specimens were tested with contact lap splices. An examination of the available literature indicated that studies which investigated non-contact lap splices in reinforced masonry construction prior to the publication of the current Canadian masonry design code, CSA S304.1-04 (CSA, 2004e) did not exist. As a result, Clause 12.5.2.2 in CSA S304.1-04 (CSA, 2004e) which addresses non-contact lap splices was likely based on studies that used reinforced concrete specimens. These types of specimens cannot model the effects of the interaction between the grout, mortar, and masonry blocks present in masonry assemblages on the tensile resistance of spliced reinforcement, especially if the lapped bars are located in adjacent cells.

A recent investigation by Ahmed and Feldman (2012) compared the tensile resistance of contact and non-contact lap splices in wall splice specimens, where the lapped bars were located in adjacent cells. The results indicated that the tensile resistance of the lapped reinforcing bars in wall splice specimens with non-contact lap splices was noticeably lower than those with contact lap splices of the same length. Ahmed and Feldman (2012) therefore recommended that the effective splice length for non-contact lap splices should be increased by 50% in relation to contact lap splices, unless other approaches of enhancing the tensile resistance of non-contact lap splices could be implemented.

A review of the available literature has indicated that there have not been research programs conducted that investigated novel methods of improving the tensile resistance of non-contact lap splices in reinforced masonry construction. Suitable technical and practical means of resolving such cases are required to maintain the viability of structural masonry construction in situations where non-contact lap splices are unavoidable. An experimental program was therefore initiated to design and test remedial splice details with the aim of increasing the tensile resistance of non-contact lap splices to that of contact lap splices of the same lap length. The following chapter

describes the various wall splice specimens with remedial procedures applied in the splice region and provides a description of the construction and testing procedures used in this current investigation.

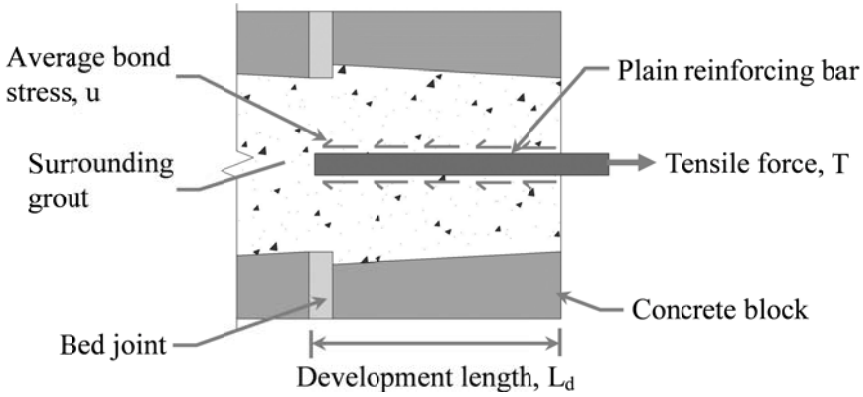

Figure 2.1: The Concept of Average Bond Stress.

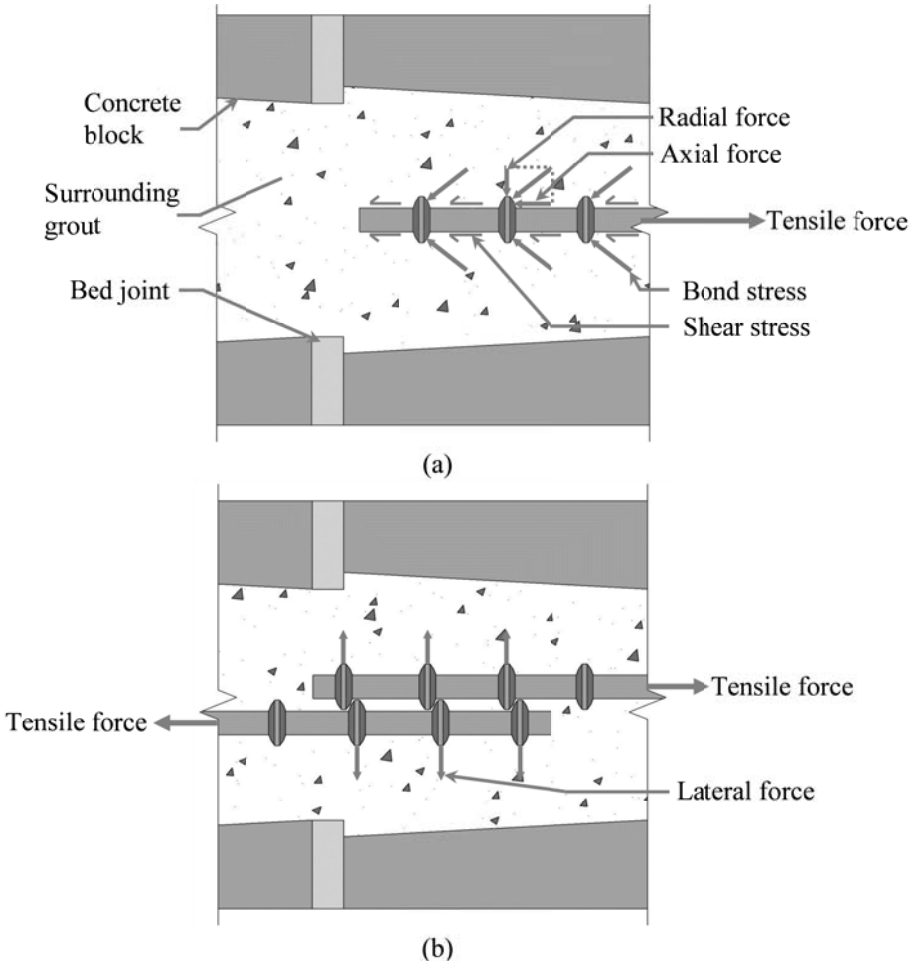

Figure 2.2: Bond Mechanisms Associated with Deformed Reinforcing Bars: (a) Bond Force Components, and (b) Lateral Force Caused by Relative Movement of Spliced Bars.

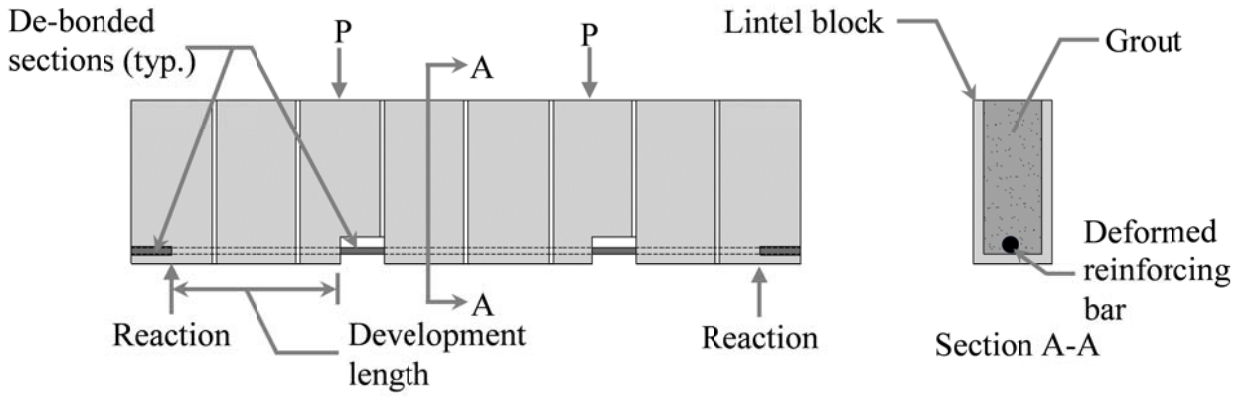

Figure 2.3: Beam Specimens (Baynit, 1980).

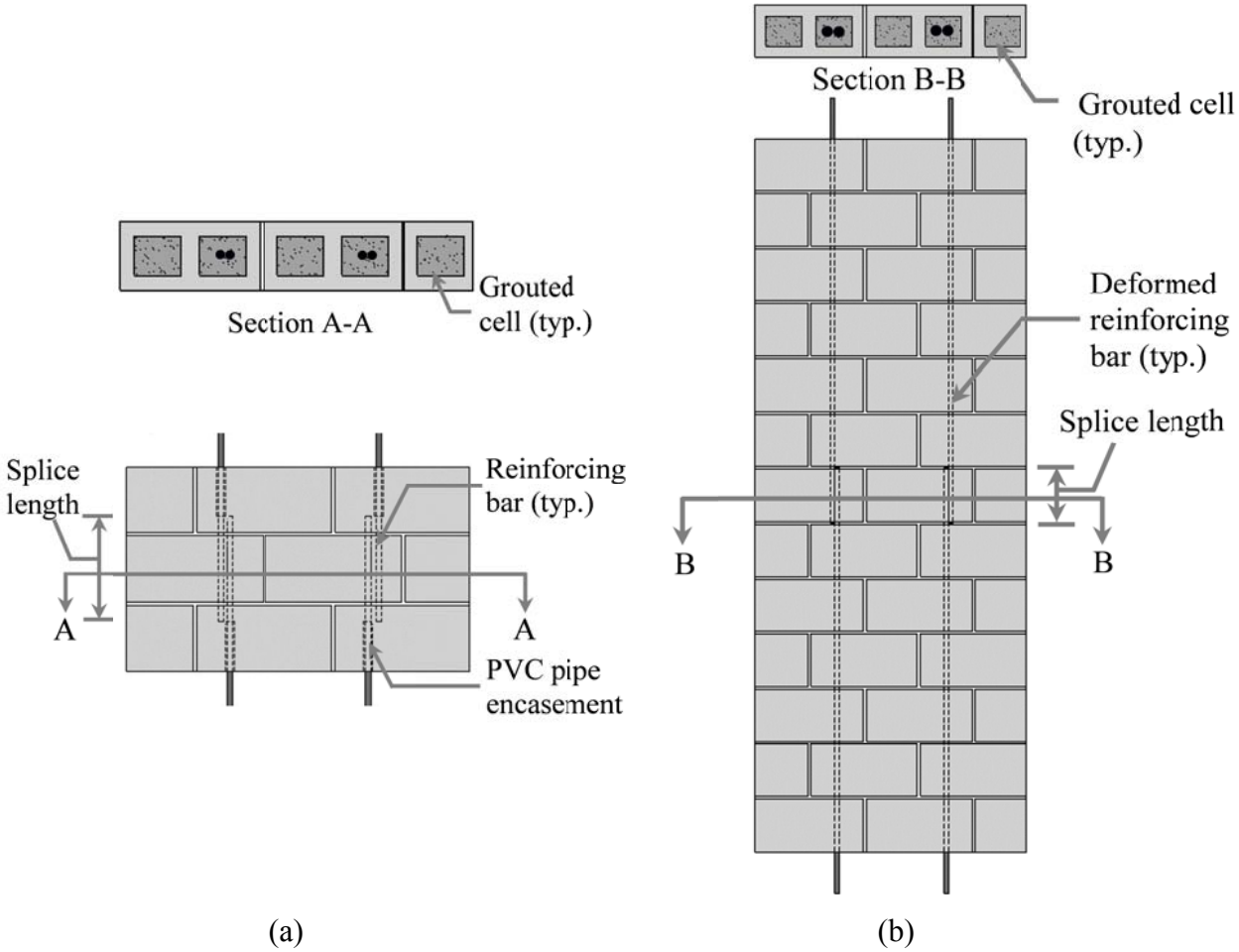

Figure 2.4: Contact Lap Splice Geometry (Ahmed & Feldman, 2012): (a) Double Pullout Specimen, and (b) Wall Splice Specimen.

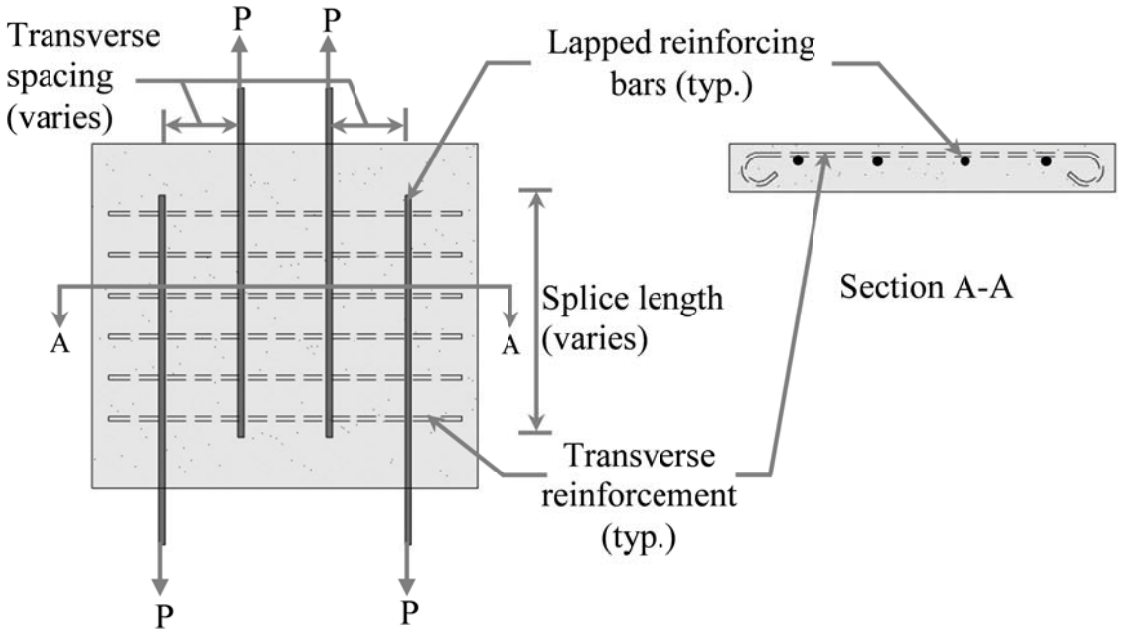

Figure 2.5: Double Pullout Specimen (Sagan et. al., 1991).

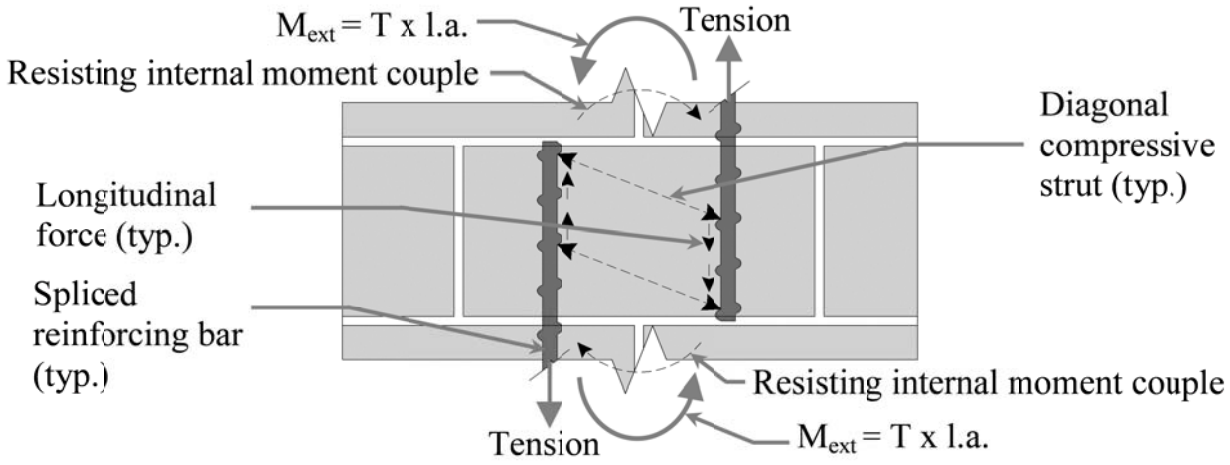

Figure 2.6: Force Transfer Mechanism Between Reinforcing Bars in Non-Contact Lap Splices (Ahmed & Feldman, 2012).

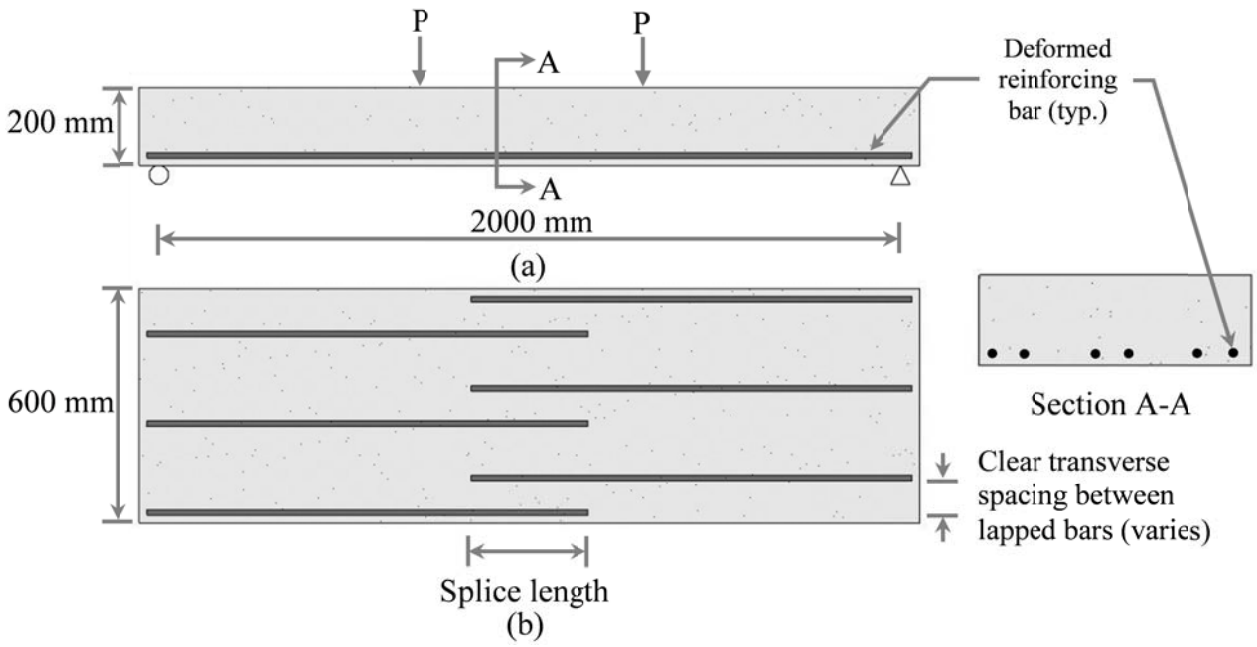

Figure 2.7: Full-Scale Reinforced Concrete Slab Specimens (Hamid & Monsour, 1996): (a) Elevation, and (b) Plan View.

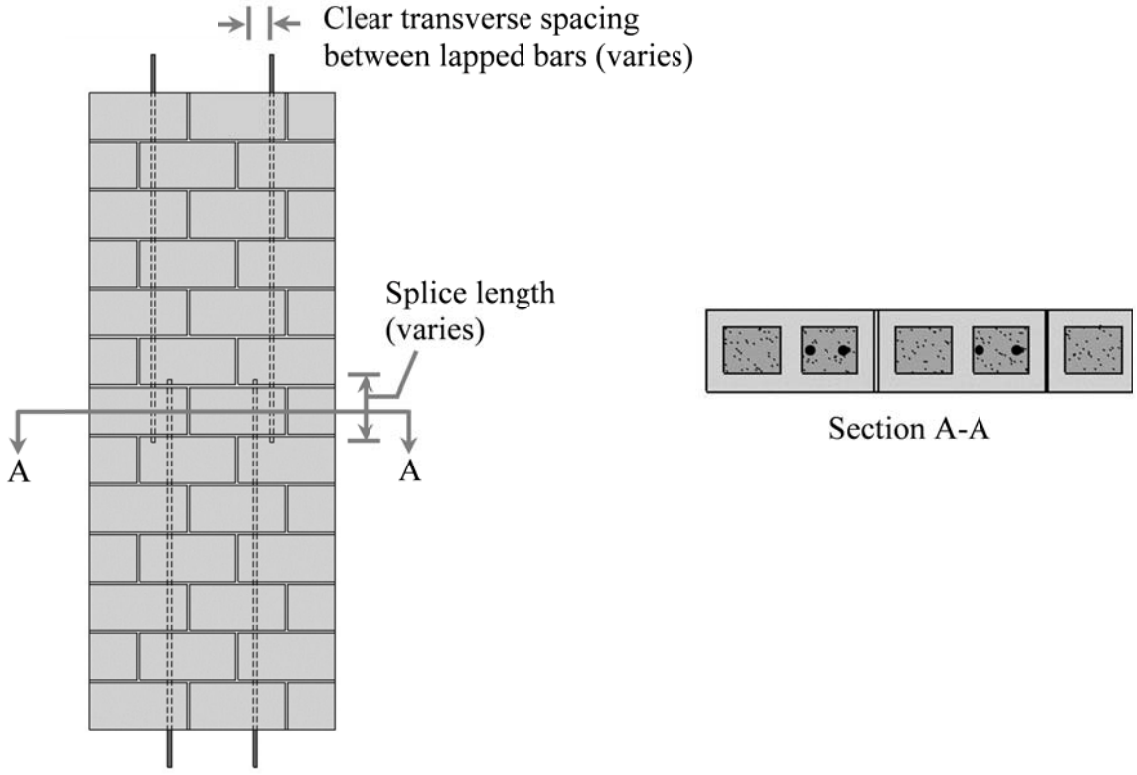

Figure 2.8: Wall Splice Specimen Geometry (Sanchez & Feldman, 2013).

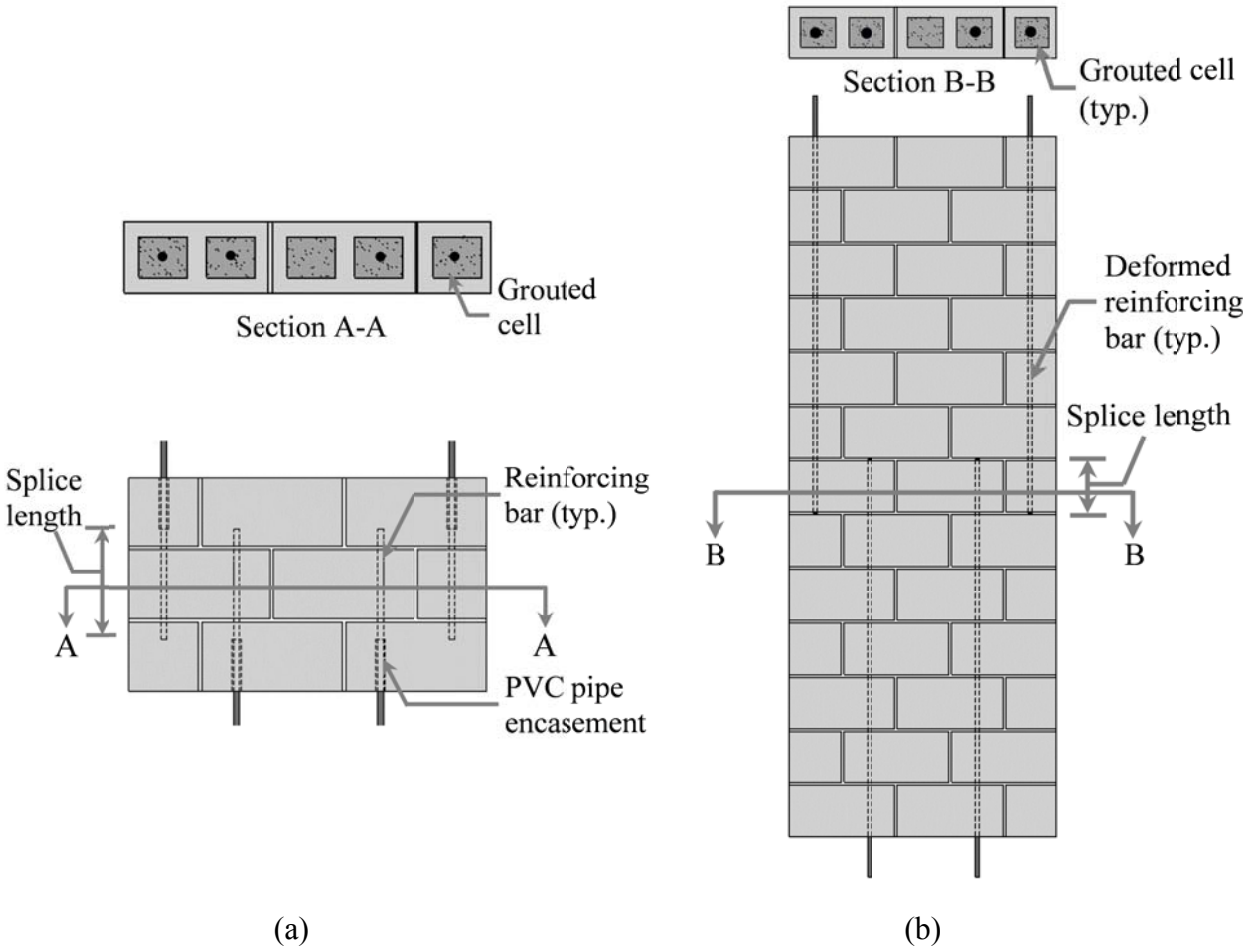

Figure 2.9: Non-Contact Lap Splice Geometry (Ahmed & Feldman, 2012): (a) Double Pullout Specimen, and (b) Wall Splice Specimen.

Figure 2.10: Shrinkage Cracks at the Grout-Block Interface.

CHAPTER 3:EXPERIMENTAL DESIGN, SPECIMEN CONSTRUCTION, AND TEST SETUP

3.1 Introduction

Eight different wall splice specimen configurations, consisting of two different control designs and six remedial measures, were designed, constructed, and evaluated in Phases 1 and 2. Three replicates of each configuration were constructed for a total of 24 wall splice specimens. An additional 12 wall splice specimens were constructed in Phase 1a, with four additional remedial measures, that were unintentionally constructed with a 240 mm lap length. The different lap length of the Phase 1a wall splice specimens does not allow for the test results to be directly compared to the wall splice specimens of Phase 1 and 2, which feature the intended 200 mm lap length. As a result, the configuration, construction, and testing process of these wall splice specimens are detailed in Appendix 3A, while the test data is located in Appendix 4A.

The appropriate standards were adhered to for both the construction and testing procedures required in this experimental program. An effort was made to keep the properties of the individual materials used to construct a masonry assemblage as constant as practically feasible for all of the wall splice specimens. The wall splice specimens were tested under monotonic, four-point loading to induce out-of-plane bending which allowed the tensile resistance of the lap splices to be calculated from the acquired load and deflection data.

3.2 Determination of Splice Length

The lap splice length used was selected to ensure that the primary mode of failure for all wall splice specimens was by bond of the reinforcement prior to yielding. Ahmed & Feldman (2012) conducted a literature review related to the development and splice length required to yield the reinforcement. This resulted in the selection a 300 mm lap length of the spliced No. 15 reinforcement in an attempt to ensure bond failure in all the specimens. This length was based on the minimum specified splice length required for all bar sizes in accordance with the current Canadian masonry design code, CSA S304.1-04 (CSA, 2004e). Following analysis of the test results, Ahmed & Feldman (2012) discovered that some of the reinforcement in the wall splice specimens featuring contact lap splices, with a 300 mm lap length, failed by the yielding of the

reinforcement and mortar crushing on the compression face, which occurred prior to bond failure. A 300 mm lap length was therefore deemed unsuitable for this study.

A test program completed by Sanchez & Feldman (2013) at the University of Saskatchewan also featured wall splice specimens reinforced with No. 15 bars with three different lap lengths (150, 200, and 250 mm) where the spliced bars were in contact. Sanchez & Feldman (2013) concluded that a 200 mm lap length, with the spliced bars in contact, was the maximum splice length in which bond failure could be consistently achieved before yielding of the reinforcement.

Based on these previous studies, a 200 mm lap splice length was selected for this investigation in an effort to ensure bond failure in all the wall splice specimens.

3.3 Determination of the Number of Replicate Specimens

A review of Ahmed & Feldman's (2012) test data suggested that six replicates are required to reasonably establish statistical parameters, the mean splice capacity, and to identify statistical outliers in masonry wall splice specimen testing. The scope of this research program focused on maximizing the number of different remediation techniques studied, given the budget and space constraints in the Structures Laboratory. As a result, a statistical evaluation of the test data was not included in the scope of this study. Three replicates of each wall splice specimen configuration, with the designations #1, #2, and #3 following the name of each specimen set, were therefore used as this was the minimum required to calculate a useable mean value and detect physical outliers, while satisfying space and cost constraints. As a result, 24 wall splice specimens were constructed with 8 different control and remedial measures.

3.4 Specimen Description

Table 3.1 shows the general description of the 24 wall splice specimens constructed over the two phases of construction prescribed in this chapter. The 24 wall splice specimens were constructed in Phase 1 and 2 and incorporated a 200 mm long lap splice length. The specimens in these two phases were therefore used for the primary analysis.

All wall splice specimens were 13 courses tall and constructed in a running bond pattern to maintain consistency with previous research conducted at the University of Saskatchewan

(Ahmed & Feldman, 2012, Sanchez & Feldman, 2013). Deformed steel reinforcing bars with a nominal diameter of 15 mm (ie No. 15 bars) were used to reinforce all the wall splice specimens. This reinforcement size was specified following consultations with professionals in the masonry industry who stated that No. 15 reinforcement was the most common bar size used in Canadian masonry construction. Each wall splice specimen featured two lapped steel bars to maintain symmetry within each specimen and eliminate the effects of the eccentricity that results when wall splice specimens are constructed with non-contact lap splices. The reinforcing bars extended 190 mm beyond the top and bottom of the wall splice specimens to accommodate the installation of end anchorages which ensured that bond failure occurred within the lap splice region. The rationale for all of the wall splice specimen configurations constructed in Phases 1 and 2 is described in the following sections; while the Phase 1a wall splice specimens are presented in Appendix 3A.

3.4.1 Contact Lap Splice (Control) Specimens (CLS)

Figure 3.1 shows the cross-section, elevation, and side view of the control wall splice specimens featuring contact lap splices (CLS) that were constructed in Phase 1. Their geometry is similar to the wall splice specimens used in the investigation conducted by Ahmed & Feldman (2012), with the exception of the lap splice length being reduced from 300 mm to 200 mm, as already discussed in Section 3.2. The CLS specimen configuration was designed to model the ideal lap splice configuration in a masonry assemblage.

Figure 3.1 shows that the steel reinforcing bars were spliced at the mid-height of the wall splice specimen. Tie wire was used to hold the lapped reinforcing bars in contact with one another until the grout placed in the reinforced cells cured. The spliced bars were centred in the cell to ensure adequate grout cover, as specified by CSA S304.1-04 Annex D (CSA, 2004e).

Results from these wall splice specimens were used as the benchmark for a quantitative comparison of all six non-contact lap splice specimens featuring remedial measures and the same lap length (GCC, 1KO, 3KO, SBAR, C-SBAR, CT-SBAR). This comparison was used to determine whether it was possible to achieve similar tensile capacities in non-contact lap splices with remedial measures applied as those achieved in specimens with contact lap splices.

3.4.2 Non-Contact Lap Splice (Control) Specimens (NCLS)

Figure 3.2 shows the cross-section, elevation and side view for the control wall splice specimens featuring non-contact lap splices (NCLS), where the lapped bars are located in adjacent cells. This wall splice specimen configuration is similar to that included in the investigation conducted by Ahmed & Feldman (2012) with the exception of the lap splice length used. This specimen geometry was designed to model a non-contact lap splice, where the lapped bars are located in adjacent cells, without any remedial measures.

Figure 3.2 shows that steel reinforcing bars were lapped at the mid-height of the wall and were centered in their respective cells. The measures taken during construction to ensure proper placement of the reinforcement are described in Section 3.6.1. Figure 3.2 also shows that the top reinforcing bars were located in the outermost cells of the wall splice specimen. Ahmed & Feldman (2012) concluded that this does not adequately model the tensile resistance of non-contact lap splices in a continuous masonry wall as the stiffness of the adjacent masonry assemblage would normally counteract the in-plane moment caused by the separation of the splice bars. However, this concern was addressed in the fully grouted confinement cell specimens (GCC), as will be discussed in Section 3.4.3.

The NCLS specimens were constructed in Phase 1; the results from the testing of these control wall splice specimens were used as a baseline for a quantitative comparison of all six non-contact lap splice designs which featured remedial measures. The results from the NCLS wall splice specimens were intended to provide a lower bound for the tensile resistance of the lap splice. This was used to determine the level effectiveness of each of the different remedial measures investigated in this study which are detailed in the following sections.

3.4.3 Fully Grouted Confinement Cell Specimens (GCC)

Most masonry walls constructed in the field are continuous, and extend beyond the cells where the lap splice is located. The stiffness of the surrounding masonry assemblage counteracts the in-plane moment caused by the separation of the spliced bars through increased confinement, as discussed in Section 2.4.1, and so increases the overall tensile resistance of the lap splice. The Fully Grouted Confinement Cell Specimen (GCC) was conceived in an effort to address this and more adequately model non-contact lap splices in continuous masonry walls.

Figure 3.3 shows the cross-section, elevation, and side view of the Fully Grouted Confinement Cell Specimens (GCC). These specimens were 3.5 blocks wide which allowed for one fully grouted unreinforced external cell on each side of the specimen. Placement of the reinforcement within the wall splice specimen was identical to that of the NCLS specimens described in Section 3.4.2. These specimens were constructed in Phase 1 and were used to determine if wider wall splice specimens would have any effect on the tensile resistance of non-contact lap splices, where the lapped bars are located in adjacent cells.

3.4.4 Single Knock-out Web Specimens (1KO)

Ahmed & Feldman (2012) noted that diagonal cracks in the grout were evident between the pairs of lapped bars in specimens with non-contact lap splices. Figure 3.4 shows that the cracks propagated diagonally from the lapped reinforcement until they reached the interface between the grout and the intact block web. The cracks then changed orientation and propagated along the interface between the grout and the intact block web. These crack patterns suggested poor bond between the grout and the concrete block which was a result of grout shrinkage during curing. Grout in masonry assemblages is susceptible to shrinkage because it is poured at a high slump, and hence high water-cement ratios, to ensure good consolidation throughout the height of the grout column. The elimination of the grout-block interface between pairs of lapped bars was the rationale behind Single Knock-out Web Specimen (1KO).

Figure 3.5 shows the cross-section, elevation, and side view of the 2.5 block wide 1KO wall splice specimens constructed in Phase 1. Placement of the reinforcement within the wall splice specimen was identical to the NCLS specimens described in Section 3.4.2. The 1KO specimens featured knock-out webs along the lap splice length which allowed for continuous grout between the pairs of lapped bars, and so eliminated the poor bond at the grout-block interface within the lap splice length of the reinforcement. Consultations with industry professionals suggested that the installation of knock-out webs in masonry construction would not affect the overall constructability of the masonry assemblage.

3.4.5 Triple Knock-out Web Specimens (3KO)

The Triple Knock-out Web Specimens (3KO) were similar in geometry and rationale to the 1KO specimens described in Section 3.4.4, and were also constructed in Phase 1. Figure 3.6 shows that

additional concrete block webs were removed in the courses directly above and below the lap splice length, for a total of three consecutive courses of knock-out webs. The multiple courses of knock-out webs were installed to more adequately accommodate the formation of inclined compressive struts, detailed in Section 2.4.1, between the spliced reinforcement. These compressive struts transfer the tensile forces in one reinforcing bar through the masonry assemblage to the other reinforcing bar in a non-contact lap splice. Since these struts are inclined, they may extend above and below the lap splice length and thus necessitate a longer uninterrupted grout region. The three courses of knock-out webs also reduced the probability of shrinkage cracks propagating from the intact webs located outside of the lap splice region into the area between the lapped reinforcement. The purpose of the 3KO specimens was to determine the effect of increasing the column of uninterrupted grout in the region of the lapped bars on the tensile resistance of non-contact lap splices.

3.4.6 Specimens with S-Shaped Reinforcement (SBAR)

Figure 3.7 shows cross-section, elevation, and side view of the 2.5 block-wide specimens reinforced with s-shaped bars at the splice level (SBAR). The location of the longitudinal reinforcing bars was identical to those detailed in the NCLS specimens in Section 3.4.2. Three courses of knock-out webs were used in the splice region, identical to the 3KO specimens described in Section 3.4.5, to provide an uninterrupted grouted region between the pairs of lapped bars. The knock-out webs also allowed for the installation of the s-shaped splice reinforcement within the splice region.

An s-shaped steel reinforcing bar was placed between the two bars that make up the non-contact lap splice and steel tie wires was used to fasten the s-shaped splice reinforcement to the longitudinal reinforcement. The s-shaped splice reinforcement consisted of No. 15 Grade 400 deformed reinforcement with two 45º bends located at such a distance to bridge the gap between the pair of lapped longitudinal reinforcing bars. The 100 mm inside radius of the 45º bends complied with CSA A23.1-04 (CSA, 2004c). The 45º bends were also designed to allow clearance between the reinforcement and the concrete blocks while minimizing dowel action, where the bar must resist shear forces, in its inclined section. This was advantageous since reinforcing steel bars are more efficient at transferring axial tension forces than shear.

The s-shaped splice reinforcement was designed to essentially transform a single non-contact lap splice into a series of two contact lap splices, both having the same lap length as the original non-contact lap splice. One limitation of the remedial measures which include the s-shaped reinforcement is that it extends beyond of the original splice length. As a result, it cannot be used in situations where the lower bar to be lap spliced has already been grouted up to the elevation of the splice region prior to the installation of the S-Bar. An example of this would be dowel protruding from a completed grade beam that does not align with the specified reinforced cell of the masonry wall above.

3.4.7 Specimens with S-Shaped Splice Reinforcement and Grouted Confinement Cells (C-SBAR)

Figure 3.8 shows the cross-section, elevation, and side view of the 3.5 block wide wall splice specimens featuring s-shaped lap splice reinforcement and confinement cells that were constructed in Phase 2. These specimens featured the same reinforcement and knock-out web geometry as the SBAR specimens detailed in Section 3.4.6; while the overall wall splice specimen geometry was identical to the GCC specimens detailed in Section 3.4.3. The design philosophy behind the C-SBAR wall splice specimens was to more accurately model the effects of s-shaped splice reinforcement in continuous masonry assemblages where the lap splices are located in the middle of the wall and not at the extremities. The stiffness of the grouted cells adjacent to the lap splice would counteract the in-plane moment caused by the straightening of the s-shaped splice reinforcement when subjected to tensile forces, therefore increasing the overall tensile resistance of the lapped bars.

3.4.8 Specimens with S-Shaped and Transverse Splice Reinforcement and Grouted Confinement Cells (CT-SBAR)

Figure 3.9 shows the cross section, elevation, and side view of the 3.5 block wide wall splice specimens featuring s-shaped and horizontal transverse reinforcement combined. The s-shaped splice reinforcement was the same as the C-SBAR wall splice specimens detailed in Section 3.4.7. The geometry of the knock-out webs was also similar to the C-SBAR specimens with the addition of further knock-out webs at splice level between the two pairs of lapped bars to allow for the placement of the horizontal transverse reinforcement at splice level.

The horizontal transverse reinforcement consisted of a No. 15 Grade 400 deformed steel bar. The bends at each end of the bar exceeded 180 degrees, featured an inside bend radius of 100 mm, and had a 85 mm straight section following the bend to comply with the specifications detailed in CSA A23.1-04 (CSA, 2004c). Figure 3.9 shows that the transverse reinforcing bar was designed to span between the two pairs of non-contact lap splices and was located at the mid-height of the wall splice specimen. The horizontal transverse reinforcement was essentially designed to behave as a stirrup to intercept the shear component of the diagonal compressive struts, detailed in Section 2.4.1, and to provide additional confinement within the lap splice region to counteract the transverse forces generated from the straightening of the s-shaped reinforcement, as discussed in Section 3.4.6.

The C-SBAR wall splice specimens were constructed in Phase 2 with the intention of determining whether the tensile resistance of non-contact lap splices could be further enhanced by combining the previously detailed s-shaped transverse reinforcement and confinement cells with horizontal transverse reinforcement.

3.5 Construction Materials

The wall splice specimens were constructed using locally sourced materials and complied with the relevant standards and codes in an effort to represent typical masonry walls as constructed locally. Materials were ordered and delivered prior to the start of each construction phase due to space restrictions in the Structures Laboratory. This resulted in a slight variability in the material properties of the various components in the masonry assemblage between two construction phases.

3.5.1 Concrete Masonry Units

Standard frogged-end concrete blocks, with overall dimensions of 390 mm x 190 mm x 190 mm and a nominal compressive strength of 15 MPa, were supplied by Cindercrete Products Ltd. of Saskatoon and adhered to the specifications detailed in CSA A165-04 (CSA, 2004a). Half concrete blocks measured approximately 190 mm x 190 mm x 190 mm and were produced by cutting the standard blocks in two equal sections using a diamond blade wet-saw in the University of Saskatchewan Structures Laboratory. Figure 3.10 (a), (b), (c), and (d) show the dimensions of the blocks in further detail. Units featuring knock-out webs, shown in Figure 3.10

(e) and (f), were also available from the supplier. However, these blocks were created by cutting out the webs using the diamond blade wet-saw. This was performed to ensure that all the blocks originated from a common batch and had similar material properties.

The concrete blocks were delivered to the Structures Laboratory on plastic wrapped pallets where they were stored, prior to being used for construction, for at least two weeks to equilibrate with laboratory humidity and temperature. The blocks were delivered in stages, one prior to each construction phase, and each stage contained concrete blocks which originated from the same production batch. Six concrete block samples from each phase were tested for compressive strength as detailed in Section 3.7.3.

3.5.2 Mortar

Mortar was hand-batched in the Structures Laboratory and was composed of cement, sand, and water. Masonry sand was supplied from a local source and stored in a steel bin in the laboratory until it was required. Lafarge Type "MCS" masonry cement was supplied in 34 kg bags and stored on a wooden pallet in the Structures Laboratory. CSA A179-04 (CSA, 2004b) specifies a minimum 28-day compressive strength of 12.5 MPa for Type "S" mortar in structural applications as well as an initial flow rate of 100-115% to maintain workability. To comply with these regulations, a cement-to-sand ratio of 1:3 and a 0.7 water-to-cement ratio were used based on data obtained by previous studies by Ahmed & Feldman (2012), Sanchez & Feldman (2013), and Udey & Sparling (2013).

A sieve analysis was performed according to the test procedure outlined in CSA A23.1-04 (CSA, 2004c) on three random 500 gram samples of masonry sand in both the first and second phases of construction. The requirements for the aggregate gradation of masonry sand are specified in CSA A179-04 (CSA, 2004b) and were met by the sand used in this study. The aggregate gradations of the mortar sand are presented in Appendix 3B.

3.5.3 Grout

Grout was also hand-batched in the Structures Laboratory. It was composed of cement, course and fine aggregates, and water. Lafarge Type "GU" Cement was supplied in 20 kg bags and stored on a wooden pallet in the Structures Laboratory until it was required for use. The aggregate was acquired from a local source, delivered to the Structures Laboratory, and placed on

the floor prior to the start of construction. The specified aggregate included a 10 mm maximum particle size and was mixed by the supplier with a ratio of 2:3 fine to coarse aggregate as required by CSA A179-04 (CSA, 2004b). A sieve analysis was performed according to the test procedure outlined in CSA A23.1-04 (CSA, 2004c) on three random 500 gram samples of grout aggregate in both the first and second phases of construction. The requirements for the aggregate gradations of are specified in CSA A179-04 (CSA, 2004b) and were met by the aggregate used in this study. The complete aggregate gradations are presented in Appendix 3B.

A mix design consisting of an 1:5 cement-to-aggregate ratio and a target slump of 250 mm was used based on consultations with local industry professionals. A 1:1 (approximate) water to cement ratio was used to attain the desired slump; however, slight variations were required to account for the varying moisture content of the delivered aggregate and how long it had been stored in the laboratory. Previous studies completed at the University of Saskatchewan by Ahmed & Feldman (2012) and Sanchez & Feldman (2013) have shown that this mix design produced minimum 28 day compressive strengths of 12.5 MPa as required by CSA A179-04 (CSA, 2004b).

3.5.4 Reinforcing Steel

Grade 400 standard deformed No. 15 steel bars were acquired from a local supplier and used as the reinforcement in the wall splice specimens. The bars were delivered to the Structures Lab in standard six meter lengths along with a mill certificate which certified that the material complied with the Standard for Carbon Steel Bars used as Concrete Reinforcement, CSA G30.18 (CSA, 2009). The six meter sections were cut to the appropriate length in the Structures Lab using a chop saw featuring an abrasive cut-off wheel. The excess lengths were saved and used to perform tension tests of the reinforcing steel.

3.6 Construction

Twenty-four wall splice specimens were constructed over two phases due to space and labour limitations. Table 3.1 details the configurations of the wall splice specimen for these two phases of construction. Phase 1 was constructed August 14th to the 23rd 2012, while Phase 2 was built between March 20th and 28th, 2013. Construction of the wall splice specimens was completed by an experienced mason. The grout and mortar preparation was performed by the graduate students

in the Structures Laboratory, under the supervision of the experienced mason. The detailed mix designs for the mortar and the grout as well as the construction processes used for each of the specimens are detailed in the following sections.

3.6.1 Splice Preparation

A single heat batch of reinforcing steel was used in Phase 1, while a second heat batch was used for the Phase 2 specimens.

Figure 3.11 shows a photograph of the contact lap splices. The lapped longitudinal reinforcing bars were fastened together using tie wire at two locations: one adjacent to each end of the lap splice length, to form a 200 mm lap splice. This was done to ensure the spliced bars were in contact in every contact lap splice specimen.

Knock-out webs were required in the splice region for multiple remedial wall splice specimen configurations (1KO, 3KO, SBAR, C-SBAR, and CT-SBAR) in both phases of construction. Figure 3.12 and Figure 3.13 (b) show that this required the use of specialty blocks with specific webs removed (Figure 3.10 (e) and (f)).

Figure 3.12 also shows the guides that were used to center the longitudinal reinforcement within the cell. These consisted of strips of 25.4 x 25.4 MW 0.102 x MW 0.102 wire mesh. The strips spanned across the reinforced cell between the fifth and sixth course and were held in place by the joint mortar. The longitudinal reinforcing bar was then threaded through the appropriate square in the welded wire mesh to ensure that the reinforcing steel remained vertical until the grout cured.

Figure 3.13 (a) shows the horizontal transverse reinforcement used in the CT-SBAR wall splice specimens. These bars were fabricated by bending a straight segment of reinforcing steel using the manual bar bender in the Structures Lab. The inside radius of the hooks was 100 mm and a 85 mm segment of straight bar followed the hooks to meet the specifications provided in CSA A23.1-04 (CSA, 2004c). Figure 3.13 (b) shows the horizontal transverse reinforcement after it was installed in the wall splice specimen. All the webs were knocked out at the splice level to accommodate the horizontal transverse reinforcing bar, similar to the knock-out web blocks used in the field to accommodate the reinforcing steel in select masonry bond beams. Each horizontal reinforcing bar was supported on the intact bottom portion of the block webs while steel tie wire

was used to fasten these bars to the bottom longitudinal reinforcing bars. This assured that the transverse reinforcement was in contact with the bottom longitudinal bars and that it remained vertical until the grout cured.

Figure 3.14 (a) shows the s-shaped splice reinforcement included in the SBAR, C-SBAR, and CT-SBAR remedial wall splice specimens. Tie wire was used to fasten the s-shaped reinforcement to the vertical longitudinal reinforcement, similar to the procedure used in the CLS wall splice specimens. The 195 mm length of the diagonal section of the s-shaped splice reinforcement was calculated to allow the longitudinal reinforcing bars to be centred in adjacent cells. Figure 3.14 (c) shows the installed s-shaped reinforcement assembly. Three courses of knock-out webs, similar to the layout shown in Figure 3.12, were used to accommodate the s-shaped splice reinforcement in the wall splice specimens. Welded wire mesh guides were once again used to centre the longitudinal bars in the required cells.

3.6.2 Mortar Preparation

Laboratory prepared mortar was used in the construction of all specimens. The proportions of cement, masonry sand, and water in each batch were based on the established mix designs provided in Section 3.5.2. The batching sequence consisted of first placing two-thirds of the sand and half of the required water into the mixer. The cement was then slowly added along with the remainder of the water. The remaining sand was then slowly added to ensure batch consistency. Finally, small amounts of additional water were added into the mix until the workability desired by the mason was achieved. Figure 3.15 (a) shows the mixer in the Structures Laboratory being used to mix a batch of mortar. All mortar batches were allowed to mix for five minutes before being transferred from the mixer and delivered to the mason. Mortar workability is known to decrease with time; therefore, additional water was added and allowed to mix as per the mason's request. This process is called tempering. The mortar batches which required tempering were noted and labeled with a "T" after the batch number. Care was taken to track the location of all mortar batches in the wall splice specimens.

Six mortar cubes were cast from each mortar batch. An additional three cubes were cast for mortar batches which required tempering to ensure the strength properties of tempered mortar complied with CSA A179-04 (CSA, 2004b). The first phase of construction required 13 batches of mortar while the second required eight. Figure 3.15 (b) shows that the cubes were cast in brass

moulds in accordance with CSA A3004-C2 (CSA, 2003). The moulds were then covered with plastic sheets for approximately 48 hours following casting, as dictated by CSA A179-04 (CSA, 2004b). The finished cubes were then de-moulded and stored under similar curing conditions to the wall splice specimens.

3.6.3 Grout Preparation

All of the grout used in the construction of the specimens was prepared in the Structures Laboratory using the concrete mixer shown in Figure 3.16 (a). The quantity of materials required per grout batch was estimated from the pre-determined mix design provided in Section 3.5.3. The batching process began by placing half of the required water into the rotating mixer and adding one-third of the gravel. Following this, the cement was placed into the rotating mixer. Next the remainder of the gravel and water was slowly added to ensure batch consistency. The grout was then allowed to mix for approximately five minutes while small amounts of additional water were added to bring the slump of the grout up to approximately 250 mm. Figure 3.16 (b) shows that a slump test was performed for every grout batch to confirm workability and ensure consistency between batches. After passing the slump test, the grout batch was then transferred from the mixer into wheelbarrows and transported to the construction location. Two types of specimens were prepared to test grout properties: absorptive grout prisms in accordance with ASTM C1019-12 (ASTM, 2012b), and non-absorbent grout cylinders in accordance with CSA A179-04 (CSA, 2004b).

Absorptive grout prisms were created by first arranging four concrete blocks, as shown in Figure 3.16 (c), to form a 100 mm x 100 mm x 190 mm mould. The moulds were then lined with paper towels to provide a bond breaker. Grout was then placed in two equal lifts, rodded 15 times per lift, covered with plastic, and then allowed to set for two days following initial casting. The prisms were stored in the laboratory following de-moulding and so were cured under the same conditions as the wall splice specimens.

Non-absorptive grout cylinders were cast in 100 mm diameter by 200 mm high plastic moulds. The moulds were filled in two equal lifts and each was rodded 20 times in accordance with CSA A179-04 (CSA, 2004b). Figure 3.16 (d) shows the cylinders covered with plastic and allowed to cure in the Structures Laboratory for approximately 48 hours. The cylinders were then stored in

the laboratory under the same conditions as the wall splice specimens following the removal of the plastic and de-moulding.

One absorptive prism and three non-absorptive cylinders were cast for each grout batch. The first phase of construction required 32 batches of grout while the second required 22. Each set of cylinders was numbered and recorded. This allowed for the appropriate grout prisms and cylinders to be tested on the same day as the corresponding wall splice specimen.

3.6.4 Prisms

Masonry prisms were constructed alongside each wall splice specimen in an effort to quantify the overall masonry assemblage strength. To achieve this, the prisms were constructed using the same batch of mortar and grout as the corresponding wall splice specimen. The mortar was allowed to set for 24 hours before the grout was placed into the cells. This ensured consistency with the procedure used for the construction of the wall splice specimens.

A total of 22 masonry prisms were constructed in Phase 1, and 15 in Phase 2. Figure 3.17 (a) shows the three block-high, stack bond masonry prism. One prism of this type was constructed alongside every wall splice specimen, resulting in 15 prisms in Phase 1 and 9 in Phase 2. This prism design was used in previous University of Saskatchewan masonry research programs (Ahmed & Feldman, 2012, Sanchez & Feldman, 2013) and was used as a baseline for comparing the remaining two masonry prism designs used in this study.

Figure 3.17 (b) shows the four block high, running bond prism. A single specimen was constructed for each set of three wall splice specimens featuring the same lap splice detail. This resulted in five prisms in Phase 1 and three in Phase 2. This prism type was constructed in an effort to more accurately determine the compressive strength of the masonry assemblage, given that these prisms featured the same bond pattern as the wall splice specimens. The additional height of this prism type should also lessen the effects of end confinement caused by the friction between the masonry and the test frame. This is the result of the zones affected by the confinement being located further away from the bed joint at the mid-height of the prism, where the cracks which result in specimen failure initiate. This results in lower f'_m values but more accurately represents the stress state in a masonry assemblage.

Figure 3.17 (c) shows the 4 block high, running bond prism featuring an O-block as was required in wall splice specimens with knock-out webs in the splice region. A single prism of this design was constructed for each set of three wall splice specimens with the same reinforcement geometry that featured knock-out webs within the splice region. Two prisms of this design were built in Phase 1 and 3 in Phase 2. This prism design modeled the effect of the discontinuity caused by knock-out webs on the overall compressive strength of the assemblage.

The completed masonry prisms were stored in the Structures Laboratory under the same climatic conditions as the wall splice specimens in an effort to ensure similar curing conditions between the two types of specimens.

3.6.5 Wall Splice Specimens

Figure 3.18 shows the plywood bases that the wall splice specimens were built on. Half inch plywood was used for the 2.5 block wide wall bases, while one inch plywood was used for the 3.5 block wide bases to prevent any excessive deflections during construction. The plywood was supported by three concrete blocks: one at each end and one at the centreline. Holes drilled through the plywood at the appropriate locations allowed the steel reinforcing bars to be accurately placed within the wall splice specimen. The bars protruded an additional 190 mm below the bottom of the splice specimens. The reinforcement extending both above and below the specimen, as shown in Figure 3.1 to Figure 3.3 and Figure 3.5 to Figure 3.9, allowed for the installation of end anchorage at the ends of the four reinforcing bar during testing to ensure bond failure occurred within the splice region.

An experienced mason was engaged to construct all of the wall splice specimens. This ensured that the workmanship was similar to masonry assemblages built in the field. The 13 course tall wall splice specimens were constructed in two lifts: the first lift consisted of eight courses while the second consisted of the remaining five. Figure 3.19 (a) shows the 25.4 x 25.4 MW 0.102 x MW 0.102 welded wire mesh. This was installed after the fifth course, within the first construction lift, with the bed joint mortar being used to maintain the position of the steel wire, to ensure the correct placement of the steel reinforcement. The remaining three courses in the first lift were laid immediately thereafter.

The upper and lower longitudinal reinforcing bars were placed into the masonry assemblage after the mortar used in the first construction lift was allowed to cure for a 24 hour period. Figure 3.19 (b) shows that the top reinforcing steel bars were centred in the appropriate cell and held in place by a plywood strip. The plywood strip featured a hole in its centre for the reinforcement to pass through. Tie wire was then placed on the top reinforcing bar at a precise elevation to maintain the reinforcing bar at the desired elevation when it was passed through the plywood strip. This ensured the appropriate lap length was achieved. Figure 3.19 (b) also shows that a steel weight was used to hamper movement of the top reinforcing bars during grout placement and subsequent curing.

The first lift of the wall splice specimen was grouted following the installation of all the steel reinforcement. Figure 3.20 (a) shows the grout being placed into the wall splice specimen, while Figure 3.20 (b) shows a mechanical vibrator being used to ensure adequate consolidation of the grout column. The plywood guide and steel weight used to secure the top reinforcing bars, shown in Figure 3.19 (b) was removed after a 24 hour curing period so construction of the second lift could proceed. The experienced mason then laid the five course second lift which brought the wall splice specimen to the design height of 13 courses. The mortar was once again allowed to cure for 24 hours before grout was placed in the second lift. Figure 3.21 shows a newly completed wall splice specimen following the successful placement and consolidation of the grout in the second lift.

3.6.6 Specimen Curing

All specimens were allowed to cure for a minimum of 28 days following construction. The specimens were stored in the Structures Laboratory where the temperature and humidity ranged from 18 to 22 degrees Celsius and 20 to 25 percent, respectively. The ranges provided were a result of the time of day that the measurements were recorded. Figure 3.22 (a) shows the wall splice specimens and prisms curing in the Structures Laboratory and Figure 3.22 (b) shows the companion specimens curing after being removed from the molds.

3.7 Instrumentation and Testing

The wall splice specimens were tested as soon as possible after the 28-day curing period had elapsed. The order of testing was based on accessibility; however, all wall splice specimens with

the same lap splice design were tested consecutively. The companion specimens were tested on the same day as the corresponding wall splice specimens in an effort to accurately measure the material properties of the wall splice specimens. The following sections detail the testing procedures as well as the instrumentation for all the different types of specimens featured in this research project.

3.7.1 Moving Frame for the Wall Splice Specimen

The wall splice specimens needed to be moved from their constructed vertical position to a horizontal orientation such that they could be tested. A specialized moving frame and the overhead crane in the Structures Laboratory were used for this purpose. Figure 3.23 shows the moving frame that was detailed in Ahmed's (2011) thesis. It was reused and modified for this study to allow for the transportation and rotation of both the 2.5 block and 3.5 block wide wall splice specimens.

The upper and lower horizontal beam assemblies were modified from the original used in Ahmed's (2011) study to accommodate both wall splice specimen widths. This was achieved by first by cutting both beam assemblies in half and welding 12.7 mm steel plates to the cut ends. Figure 3.23 shows the 500 mm long back-to-back C250 x 23 drop-in section that was added to both the upper and lower horizontal beam assemblies to accommodate the 3.5 block wide wall splice specimens. The 12.7 mm steel plates were also welded to the ends of the drop-in sections to allow them to be connected to the lower and upper horizontal beam assemblies. The location of the bolt holes drilled in on both the drop-in sections and the horizontal beam assemblies lined up to allow for the different elements to be fastened together and so form extended upper and lower horizontal beam assemblies as shown in Figure 3.23 (a).

The first step in the installation of the moving frame around a given wall splice specimen involved lowering the lower horizontal beam assembly over the wall splice specimen using the overhead crane. Next, a pair of 19 mm steel bearing plates were fastened to the bottom flanges of the bottom horizontal beam assembly with bolts. Following this, the upper horizontal beam assembly was lowered to encompass the top two courses of the wall splice specimen and was held in place using the overhead crane. Four threaded 16 mm diameter steel rods were then used to connect the upper and lower horizontal beam assemblies. Figure 3.23 shows the location of these four connector rods.

Figure 3.24 (a) shows that the assembled moving frame and wall splice specimen were lifted by the overhead crane using the lift points. The slings were attached on the inside of the frame to prevent them from slipping off during the lifting procedure. The lifting of the frame caused the wall to be supported by the bearing plates bolted to the horizontal beams of the lower moving frame assembly. The load was transferred from the bearing plates to the horizontal beams of the lower moving frame assembly through the four threaded bars to the horizontal members in the upper moving frame assembly and so ensured that no tensile forces were induced within wall splice specimen during transportation. The pivot points used to rotate the wall splice specimen to the horizontal position are shown at the bottom of Figure 3.24 (b). The moving frame was then dismantled and removed and the wall splice specimen was then lifted using slings and the overhead crane to allow it to be maneuvered into the test frame. The slings were positioned to minimize the bending moment in the splice region and prevent cracking.

3.7.2 Wall Splice Specimen Loading Frame and Test Procedure

The wall splice specimens were positioned in the test frame on two 50 mm steel rollers that were each supported by a pivoting base. The upper section of the bases was hinged in the transverse direction to the fixed lower section to allow for rotation of the specimen about the transverse axis of the assembly. Figure 3.25 shows that the upper sections of the bases consisted of a channel section used to support the steel rollers. The rollers were located 2400 mm apart with one roller designed to simulate a pin support (Figure 3.25 (a)) while the other, a roller support (Figure 3.25 (b)). The rollers allowed for rotation of the wall splice specimen at the supports while the screw in the base of the pin support prevented lateral translation of the steel roller, simulating a pin support condition. The absence of the screw in the base of the roller support allowed for lateral translation of the steel roller. These support details allowed the wall splice specimens to be simply supported.

Figure 3.26 shows the frame used to test the wall splice specimens in this study. Two computer controlled hydraulic actuators, manufactured by Material Testing Systems, applied the load to the wall splice specimens. The hydraulic actuators included a 300 mm stroke, with a combined capacity of 1000 kN, and were simultaneously operated in deflection control at a rate of 0.5 mm per minute. Two hydraulic actuators were required to accommodate both the 2.5 block and 3.5 block wide wall splice specimens since the wider walls could not be placed directly under a

single actuator due to inadequate clearance between the columns of the test frame. As a result, the test frame geometry shown in Figure 3.26 was adopted, and included an upper steel spreader beam to transfer the load from the two hydraulic actuators to a single point load at the transverse midspan of each specimen. A roller was positioned below the upper spreader beam at the transverse midspan to eliminate the effects of any potential differences between the deflection rates of the two hydraulic actuators.

Figure 3.27 shows the four-point loading geometry applied to the wall splice specimen. The upper spreader beam, detailed in the previous paragraph, has been omitted from Figure 3.27 for simplicity. A simply supported steel I-section distributed the force equally 400 mm on either side of the midspan of the horizontally positioned wall splice specimen. The resulting four-point loading induced a constant moment region within the lap splice length to simplify the subsequent modeling.

Figure 3.26 and Figure 3.27 both show the end anchorage installed on the steel reinforcing bars that extended beyond both ends of the wall splice specimen. This was done to ensure that the bond failure would occur within the lap splice length and not at the end anchorage. A thin layer of grout was placed at the ends of the wall splice specimen prior to the installation of the end anchorage to fill any voids and so ensuring an even bearing surface. The anchorage itself consisted of 12 mm thick, 200 mm square steel plates which were held in place against the wall splice specimen using Type 2 ZAP Screwlock mechanical couplers supplied by Bar Splice Products Inc.

Figure 3.27 also shows the arrangement of the instrumentation of the wall splice specimens. A 250 kN load cell was placed at the midspan of the lower spreader beam to record the force exerted by the hydraulic actuators. The self-weight of the lower spreader beam and the pin and roller supports below the lower spreader beam (0.73 kN and 0.74 kN for the 2.5 and 3.5 block wide wall splice specimen tests, respectively) were added to the recorded data in the analysis phase to more accurately represent the total applied load exerted on the wall splice specimen.

Figure 3.27 shows the location of the six LVDTs, each with a 50 mm stroke, that were used to record the vertical deflection profile of the wall splice specimens. Two LVDTs were placed at the midspan of the wall splice specimen, one on either side. The data from these two LVDTs were

averaged during the analysis phase in an effort to obtain a more accurate midspan deflection values. Two LVDTs were additionally placed 200 mm from either side of the midspan of the wall splice specimen and the remaining two LVDTs were placed 600 mm from either side of the midspan of the wall splice specimen. Instrument readings were sampled at a frequency of 2 Hz by a computer controlled data acquisition system manufactured by National Instruments running LabView^{TM} software.

Crack patterns were recorded in the region extending 500 mm to either side of the midspan as well as the entire upper face of the wall splice specimen throughout testing. Failure was defined as when the applied load decreased to 40% of the maximum load that the wall splice specimen was able to withstand.

3.7.3 Companion Specimen Testing

Tests of the companion specimens were performed to evaluate the compressive strength of the mortar, grout, and the masonry assemblage as well as the stress versus strain properties of the reinforcing steel. The companion tests were completed in accordance to all the relevant CSA and ASTM standards. The results of the companion tests were used in the subsequent analysis and to confirm the minimum strength requirements of each material.

Mortar Cube Testing

Ninety-six and 57 mortar cubes were tested in Phases 1 and 2, respectively. The compressive tests were conducted in accordance to A3004-C2 (CSA, 2003) using the Instron 600DX Universal Testing Machine with a constant load rate of 10 kN per minute being applied to the specimen. Figure 3.28 (a) shows a mortar cube in the Universal Testing Machine. The smooth surfaces produced by the brass molds, used to cast the mortar cubes, were in contact with the load plates of the Universal Testing Machine to ensure the specimen was loaded uniformly. A computer controlled data acquisition system recorded the applied load and vertical deformation of the mortar cubes at a rate of 10 Hz.

Non-Absorbent Grout Cylinder Testing

The Instron 600DX Universal Testing Machine was also used to test the compressive strength of the grout cylinders that were cast in non-absorbent molds. The compressive tests were conducted

in accordance to CSA A179-04 (CSA, 2004b) with a constant load rate of 70 kN per minute being applied. Figure 3.28 (b) shows that both ends of the cylinder were capped with sulfur to ensure uniform load application. Ninety-six and 66 grout cylinders were tested in Phase 1 and 2, respectively. A computer controlled data acquisition recorded the applied load and vertical deformation of the grout cylinders at a rate of 10 Hz.

Absorbent Grout Prism Testing

The compressive strength tests for the absorbent grout prisms were conducted in accordance to ASTM C1019-12 (ASTM, 2012b) with a constant load rate of 70 kN per minute. Once again, the Instron 600DX Universal Testing Machine was used to test the compressive strength of the absorbent grout prisms. Figure 3.28 (c) shows that fibre board was placed at both ends of the prism to ensure uniform load application on the specimen. Thirty-two and twenty-two grout prisms were tested in Phase 1 and 2, respectively. A computer controlled data acquisition system recorded the applied load and vertical deformation of the grout prisms at a rate of 10 Hz.

Concrete Masonry Unit Testing

The compressive strength tests for the concrete masonry units were conducted in accordance to ASTM C140-12 (ASTM, 2012c). Six samples were randomly selected from each phase of construction when the concrete masonry units were delivered to the laboratory. The 200 tonne capacity Amsler beam bender, located in the Structures Laboratory, was used to test the concrete masonry units. A steel spreader beam and a 25 mm thick steel plate were placed above the concrete masonry units to ensure that the compressive force was uniformly applied to the entire specimen. Fibre board was also placed above and below the prism to ensure the force was applied uniformly along the entire contact area of the prism and surrounding test frame. A 1500 kN load cell was used to measure the applied load and a computerized data acquisition system controlled by LabView^{TM} software with a sampling frequency of 10 Hz was used to record the data.

Masonry Prism Testing

All prisms were tested in accordance to CSA S304.1-04 Annex D (CSA, 2004e). The masonry prisms were tested on the same day as the corresponding wall splice specimen in an effort accurately represent the compressive strength of the masonry assemblage at the time of testing.

Figure 3.29 (a) shows the loading geometry and instrumentation used for the prism test. Steel angles were affixed with epoxy along the center line of the prism as reference points for the LVDTs that were used to measure the vertical deflection. These angles were located 400 mm and 600 mm apart for the three and four block prisms, respectively. A 1500 kN load cell was located between the beam bender cross-head and the steel spreader beam above the masonry prism and was used to measure the applied load. The two LVDTs and the load cell were connected to a computerized data acquisition system controlled by LabView^{TM} software with a sampling frequency of 10 Hz.

Figure 3.29 (b) shows that the 200 tonne Amsler beam bender, located in the Structures Laboratory, was used for the masonry prism tests. The overhead crane was used to first lift the prism into position under the cross-head of the beam bender. Once in position, a steel spreader beam and a 25 mm thick steel plate were placed above the prism to ensure that the compressive force was uniformly applied to the entire prism. Fibre board was also placed directly above and below the prism to ensure the force was applied uniformly along the entire contact area of the prism and surrounding test frame. The LVDTs were installed in the locations shown in Figure 3.29 (b). A compressive force was then applied to the masonry prism until failure occurred. The data acquired from the masonry prism tests was ultimately used in the analysis of the wall splice specimens.

Reinforcing Steel Testing

A total of nine reinforcing bar specimens were tested from the reinforcing steel used in Phase 1 and eight were tested from the reinforcing steel used in Phase 2, as the material came from different heat batches. Specimens were loaded in tension using the Instron 600DX universal testing machine at a uniform rate of 0.315 mm/s in accordance with ASTM A370-12 (ASTM, 2012a). Figure 3.30 shows that an extensometer with a 200 mm gauge length was fabricated and attached to the bar sample to measure bar elongation. The applied load and corresponding strain in the bar samples was then recorded using LabView software at a sampling rate of 10Hz.

This chapter included a description of the specimen geometries as well as the rationale behind their design. The construction processes followed to build the specimens, as well as the testing equipment and procedures used to evaluate all the specimens in this research program were also

described. The next chapter presents the results of this investigation. The results of the companion testing are presented and discussed first followed by the visual observations noted during wall splice specimen testing. Next, the load-deflection behaviour of each set of wall splice specimens is discussed. The modelling of the wall splice specimens is then presented followed by a review of the analyzed data. The maximum tensile resistance of each wall splice specimen is presented and compared to the two control lap splice detail. The practical implications of the results are then discussed.

Table 3.1: Specimen Construction Schedule

Phase	Specimen Width [Blocks]	Specimen ID	Specimen Configuration	Splice Length [mm]
1	2.5	CLS	Contact lap splice (Control).	200
	2.5	NCLS	Non-contact lap splice (Control).	200
	2.5	1KO	A single knock-out web course allowing for uninterrupted grout placement between cells along the splice length.	200
	2.5	3KO	placement between cells within, above, and below the splice length.	200
	3.5	GCC	Grouted confinement cells.	200
2	2.5	SBAR	Three knock-out web courses allowing for uninterrupted grout placement between cells within, above, and below the splice length with an s-shape splice bar included.	200
	3.5	C-SBAR	Three knock-out web courses allowing for uninterrupted grout placement between cells along, above, and below the splice length with an s-shape splice bar included. The outside and centre un-reinforced cells are also fully grouted.	200
	3.5	CT-SBAR	Three knock-out web courses allowing for uninterrupted grout placement between cells within, above, and below the splice length. S-shape splice bar and transverse reinforcement are also installed at splice level. All cells are fully grouted.	200

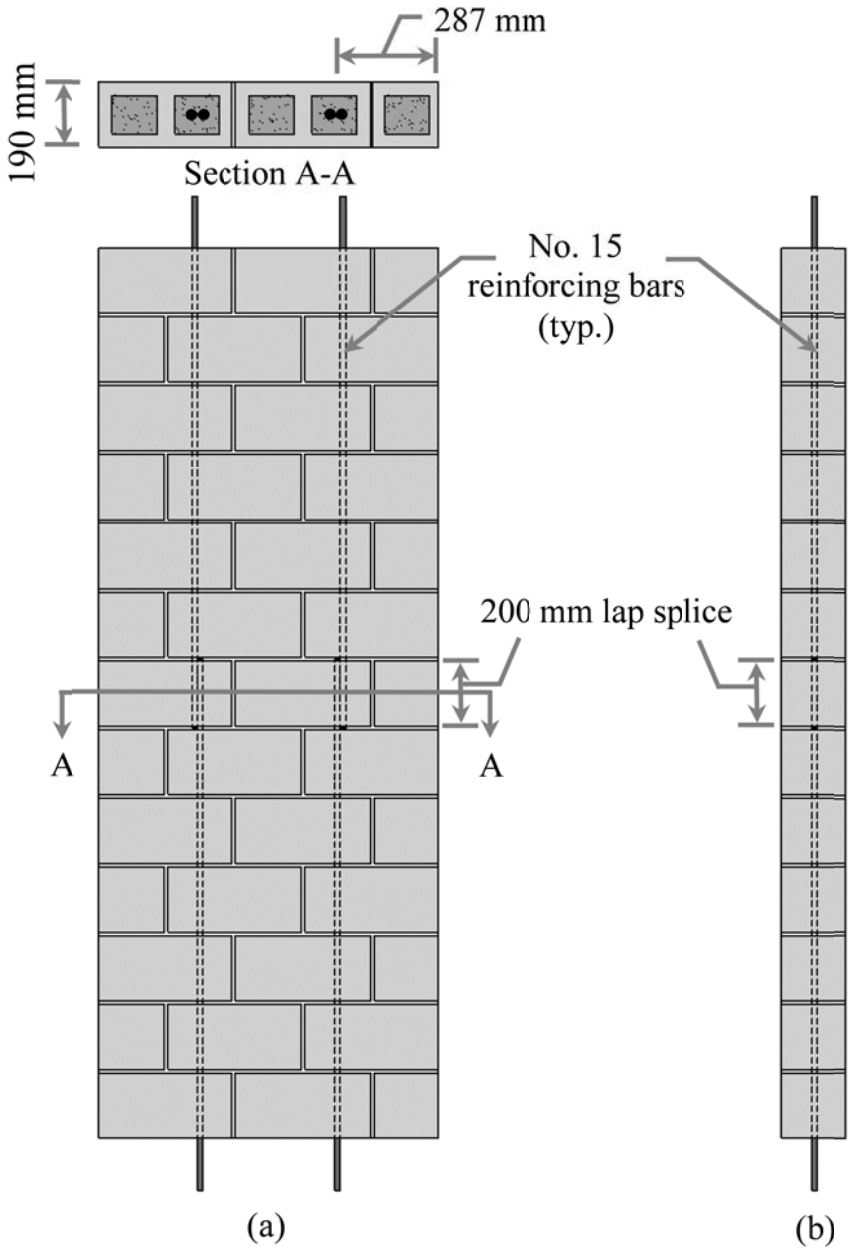

Figure 3.1: Control Wall Splice Specimen with Contact Lap Splices (CLS): (a) Elevation Including a Section at Splice Level, and (b) Side Profile.

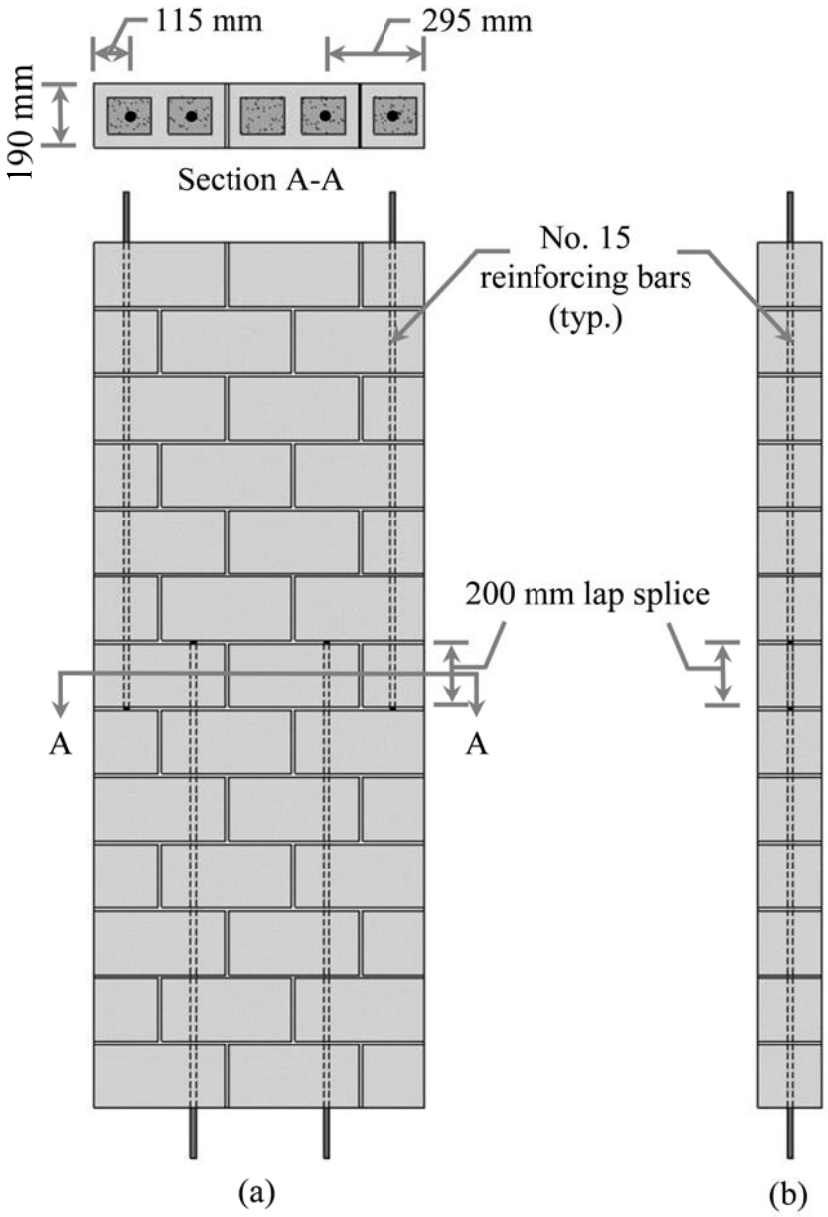

Figure 3.2: Control Wall Splice Specimens with Non-Contact Lap Splices (NCLS): (a) Elevation Including a Section at Splice Level, and (b) Side Profile.

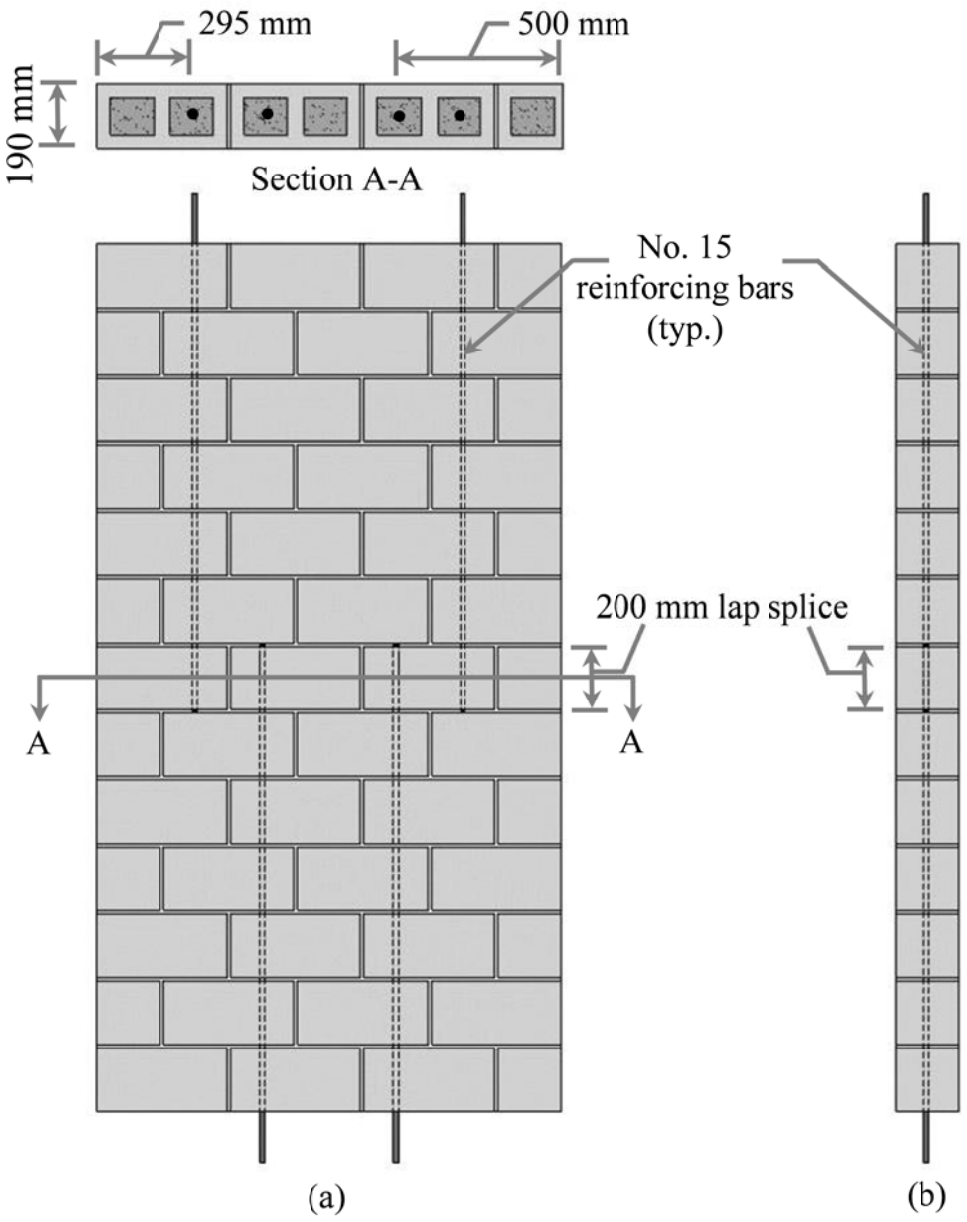

Figure 3.3: Remedial Wall Splice Specimen with Grouted Confinement Cells (GCC): (a) Elevation Including a Section at Splice Level, and (b) Side Profile.

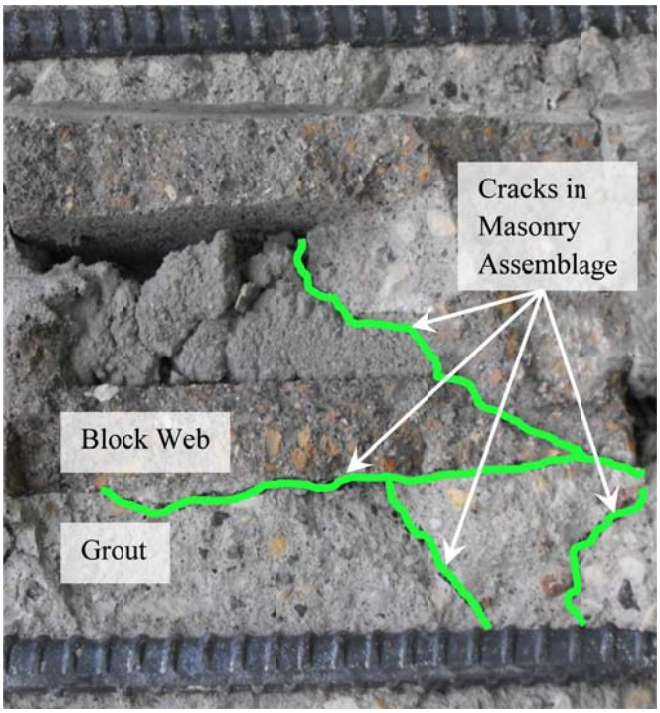

Figure 3.4: Crack Pattern in Wall Splice Specimens Featuring Non-Contact Lap Splices (Ahmed & Feldman, 2012)

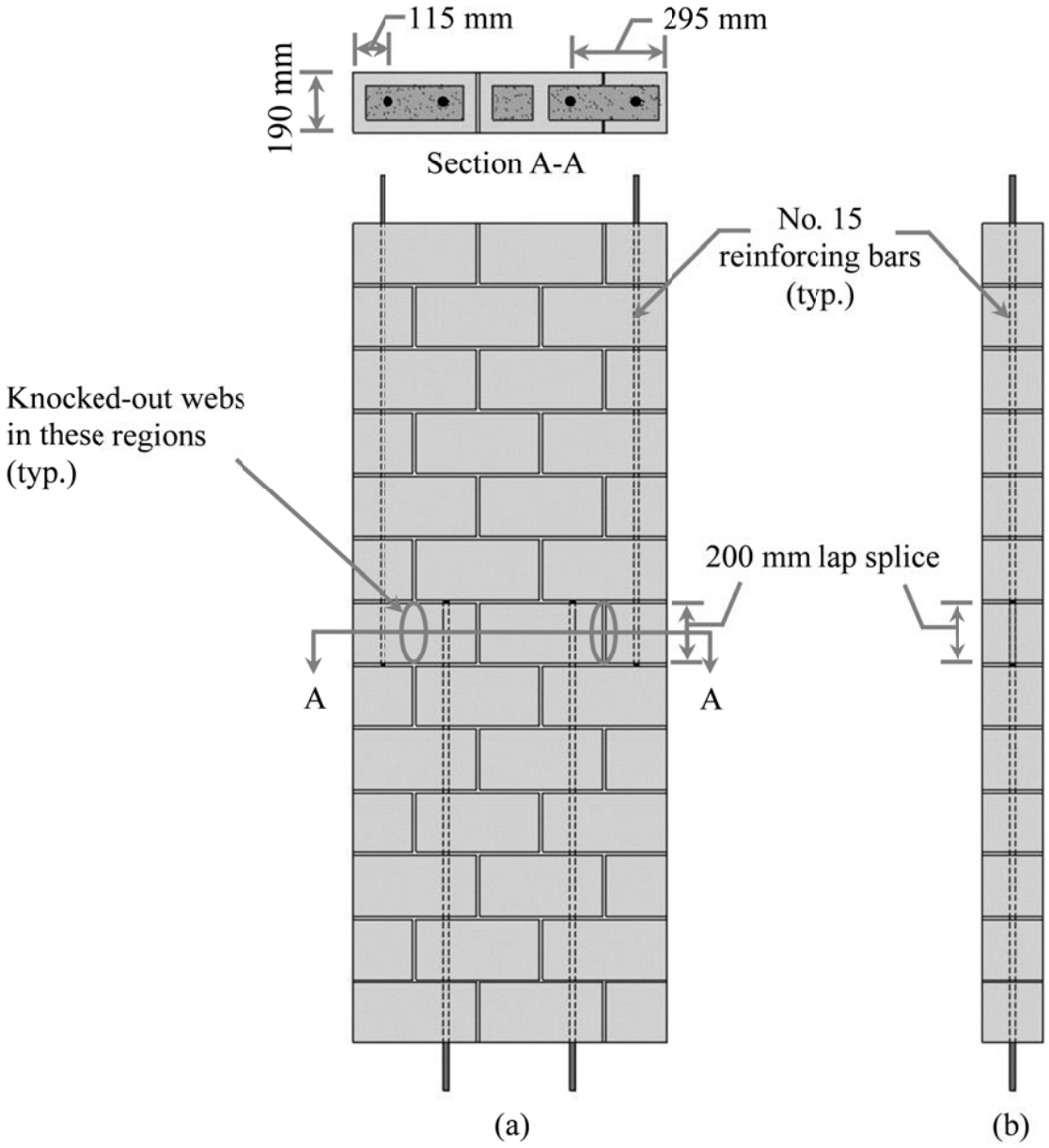

Figure 3.5: Remediated Wall Splice Specimen Featuring a Single Course of Knock-Out Webs (1KO)：(a) Elevation Including a Section at Splice Level, and (b) Side Profile.

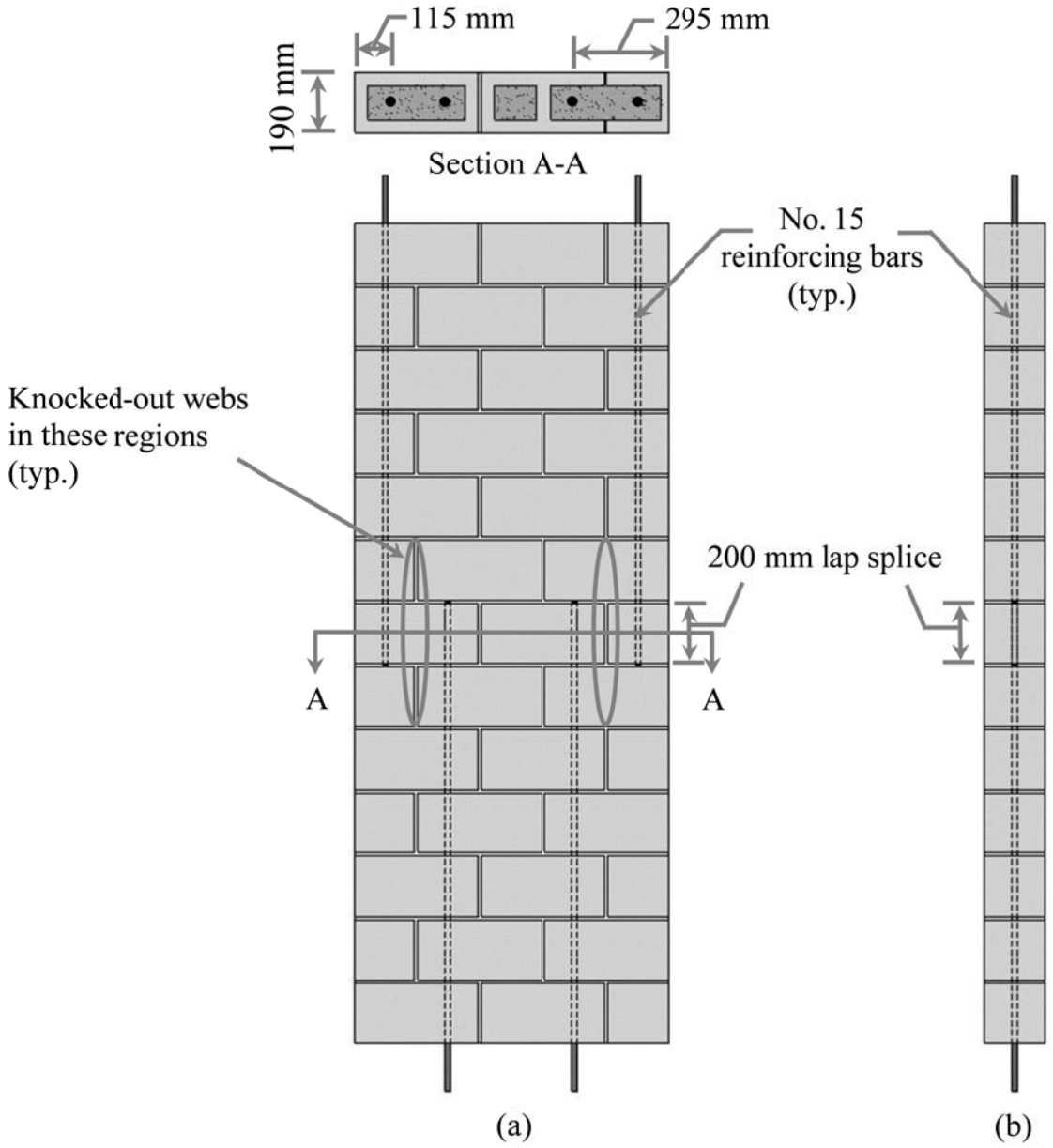

Figure 3.6: Remediated Wall Splice Specimen with Three Courses of Knock-Out Webs (3KO)：(a) Elevation Including a Section at Splice Level, and (b) Side Profile.

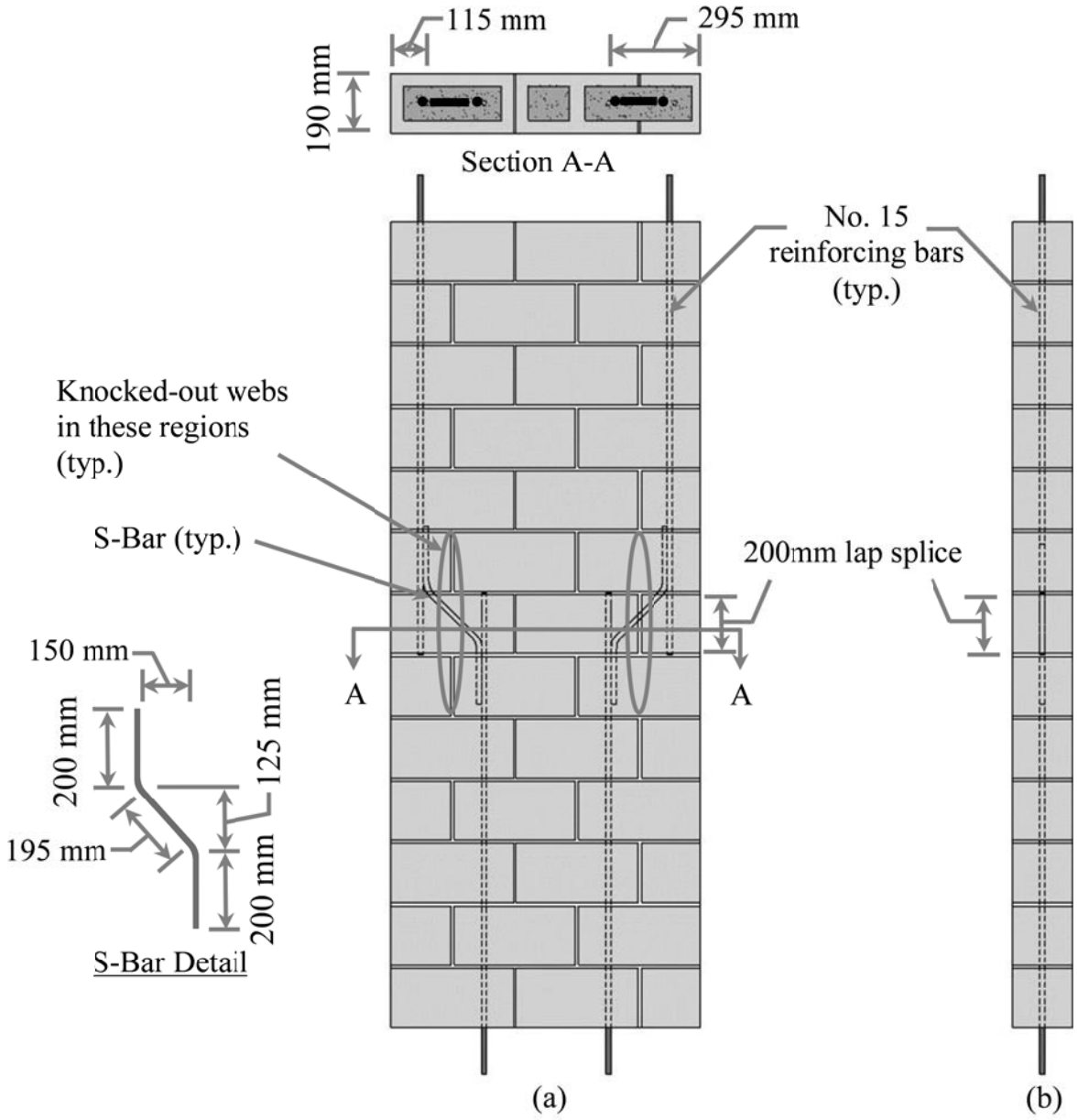

Figure 3.7: Remedial Wall Splice Specimen with S-Shaped Splice Reinforcement (SBAR): (a) Elevation Including a Section at Splice Level, and (b) Side Profile.

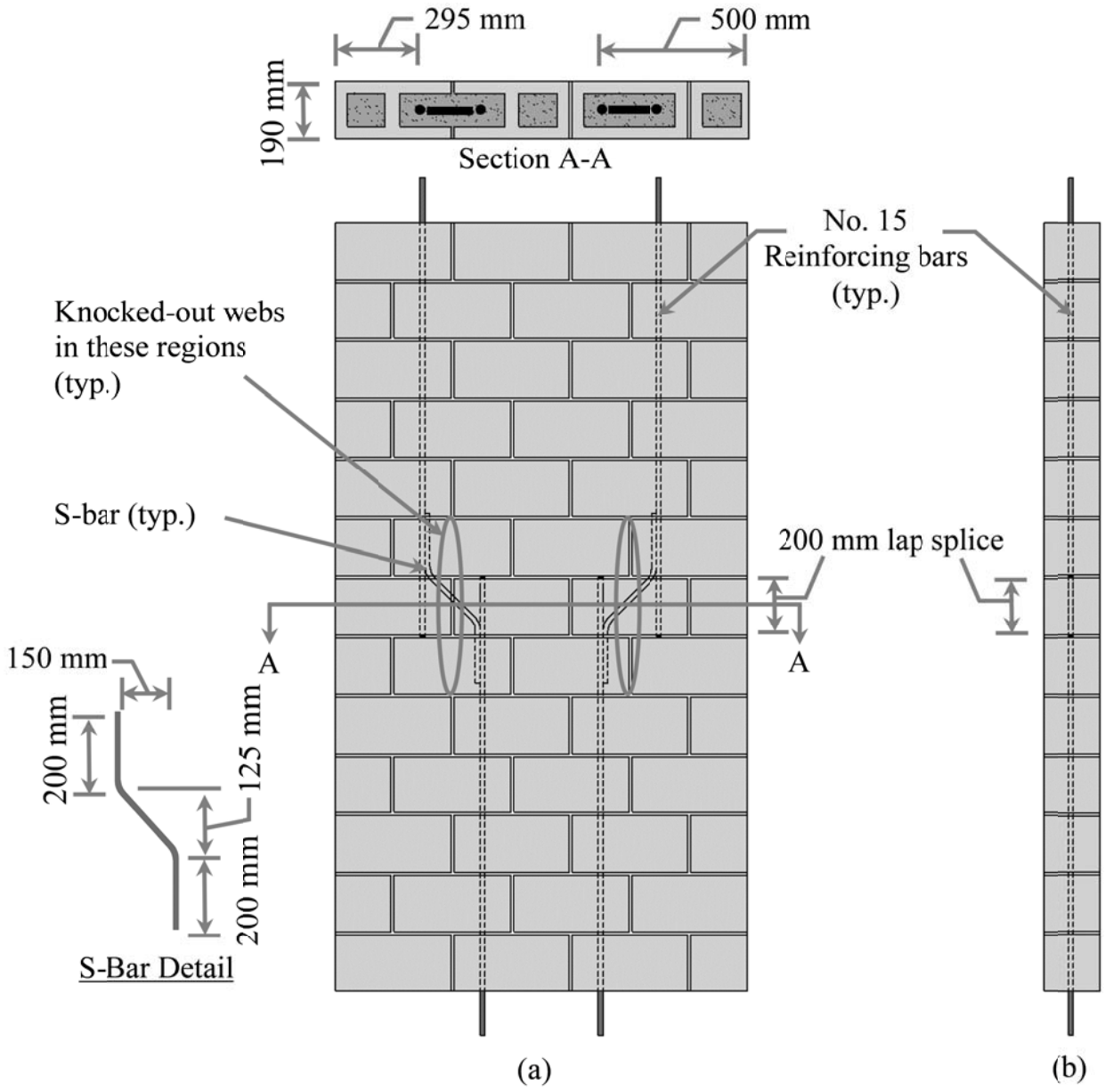

Figure 3.8: Remedial Wall Splice Specimen with S-Shaped Splice Reinforcement and Grouted Confinement Cells (C-SBAR): (a) Elevation Including a Section at Splice Level, and (b) Side Profile.

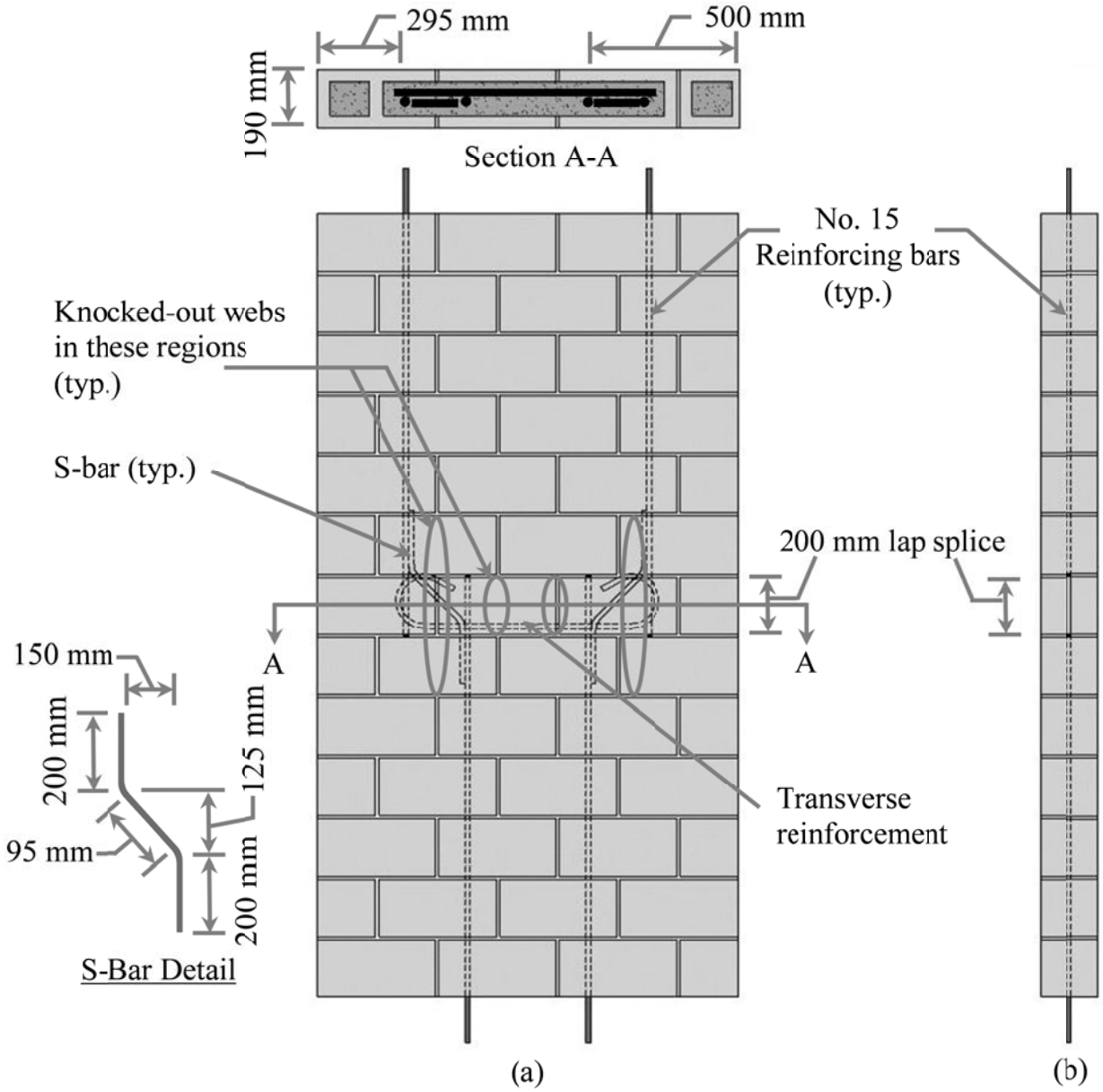

Figure 3.9: Remedial Wall Splice Specimen with S-Shaped and Transverse Splice Reinforcement, and Grouted Confinement Cells (CT-SBAR): (a) Elevation Including a Section at Splice Level, and (b) Side Profile.

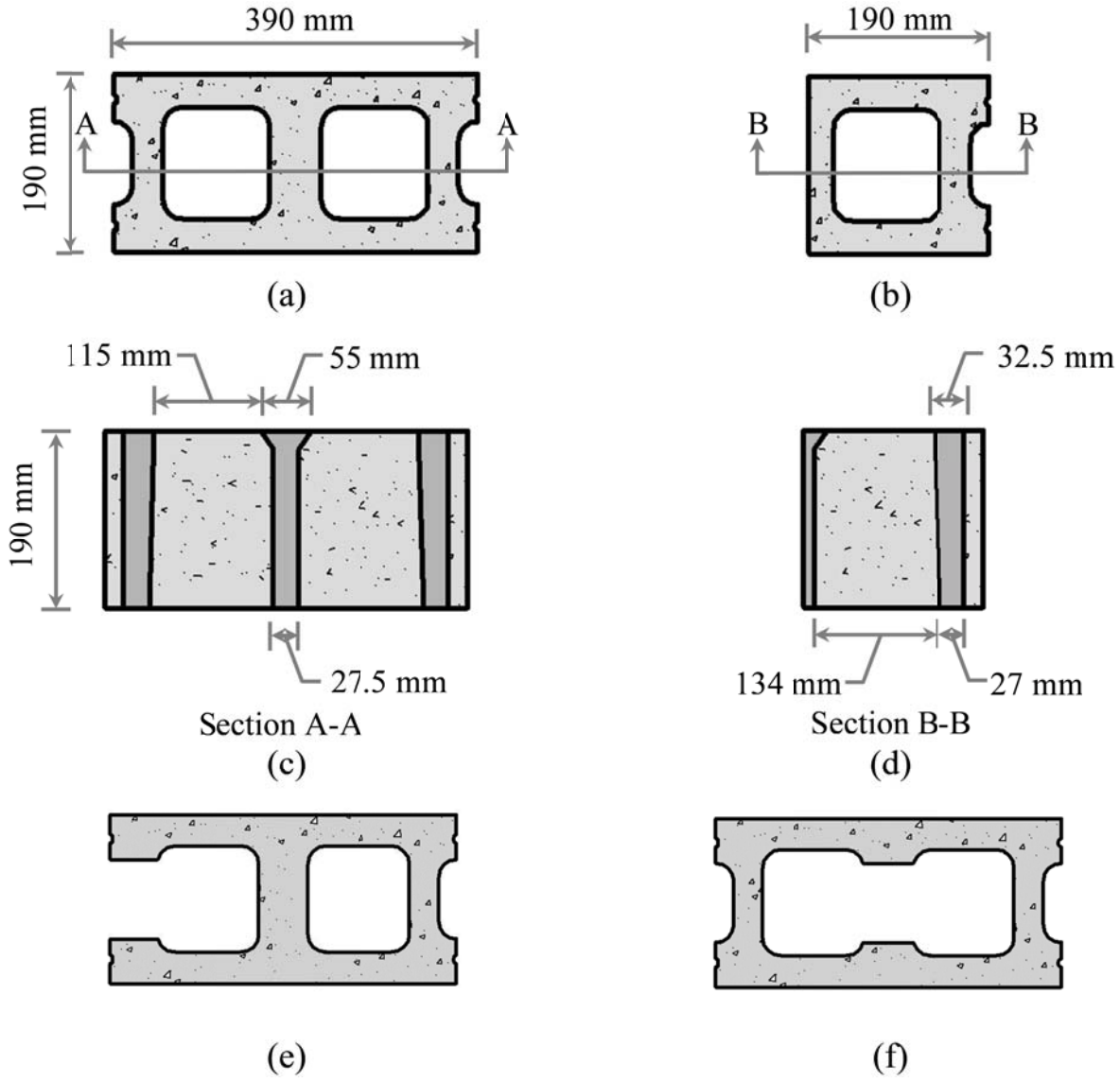

Figure 3.10: Concrete Masonry Units: (a) Standard Frogged End Block, (b) Half Block, (c) Section of Standard Frogged End Block, (d) Section of a Half Block, (e) Block with Exterior Knock-Out Web (A-Block), and (f) Block with Interior Knock-Out Web (O-Block).

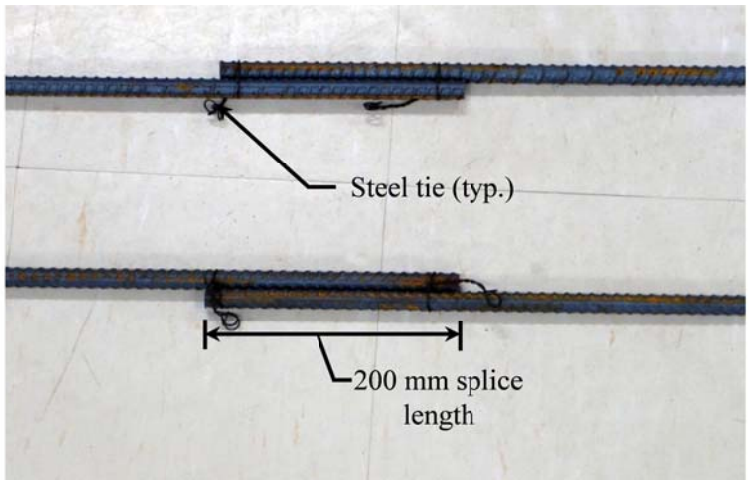

Figure 3.11: Tied Reinforcing Bars Used in Contact Lap Splice Specimens (CLS).

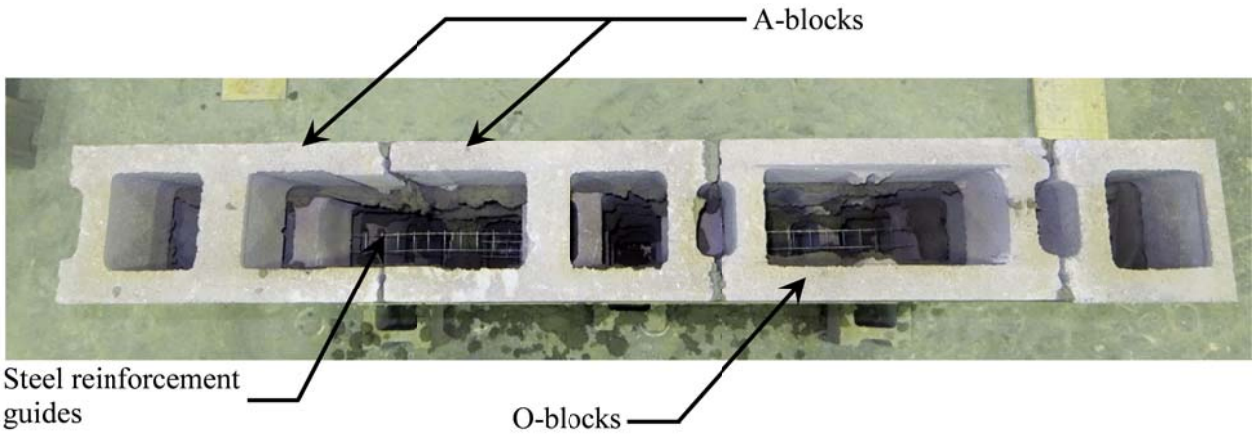

Figure 3.12: Courses of Modified Blocks at Splice Level in Wall Specimens Featuring Knock-out Webs and S-Bars.

(a)

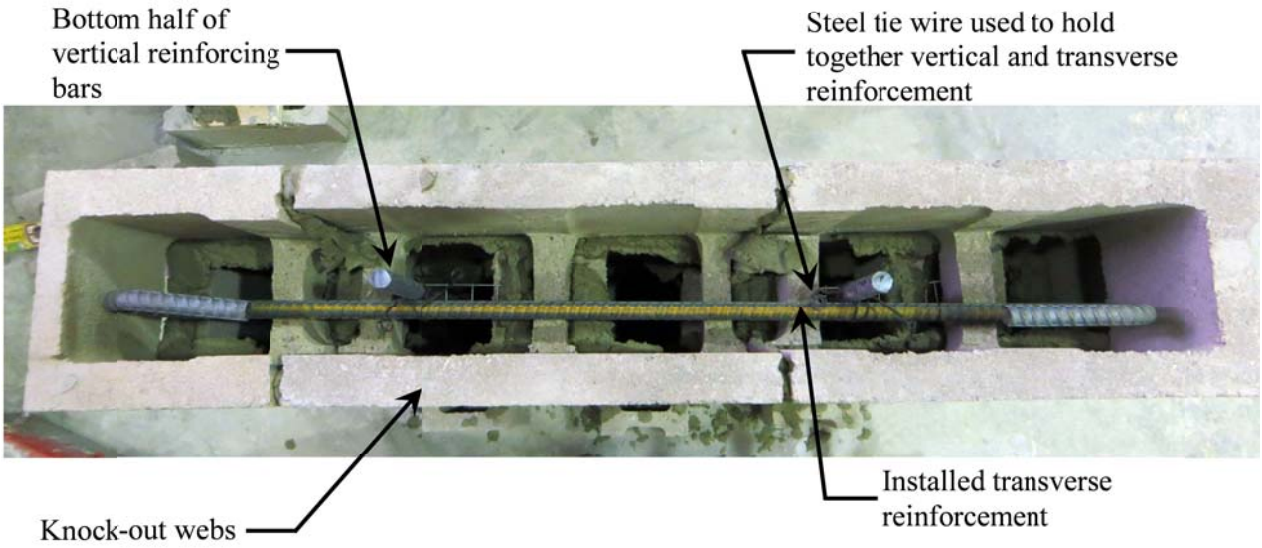

(b)

Figure 3.13: Wall Splice Specimen Featuring Horizontal Transverse Reinforcement: (a) Transverse Reinforcing Bar and (b) Installed Knock-out Webs and Horizontal Transverse Reinforcement at Splice Level.

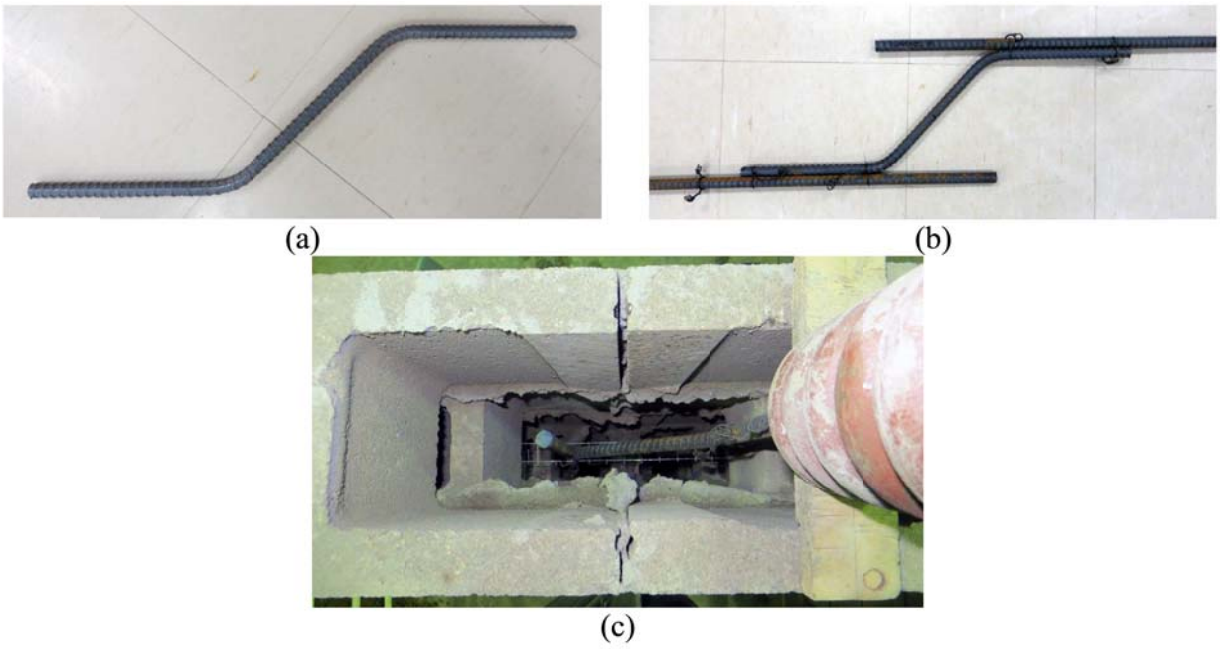

Figure 3.14: Wall Splice Specimens Featuring S-Shaped Splice Reinforcement: (a) S-Shaped Reinforcing Bar, (b) Installed S-Bar Prior to Grouting, and (c) S-Shaped Reinforcing Bar Tied Together With Longitudinal Reinforcing Bars.

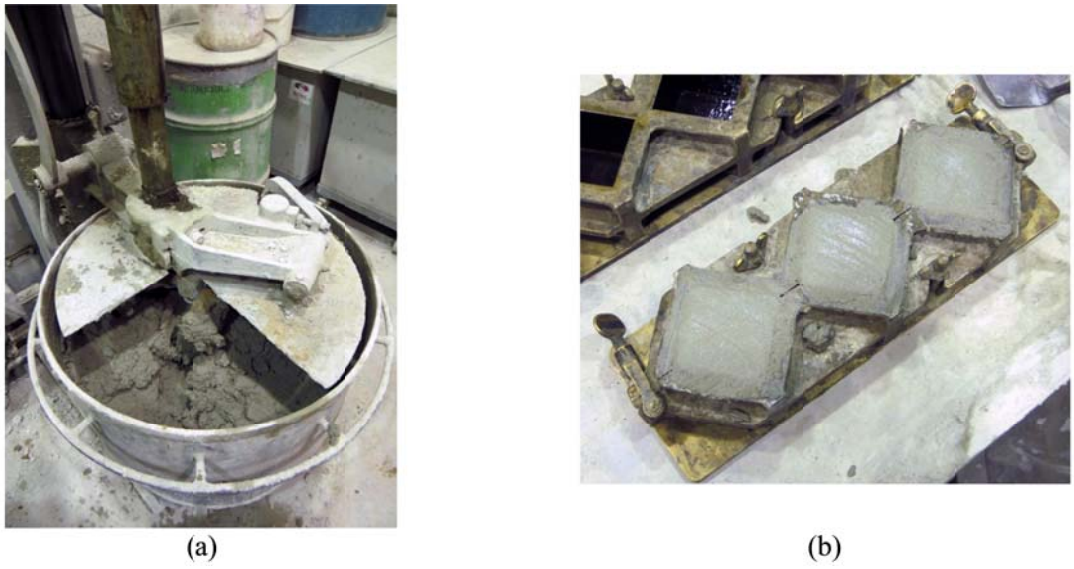

Figure 3.15: Mortar Preparation: (a) Mixing Mortar with Mechanical Mixer, and (b) Casting Mortar Cubes.

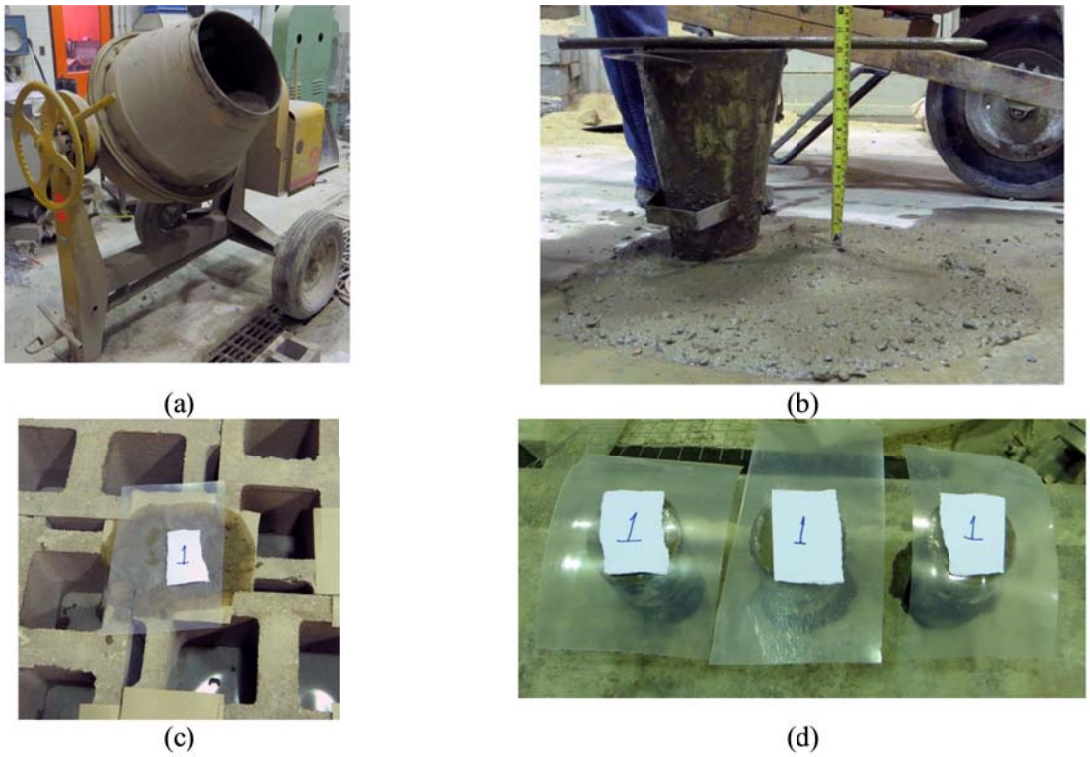

Figure 3.16: Grout Preparation: (a) Mixing Grout with Mechanical Mixer, (b) Slump Test, (c) Cast Absorbent Grout Prism in Previously Prepared Mould, and (d) Cast Non-Absorbent Grout Cylinders.

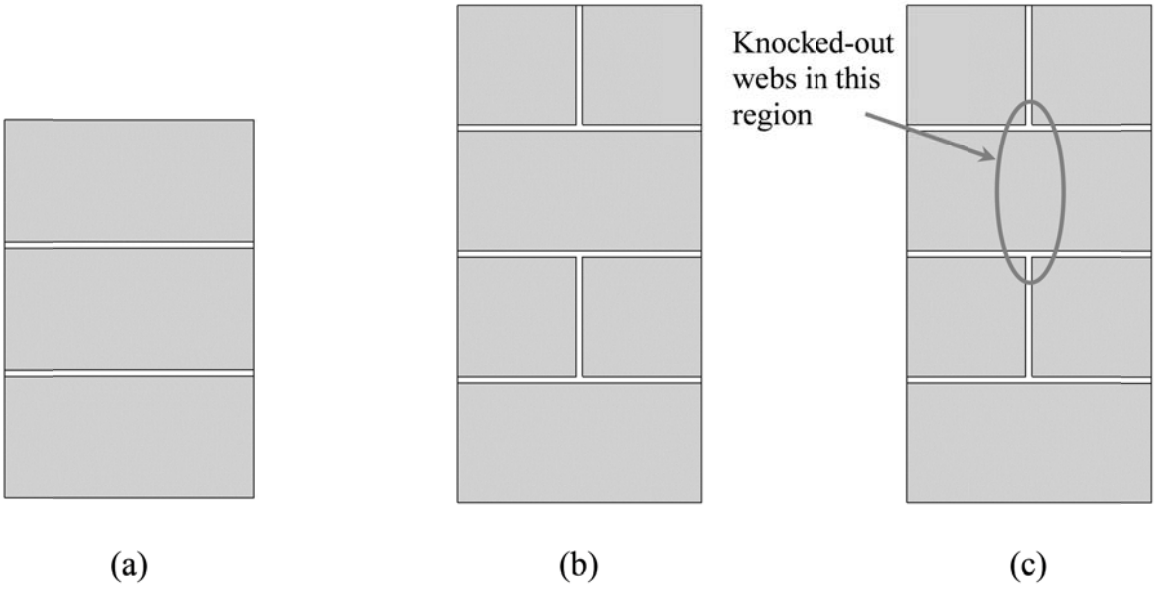

Figure 3.17: Plans of Masonry Prisms: (a) 3-Course High Stack Bond, (b) 4-Course High Running Bond, and (c) 4-Course High Running Bond Featuring a Knock-out Web.

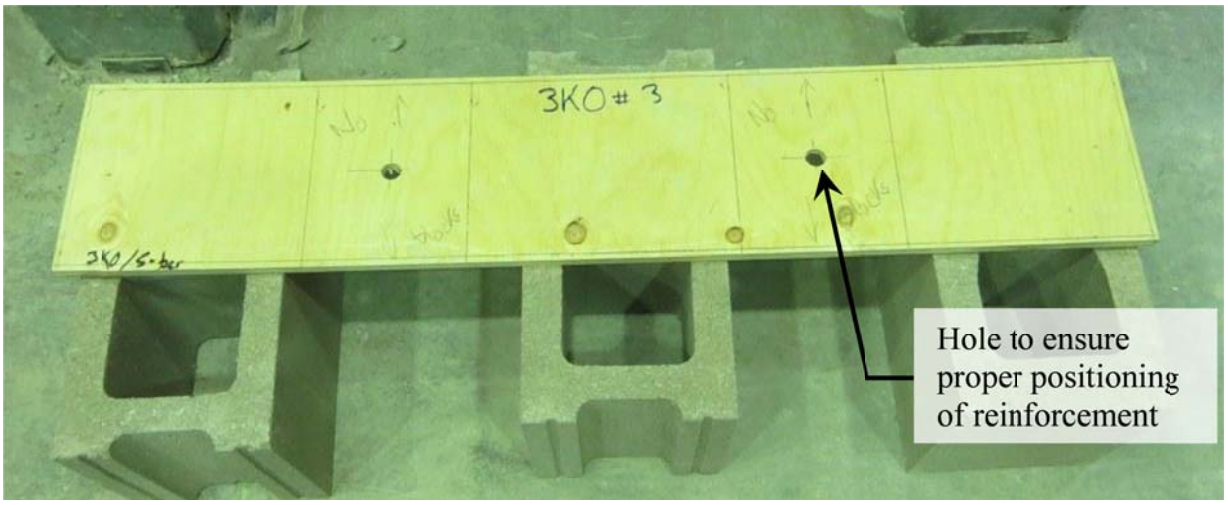

Figure 3.18: Base Used to Construct Wall Splice Specimens.

(a) (b)

Figure 3.19: (a) Welded Wire Mesh Guides for Placement of Longitudinal Reinforcement, and (b) Wooden Template and Weight Used to Align Top Reinforcement Bars Prior to Grouting.

(a) (b)

Figure 3.20: Grouting the First Lift of the Wall Splice Specimens: (a) Grout Placement, and (b) Consolidation Using Mechanical Vibration.

Figure 3.21: Newly Completed Wall Splice Specimen.

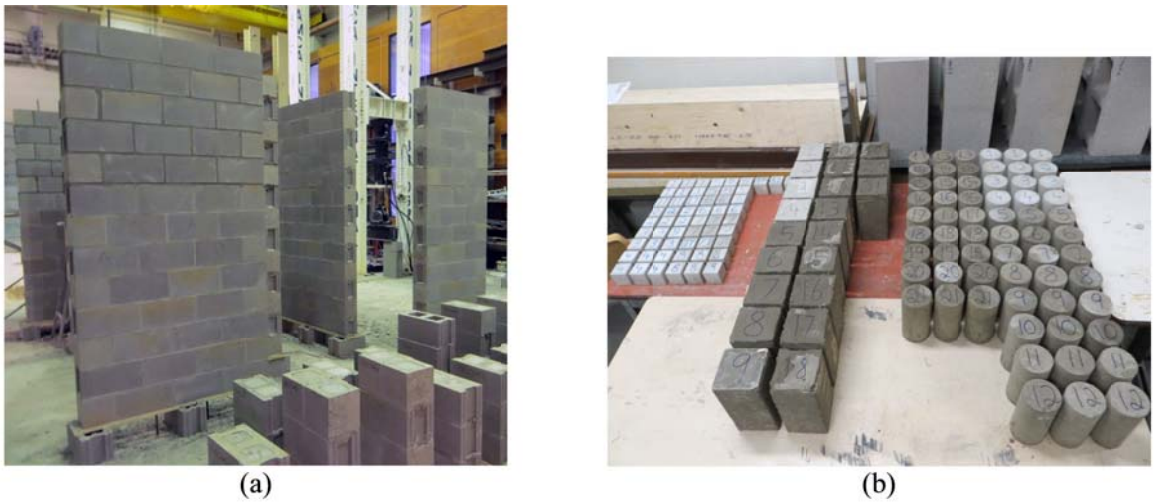

Figure 3.22: Specimens Curing in the Structures Laboratory Following Construction: (a) Wall Splice Specimens, and (b) Companion Specimens.

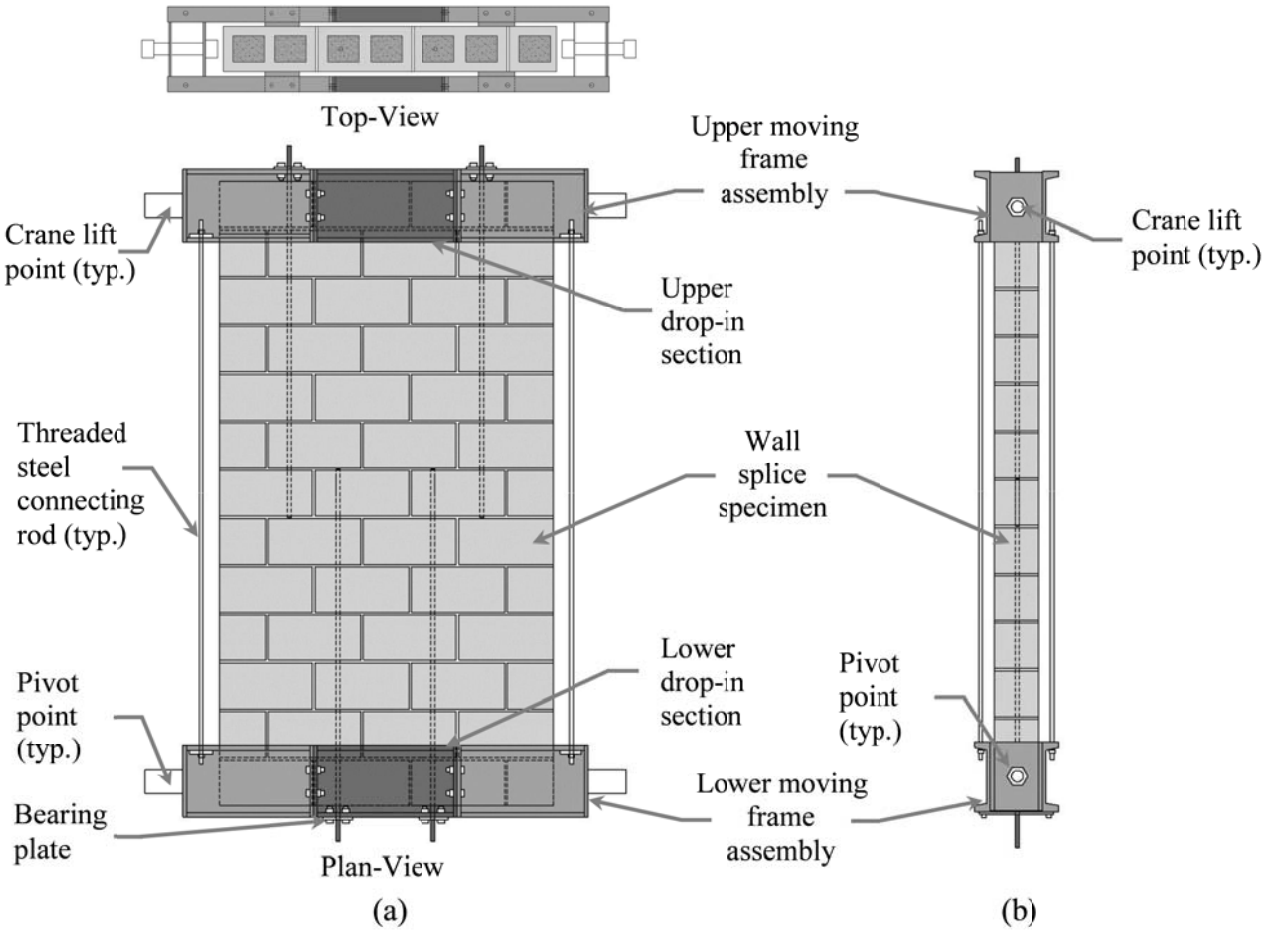

Figure 3.23: Moving Frame: (a) Plan and Top View, and (b) Side View.

(a) (b)

Figure 3.24: Wall Specimen Transport: (a) Lifting the Wall Specimen Using Overhead Crane and Moving Frame, and (b) Rotating the Wall Specimen to the Horizontal Position.

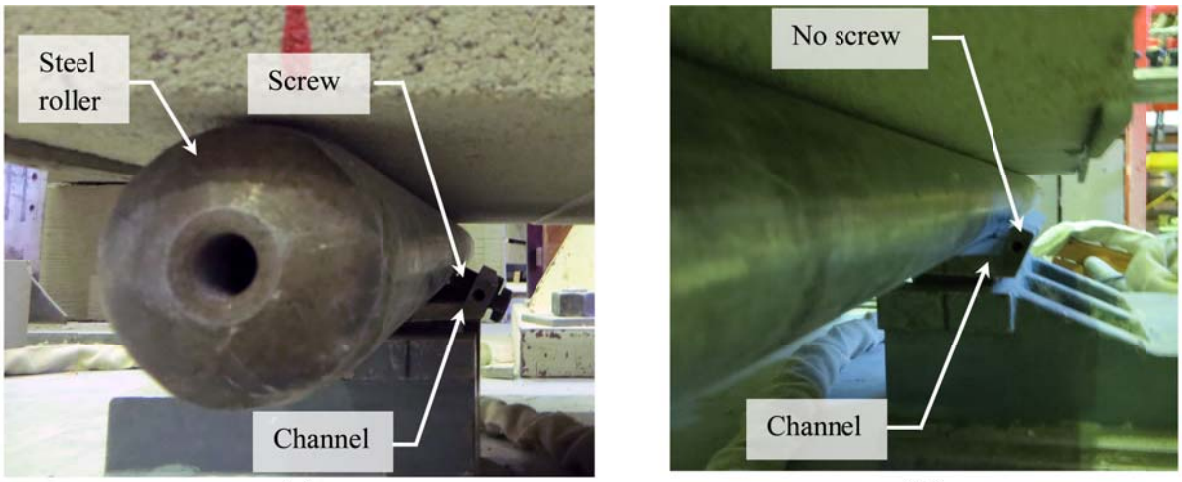

(a) (b)

Figure 3.25: Support Conditions: (a) Pin, and (b) Roller.

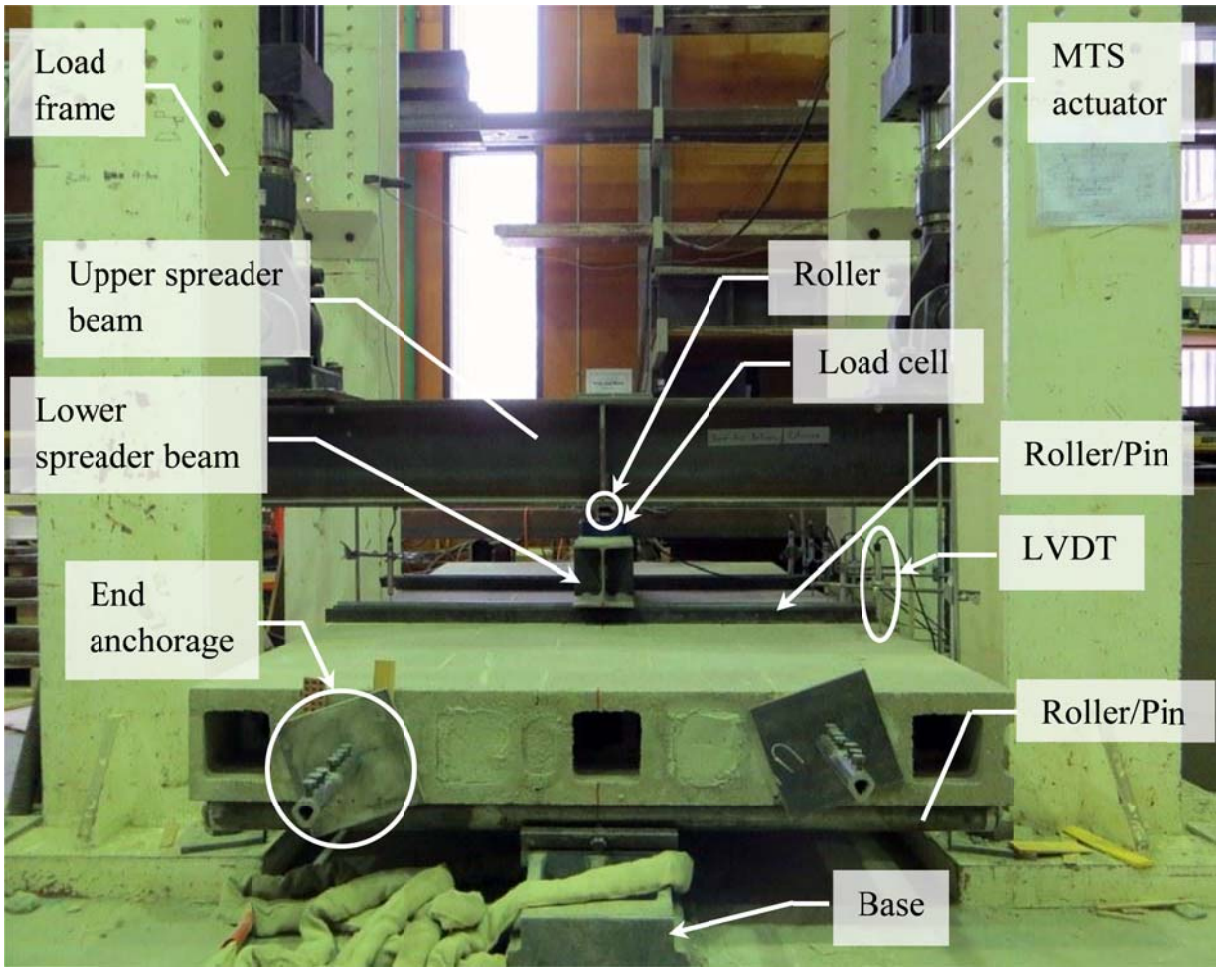

Figure 3.26: Test Frame.

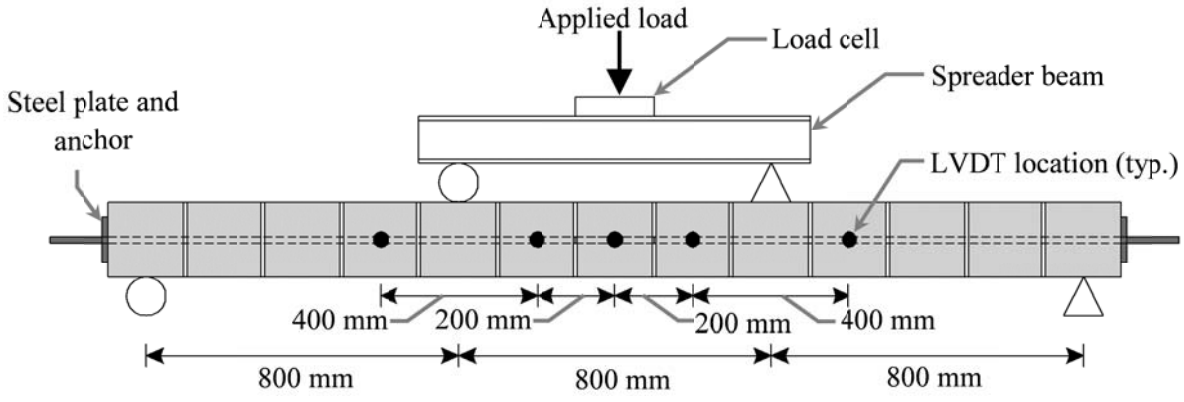

Figure 3.27: Loading Geometry and Instrumentation of Wall Splice Specimen.

Figure 3.28: Companion Tests: (a) Mortar Cube, (b) Non-Absorbent Grout Cylinder, and (c) Absorbent Grout Prism.

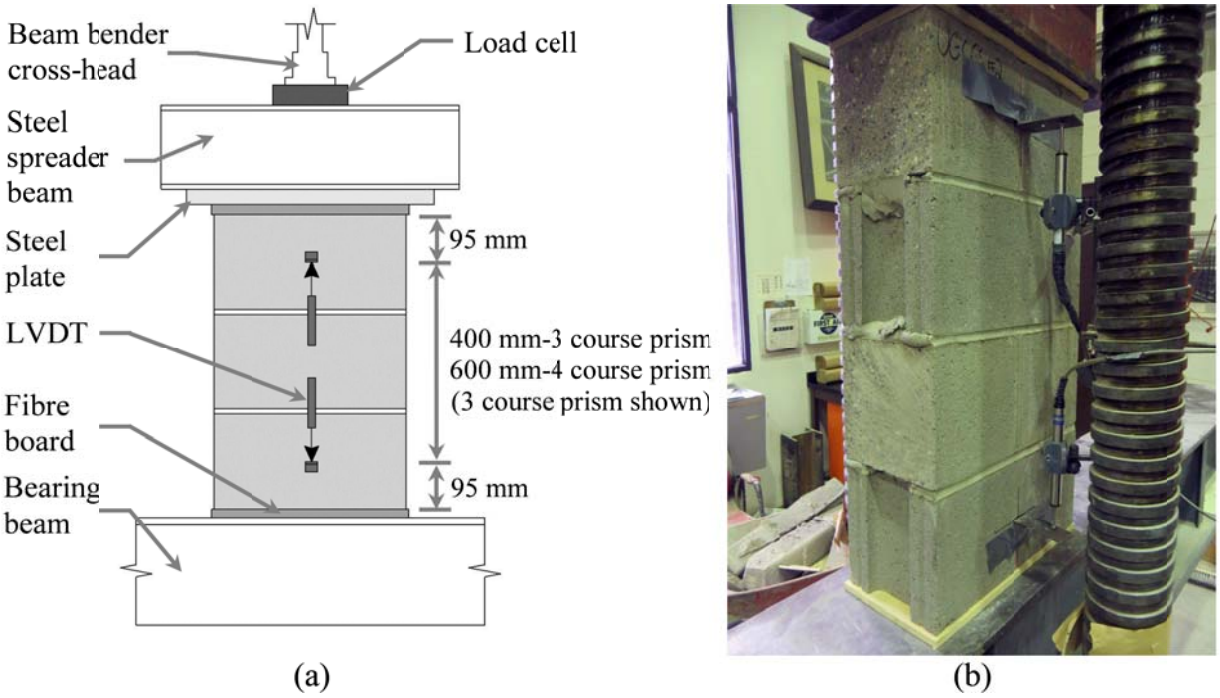

Figure 3.29: Prism Test Geometry: (a) Instrumentation, and (b) Masonry Prism Test.

Figure 3.30: Extensometer Used to Measure Displacement of the Bar Sample of an 200 mm Gauge Length.

CHAPTER 4: EXPERIMENTAL RESULTS AND ANALYSIS

This chapter discusses the experimental results for the 24 wall splice specimens and the associated companion specimens tested in Phases 1 and 2 of this research program. Table 4.1 shows the construction and test schedules for the two phases along with the number of test specimens included in each phase. Visual observations of the external crack patterns are presented and compared for the different control specimens and rehabilitative techniques evaluated. Representative wall splice specimens were selected and cut open to reveal the internal distress within the lap splice region. The load versus displacement behaviour of the wall splice specimens is also presented along with the moment-curvature data that was used in the analytical model.

A finite difference model used to determine the theoretical moment-curvature and deflection of the wall splice specimens and the tensile capacity of the various lap splice details is also described. The results of the model were used to compare the structural performance of the six remedial measures to the two control lap splice designs of the same lap length.

The results of the 12 wall splice specimens and the associated companion specimens tested in Phase 1a are presented in Appendix 4A as the lap splices in the wall splice specimens in this phase were unintentionally constructed with a different splice length. These specimens were constructed in addition to the 24 wall splice specimens discussed above. The difference in the lap splice lengths did not allow for the results from the Phase 1a wall splice specimens to be directly compared to the specimens in Phases 1 and 2.

4.1 Companion Specimen Test Results

The following subsections describe the results of the companion specimens tested in this research program. Table 4.2 presents the mean maximum stress for each specimen type and the coefficient of variation while Table 4.3 shows the results summary of the steel reinforcement tensile testing.

4.1.1 Mortar Cubes

The mortar cube construction and testing procedures are detailed in Sections 3.6.2 and 3.7.3, respectively. A review of the logged data confirmed that the Instron 600 DX universal testing machine accurately controlled the load rate to within 1% of the value stated in Section 3.7.3.

Three statistical outliers, two in the first construction phase and one in the second, were identified at the 95% confidence level using the procedure detailed in ASTM E178-08 (ASTM, 2008). The possibility of poor casting resulting in the formation of voids at the corners of the mortar cubes may have affected the performance of those mortar cubes as the voids would cause stress concentrations which would result in premature failure of the specimen. The results from those three mortar cube tests were not included in the calculation of the mean maximum stress and the coefficient of variation of the two respective phases.

Table 4.2 shows the mean maximum strength and the coefficient of variation of the mortar cubes tested in the two respective phases. The mean maximum strength of the mortar cubes tested in Phases 1 and 2 was 17.0 MPa and 16.7 MPa, respectively. Both of these values exceeded the minimum compressive strength for mortar cubes of 12.5 MPa as specified in CSA S304.1-04 (CSA, 2004e). The difference between the mean maximum compressive strengths of the mortar cubes between Phases 1 and 2 is not statistically significant at the 95% confidence interval. The results from the individual mortar cube tests are shown in Appendix 4B.

4.1.2 Grout Tests

Both non-absorptive grout cylinders and absorptive grout prisms were tested to determine the compressive strength of the grout used in the wall splice specimens. The construction and testing procedures of both specimen types are detailed in Sections 3.6.3 and 3.7.3, respectively. A review of the logged data confirms that the Instron 600 DX universal testing machine accurately controlled the load to within 1% of the value rate stated in Section 3.7.3 for both the non-absorptive grout cylinder and absorptive grout prism tests.

Six non-absorptive grout cylinders were identified as statistical outliers at the 95% confidence level using the procedure detailed in ASTM E178-08 (ASTM, 2008). Four of these cylinders were from the first construction phase, while the remaining two were from the second. These outliers were possibly the result of poor capping of the cylinders which may have resulted in non-level surfaces causing bending. This would have resulted in an uneven stress distribution within the specimen and also contributed to the premature failure in some of the specimens. The results from these six non-absorptive grout cylinder tests were not included in the calculation of the mean maximum stress and the coefficient of variation as reported for the two construction phases.

Table 4.2 shows the mean maximum strength and the coefficient of variation of the non-absorptive grout cylinders tested in the two respective phases. The detailed results from the individual grout cylinder tests are shown in Appendix 4B. The mean maximum strength of the non-absorptive grout cylinders tested in Phases 1 and 2 was 14.1 MPa and 12.5 MPa, respectively. Both of these values met or exceeded the minimum compressive strength for non-absorptive grout cylinders of 12.5 MPa as specified in CSA S304.1-04 (CSA, 2004e).The non-absorptive grout cylinders tested in Phase 1 had a 13.6% higher mean maximum compressive strength as compared to the cylinders tested in Phase 2. This represents a statistically significant difference in the mean maximum compressive strength between the Phase 1 and 2 non-absorptive grout cylinders at the 95% confidence interval. Previous research by Hamid and Drysdale (2005) concluded that a 50% increase in the grout strength only resulted in a 5% increase in the compressive strength of the masonry assemblage. It can therefore be assumed that the splice resistance of the wall splice specimens was not sensitive to the 13.6% difference in the mean grout strengths between Phase 1 and 2.

Absorptive grout prisms were also tested in an effort to more accurately model the compressive strength of the grout used to construct the wall splice specimens. The casting of the grout prisms, detailed in Section 3.6.3, results in the ability to model the effect of the reduction in the water-to-cement ratio in the grout mix due to the absorption by the concrete blocks (Drysdale and Hamid, 2005).

Table 4.2 shows the mean maximum compressive strength and coefficient of variation of the absorptive grout prisms tested in Phases 1 and 2, while the detailed results from the individual grout prism tests are shown in Appendix 4B. The mean maximum strength of the absorptive grout prisms tested in Phases 1 and 2 was 14.1 MPa and 15.5 MPa, respectively. Both of these values exceeded the minimum compressive strength for absorptive grout prisms of 12.5 MPa as specified in CSA S304.1-04 (CSA, 2004e).Two statistical outliers, one in each phase, were identified using the procedure detailed in ASTM E178-08 (ASTM, 2008) at the 95% confidence interval. The mean maximum compressive strength of the Phase 2 absorptive grout prisms was 9.0% higher than those tested in Phase 1. This represents a statistically significant difference in the mean maximum compressive strength between the Phase 1 and 2 non-absorptive grout cylinders at the 95% confidence interval.

Previous research by Hamid and Drysdale (2005) concluded that a 50% increase in the grout strength only resulted in a 5% increase in the compressive strength of the masonry assemblage. It can therefore be assumed that the splice resistance of the wall splice specimens between Phases 1 and 2 was not sensitive to the 13.6% and 9.0% difference in the mean grout strength represented by the non-absorptive grout cylinders and the absorptive grout prisms, respectively.

4.1.3 Concrete Blocks

Six concrete blocks were selected at random during each construction phase and set aside for compression testing. Table 4.2 shows the mean ultimate compressive strength and coefficient of variation for the concrete blocks tested in Phases 1 and 2. The detailed results from each block test are shown in Appendix 4B. All the blocks tested achieved, as a minimum, the nominal compressive strength of 15 MPa and there were no outliers identified using the procedure detailed in ASTM E178 (ASTM, 2008) at the 95% confidence level. The difference in the mean compressive strength of the blocks between Phases 1 and 2 was not found to be statistically significant at the 95% confidence level.

4.1.4 Masonry Prisms

Three different masonry prism geometries were tested in this investigation. The geometry and construction procedure of the prisms is discussed in Section 3.6.4, while the testing procedure is detailed in Section 3.7.3.

A review of the resulting test data confirmed that the load rate conformed to the specifications included in CSA S304.1-04 Annex D (CSA, 2004e).The results from the three block-high, stack bond prisms are discussed in this chapter as only their results were used acquire the material properties of their representative wall splice specimens. The results from the two four block-high prism designs could not be used for this purpose as they were not constructed for every wall splice specimen. However, a comparative analysis between the three different masonry prism designs is located in Appendix 4C.

Table 4.2 shows the mean maximum compressive strength and coefficient of variation for the three block-high, stack bond masonry prisms. The results from each individual prism are presented in Appendix 4C.

A total of 24 three block-high stack bond prisms were tested in Phases 1 and 2. The compressive strength of each prism was comparable to the theoretical values calculated using Table 4 in CSA S304.1-04 (CSA, 2004e). No statistical outliers were identified at the 95% confidence level using the procedure detailed in ASTM E178-08 (ASTM, 2008). It was also established that the difference between the mean maximum strengths of the Phase 1 and 2 three block-high, stack bond prisms was not statistically significant at the 95% confidence level.

Figure 4.1 shows a representative experimental stress versus strain curve for a three block-high, stack bond masonry prism plotted against the theoretical curve. A Kent-Park (1971) curve was used to develop the theoretical stress versus strain relationship for the masonry prisms using modulus of elasticity, $E'_{m,}$ and compressive strength, f'_{m}, values acquired from the test data. A parabolic rising curve was used to represent the stress versus strain relationship of the masonry prism up to the maximum stress followed by a linearly decreasing segment. The stress versus strain curves for individual masonry prisms are presented in Appendix 4C.

The two curves show a good agreement up to the maximum compressive stress. At this point, the prisms tested in the laboratory failed suddenly and so the decreasing segment could not be captured.

4.1.5 Reinforcing Steel

Table 4.3 shows a summary of the properties acquired from the tensile tests of the steel reinforcing bars that were used to capture their material properties in the wall splice specimens. Appendix 4B presents the results of the individual tensile tests. A review of the test data shows that the loading rate was within 1% of the 0.315 mm/s target value detailed in Section 3.7.3.

Table 4.3 also presents the mean values and coefficient of variation for the yield stress and modulus of elasticity. No outliers were identified using the procedure detailed in ASTM E178-08 (ASTM, 2008) at the 95% confidence interval. The difference in the mean modulus of elasticity between the reinforcing steel used in Phases 1 and 2 was also not statistically significant when evaluated at the 95% confidence level. The reinforcing bars tested in the first phase had a 1.6% higher mean yield strength as compared to the steel bars tested in Phase 2. This represented a statistically significant difference at the 95% and was a result of the reinforcing steel from Phase 1 and 2 originating from different heat batches.

A previous investigation by Sanchez & Feldman (2013) concluded that wall splices specimens with similar geometry will fail in bond prior to the yielding of the reinforcement. It was therefore assumed that the resistance of the reinforcement in the wall splice specimens constructed in Phases 1 and 2 was not sensitive to the differing mean yield stresses.

Figure 4.2 shows a representative stress versus strain curve for a steel reinforcing bar specimen. The corresponding theoretical curve is also shown and agrees well with the test data. The theoretical curve was comprised of three sections: the first section was the linear elastic portion which was calculated based on the mean modulus of elasticity of the steel test specimens, the yield plateau followed and its location was based on the average yield strength of the steel bars tested, and the final segment comprised of a cubic function which was used to represent the strain hardening region. The material properties acquired from the tensile tests of the reinforcing steel were used as boundary conditions to determine the coefficients in the cubic equation.

Figure 4.2 shows that the theoretical curve produced by the analytical model agrees with the test data up to the ultimate stress. The analytical model was only capable of predicting specimen behaviour up to the ultimate stress; however, the Instron 600 DX Universal Testing Machine continued to record load and strain data until specimen rupture. The inability of the analytical model to predict the behaviour beyond the ultimate stress did not affect the modelling of the wall splice specimens as the steel reinforcement did not yield in any of the wall splice specimen tests. Appendix 4D details the complete procedure used to model the theoretical curve representing the reinforcing steel. One theoretical curve was created using the average tensile properties from the bar tests coinciding with the steel reinforcement used in Phase 1 while another was created to represent the steel reinforcement used in the Phase 2 specimens.

4.2 Visual Observations

This section presents the visually observed behaviour of the 24 wall splice specimens tested in Phases 1 and 2. The wall splice specimens were tested under four-point loading, as described in Section 3.7.2. Crack propagation on the compression face and the side of the wall splice specimens were recorded in addition to the load and deflection data. Visual observations of the different wall splice specimens provided a better understanding of their overall performance and indication of their failure mode. Cracks on the tension face were not recorded due to accessibility

and safety concerns since there was only 230 mm of clearance between the laboratory floor and the tension face of the wall splice specimens. The face shell from at least one specimen with each remedial method considered in Phases 1 and 2 was removed after testing to examine the internal distresses in the region of the lapped bars. Visual observations were also used to identify physical outliers and so exclude the resulting data from the calculation of mean values for the respective wall splice specimen set.

Figure 4.3 shows the typical crack propagation pattern observed on the side face of all the wall splice specimens. The first vertical flexural cracks appeared in the bed joints adjacent to the load application points within constant moment region. The next flexural cracks appeared in the two bed joints adjacent to the specimen midspan followed by the bed joints outside the constant moment region, directly adjacent to the load application points. The flexural cracks in the bed joint within the constant moment region adjacent to the load application points propagated in length and width the fastest as the load increased, followed by the flexural cracks in the two bed joints adjacent to the specimen midspan. Cracking in the bed joints adjacent to the specimen midspan continued to lengthen until approximately 90% of the ultimate load was reached. Further application of the load only caused these cracks to widen.

Crushing of the block or mortar was not observed on the compression face of any wall splice specimens during testing. Minor cracking was observed on the compression face of some wall splice specimens close to the bar anchorage at the ends of the specimens but the cracks did not continue to propagate at higher load levels. Such behaviour confirmed that the end anchorages were effective in preventing a bond failure at the ends of the specimen.

Different crack patterns were observed in the various splice details tested in this investigation. The individual analysis of the external and internal crack patterns for each of the two control and six remedial splice details provided a better understanding of their structural performance during testing. It also permitted a comparative analysis of the six remedial measures to the two control specimen types. These visual observations and comparisons are detailed in the following sections.

Control Contact Lap Splice Specimens (CLS)

Figure 4.4 shows the representative internal distress for the CLS wall splice specimens. The end slip of the steel reinforcement suggests that a bond failure occurred. Bond failure is also demonstrated in Figure 4.4 by the apparent movement of the spliced reinforcing bars relative to one another until the bar deformations began to bind on each other. These distresses were similar to those observed in the wall splice specimens with contact lap splices tested by Ahmed & Feldman (2012).

Control Non-Contact Lap Splice Specimens (NCLS) and Grouted Confinement Cell Specimens (GCC)

Figure 4.5 shows the representative internal distress for the NCLS and GCC wall splice specimens. The internal distress for these two wall splice specimen designs were similar to each other as they were both dominated by voids between the frog-ended blocks, diagonal cracks forming between the lapped reinforcing bars, and significant cracking at the bed joints. The void between the two ends of the frog-ended blocks was a result of the running bond geometry which made it difficult to consolidate grout in these regions as the area was obstructed by the course of blocks directly above. This resulted in stress concentrations around these voids and offered a path for crack propagation.

Figure 4.5 also shows that diagonal splitting cracks formed between the lapped bars. The formation of these cracks was the result of a tensile force that developed at each of the lapped steel reinforcing bars when the horizontal component of the diagonal compressive struts, detailed in Section 2.4.1, exceeded the shear strength of the masonry assemblage. This unbalanced force resulted in the formation of the diagonal splitting cracks. These cracks then changed orientation and proceeded to propagate along the grout-block interface which suggested a poor bond between the grout and surrounding block. This behaviour was also similar to the observations made by Ahmed & Feldman (2012) for wall splice specimens with non-contact lap splices where the lapped bars were placed in adjacent cells. Splitting failure occurred when the propagation of the diagonal splitting cracks spanned from one spliced bar to the intact web of the concrete block.

Figure 4.5 shows that significant internal cracking also occurred at the bed joints, in which the lapped reinforcing bars terminated. This led to failures shown in Figure 4.6 where cracks

propagated along the bed and head joints in the lap spice region resulting in reduced flexural capacity. All of the lapped reinforcing bars in the wall splice specimen examined in this investigation terminated at a bed joint. Therefore, the relative performance between the different splice details could still be evaluated.

The NCLS#3 and GCC#2 wall splice specimens were deemed to be physical outliers based upon their observed behaviour during testing. Figure 4.7 and Figure 4.8 show that voids were present around the longitudinal reinforcing bars in the splice region of both of these specimens and were likely due to inadequate grout consolidation. These specimens were therefore excluded in the calculation of the mean performance of the respective wall sets.

Single and Triple Knock-out Web Specimens (1KO & 3KO)

Figure 4.9 shows that the addition of knock-out webs in the 1KO and 3KO specimens reduced the external head joint cracking in the lap splice zone. The knock-out webs eliminated the grout-block interface within the lap splice region. This eliminated the possibility of voids forming between the frog-end blocks and delayed splitting failure.

Figure 4.10 shows the representative internal distress for both the 1KO and 3KO wall splice specimens as post-test investigations revealed that both remedial measures resulted in similar distress. The removal of the face shell and sufficient grout to expose the steel reinforcement revealed good grout consolidation between the lapped bars in the knock-out web regions. The uninterrupted area of grout between the lapped bars increased the capacity of the shear component of the diagonal compressive struts, discussed in Section 2.4.1 and shown in Figure 2.6. This resulted in a more effective transfer of the tensile forces between the lapped bars.

Figure 4.10 also shows large cracks at the bed joints directly above and below the lap splice. These cracks were a result of the longitudinal steel reinforcement terminating at these bed joints. Failure of the wall splice specimens featuring knock-out webs alone (ie. the 1KO and 3KO specimens) was likely the result of these bed joint cracks propagating through the wall cross-section. These cracks decreased the compression block depth, which in turn resulted in higher stress levels in the masonry assemblage and thus accelerated further crack propagation. A bond failure of the wall splice specimens with these remedial measures resulted.

Wall Splice Specimens with S-Shaped Reinforcement at Splice Level (SBAR, C-SBAR, & CT-SBAR)

The three remedial measures that included s-shaped reinforcement in the lap splice region all had similar external and internal distresses. Marginal differences in crack patterns were noted with the systematic addition of confinement cells and transverse reinforcement. The visually observed distresses of the SBAR, C-SBAR, and CT-SBAR wall splice specimens are discussed simultaneously for this reason.

Figure 4.11 shows the typical longitudinal crack pattern which formed on the compression face of the SBAR wall splice specimens. Additional confinement would assist in counteracting the bearing forces caused by the straightening of the s-shaped reinforcement as the tensile force increases.

Figure 4.12 shows that the straightening of the s-shaped reinforcement, as caused when the internal tension in the bar increases, resulted in a bearing force to be imparted on the surrounding cementitious material. The bearing force consisted of a longitudinal component, $B_{rl,}$ and a transverse component, B_{rt}. The transverse component of this bearing force, B_{rt}, exceeded the bearing capacity of the surrounding masonry assemblage as there was not masonry stiffness from the masonry assemblage to provide the necessary confinement to counteract this force at higher load levels. This is indicated by the longitudinal cracks, as shown in Figure 4.11, which appeared between the lapped longitudinal reinforcing bars.

A comparison of the external longitudinal crack propagation between the C-SBAR and CT-SBAR wall splice specimens is shown in Figure 4.13. Figure 4.13 (a) shows that the added confinement of an additional grouted cell on each side of the C-SBAR wall splice specimens did not noticeably decrease the extent of the longitudinal crack propagation when compared to those on the SBAR specimens shown in Figure 4.11. However, Figure 4.13 shows that there was a reduction in the extent of the longitudinal cracking on the CT-SBAR wall splice specimens (Figure 4.13 (b)) as compared to the C-SBAR wall splice specimens (Figure 4.13 (a)). The horizontal reinforcement at the splice level in the CT-SBAR specimens increased lateral confinement in the region and improved the cracking performance of the CT-SBAR wall splice specimens.

Figure 4.14 shows the typical internal distresses for all three wall splice specimen sets with s-shaped reinforcement in the splice region. The cracks in the bed joints located directly above and below the splice region were noticeably narrower than those observed in the other wall splice specimens with non-contact lap splices. Figure 4.14 also shows evidence that bond failure occurred during testing similar to the CLS wall splice specimens shown in Figure 4.4 as end slip is observed in both figures. This type of bond failure was seen in all three splice details with s-shaped reinforcing in the splice region (SBAR, C-SBAR, CT-SBAR). The internal distress in all three wall splice specimen sets with s-shaped reinforcement indicated that they likely were subject to the same failure mode as the control wall splice specimens with contact lap splices (CLS).

Figure 4.15 shows a large void that was discovered in the SBAR#3 wall splice specimen upon removal of the face shell. The likely cause of this void was a combination of inadequate grout consolidation by the mechanical vibrator and excess mortar at the bed joint that seeped into the cell impeding grout flow during placement. However, this void was located outside of the lap splice length and thus the longitudinal reinforcing bar acted as a tension tie in this region. The reinforcement in the splice region remained fully encapsulated in grout and thus the force transfer mechanism between the lapped bars was likely not affected. This specimen was therefore not deemed to be a physical outlier.

4.3 Load-Deflection Behaviour

Figure 4.16 shows the representative load versus deflection relationships for each of the control and remedial measures. Figure 4.16 (a) shows the plots for the 2.5 block-wide specimens, while Figure 4.16 (b) shows the 3.5 block-wide specimen plots. The plots for the two wall widths could not be compared directly since their stiffness differed. Appendix 4E presents the load versus deflection plots for all of the individual wall splice specimens.

The “loops” in the load-deflection data for the SBAR specimens, as shown in Figure 4.16 (a), were the result of a malfunction in the west hydraulic actuator. An error in the control program caused the west actuator to overshoot its intended set-point. The program then instructed the actuator to retract its position once the computer detected the overshoot. This resulted in a momentary decrease in both the load and deflection as represented by the loops in the load-

deflection data. However, the behaviour remained linear between the loops, similar to the wall splice specimen tests where the load frame operated correctly and so the data was included in the overall results database. The programming error was successfully addressed prior to testing the other Phase 2 specimens.

The change in slope near the beginning of the curves shown in Figure 4.16 represents the transition between the un-cracked and cracked behaviour of the wall splice specimens. Table 4.4 presents the actual cracking load for each individual specimen. The mean experimental cracking load for the 2.5 and 3.5 block-wide wall splice specimens were 5.67 kN and 5.99 kN, respectively. However, the theoretical cracking load, as calculated in accordance to CSA S304-04 (CSA, 2004e), were 2.71 kN and 4.26 kN for the 2.5 and 3.5 block-wide wall splice specimens, respectively. The increased observed cracking loads may have resulted due to a higher tensile resistance of the masonry assemblages tested in this investigation compared to that recommended in Table 5 of CSA S304-04 (CSA, 2004e).

The applied load increased in a linearly manner with midspan deflection following the onset of crack propagation until the ultimate applied load was reached. Figure 4.16 shows that the slope of the load- deflection plot decreased as the ultimate applied load was approached. This was likely the result of a decrease in the flexural rigidity of the wall splice specimen cross-section as cracks continued to propagate from the tension to the compression face, as shown in Figure 4.3. The ultimate applied load was defined by the maximum applied load resisted by the wall splice specimen.

Table 4.4 shows the values of the ultimate applied load for each wall splice specimen. Figure 4.17 shows a graphical comparison of the ultimate applied loads for each of the control and remedial measures tested. The control NCLS specimens had the lowest mean ultimate load at 9.92 kN (COV = 18.2%) while the C-SBAR, CT-SBAR, and the control CLS specimens had the highest, with each of the three wall splice specimen sets having a mean ultimate applied load of over 26 kN. This represented an over 160% improvement in the mean ultimate applied load compared to the control NCLS specimens. The explanations attributed to the difference in the mean applied ultimate load of the all remedial measures are the same as those discussed for the differences in the tensile capacity and will be discussed later in this chapter.

A 34.2 kN applied load was calculated, based on the cross-sectional geometry and average material properties of the wall splice specimens, to initiate yielding in the steel reinforcement. The resulting test data listed in Table 4.4 shows that the ultimate applied loads all of the wall splice specimens fell below 34.2 kN. This result corresponds with the findings by Sanchez & Feldman (2013) discussed in Section 3.2 and provided further evidence that all specimens failed in bond.

4.3.1 Midspan Deflection at the Ultimate Applied Load

Table 4.4 shows the maximum midspan displacement at the ultimate applied load for each of the wall splice specimens. Figure 4.16 shows that the increase in the deflection for the various splice details was proportional to the increase in the ultimate applied load. The average maximum midspan deflection for the NCLS and CLS wall splice specimen sets, which were the two control groups in this research program, was 5.35 mm (COV 24.3%) and 17.0 mm (COV 2.75%), respectively. This equated to a 218% increase in the maximum midspan deflection and an 800% decrease in the coefficient of variation. A decreased coefficient of variation is a desirable characteristic in engineering design as it represents a more predictable structural behaviour. These performance gains were the result of the different failure modes between the NCLS and CLS specimens. Figure 4.4 shows that the CLS wall splice specimens failed by the pulling out of the steel reinforcing bars. This failure mode typically results in larger displacements prior to failure and is mainly dependent on the overlap length of the spliced bars. In comparison, Figure 4.5 shows that the NCLS wall splice specimens failed due to the propagation of splitting cracks between the overlapped bars. This is a more brittle failure mode and is dependent on the highly variable properties of cementitious materials in tension (Ahmed & Feldman, 2012), which are more variable than those of steel reinforcement since cementitious materials are a heterogeneous material. In addition, the properties of cementitious materials are dependent on the quality of on-site batching and placement which can be highly variable; whereas reinforcing steel is less variable as it is manufactured in a more controlled environment.

The 1KO wall splice specimens achieved a 53% increase in the mean midspan deflection at the applied ultimate load as compared to the control NCLS specimens. The 3KO specimens achieved a further 20% increase in the mean midspan deflection at the applied ultimate load as compared to the 1KO specimens. These increases in the midspan deflection were the result of the

elimination of the grout-block interface between the lapped bars which delayed the onset of splitting cracks. The increase in the midspan deflection between the 1KO and 3KO specimens also showed that eliminating the grout-block interface along a greater length into the courses directly above and below the splice region had a positive impact on the structural performance of the lap splice. The increase in the midspan deflection was due to the geometry of the additional knock-out webs which allowed the compressive struts, shown in Figure 2.6, to form in a larger region of uninterrupted grout between the spliced reinforcement and thus increased the effective lap length of the lapped bars.

The mean midspan deflection at the ultimate applied load of the SBAR wall splice specimens was 17.2 mm (COV 26%). This represented a 75% increase in the midspan deflection at the ultimate load as compared to the 3KO specimens. This resulted in the SBAR specimens achieving approximately the same mean midspan deflection at ultimate applied load as the control CLS specimens; however, the deflection data from the SBAR specimens had a noticeably higher coefficient of variation. The increase in the coefficient of variation of the midspan deflection at the ultimate load among the SBAR specimens was likely the result of poor grout consolidation in the splice region due to a localized increase in the reinforcing steel in this area and the requirement for portions of the knock-out webs in the half blocks to remain intact, as shown in Figure 4.18, to maintain the structural integrity of the concrete block during construction. This reduced the available room to maneuver the mechanical vibrator within the reinforced cell and ensure complete consolidation of the grout. These constructability concerns did not occur for the C-SBAR and CT-SBAR specimens as the knocked-out webs of the half blocks were not located between the lapped bars.

The average maximum midspan deflection at the maximum applied load for the GCC and C-SBAR wall splice specimen sets was 5.95 mm (COV 21.8%) and 18.4 mm (COV 6.63%) respectively. This equated to a 209% increase in the maximum midspan deflection at the ultimate applied load and a 228% decrease in the coefficient of variation between these two remedial measures. This increase in the midspan deflection was the result of the elimination of the grout-block interface between the lapped bars which delayed the propagation of splitting cracks. Another reason for the increased midspan deflection, as shown in Figure 4.14, was that the installation of the s-shaped bars in the C-SBAR specimen resulted in failure due to pullout of the

longitudinal reinforcing steel. The addition of the transverse reinforcement at the splice level of the CT-SBAR specimens resulted in a further 16% increase to the average midspan deflection at the ultimate applied load as compared to the C-SBAR specimens. The transverse reinforcement in the CT-SBAR specimens provided additional confinement in the splice region and so inhibited the formation of the longitudinal cracks which formed between the lapped bars as shown in Figure 4.13.

The midspan displacement results indicate that the installation of remedial measures in the splice region resulted in noticeable increases in the maximum midspan deflection at the ultimate applied load compared to the control NCLS specimens. However, this increase in the midspan deflection was proportional to the increase in the applied load and did not represent an increase in the flexibility of the wall splice specimens. Certain remedial measures applied to the non-contact lap splices, where the lapped bars were centered in adjacent cells, were able to match the midspan deflection of the control CLS specimens that contained contact lap splices.

4.4 Wall Splice Specimen Modelling and Analysis

The wall splice specimens were not internally instrumented since doing so would affect the bond between the steel reinforcement and the surrounding cementitious materials. The tension in the reinforcing steel was therefore not measured directly. A numerical moment-curvature model was therefore developed to determine the tension in the steel reinforcement indirectly using the experimental load and deflection data as input. Material properties were obtained from the various companion specimens tested alongside the wall splice specimens. An iterative finite difference approach was then used to conduct a sectional analysis and so determine the depth of the compression block. The tensile force in the steel reinforcement was then calculated using force equilibrium.

4.4.1 Moment-Curvature Analysis

The displacement data used in the moment-curvature analysis was acquired from six LVDTs located along the length of the horizontally tested wall splice specimens. The location of the LVDTs is detailed in Section 3.7.2 and shown in Figure 3.27. The data was then compiled to create deflection profiles of each wall splice specimen. Figure 4.19 shows the deflection profile of a representative wall splice specimen along with the parabolic approximation at ultimate

applied load level. The deflected profile of the wall splice specimens was significantly influenced by rigid body flexural motion between the cracks that formed in the bed joints. The widening of these cracks at these locations caused the un-deformed wall segments between the cracks to rotate. The agreement between the LVDT data at the various locations along the length of the wall splice specimen and the parabolic approximation was therefore predominantly influenced by the crack locations. However, the LVDT deflection data at the ultimate applied load and the corresponding points on the parabolic approximation showed good agreement as the root mean square error (RMSE) was typically within 10% of the midspan deflection. The parabolic approximation of the deflection was then used in the moment curvature analysis to determine the experimental curvature at the ultimate applied load. This was achieved by differentiating the equation twice to obtain the curvature. The experimental moment-curvature was then compared to the theoretically derived moment-curvature as was obtained using the process detailed in the following paragraphs.

A modified Kent-Park curve (1971) with the maximum stress occurring at 0.002 strain was used as the theoretical stress versus strain profile for the masonry prisms. The curve included a parabolic rising segment from 0 to 0.002 strain, followed by a linear drop in stress at strains higher than 0.002. The detailed expressions used to derive the Kent-Park (1971) curve are presented in Appendix 4F. Figure 4.1 shows that the experimental prism data exhibited good agreement with the theoretical curve up until a strain of 0.002 where the masonry prism underwent a brittle failure and further data could not be collected. The modulus of elasticity for the masonry assemblage, E'_m, was obtained from the plotted data by determining the average slope of the rising segment from the stress-strain curve, while the compressive strength, f'_m, was obtained from each masonry prism test. The material properties from each prism test were used solely for the analysis of the corresponding wall splice specimen.

The theoretical stress versus strain profile for the reinforcing steel, shown in Figure 4.2, was developed using the mean tensile properties from the reinforcing bar tests for each construction phase. Table 4.3 summarizes these results. As previously stated, the theoretical curve was comprised of three segments. The first segment of the theoretical curve was the linear elastic zone. The slope of the linear elastic portion up to the yield point, f_y, is equal to the modulus of elasticity, E_s. The next segment of the theoretical stress versus strain profile was the yield plateau

which continued until the onset of strain hardening. The strain hardening region consisted of a third order curve derived using the following four boundary conditions established from the tension test on the reinforcing steel bars: strain at the initiation of strain hardening, ε_{sh}; the instantaneous slope at the initiation of strain hardening, E_{sh}; the strain at the ultimate stress, ε_u; and the ultimate stress in the steel, f_u. Appendix 4D presents the detailed derivation of the theoretical stress versus strain profile of the steel reinforcement. Figure 4.2 shows that good correlation was observed between the theoretical stress versus strain profiles derived using the average material properties obtained from the individual tension tests. Appendix 4B presents the material properties obtained from all the individual tension tests.

The material properties of the masonry assemblage and the steel reinforcement were then used in a sectional analysis to determine the theoretically applied moment corresponding to any given curvature. It was assumed that plane sections remained plane after bending and that perfect bond between the masonry assemblage and the steel reinforcement existed up until specimen failure. Ideal support conditions were assumed such that the wall splice specimens did not experience any axial compression. The model also assumed that curvature was symmetric about the midspan of the horizontally tested wall splice specimen.

The curvature prior to cracking of the wall splice specimen, ϕ_{uc}, was calculated by assuming linear behaviour and determining the ratio of the applied moment to the flexural rigidity of the un-cracked cross section:

$$\phi_{uc}=\frac{M_a}{E'_m I_g} \qquad [4\text{-}1]$$

where M_a is equal to the applied moment, calculated using the applied load data and the loading geometry shown in Figure 3.27; E'_m is the modulus of elasticity for masonry; and I_g is the moment of inertia of the gross cross-section.

The experimental cracking load, P_{cr}, for each wall splice specimen was identified as the load level where the slope of the load-deflection data decreased from an almost vertical orientation to a more shallow trajectory, as shown in Figure 4.16. The experimental cracking moment, M_{cr}, for each wall splice specimen was then calculated by using the experimental cracking load, P_{cr}, and the loading geometry shown in Figure 3.27. Following cracking, the effective flexural rigidity,

$E'_m I_g$, became a function of the applied moment. A flexural analysis was used to determine the analytical moment-curvature relation for the cracked sectional analysis. A partially cracked section was not considered since its inclusion would not affect the modeling of the wall splice specimens at the ultimate load.

The flexural analysis of the cracked section was completed using a finite difference approach. Figure 4.20 shows the sectional analysis used given the stress versus strain behaviour of the masonry assemblage. The compression zone was therefore divided into 100 segments of equal thickness, with the distance from the centre of a given segment to the neutral axis being denoted as y_i. Calculations presented in Appendix 4G show that the error associated with dividing the compression zone into 100 segments was determined to be less than 0.1% and was thus considered to be negligible.

An iterative finite central difference program was then initiated using the geometry of the compression block. The first step of this program was to input the wall width, b, and a value for the curvature, ϕ. A neutral axis depth, c, was then assumed so the strain at the extreme compressive fibre, ε_c, could be calculated by multiplying the curvature obtained from the test data at the ultimate load, ϕ, and the assumed depth to the neutral axis, c. Figure 4.20 (b) shows how a linear strain profile and similar triangles were used to calculate the strain in the reinforcing steel, ε_s, and at the centre of each of the 100 compression strips, ε_i. The tensile stress in the reinforcing steel, f_s, was then determined using the theoretically developed stress versus strain curve. The resulting tensile stress was then multiplied by the cross-sectional area of longitudinal steel reinforcing bars, A_s, to calculate the total tensile force in the steel reinforcement, T.

The compressive force in each of the 100 segments, C_i, was obtained by first determining the compressive stress, f_{mi}, corresponding to the calculated strain, ε_i, in the given segment assuming the theoretically derived compressive stress versus strain relationship. The resulting compressive stress was then multiplied by the cross-sectional area of the segment, equal to the product of the width of the wall splice specimen, b, and the thickness of the segment. The segment's thickness was the quotient of the depth to the neutral axis, c, divided by the total number of segments, 100. The total compressive force in the cross-section of the masonry assemblage, C, was then calculated by summing the compressive force in all of the segments, as illustrated in Figure 4.20 (c) and Figure 4.20 (d).

The resulting total compressive force, C, and the total tensile force in the reinforcing bars, T, were then compared to determine if the two values were within 0.5% of each other to ensure that force equilibrium had been satisfied. If this criterion was not satisfied, the neutral axis was decreased by 0.1 mm and the process was repeated. Alternatively, if the criterion was satisfied, the resulting moment was then calculated.

Figure 4.20 (d) shows how the resisting moment was calculated. The compressive forces in each segment were first multiplied by the respective distance between the centroid of the segment and the neutral axis. These values were then added to the product of the tensile force in the reinforcing steel and the distance between the centroid of the steel reinforcement and the neutral axis. The resulting value was equal to the resisting moment of the reinforced masonry cross-section.

Figure 4.21 shows a representative moment-curvature plot that was developed using the finite difference approach as described. Segment 1 of the plot is a short near-vertical section which represents the un-cracked moment-curvature behaviour of the wall splice specimen. This is followed by a linearly increasing section (Segment 2) that represents the cracked moment-curvature behaviour of the wall splice specimen prior to the yielding of the steel reinforcement. Segment 3 of the plot represents the moment-curvature behaviour of the wall splice specimens once the reinforcement was yielding. This is followed by Segment 4 which represents the moment-curvature behaviour of the wall splice specimen when the steel reinforcement has entered the strain hardening region. Segment 5 of the plot represents the moment-curvature behaviour of the wall splice specimen where the reinforcing steel has exceeded its ultimate stress and the tensile stress decreases prior to failure. Appendix 4G presents the detailed expressions and MathCAD code for the theoretical moment-curvature analysis using the finite difference approach.

Figure 4.22 (a) and (b) show the representative experimental and theoretically derived moment-curvature plots for the 2.5 and 3.5 block-wide wall splice specimen sets, respectively. Appendix 4H includes the individual moment-curvature plots for each wall splice specimen. The theoretical curves shown in Figure 4.22 do not have the same proportional relationship shown by the theoretical moment-curvature plot in Figure 4.21. This difference was a result of the theoretical curves shown in Figure 4.22 taking into account the self-weight of the wall splice specimen and

the weight of the lower spreader beam assembly (3.25 kN·m and 4.00 kN·m for the 2.5 and 3.5 block wide wall splice specimens, respectively) into their derivation. The change in the slope between the segments of the curve representing the un-cracked and cracked moment-curvature behavior was noticeably more gradual than what was represented by the theoretical curves. This showed that the flexural rigidity of the section changed gradually from an un-cracked state to a fully cracked section as new cracks formed and propagated. Figure 4.22 and the individual moment-curvature plots in Appendix 4H show that all 24 wall splice specimens failed prior to yielding of the steel reinforcement. They also show that the experimental moment-curvature plots exhibited relatively bi-linear behaviour. The curves shown in Figure 4.22 are marginally above the theoretically derived counterparts for the entire loading range. This is likely due to effects of tension stiffening which results in a slight increase in the flexural rigidity of the masonry assemblage. However, Figure 4.22 shows that good overall agreement was achieved between the experimental and theoretically derived curves representing the moment-curvature behaviour of the wall splice specimens. This result validated the iterative finite central difference program to calculate the tension in the lapped reinforcement.

4.4.2 Theoretical Deflection

The theoretical deflection at the midspan of the wall splice specimens was calculated using a finite difference approach founded on the conjugate beam method. Appendix 4I presents the detailed MathCAD code detailing this finite difference program. The first step in the derivation of the theoretical midspan deflection was to divide the 2400 mm clear-span of the wall splice specimen into 10 mm lengths, for a total of 240 segments. The error associated for this number of segments, as presented in Appendix 4I, was determined to be less than 0.01% and was thus considered to be negligible. The moment at the midspan of each 10 mm segment was then determined using statics as based on the loading arrangement. The curvature was then determined using the calculated moment at the midspan of the segment. An effective moment of inertia was used to interpolate the curvature of the un-cracked and fully transformed sections in an effort to model a gradual change between the two sets of section properties.

Bischoff`s (2005) equation was used to calculate the effective moment of inertia that was required to determine the deflections of the individual 10 mm wall segments. Although the Canadian masonry design code, CSA S304-04 (CSA, 2004e), uses Branson`s (1965) equation,

which is based on research conducted on reinforced concrete beams. However, Bischoff (2005) showed that Branson`s (1965) equation is not well suited for reinforced concrete beams and slabs with reinforcement ratios under 1%. This is noticeably more than the reinforcement ratios for the 2.5 and 3.5 block-wide wall splice specimens used in this study which, were 0.21% and 0.15% respectively. Ahmed and Feldman (2011) also used the Bischoff's (2005) equation to determine the theoretical midspan deflections of the masonry wall splice specimens in their study which resulted in a good correlation between the experimental data and the theoretically derived values. For these reasons, Bischoff's (2005) equation was used to calculate the effective moment of inertia in this study.

The deflection of the 240 individual segments was calculated using the conjugate beam method. The effective curvature caused by the application of a fictitious load was first calculated for each segment. The moment at the midspan of each segment was then determined given this curvature and the moment-curvature relationship established from the material properties as described in Section 4.4.1. The midspan deflection of each respective segment was then set to this moment. The midspan deflection of the overall wall splice specimen was then calculated as the sum of the individual segment deflections from one end of the wall splice specimen to the midspan. Figure 4.16 shows a good agreement between the load-deflection data acquired during testing and the theoretical load-deflection plot derived by using this method.

4.4.3 Tensile Resistance

The tensile resistance was then calculated using the ultimate moments, reported in Table 4.4, and the moment-curvature analysis detailed in Section 4.4.1. Figure 4.23 shows the variations in the tensile resistance of the spliced reinforcement in the different wall splice specimen sets. The magnitude of these variations appear to be similar to the variations in the mean ultimate applied load each of the different wall splice specimen sets as shown in Figure 4.17. However, closer inspection of the values presented in Table 4.4 reveals that there is up to a 150% variance in the magnitude of the difference between the tensile capacity and the ultimate applied load of the various remedial measures. These differences were the result of the calculation of tensile capacity being based on the curvature of the wall splice specimen, the material properties acquired from the prism and tension test results, and the ultimate load. The inclusion of these various

parameters in the calculation of the tensile capacity allowed for a more meaningful comparative analysis.

4.5 Tensile Capacity of the Spliced Reinforcement

Table 4.4 shows that the average tensile resistance of the pair of lapped bars in the control NCLS and CLS wall splice specimens sets was 43.5 kN (COV 24.3%) and 129.0 kN (COV 3.47 %), respectively. This equated to a 197% increase in the average tensile capacity of the lap splices and an 86% decrease in the coefficient of variation. The reduction in the coefficient of variation can be attributed to the different failure modes of the two wall splice specimen sets, as discussed in Section 4.3.

The GCC wall splice specimens exhibited a marginally higher average tensile resistance of the lapped reinforcement (53.3 kN, COV 23.6%) compared to the control NCLS wall splice specimens. This increase in performance was the product of the increased stiffness due to the increased specimen width. The additional confinement that was provided delayed splitting cracks from developing between the lapped bars. The coefficient of variation remained relatively constant as the failure mode of the NCLS and GCC wall splice specimens both involved poor bond at the interface of the grout and block between the lapped bars.

The mean tensile resistance of the 1KO lap splices was 63% higher than the lap splices in the control NCLS specimens with a 69% decrease in the coefficient of variation. The results of the 3KO wall splice specimens showed an additional 7.5% increase to the mean tensile resistance of the lapped bars, with a further 10% decrease in the coefficient of variation, as compared to the 1KO wall splice specimens. These increases in performance were the result of the installation of knock-out webs within the splice region. This eliminated the grout-block interface and allowed for the diagonal compressive struts to more effectively transfer the tensile forces in the lapped reinforcement through the masonry assemblage, as discussed in Section 4.3. The minor increases in the tensile capacity between the 3KO and 1KO specimens showed that the diagonal compressive struts are mainly confined to within the lap region and crack propagation into the lap splice region was not a major concern.

The addition of the s-shaped reinforcement in the lap splice region of the SBAR specimens resulted in a further 47% increase in the mean tensile capacity of the lapped reinforcement

compared to the 3KO wall splice specimens, but came with a 75% increase in the coefficient of variation. The increase in the tensile capacity of the lap splices was the result of s-shaped reinforcement transferring a portion of the tensile forces between the longitudinal reinforcing bars. This allowed for a lower stress state in the cementitious material between the lapped longitudinal reinforcement and thus delayed splitting cracking. The explanation for the increase in the coefficient of variation for the tensile resistance of the SBAR specimens was discussed in Section 4.3.1.

The lap splices in the SBAR specimens developed the highest tensile resistance of all of the 2.5 block-wide wall splice specimens with remedial measures. However, the tensile resistance of the pair of lapped bars in the SBAR specimens was 13% lower than the CLS specimens which had contact lap splices of the same lap length. The lack of confinement likely prevented the SBAR specimens from equaling the performance of the CLS specimens.

The confinement cells added to the C-SBAR specimens resulted in an additional 7.1% increase in the mean tensile capacity of the lapped reinforcing bars and a 72% decrease in the coefficient of variation as compared to the 2.5 block-wide SBAR specimens. The addition of the transverse reinforcement in the splice region of the CT-SBAR specimens resulted in a 14% increase in the mean tensile resistance of the lapped bars but also resulted in a 56% increase in the coefficient of variation compared to the C-SBAR wall splice specimens. The rationales behind the comparative performance of the SBAR, C-SBAR, and CT-SBAR rehabilitation measures are the same as those discussed for the differences in observed crack patterns and ductility in Sections 4.2 and 4.3, respectively.

The lapped reinforcing bars in the CT-SBAR specimens had the highest tensile resistance of the six different wall splice specimen sets with remedial measures tested in Phase 1 and 2. The mean tensile resistance of the lapped bars in the CT-SBAR specimens represented 215% increase in the tensile capacity and a 28% decrease in the coefficient of variation as compared to the control NCLS wall splice specimens. The mean tensile resistance of the lapped bars in the CT-SBAR specimens also represented a 6.2% increase in the tensile capacity compared to the control CLS wall slice specimens. However, this modest increase cannot be statistically proven to be significant as there were an insufficient number of replicates constructed. The coefficient of variation in the lap splice capacities of the CT-SBAR specimens was noticeably higher than that

of the CLS specimens. This was a result of the tensile capacity of the spliced reinforcement in the CT-SBAR specimens relying on the proper placement and material properties of multiple reinforcing bars, and the proper consolidation of the grout in the entire region between the lapped longitudinal reinforcing bars. The tensile capacity of the contact lap splices in the CLS specimens mainly depended on the length of the overlap and the material properties of the longitudinal reinforcing steel.

4.6 Practical Implications

One of the intents of this research project was to provide engineers with options to improve the structural response of non-contact lap splices, where the lapped bars are in adjacent cells. The remedial measures tested in Phase 1 and 2 were designed to be applied either in the design or construction phase. The results have shown that the addition of knock-out webs and s-shaped splice reinforcement noticeably improved both the flexibly of the reinforced masonry assemblage and the tensile capacity of the lap splice.

Knock-out webs between the lapped bars, as provided in the 1KO and 3KO wall splice specimens, can be installed in construction situations where the non-contact lap splice was not anticipated in the design phase or to address constructability concerns by the masonry contractor. Figure 4.24 (a) shows a construction situation that is well suited for the installation of knock-out webs within the lap length: a misaligned dowel protruding from a previously cast grade beam. A knock-out web can also be installed in just the course above the splice length to gain additional structural capacity. This geometry was not tested in this investigation since the parabolic approximation used in the moment-curvature analysis is best suited for horizontally tested wall splice specimens that are symmetric about the midspan. Blocks with knocked-out webs, including A-blocks, H-blocks, and knock-out blocks, are available from local suppliers or can be easily fabricated on site using a masonry saw. These blocks are then laid in the same manner as a typical concrete block. The knock-out webs also do not affect the exterior appearance or dimensions of the masonry assemblage. Knock-out webs within the splice length can be applied to any non-contact lap splice situation in the field and will provide reasonable improvements in structural response. The installation of additional knock-out webs directly above and below the lap length, as represented with the 3KO specimens, has been shown to yield further modest increases in structural performance. However, the location of the non-contact lap splice must be

known at least one course prior to the lap level to make use of this structural detail and it cannot be applied to misaligned dowels protruding from a grade beam.

The installation of s-shaped splice and transverse reinforcement, in addition to knock-out webs, within the splice region has been shown to additionally increase structural performance. Consultations with industry professionals have concluded that the level of difficulty associated with their fabrication and installation would not be high in field situations. In addition, typical masonry structures are wider than those tested in the lab and thus will provide higher levels of confinement, further increasing the performance of the s-shaped splice reinforcement and non-contact lap splice. One shortcoming of the installation of s-shaped splice reinforcement is that it requires that the reinforced cell remains ungrouted at least one lap length below the splice region prior to their installation. This limits their use to situations where the non-contact lap splices are identified in the design phase. Figure 4.24 (b) shows an example of such a condition where non-contact lap splices are required to accommodate the bond beam reinforcement located above the opening. S-shaped splice reinforcement can be used in this situation to strengthen non-contact lap splice without increasing the splice length.

Table 4.5 presents the recommended multiplication factors for four different remedial measures which can be applied to the available tensile resistance of remediated non-contact lap splices in structural masonry assemblages. These factors were based on the correction factor of 1.5 recommended for a non-contact lap splice with no applied remedial measures by Ahmed & Feldman (2012) and the test results of the wall splice specimens with remedial measures obtained from this investigation. The results were not compared to non-contact lap splices where the lapped bars are located in a single cell as this was not within the scope of this research program.

The factor of 1.5 conservatively represents Ahmed & Feldman's (2012) findings that the lapped reinforcement located within adjacent cells in concrete block masonry construction developed only 71% of the tensile resistance of bar in contact. The difference in the tensile resistance of the control non-contact lap splice and contact lap splice specimens in this investigation compared to Ahmed & Feldman (2012) was larger; however, Ahmed & Feldman's (2012) recommended correction factor of 1.5 was still used as the basis for the multiplication factors for this study because that investigation included a greater number of replicate specimens and the geometry of the specimens did not result in having the lapped bars terminate in a bed joint.

The multiplication factors for remediated non-contact lap splices, F_{splice}, presented in Table 3 were calculated using:

$$F_{splice}=[(1-n_{cls})\cdot(1.5-1)+1]^{-1} \quad [4\text{-}2]$$

where n_{cls} is the percent difference between the mean tensile capacity of the non-contact lap splice specimen with remedial measures and the control contact lap splice specimens. This was then multiplied by the difference between Ahmed & Feldman's (2012) correction factor, 1.5, and the factor for contact lap splices, 1. This represents the increase required for the tensile resistance of the non-contact lap splice with the specified remedial method as compared to the contact lap splice length. Adding unity to the product provides for the necessary correction factor. The inverse of this sum was then taken to obtain a multiplier of the available tensile resistance expected with the implementation of a specified remedial method in relation to a contact lap splice of the same lap length. The multiplication factors presented in Table 4.5 quantify the available tensile resistance of remediated non-contact lap splices in masonry construction compared to the un-remediated non-contact lap splices recommended by Ahmed and Feldman (2012). It is also recommended that splice details, such as those presented in Figure 4.24, be included in construction guides to provide engineers with visuals of potential solutions when non-contact lap splices are encountered in the design or construction phase of masonry structures.

4.7 Summary

The visual observations, vertical deflection, member capacity, and tensile resistance of the reinforcement of the two control and six remedial lap splice details were analyzed to determine if it was possible enhance the structural performance of non-contact lap splices, where the lapped bars are located in adjacent cells.

Large cracks were observed in the bed joints directly above and below the lap region, in the same plane as the termination of the longitudinal reinforcement in wall splice specimens with non-contact lap splices. This led to specimen failures where cracks propagated along the bed and head joints in the lap spice region which resulted in reduced flexural capacity. All of the lapped reinforcing bars in the wall splice specimens in this investigation terminated in the plane of the bed joint. Therefore, the relative performance between the different splice details could still be

evaluated. This phenomenon must be considered when evaluating bond in masonry construction as it may result in reduced tensile capacity of the reinforcement.

The theoretically derived deflection and moment-curvature plots showed good correlation with the LVDT measured data. A moment-curvature analysis incorporating a finite central difference approach was then completed to determine the tensile force in the steel reinforcement.

The installation of remedial measures in the splice region resulted in improved structural performance compared to the control non-contact lap splice specimen set. The installation of knock-out webs between the lapped bars delayed the propagation of splitting cracks and increased the tensile capacity of the spliced reinforcement. The addition of s-shaped steel reinforcement in the lap splice region resulted in a failure mode similar to that of the contact lap splices where a bond pullout failure was observed. An additional increase in the tensile capacity of the lapped bars as compared to the wall splice specimen sets with just knock-out webs also resulted.

The 3.5 block wide wall splice specimens with s-shaped and transverse splice reinforcement had the greatest increase in the vertical deflection and the tensile capacity of the lapped bars out of six lap splice details with remedial measures tested in Phase 1 and 2 of this research program. These wall splice specimens were able to match the performance of the control specimens with contact lap splices of the same lap length both in terms of the tensile resistance of the lapped bars and the ductility of the wall splice specimen.

A statistical review of the data could not be conducted given the scope of the experimental program since only three replicates of each mitigative technique were constructed. However, noticeable increases in both the vertical deflection of the wall splice specimens and the tensile capacity of the splice reinforcement were observed when the data from the eight different wall splice specimen sets were compared.

The results of the analysis in this chapter were used to quantify the performance of the proposed remedial measures for non-contact lap splices. The resulting multiplication factors will allow engineers to more accurately predict the tensile resistance of non-contact lap splices if the prescribed remedial measures are implemented.

Table 4.1: Test Schedule.

Construction Phase	Construction Dates	Test Dates	Specimen Age Range (Average) [Days]	Number of Specimens Tested				
				Wall Splice Specimens	Masonry Prisms	Mortar Cubes	Grout Prisms	Grout Cylinders
1	Aug. 14-23, 2012	Oct. 9-Nov. 13, 2012	42-82 (61)	15	22	96	32	96
2	March 20-28, 2013	April 20-May 10, 2013	41-51 (47)	9	15	57	22	66

Table 4.2: Cementitious Companion Specimen Summary.

Companion Test	Construction Phase	Number of Specimens Used for Analysis	Mean Maximum Stress [MPa]	COV
Masonry Block	1	6	19.7	10.5%
	2	6	21.5	8.39%
Mortar Cubes	1	94*	17.0*	16.1%*
	2	56*	16.7*	10.9%*
Absorbent Grout Prisms	1	31*	14.1*	12.5%*
	2	21*	15.5*	8.08%*
Non-Absorbent Grout Cylinders	1	92*	14.1*	13.3%*
	2	64*	12.5*	11.7%*
3-High, Stack Bond Masonry Prism	1	15	13.4	10.2%
	2	9	12.5	20.2%

* Excludes statistical outliers identified at the 95% confidence interval using the procedure detailed in ASTM E178 (ASTM, 2008) (3-mortar cubes, 2-absorbent grout prisms, 6-non-absorbent grout cylinders).

Table 4.3: Summary of Reinforcing Steel Test Results.

Test Phase		Dynamic yield stress f_y [MPa]	Modulus of elasticity E_s [GPa]	Strain at the initiation of strain hardening ε_h	Slope at initiation of strain hardening E_{sh} [MPa]	Ultimate steel stress f_{ult} [MPa]
1*	Average	442	192	0.0146	6942	666
	COV	0.65%	11.44%	11.45%	16.3%	0.38%
2	Average	435	180	0.0134	2715	594
	COV	0.64%	18.7%	22.5%	13.9%	0.46%

*This data also applies for the reinforcement used in specimens constructed during Phase 1a as all originated from a common batch.

Table 4.4: Resulting Wall Data.

Wall Set	Wall Number	Age @ Test [days]	Cracking Load [kN]	Max Applied Load [kN]	Max Midspan Moment [kNm]	Midspan Displacement @ Max Load [mm]	Curvature @ Max Load [1/m]	Tension in Spliced Reinforcing Bars [kN]	f'_m [MPa]	E_m [MPa]
NCLS	1	43	5.70	11.7	7.62	6.67	0.0103	54.1	12.9	8910
	2	42	5.30	8.11	6.16	4.02	0.00617	32.9	13.5	8590
	3*	49	6.10	7.57	5.95	3.15	0.00510	28.6	11.9	10500
	Average		5.50	9.92	6.89	5.35	0.00824	43.5	13.2	8750
	COV [%]		3.64	18.2	10.6	24.8	25.1	24.3	2.16	1.83
GCC	1	78	6.70	12.8	8.83	7.24	0.0116	65.9	14.8	7770
	2*	82	7.60	9.08	7.35	1.62	0.00310	17.6	14.2	10100
	3	75	8.50	13.4	9.08	4.65	0.00740	40.7	11.9	7450
	Average		7.60	13.1	8.96	5.95	0.00950	53.3	13.4	7610
	COV [%]		11.8	2.41	1.40	21.8	22.1	23.6	10.9	2.10
1KO	1	67	6.20	12.2	7.80	8.89	0.0141	76.5	15.9	14900
	2	69	6.80	13.3	8.24	7.01	0.0124	63.7	11.7	11100
	3	70	6.00	16.5	9.51	8.62	0.0135	72.8	15.2	10900
	Average		6.33	14.0	8.52	8.17	0.0133	71.0	14.3	12300
	COV [%]		5.37	13.0	8.51	10.2	5.28	7.58	12.8	15.0
3KO	1	54	5.70	17.5	9.92	10.9	0.0159	83.0	12.9	7210
	2	57	7.30	17.6	9.96	9.44	0.0142	75.8	14.4	10900
	3	50	7.20	15.7	9.20	9.12	0.0137	70.3	11.5	9990
	Average		6.73	16.9	9.69	9.81	0.0146	76.3	12.9	9370
	COV [%]		10.9	5.13	3.60	7.80	6.45	6.81	9.19	16.8
SBAR	1	36	3.90	19.3	19.6	13.0	0.0178	84.8	15.5	8350
	2	34	3.80	25.2	13.0	23.6	0.0335	154	13.8	8560
	3	33	3.30	24.3	12.7	14.9	0.0209	97.5	13.9	8700
	Average		3.67	22.9	15.1	17.2	0.0241	112	14.4	8540
	COV [%]		7.16	11.4	21.2	26.9	28.2	26.9	5.41	1.68
C-SBAR	1	42	4.70	29.6	15.6	20.0	0.0272	133	13.4	8120
	2	41	4.60	24.9	13.7	17.1	0.0229	111	12.7	7970
	3	40	6.90	25.7	14.0	18.0	0.0258	116	8.75	6460
	Average		5.40	26.8	14.4	18.4	0.0253	120	11.6	7520
	COV [%]		19.7	7.7	5.69	6.63	7.08	7.67	17.7	10.0
CT-SBAR	1	39	6.10	26.1	14.2	17.0	0.0231	110	11.4	20200
	2	43	6.00	27.3	14.7	22.1	0.0297	132	7.9	9430
	3	42	4.40	26.1	14.2	25.0	0.0338	168	15.2	8420
	Average		5.50	26.5	14.3	21.4	0.0289	137	11.5	12700
	COV [%]		14.2	2.2	1.60	15.4	15.3	17.5	25.8	42.0
CLS	1	63	6.10	29.6	14.8	16.4	0.0240	123	12.5	10100
	2	62	5.10	22.9	12.1	17.5	0.0253	130	12.5	6890
	3	60	7.20	25.8	13.2	17.1	0.0253	134	14.9	8710
	Average		6.13	26.1	13.4	17.0	0.0249	129	13.3	8570
	COV [%]		14.0	10.6	8.32	2.75	2.46	3.47	8.45	15.3

*Physical outliers as identified in the accompanying text. The resulting data from these specimens have been excluded in the averages and coefficients of variation as reported.

Table 4.5: Recommended Correction Factors for the Available Tensile Resistance When the Lapped Bars are Located in Adjacent Cells.

Remedial Measure	Multiplication Factor
S-shaped and transverse reinforcement at splice level with at least one grouted confinement cell on either side of the lap splice	1
S-shaped reinforcement at splice level with at least one grouted confinement cell on either side of the lap splice	0.95
S-shaped reinforcement at splice level at the edge of a masonry assemblage (ie. No confinement)	0.90
Knock-out webs installed in the splice length only	0.80
No remedial measures applied	0.70

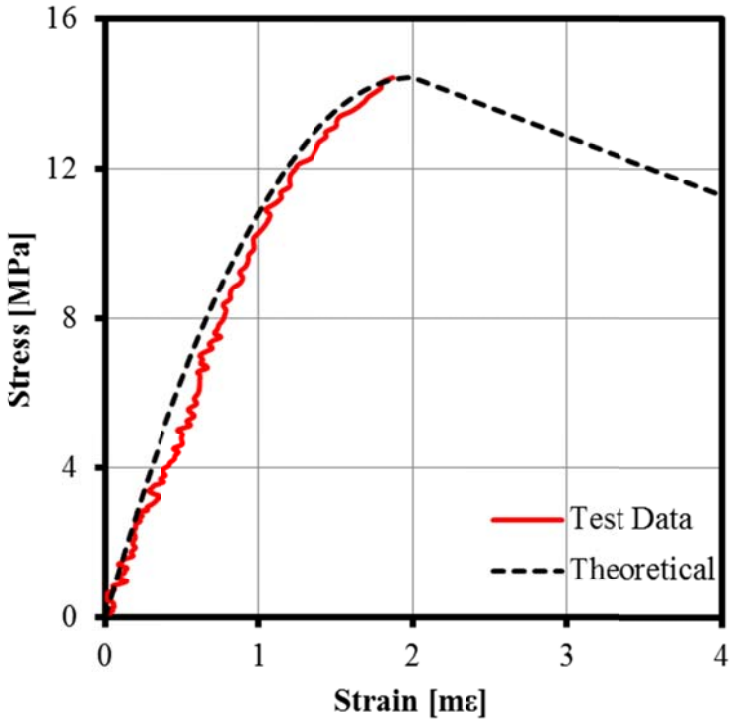

Figure 4.1: Representative Stress Versus Strain Data for a Masonry Prism.

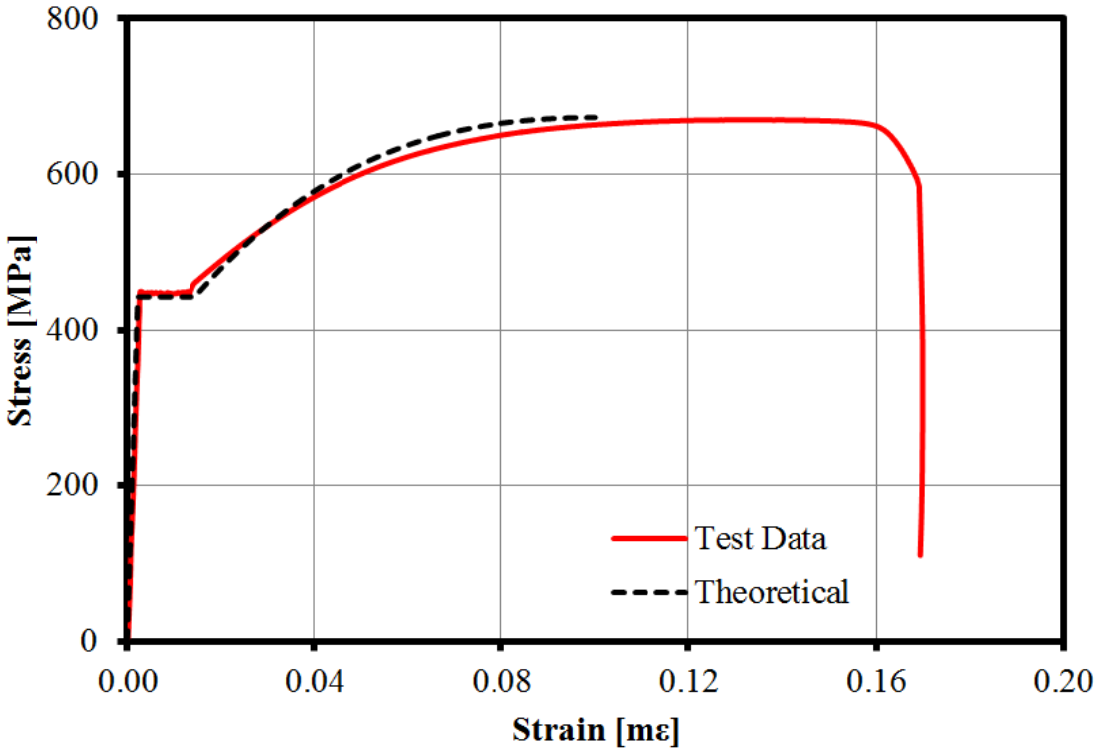

Figure 4.2: Representative Stress Versus Strain Data for a Steel Coupon Plotted Alongside the Analytical Curve for the Steel Reinforcement.

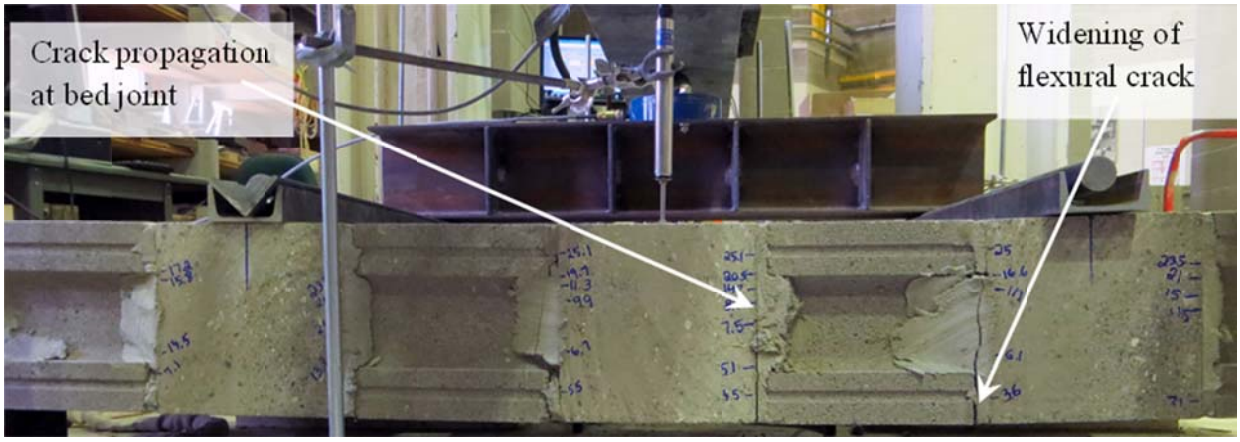

Figure 4.3: Typical Flexural Bed Joint Crack Patterns at the Ultimate Load Level.

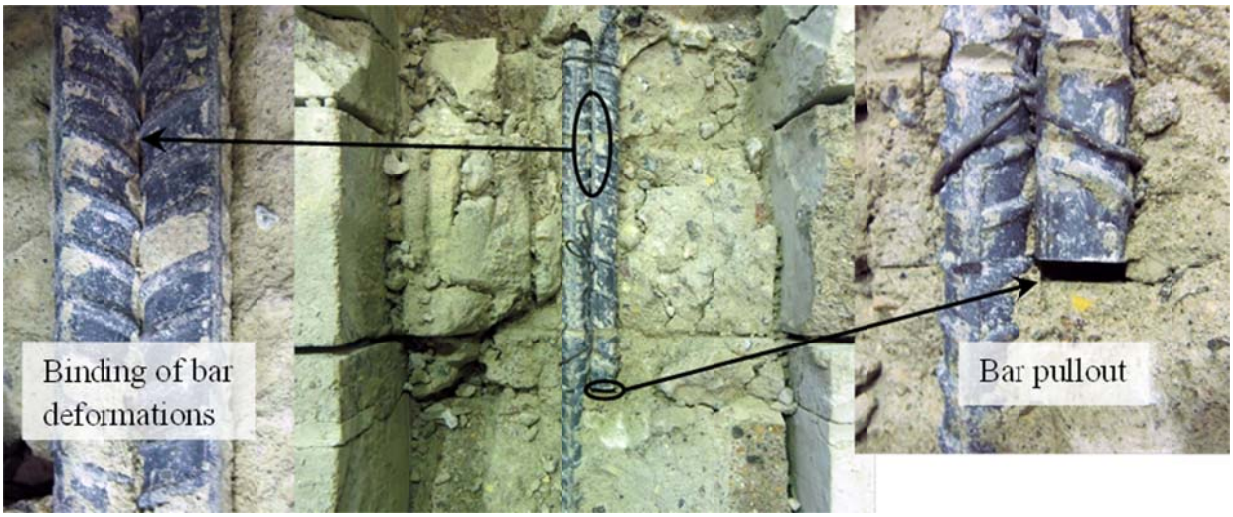

Figure 4.4: Representative Internal Distress of the CLS Specimens.

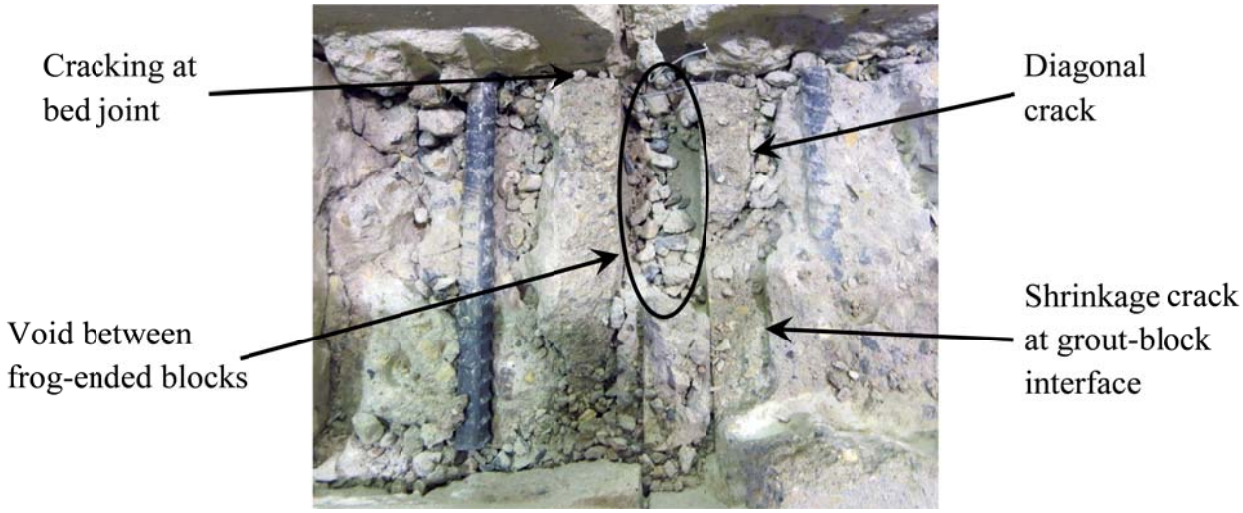

Figure 4.5: Representative Internal Distress of the NCLS and GCC Specimens.

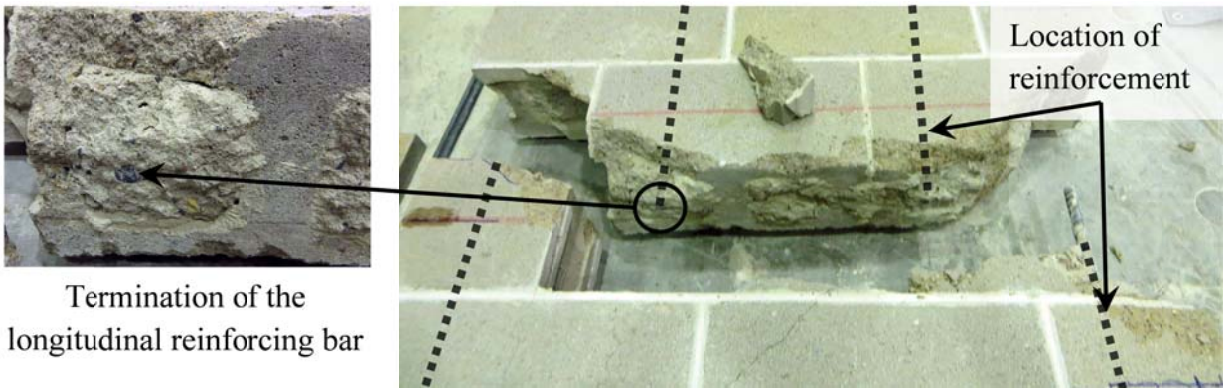

Figure 4.6: Bed and Head Joint Crack Pattern in Specimens Without Knock-out Webs.

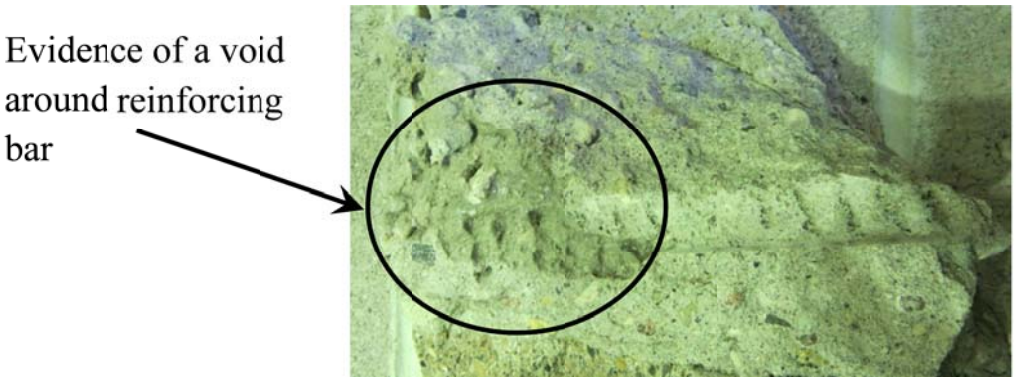

Figure 4.7: Inadequate Grout Consolidation Around the Longitudinal Reinforcing Bar in the Splice Region of the NCLS#3 Wall Splice Specimen.

Figure 4.8: Inadequate Grout Consolidation Around the Longitudinal Reinforcing Bar in the Splice Region of the GCC#2 Wall Splice Specimen: (a) End View, and (b) Side View.

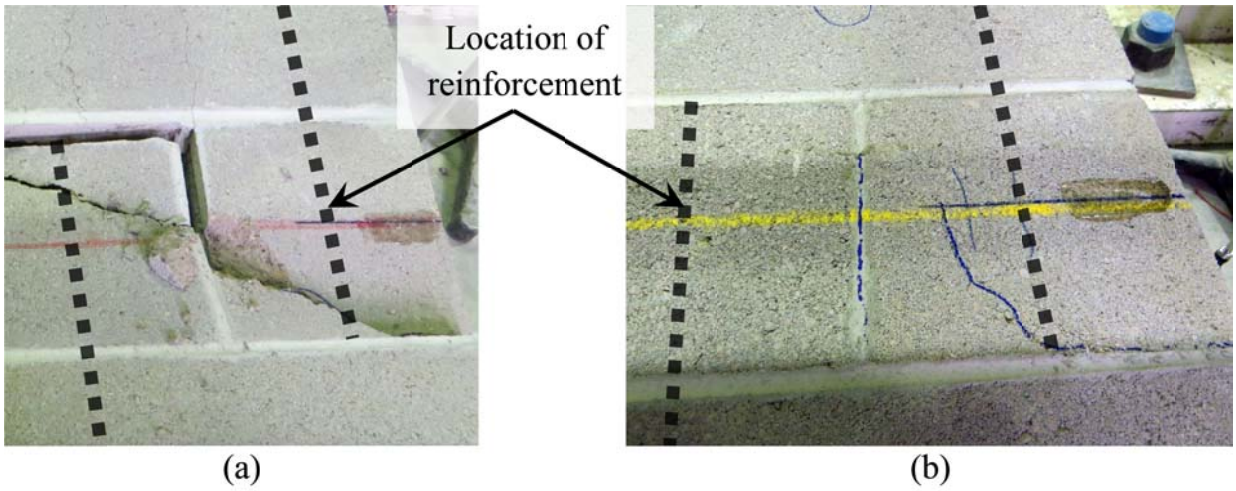

Figure 4.9: Typical Midspan Crack Pattern on the Compression Face at Failure: (a) NCLS, and (b) 1KO and 3KO Wall Splice Specimens.

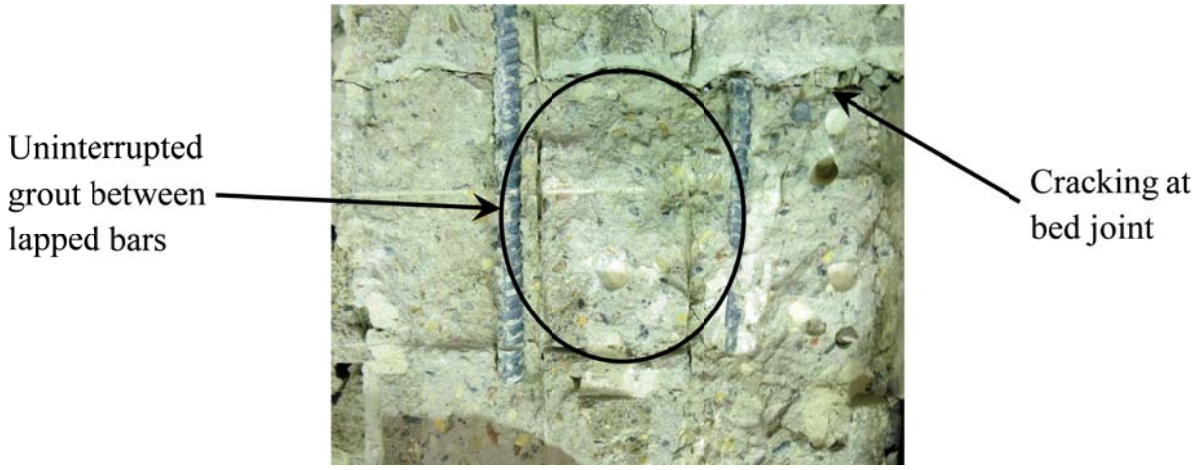

Figure 4.10: Representative Internal Distress of the 1KO and 3KO Wall Splice Specimens.

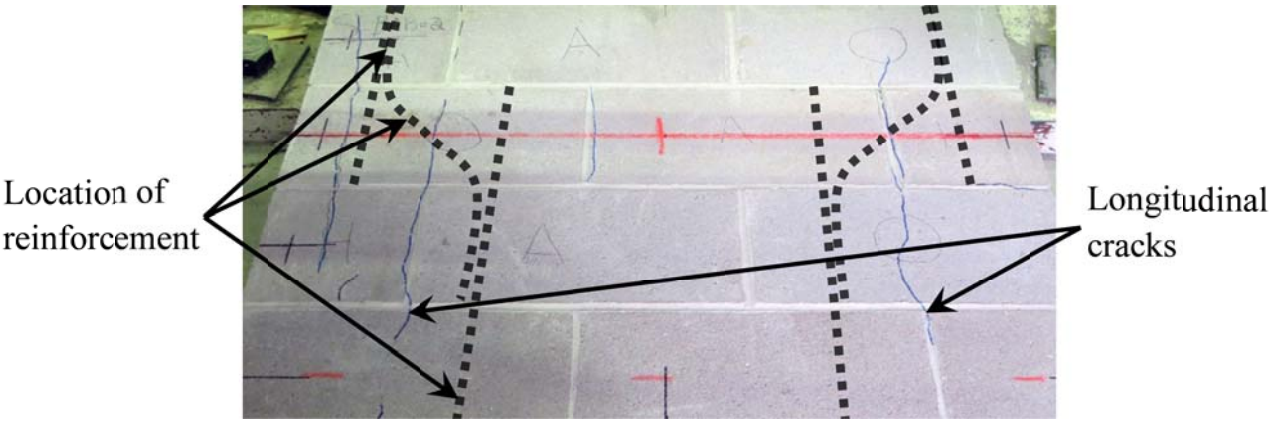

Figure 4.11: Longitudinal Cracks on the Compression Face of a Representative SBAR Wall Splice Specimen.

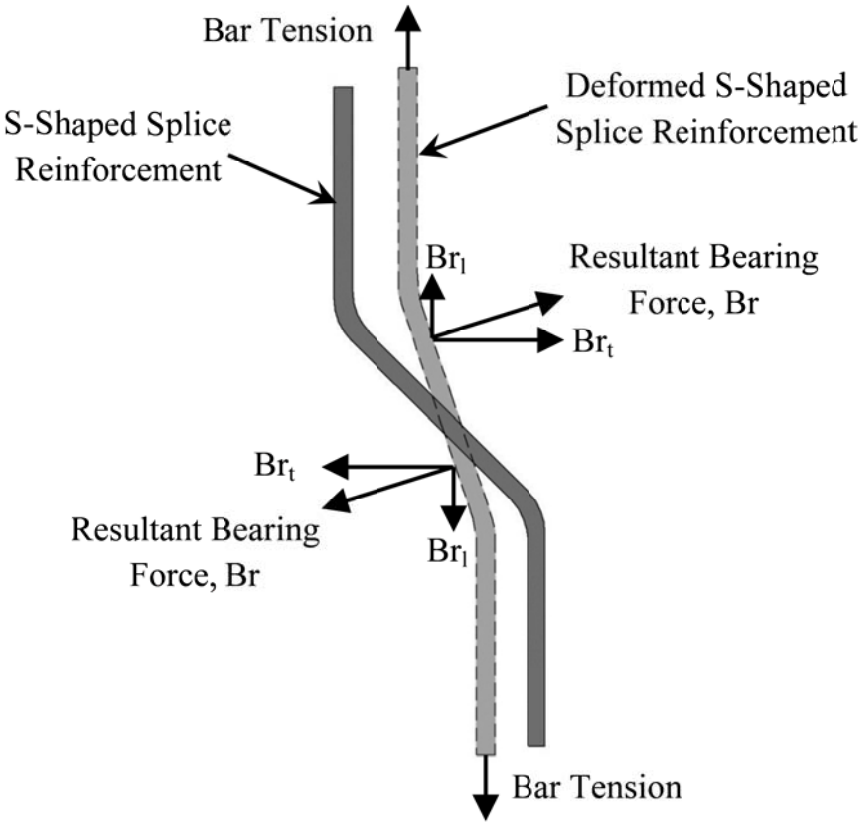

Figure 4.12: Bearing Forces Caused by the Straightening of the S-Shaped Splice Reinforcement When Subjected to Tension.

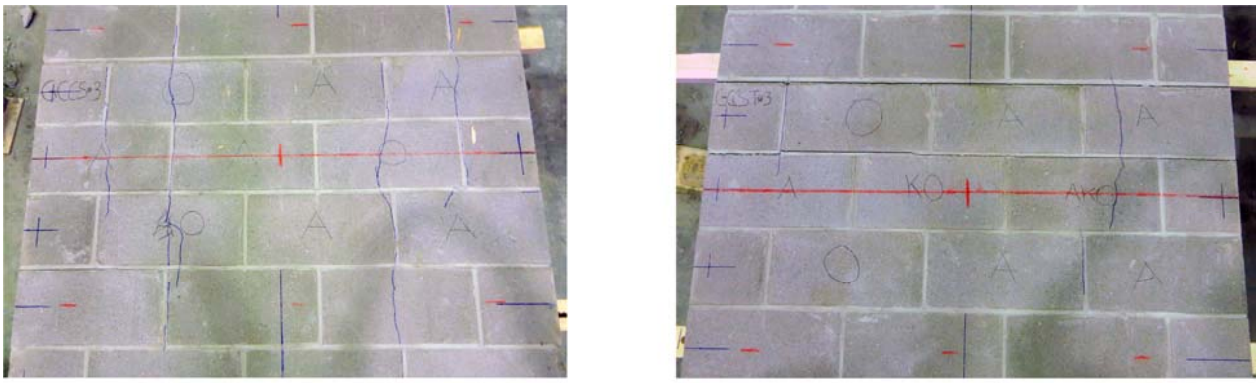

(a) (b)

Figure 4.13: Comparison of Longitudinal Cracks on the Compression Face: (a) Representative C-SBAR, and (b) Representative CT-SBAR Wall Splice Specimens.

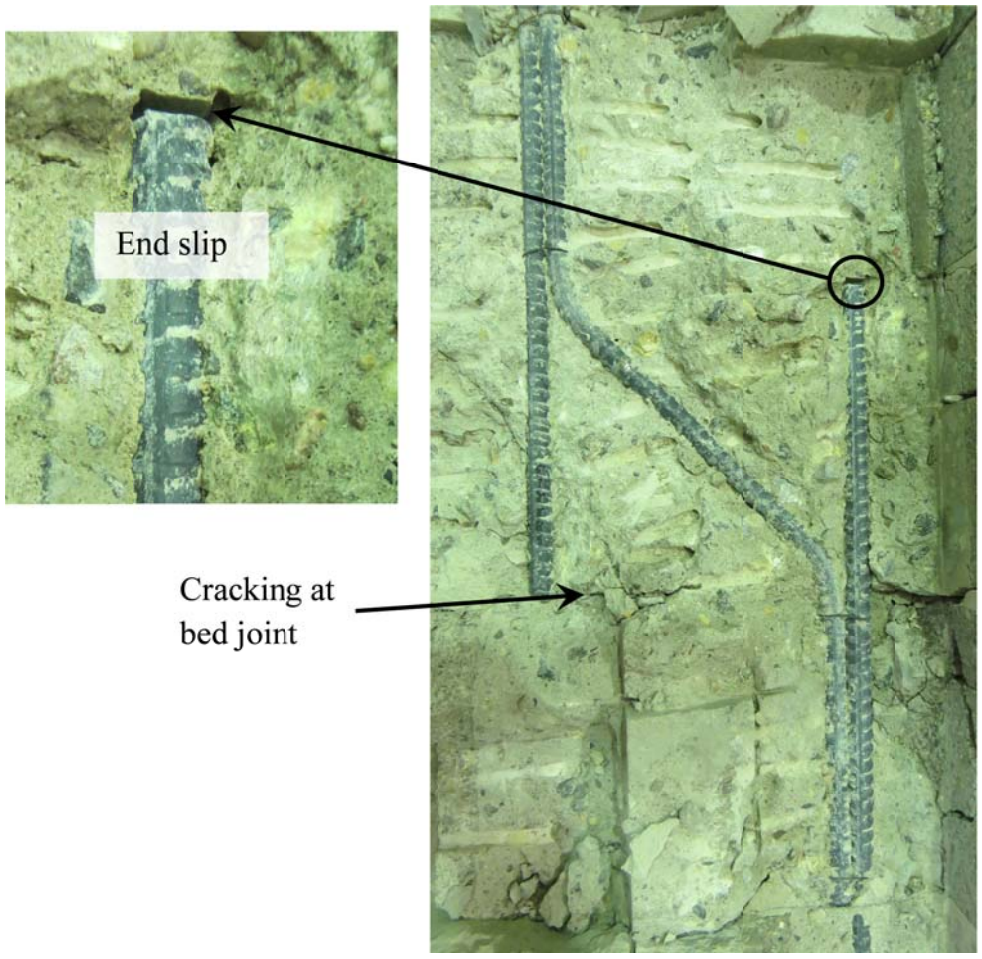

Figure 4.14: Representative Internal Distress of the SBAR Wall Splice Specimens.

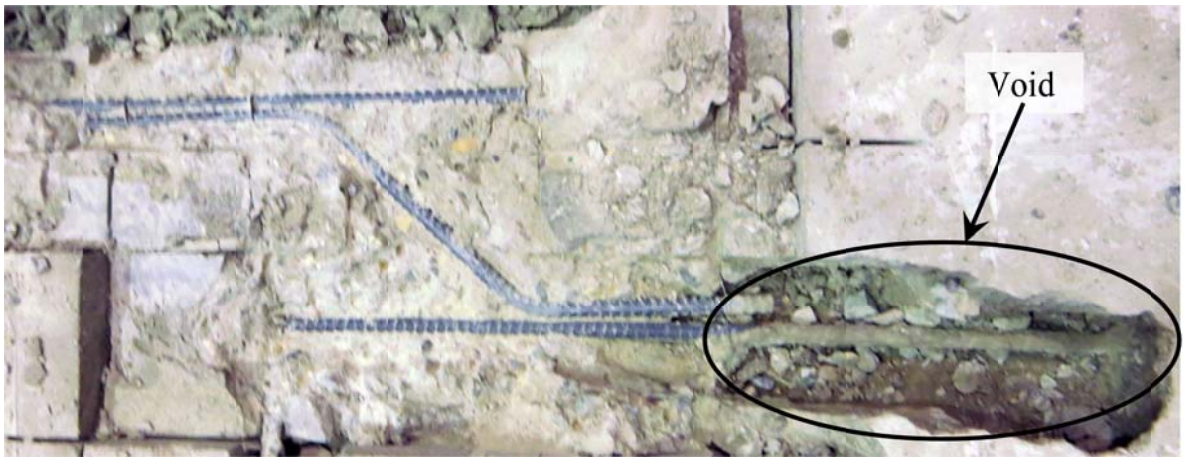

Figure 4.15: Inadequate Grout Consolidation Around Longitudinal Reinforcing Bar Outside the Splice Region of the SBAR#3 Wall Splice Specimen.

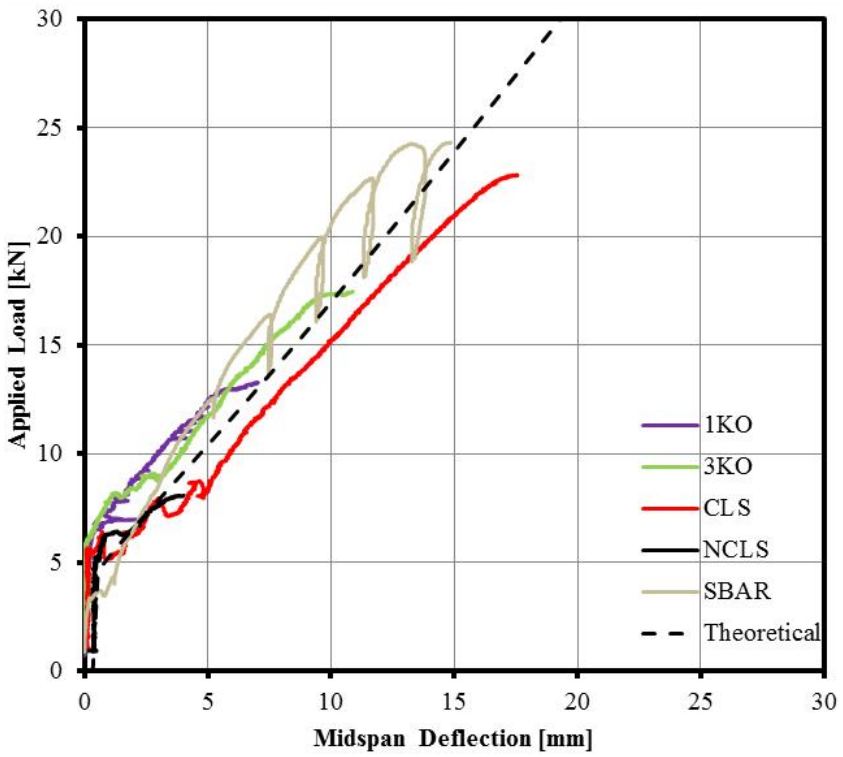

(a)

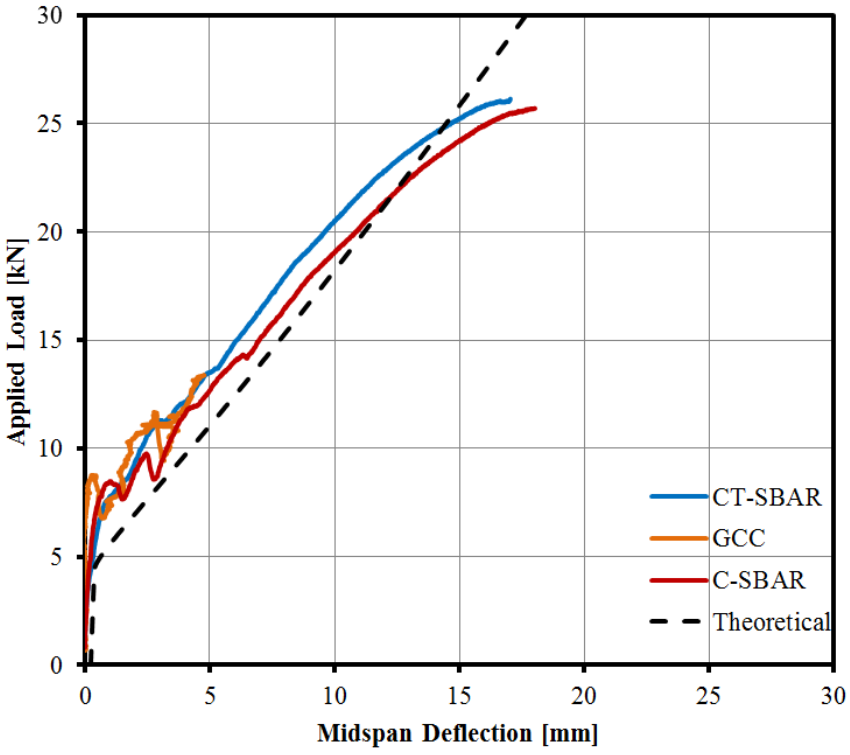

(b)

Figure 4.16: Representative Load Versus Deflection Relationships: (a) 2.5 Block-Wide Wall Splice Specimens, and (b) 3.5 Block-Wide Wall Splice Specimens.

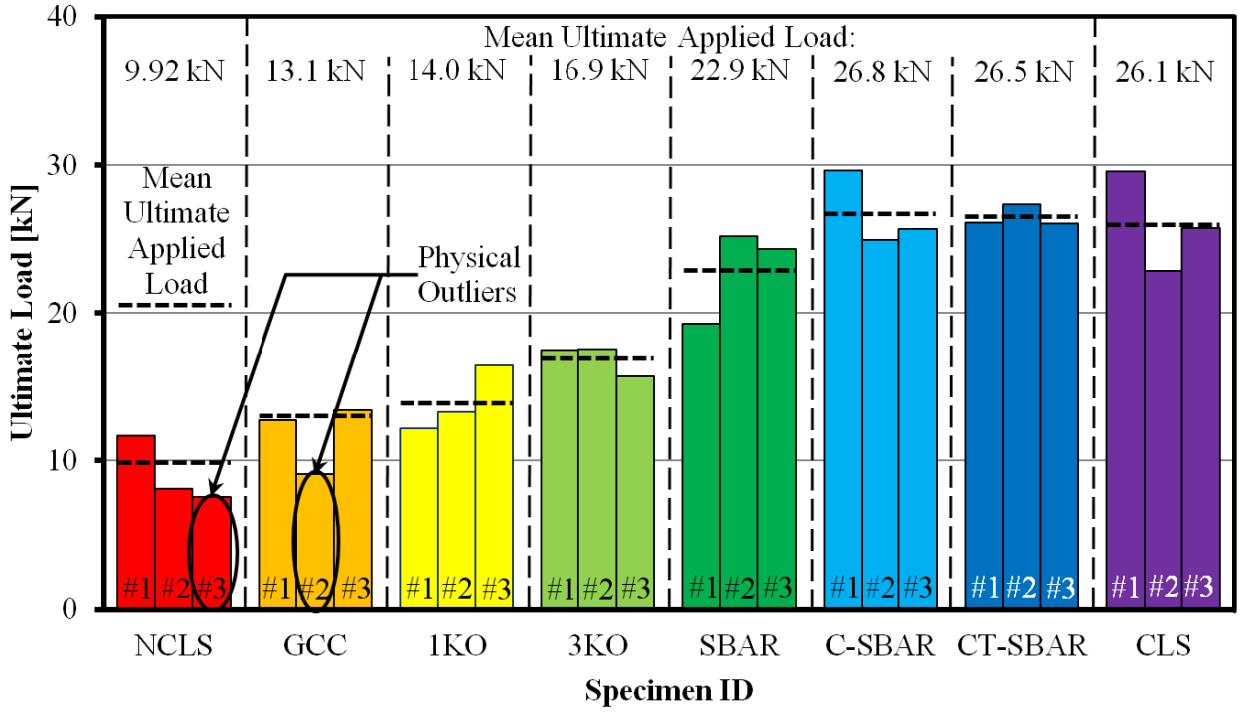

*Physical outliers contained air pockets around the reinforcing steel in the lap splice region; therefore, they were not included in the calculation of the average ultimate load for each wall splice specimen set.

Figure 4.17: Ultimate Load Comparison for the Different Wall Splice Specimen Sets

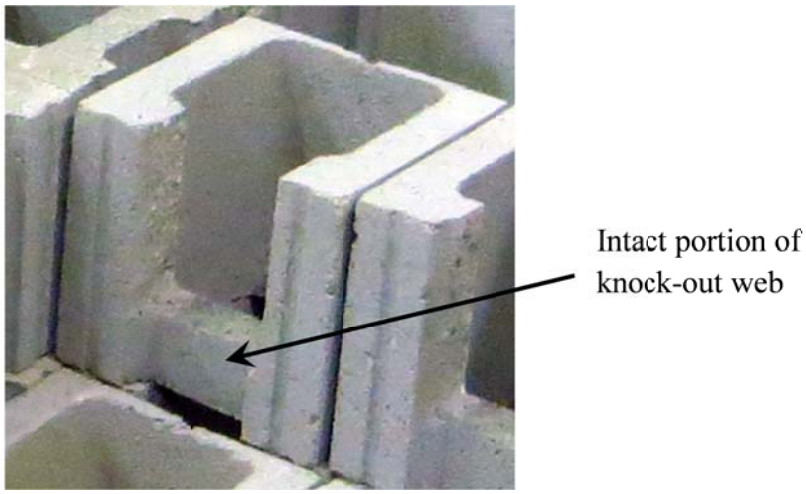

Figure 4.18: Intact Portion of Knock-out Web on Half Block to Facilitate Construction.

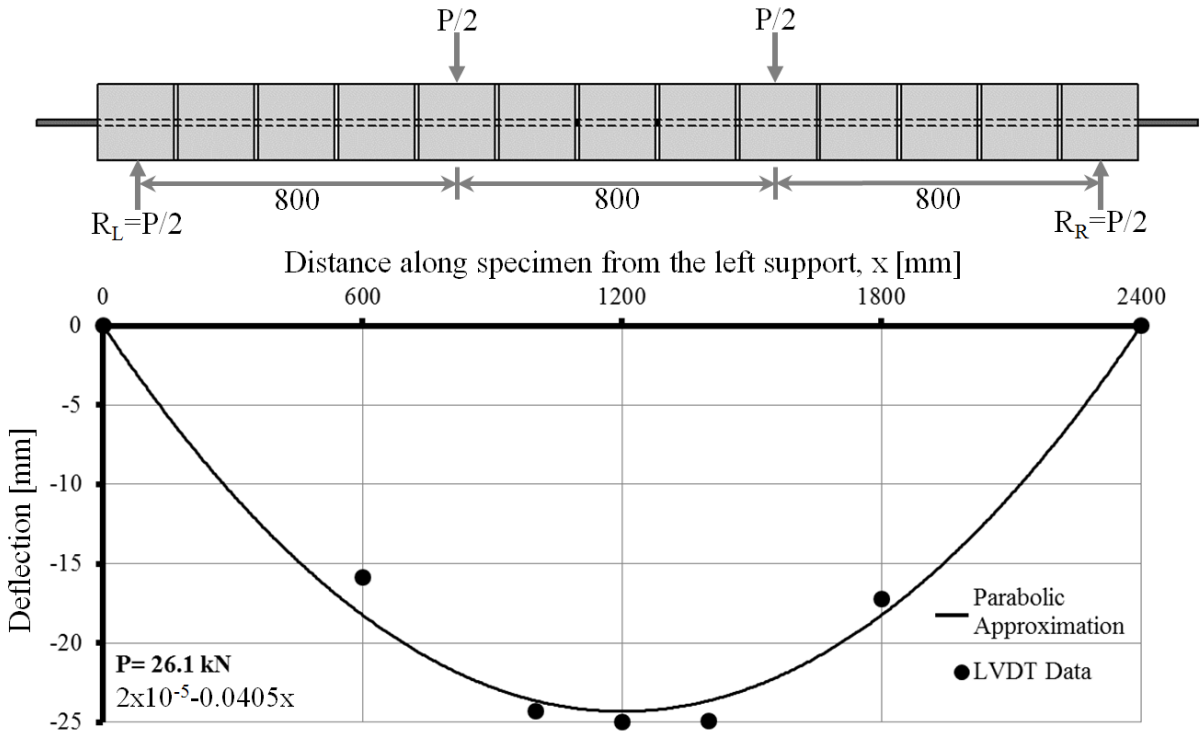

Figure 4.19: Experimental Deflection Profile Plotted with Parabolic Approximation at the Ultimate Applied Load – Specimen CT-SBAR#3.

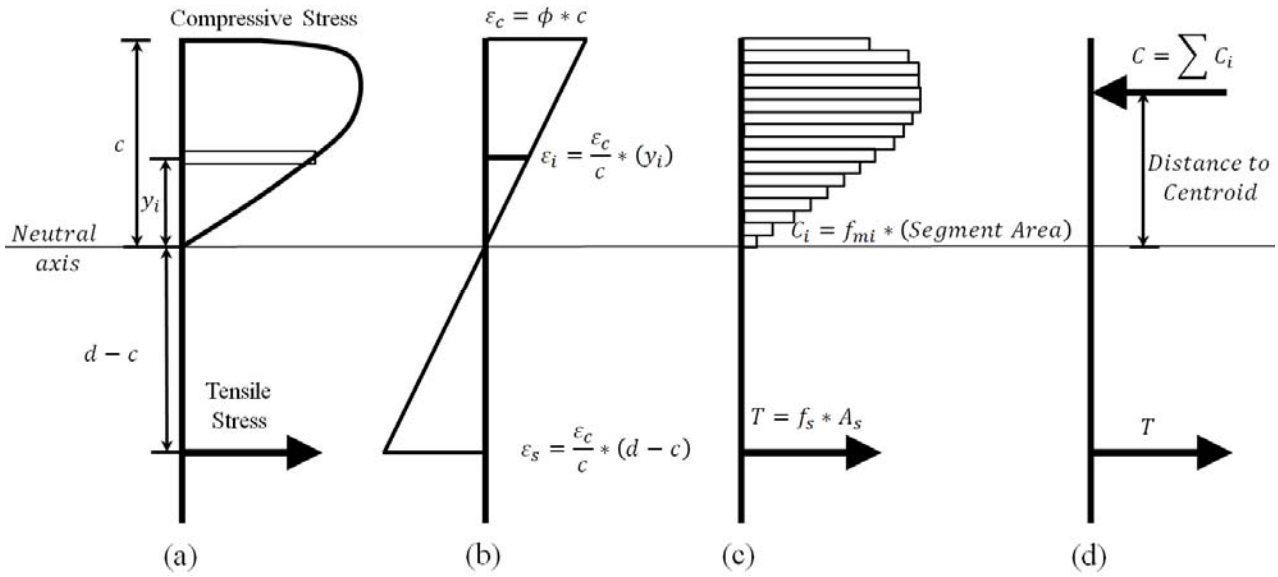

Figure 4.20: Wall Splice Specimen-Sectional Analysis: (a) Stress Distribution, (b) Strain Profile, (c) Force Distribution, and (d) Simplified Force Distribution.

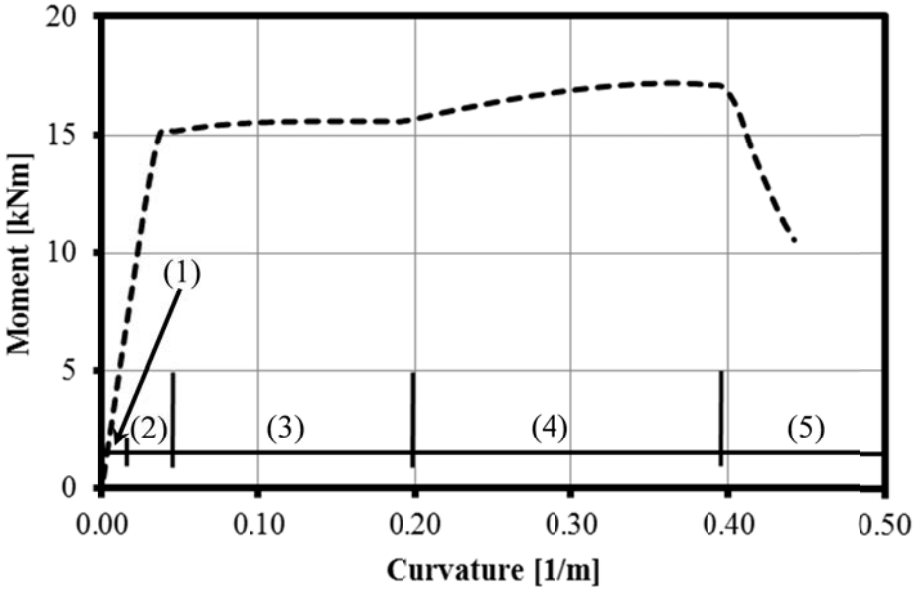

Figure 4.21: Representative Theoretical Moment – Curvature Profile Used for Wall Splice Specimen Analysis.

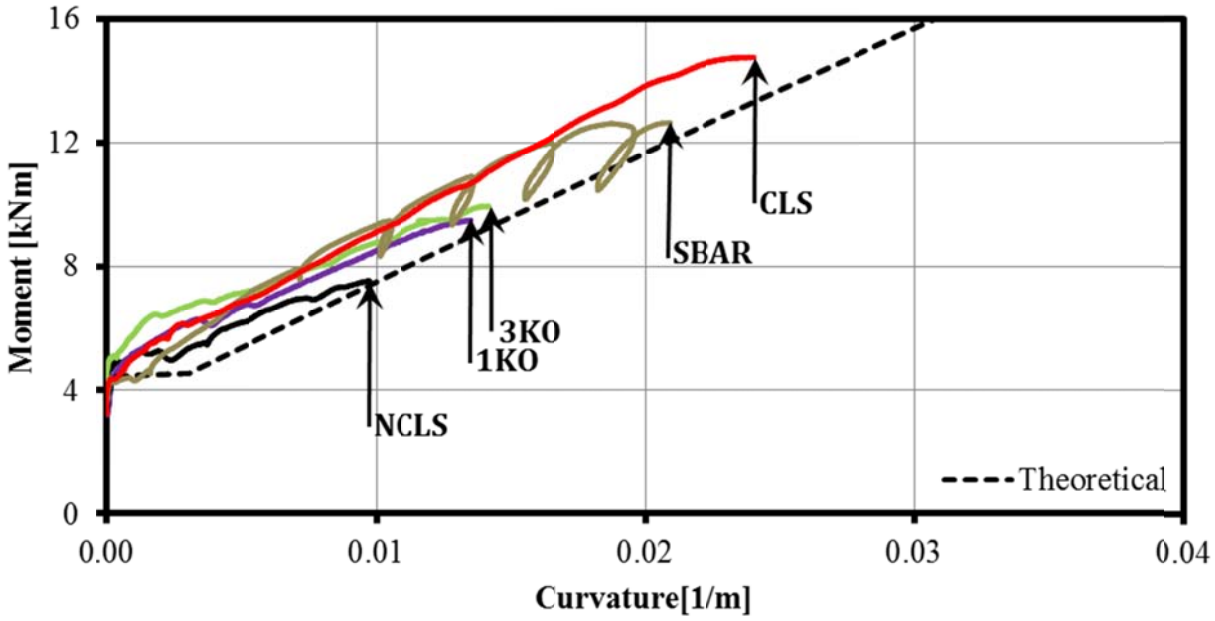

(a)

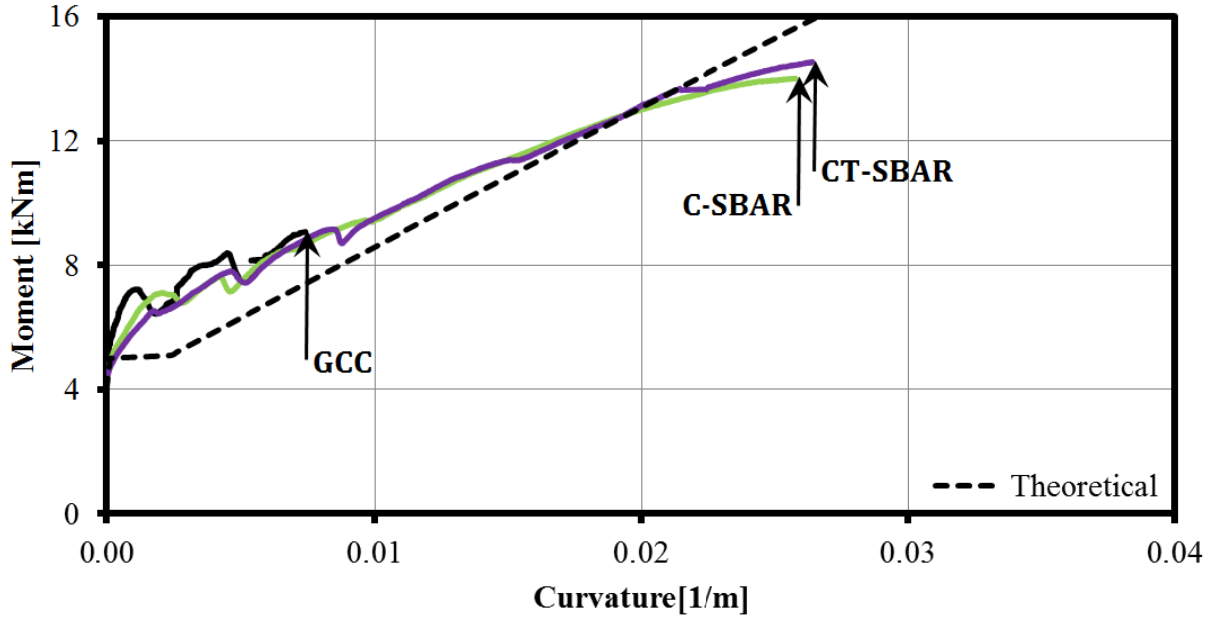

(b)

Figure 4.22: Representative Experimental and Theoretical Moment Curvature Relationships: (a) 2.5 Block-Wide Wall Splice Specimens, and (b) 3.5 Block-Wide Wall Splice Specimens.

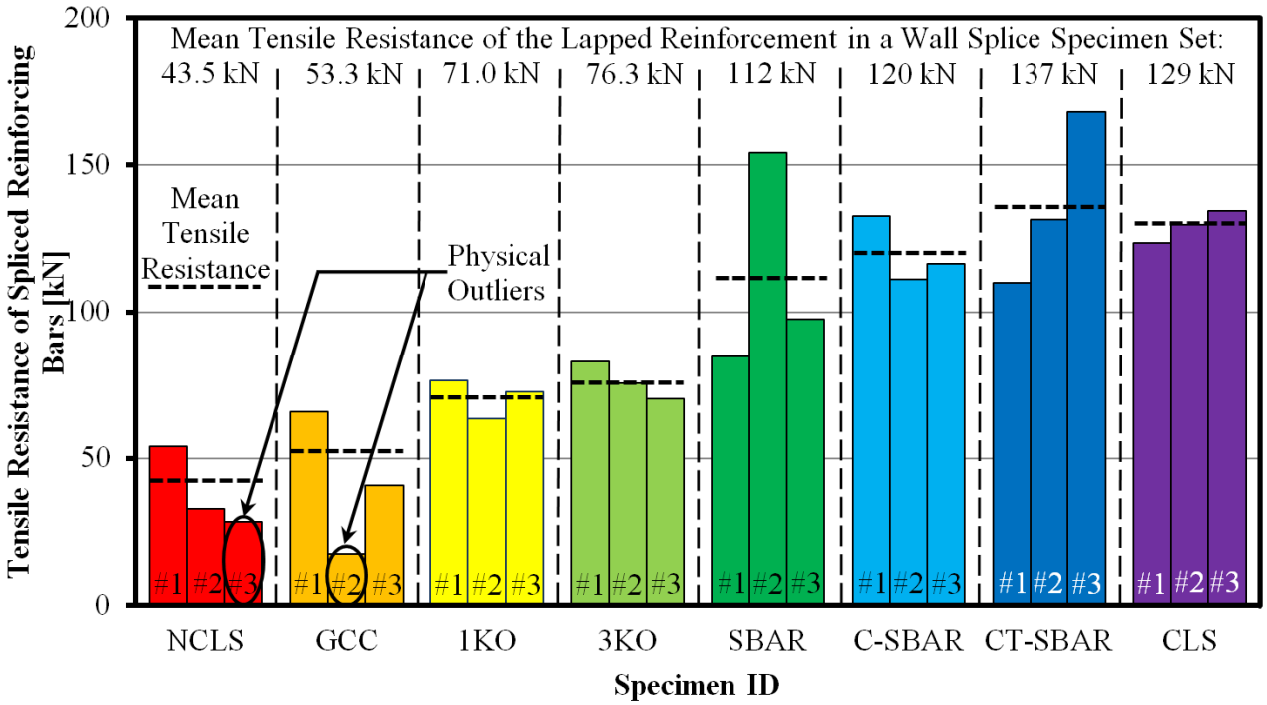

*Physical outliers contained air pockets around the reinforcing steel in the lap splice region; therefore, they were not included in the calculation of the average tensile resistance of each wall splice specimen set.

Figure 4.23: Tensile Resistance Comparison for the Different Wall Splice Specimen Sets.

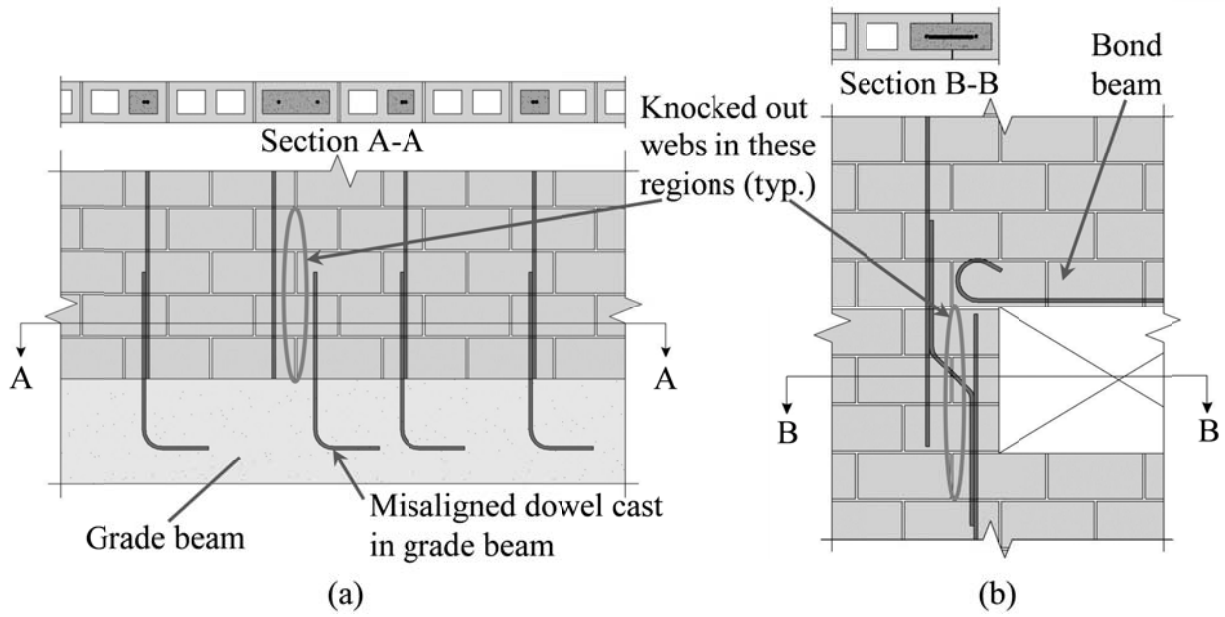

Figure 4.24: Practical Implications: (a) Knock-out Webs to Compensate for Misaligned Dowel and (b) S-Shaped Splice Reinforcement Adjacent to an Opening.

CHAPTER 5: CONCLUSIONS AND RECOMMENDATIONS

5.1 Overview

Twenty-four wall splice specimens were tested over two construction phases. Six unique remedial techniques applied to non-contact lap splices were tested and the results were compared to unaltered contact and non-contact lap splices which were constructed as controls. Three replicate specimens for each remedial and control splice detail were constructed in an effort to obtain a meaningful mean tensile resistance for each specimen set. Every wall splice specimen was reinforced with No. 15 Grade 400 deformed reinforcing bars with a 200 mm lap splice length at the midspan. The properties of the materials that were used to construct the reinforced masonry assemblages were maintained as consistently as was practically possible between the construction phases and the individual batches within each phase. Companion testing confirmed the properties of the materials used in the construction of the wall splice specimens conformed to relevant CSA and ASTM standards.

The wall splice specimens were tested horizontally under a monotonic, four-point loading geometry. Load and deflection data were recorded throughout testing at a rate of 2 Hz by an automated data acquisition system. The resulting data, along with the self-weight of the specimen, were then used in an iterative moment-curvature analysis to calculate the maximum tensile resistance of the two pairs of spliced reinforcing bars used to reinforce each wall splice specimen. The calculated maximum tensile resistance and the recorded midspan deflection at the ultimate applied load were then each averaged to determine the respective mean values for each of the eight specimen sets. The resulting mean values for the maximum tensile resistance and midspan deflection at the ultimate applied load where then compared to determine comparative structural performance for all specimen sets. Recommended multiplication factors to quantify the tensile resistance of non-contact lap splices with applied remedial measures were then calculated. These values were based on the comparison of the maximum tensile resistance of the various lap splice details tested in this investigation.

Practical implications of each splice detail were then assessed based on the qualitative data gathered from the construction process and discussions with industry professionals. Examples of potential designs and select construction situations where the remedial measures could be

implemented were presented. The summarized conclusions addressing the primary objectives stated in Section 1.2 are reported in the following section.

5.2 Summary of Findings

The following conclusions are based on the testing and analysis summarized in the previous section, and address each of the specific objectives presented in Section 1.2.

5.2.1 Establishing the Increase in the Capacity of Non-Contact Lap Splices Using Remedial Measures

The results of the theoretical analysis showed that the mean maximum tensile resistance of the lapped reinforcement in the control specimens with contact lap splices was 129 kN. The mean maximum tensile resistance of the lapped reinforcement in the 3.5 block-wide wall splice specimens with three courses of knock-out webs, s-shaped, and transverse splice reinforcement was 137 kN. These results indicated that this non-contact lap splice detail was able to achieve a similar magnitude of tensile resistance as contact lap splices. It also shows that noticeable improvements were made to the tensile resistance of the lapped reinforcement since the spliced reinforcing bars in the control wall splice specimens with standard non-contact lap splices of the same splice length had a mean maximum tensile resistance of 43.5 kN. This represents a 215% increase in the mean maximum tensile resistance of the lapped reinforcement with the combination of previously stated remedial measures, compared to the wall splice specimens with standard non-contact lap splices. The increase in the tensile resistance of the spliced reinforcing bars was the result of a combination of different factors. The additional stiffness from the larger specimens as well as the installation of the transverse reinforcement at splice level increased the confinement in this region and likely delayed the onset of splitting failure. The installation of the knock-out webs and s-shaped reinforcement allowed for a more adequate force transfer between the lapped bars which increased the tensile resistance of the spliced reinforcement.

5.2.2 Formulation of Multiplication Factors for Remediated Non-Contact Lap Splices

A set of multiplication factors, based on the test results of the remedial measures, was calculated to quantify the available tensile resistance of non-contact lap splices with remedial measures. These results were scaled to the findings by Ahmed and Feldman (2012) which indicated that non-contact lap splices had only 71% of the available tensile resistance compared to lapped bars

that were in contact. A factor of 0.80 was recommended for non-contact lap splices where knock-out webs are installed within the splice length of the lapped reinforcing bars. Non-contact lap splices located at the edge of a masonry assemblage (ie. no confinement) with s-shaped reinforcement installed at the splice level were assigned a correction factor of 0.90. A factor of 0.95 was recommended for non-contact lap splices with s-shaped reinforcement installed at splice level that have at least one grouted confinement cell on either side of the lapped reinforcing bars. If transverse reinforcement is also installed with this splice geometry, the multiplication factor can be increased to 1.0.

5.2.3 Deflection Profiles of the Remediated Non-Contact Lap Splices

The mean midspan deflection at the ultimate load for the control wall splice specimens with contact lap splices was 17.0 mm. The 2.5 block-wide wall splice specimens with s-shaped splice reinforcement within the splice region was the only wall splice specimen set with this type of splice reinforcement that could be compared to the control contact lap splice specimen set as they were both 2.5 blocks wide. The mean midspan deflection at the ultimate applied load of the 2.5 block-wide specimens with s-shaped reinforcement was 17.2 mm, thus matching performance of the wall splice specimens with contact lap splices. However, the increase in the midspan deflection was almost proportional to the increase in the ultimate applied load. This does not represent a noticeable increase in the flexibility of the masonry assemblage as a result of the installation of remedial measures within the splice region.

5.2.4 Failure Modes Observed for the Remedial Measures

Cracking in the bed joint located in the same plane as the termination of the longitudinal reinforcing bars was prominent in every wall splice specimen tested. Internal distresses were also examined as the block face shell and grout were incrementally removed in the splice region. Loss of bond between the steel reinforcement and the grout was observed in the control wall splice specimens with contact lap splices. This was demonstrated by the gap between the location where the encapsulated end of the longitudinal reinforcing bar was at the time of grout consolidation and the post-test position. A comparison of the internal distresses of the wall splice specimens with remedial splice details revealed that the remedial measures which included the installation of s-shaped reinforcement and knock-out webs within the splice region also showed similar internal

distresses. This indicates that they were likely subject to the same failure mode as the control wall splice specimens with contact lap splices.

5.2.5 Ease of Implementation of the Remedial Measures

Industry professionals have indicated that the production of knock-out webs and splice reinforcement would not be difficult in field situations. Installing knock-out webs within the length of a non-contact lap splice can be achieved in any situation since the remedial measure is confined within the splice length. This makes it suitable for the remediation of non-contact lap splices identified in construction situations. This includes situations where the splice length is governed by the length of dowel projecting above a previously cast grade beam or when a non-contact lap splice is requested by the mason to alleviate reinforcement crowding. Test results indicated that the installation of s-shaped reinforcement within the splice region enhances the tensile resistance of the lapped bars to similar levels as contact lap splices. However, the proper installation of this remedial measure requires that the location of the non-contact lap splice be known and accessible at least one lap length below the splice region such that the s-shaped reinforcing bar can be spliced with the lower lapped longitudinal bar. This remedial technique is therefore more suited for non-contact lap splices identified in the design phase and cannot be used for misaligned dowels protruding from a previously cast grade beam.

5.3 Recommendations for Future Investigations

Financial and practical considerations provided a limited scope for the investigation of remedial measures applied to non-contact lap splices in masonry construction: three replicates of eight unique splice details were constructed and evaluated. Useful information was gathered from this research program but further investigations related to non-contact lap splices in masonry construction would supplement the findings from this study. The recommendations for future investigations include:

- The construction of sufficient replicates of full-scale, 3.5 block-wide, wall splice specimens with combinations of knock-out webs, s-shaped, and transverse reinforcement installed in the splice region to allow for a statistical comparison to control wall splice specimens with standard contact and non-contact lap splices.

- A parametric investigation of different splice lengths and bar sizes in full-scale, 3.5 block-wide, wall splice specimens with combinations of knock-out webs, s-shaped, and transverse reinforcement. This will provide a database of test results for the development of reliability-based design provisions for non-contact lap splices in masonry design codes and guides.

- In the current investigation, the lapped longitudinal reinforcing bars terminated within the bed joint, which is a known plane of weakness for masonry assemblages in flexure. The results of each wall splice specimen set were still valid and could be compared since all of the lapped longitudinal reinforcing bars terminated in the bed joints. Spliced reinforcing bars which terminate within the bed joints should be compared to lapped bars of the same splice length which terminate at the mid-height of the masonry block to determine the magnitude of the effect this has to the flexural capacity of the masonry assemblage. This can be achieved by replacing a course of full-height masonry blocks with a course of half-height masonry blocks at the bottom and top of the wall splice specimen. This would provide a quantitative data set to determine the sensitivity of the flexural capacity for these two geometries.

- The s-shaped reinforcing bars evaluated in this investigation were symmetrically installed within the lap splice length. This caused the s-shaped splice reinforcement to extend one lap length below the original splice length of the lapped longitudinal bars and thus limited type of splice situations this remedial measure could be used in. A future study should examine the possibility of a non-symmetrical remedial measure where the s-shaped reinforcing bar is installed at a higher elevation so that its bottom end does not extend below the elevation of original lap length. This could potentially still allow for the s-shaped reinforcement to transfer the tensile forces between the lapped bars while permitting it to be installed in a wider array of situations where non-contact lap splices are unintentionally encountered. This includes situations where the splice length is governed by the length of dowel projecting above a previously cast grade beam.

REFERENCES

Abrams, D.A., “Tests of Bond Between Concrete and Steel,” University of Illinois Bulletin No. 71, University of Illinois Urbana-Champaign, Urbana, IL, 1913.

Ahmadi, B.H., “Effect of Loss of Bond in Lap Splices of Flexurally Loaded Reinforced Concrete Masonry Walls,” Material and Structures, Vol. 34, October, 2001, pp. 475 -478.

Ahmed, K., “Evaluation of Contact and Non-Contact Lap Splices in Concrete Block Masonry Specimens,” M.Sc. Thesis, University of Saskatchewan, Saskatoon, SK, 2011.

Ahmed, K., Feldman, L.R., “Evaluation of Contact and Noncontact Lap Splices in Concrete Block Masonry Construction,” Canadian Journal of Civil Engineering, Vol. 39 Issue 5, pp. 515-523, 2012.

ASTM International. (2008) “E178-08: Standard Practice for Dealing with Outlying Observations” ASTM Standards, West Conshohocken, PA, USA.

ASTM International. (2012a) “A370-12: Standard Test Methods and Definitions for Mechanical Testing of Steel Products” ASTM Standards, West Conshohocken, PA, USA.

ASTM International. (2012b) “C1019-12: Standard Test Method for Sampling and Testing Grout” ASTM Standards, West Conshohocken, PA, USA.

ASTM International. (2012c) “C140-12: Standard Test Methods for Sampling and Testing Concrete Masonry Units and Related Units” ASTM Standards, West Conshohocken, PA, USA.

Baynit, A.R., “Bond and Development Length in Reinforced Concrete Block Masonry,” M. Eng. Thesis, Carleton University, Ottawa, ON, 1980.

Bischoff, P.H., Moxon, D., “Shrinkage Wreaks Havoc with Tension Stiffening in Reinforced Masonry Test Specimens,” 10 page paper published in the CD-ROM proceedings of the 9th Canadian Masonry Symposium, June 4 – 6, 2005, Fredericton, New Brunswick.

Branson, D.E., “Instantaneous and Time Dependant Deflections of Simple and Continuous Reinforced Concrete Beams” HPR Report No. 7, Part 1, Alabama Highway Department, Bureau of Public Roads, Alabama, 1965.

Canadian Standards Association. (1977) “CAN/CSA S304-77: Masonry Design and Construction for Buildings” CSA, Rexdale, Ontario, Canada.

Canadian Standards Association. (2003) “CAN/CSA A3004-C2: Test Method for the Determination of Compressive Strengths” CSA, Rexdale, Ontario, Canada.

Canadian Standards Association. (2004a) “CAN/CSA A165-04: Concrete Masonry Units” CSA, Rexdale, Ontario, Canada.

Canadian Standards Association. (2004b) “CAN/CSA A179-04: Mortar and Grout for Unit Masonry” CSA, Rexdale, Ontario, Canada.

Canadian Standards Association. (2004c) “CAN/CSA A23.1-04: Concrete Materials and Methods of Concrete Construction” CSA, Rexdale, Ontario, Canada.

Canadian Standards Association. (2004d) “CAN/CSA A23.3-04: Design of Concrete Structures” CSA, Rexdale, Ontario, Canada.

Canadian Standards Association. (2004e) “CAN/CSA S304.1-04: Design of Masonry Structures” CSA, Rexdale, Ontario, Canada.

Canadian Standards Association. (2009) “CAN/CSA G30.18-09: Carbon Steel Bars for Concrete Reinforcement” CSA, Rexdale, Ontario, Canada.

Cheema, T.S., Klingner, R.E., “Design Recommendations for Tensile Anchorages of Deformed Reinforcement in Grout Concrete Masonry,” ACI Journal, September – October, 1985, pp. 616 - 621.

Drysdale, R.G., Hamid, A.A., “Masonry Structures: Behaviour and Design” Canadian Masonry Design Centre, Mississauga, ON, 2005.

Feldman, L.R., Bartlett, F.M., “Bond Stresses Along Plain Steel Reinforcing Bars in Pullout Specimens,” ACI Structural Journal, V-104, No. 6, November – December, 2007, pp. 685 - 692.

Hamid, A., “Design and Construction of Reinforced Masonry in North America,” Proceedings of the 6th Conference of Seismology and Earthquake Engineering, pp. 179-196, 2004, Guimarães, Portugal.

Kent, D.C., Park, R. (1971) “Flexural Members with Confined Concrete,” Journal of the Structural Division, ASCE, Vol. 97, No. ST7, pp 1969-1990.

Kisin, A., Feldman, L.R., “Construction Solutions for Non-Contact Lap Splices in Concrete Block Construction,” 11 page paper published in the USB proceedings of the 12th Canadian Masonry Symposium, June 2 – 5, 2013, Vancouver, British Columbia.

NCMA, “Evaluation of Minimum Reinforcing Bar Splice Criteria for Hollow Clay Brick and Hollow Concrete Block Masonry,” National Concrete Masonry Association, Report No. 12, Herndon, Virginia, July, 1999.

Sagan, B.E., Gergely, P., White, R.N., “Behaviour and Design of Non-Contact Lap Splices Subjected to Repeated Inelastic Tensile Loading,” ACI Structural Journal, V-88, No. 4, July – August, 1991, pp. 420 - 431.

Sanchez, D., Feldman, L.R., “The Effect of Transverse Bar Spacing on the Resistance of Lap Spliced Bars in Concrete Block Construction,” 11 page paper published in the USB proceedings of the 12th Canadian Masonry Symposium, June 2 – 5, 2013, Vancouver, British Columbia.

Soric, Z., Tulin, L.G., “Bond Stress Deformation in Pull-out Masonry Specimens,” ASCE Journal of Structural Engineering, Vol. 115 No. 10, October 1989, pp. 2588-2602.

Schuller, M.P., Hammons, M.I., Atkinson, R.H., “Interim Report on a Study to Determine the Lap Splice Requirements for Reinforced Masonry,” ASTM Special Publication STP 1180: Masonry: Design and Construction Problems and Repairs, eds. J.M Melander & L.R. Lauersdorf, Philadelphia, PA, 1993, pp. 75 – 90.

Suter, G.T., Fenton, G.A., “Splice Length Tests of Reinforced Masonry Walls,” Proceedings of the 3rd North American Masonry Conference, June 3-5, 1985, Arlington, Texas.

Udey, A., Sparling, B.F., “Realistic Wind Loading on Unreinforced Masonry Walls,” 11 page paper published in the USB proceedings of the 12th Canadian Masonry Symposium, June 2 – 5, 2013, Vancouver, British Columbia.

Uniat, D.B., “Lap Splices of Deformed Bars in Reinforced Concrete Block Masonry Walls,” M. Eng. Thesis, Carleton University, Ottawa, ON, 1983.

APPENDICES

APPENDIX 3A: PHASE 1A SPECIMEN GEOMETRY

This appendix presents the configuration, construction, and testing method associated with the specimens tested in Phase 1a. These wall splice specimens were mistakenly constructed with a 240 mm lap splice length and therefore could not be compared directly to the specimens constructed in Phases 1 and 2 that had the intended 200 mm splice length. The results for the Phase 1a specimens are located in Appendix 4A.

Table 3A-1 shows the general description of the 12 wall splice specimens constructed in Phase 1a. All wall splice specimens were 13 courses tall and constructed in a running bond and were reinforced with No. 15 Grade 400 deformed steel bars. Each wall splice specimen contained two lapped bars to maintain symmetry within each specimen and eliminate the effects of the eccentricity that result when wall splice specimens are constructed with non-contact lap splices. The reinforcing bars extended 190 mm beyond the top and bottom of the wall splice specimens to accommodate the installation of end anchorages which ensured that bond failure occurred within the lap splice region. The rationale for all the wall splice specimens constructed in Phase 1a is described in the following sections.

Transverse Reinforcement Specimen (TBAR)

Sagan et. al. (1991) showed that the addition of transverse reinforcement in the splice region of non-contact lap splices in reinforced concrete specimens resulted in a 30 to 40% increase in the tensile capacity of the lapped bars. The rationale behind the TBAR wall splice specimens was to see whether the addition of transverse reinforcement had the same effect for non-contact lap splices in masonry construction.

Figure 3A-1 shows the cross-section, elevation, and side view of the 2.5 block-wide TBAR wall splice specimens. The placement of the longitudinal reinforcing bars within the wall splice specimen was identical to the NCLS specimens described in Section 3.4.2. The webs of the masonry at splice level were knocked out using the same techniques employed on the Phase 1 and 2 specimens that included knock-out webs. This allowed for the installation of the transverse reinforcing bar, shown in Figure 3A-1, within the splice region. The transverse reinforcing bars consisted of No. 15 Grade 400 deformed reinforcing steel bar with a hook in the excess of 180 degrees at each end. The 100 mm inside radius of these hooks complied with CSA A23.1-04

(CSA, 2004c). The transverse reinforcing bar was installed prior to the placement of the eighth course and was tied to the lower longitudinal bars to ensure its proper positioning during grout placement. Consultations with industry professionals suggested that the installation of knock-out webs in masonry construction does not affect the overall constructability of the masonry assemblage.

Specimens with S-Shaped Reinforcement (SBAR-1a)

Figure 3A-2 shows the cross-section, elevation, and side view of the 2.5 block-wide SBAR-1a wall splice specimens. The description and rationale behind these specimens is identical to the SBAR specimens described in Section 3.4.6.

Ungrouted Confinement Cell Specimen (UGCC)

The rationale behind the UGCC specimens is similar to the Fully Grouted Confinement Cell Specimens (GCC) detailed in Section 3.4.3. Grout was not placed in the cells that did not contain longitudinal reinforcement to simulate a partially grouted masonry wall. Minimizing the number of grouted cells in a masonry wall reduces labour and materials which results in a more cost effective design. This makes partially grouted masonry walls common in many field situations.

Figure 3A-3 shows the cross-section, elevation, and side view of the Ungrouted Confinement Cell Specimens (UGCC). These specimens were 3.5 blocks wide which allowed for one un-grouted external cell on each side of the specimen. Placement of the reinforcement within the wall splice specimen was identical to the NCLS specimens described in Section 3.4.2. These specimens were used to determine if wider, partially grouted wall splice specimens have any effect on the tensile resistance of non-contact lap splices, where the lapped bars are located in adjacent cells.

Specimens with S-Shaped Reinforcement and Un-Grouted Confinement Cells (UGC-SBAR)

The rationale behind the UGC-SBAR specimens is similar to the specimens with s-shaped splice reinforcement and grouted confinement cells (CT-SBAR). Grout was not placed in the cells that did not contain longitudinal reinforcement for the same reason explained in the section describing the UGCC specimens above.

Figure 3A-4 shows the cross section, elevation, and side view of the UGC-SBAR. The s-shaped splice reinforcement was the same as the C-SBAR wall splice specimens detailed in Section 3.4.7. The geometry of the knock-out webs was also similar to the C-SBAR specimens with the addition of further knock-out webs at splice level between the two pairs of lapped bars to allow for the placement of the horizontal transverse reinforcement at splice level.

The UGC-SBAR wall splice specimens were constructed with the intention of determining whether the tensile resistance of non-contact lap splices could be further enhanced by combining the previously detailed s-shaped transverse reinforcement and un-grouted confinement cells.

Construction and Testing

The construction and testing of these specimens was identical to the wall splice specimens constructed in Phases 1 and 2 and is detailed in Section 3.6 and 3.7, respectively.

Table 3A-1: Phase 1a Specimen Construction Schedule

Phase	Specimen Width [Blocks]	Specimen ID	Specimen Configuration	Splice Length [mm]
1a	2.5	TBAR	Three knock-out web courses allowing for uninterrupted grout placement between cells within, above, and below the splice length as well as transverse reinforcement at splice level.	240
	2.5	SBAR-1a	Three knock-out web courses allowing for uninterrupted grout placement between cells within, above, below the splice length, with s-shape splice bars also included.	240
	3.5	UGCC	Un-grouted outside and centre cells (ie unreinforced cells).	240
	3.5	UGC-SBAR	Three knock-out web courses allowing for uninterrupted grout placement between cells within, above, below the splice length, and a s-shape splice bar is also included. The outside and centre un-reinforced cells remain un-grouted.	240

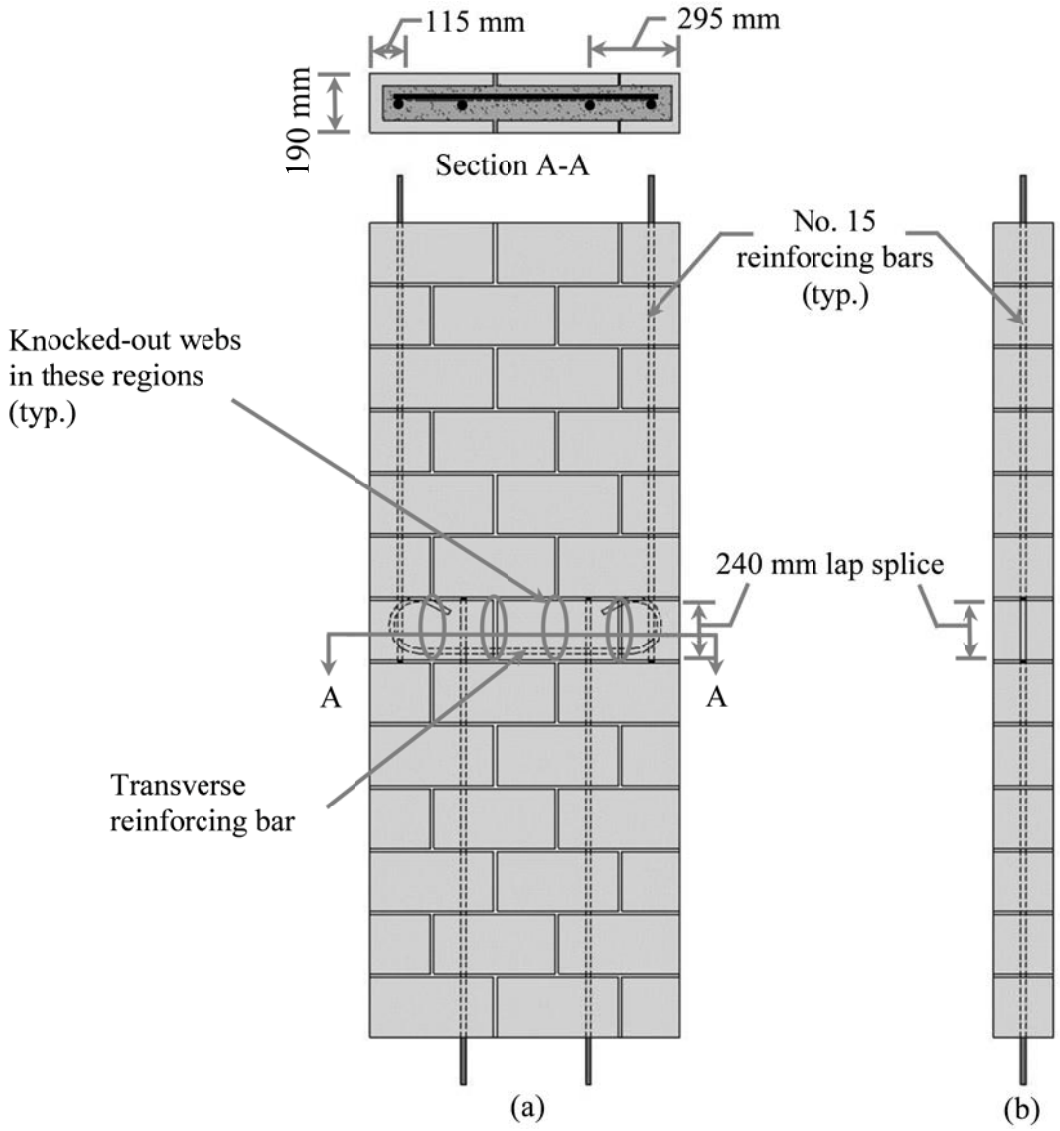

Figure 3A-1: Remedial Wall Splice Specimen with Transverse Splice Reinforcement (TBAR): (a) Elevation Including a Section at Splice Level, and (b) Side Profile.

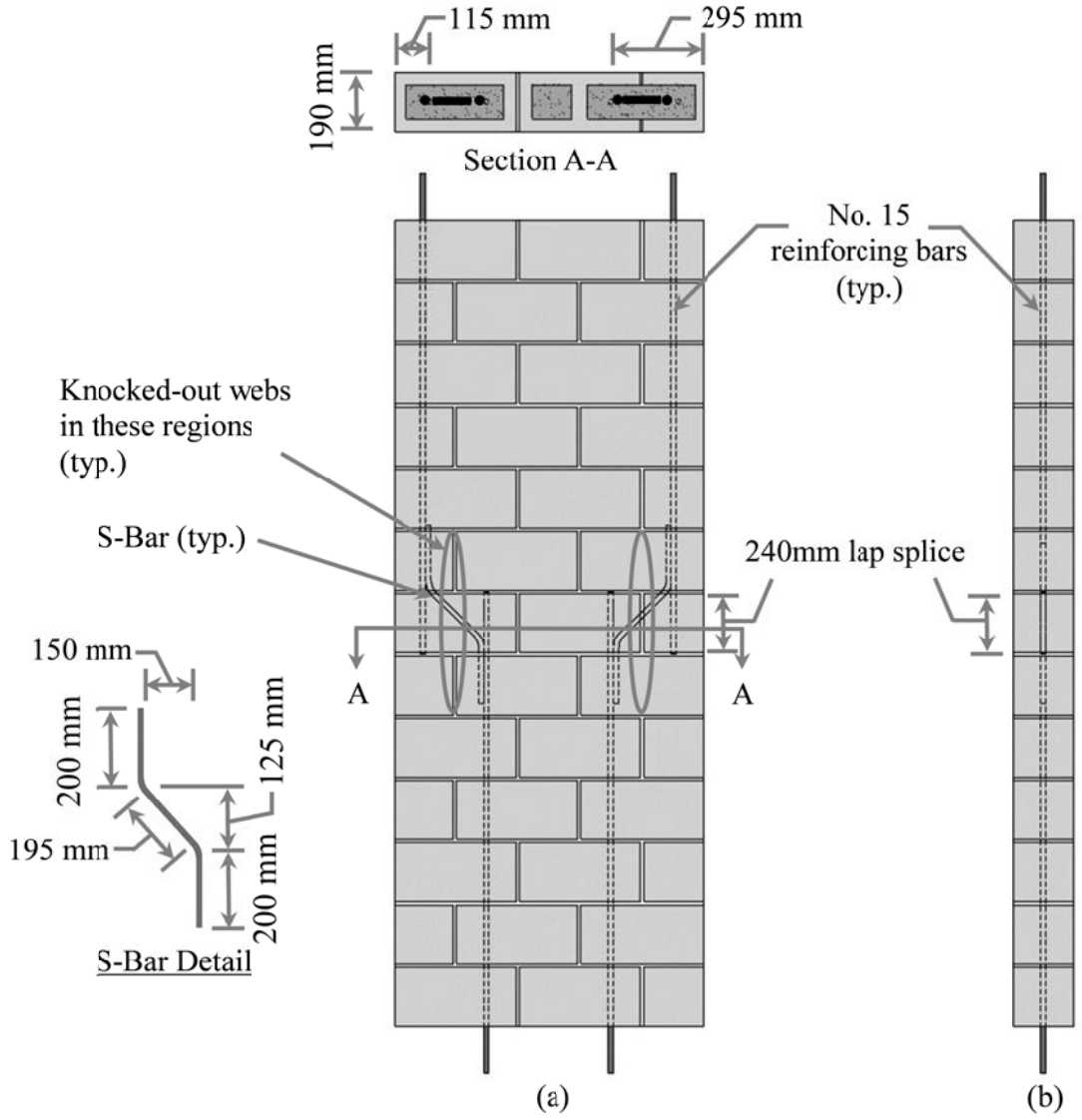

Figure 3A-2: Remedial Wall Splice Specimen with S-Shaped Splice Reinforcement (SBAR-1a)：(a) Elevation Including a Section at Splice Level, and (b) Side Profile.

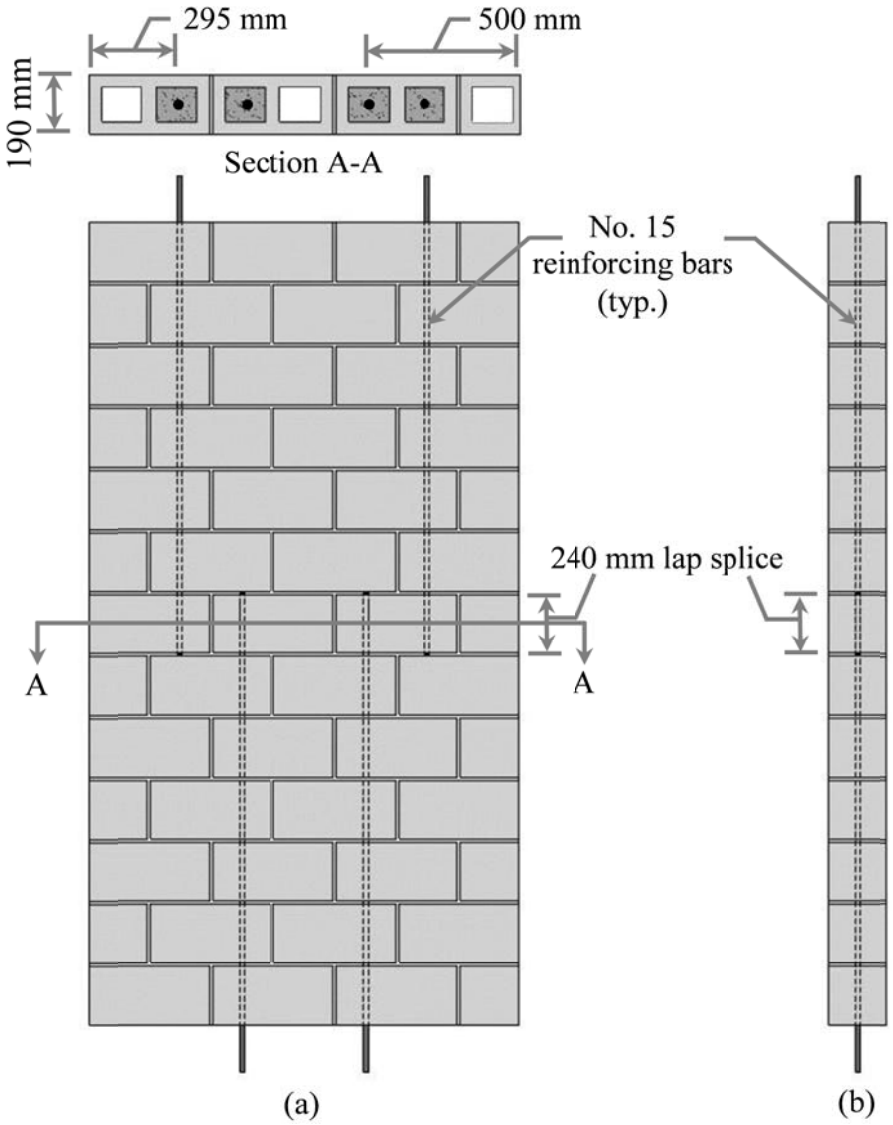

Figure 3A-3: Remedial Wall Splice Specimen with Un-Grouted Confinement Cells (UGCC): (a) Elevation Including a Section at Splice Level, and (b) Side Profile.

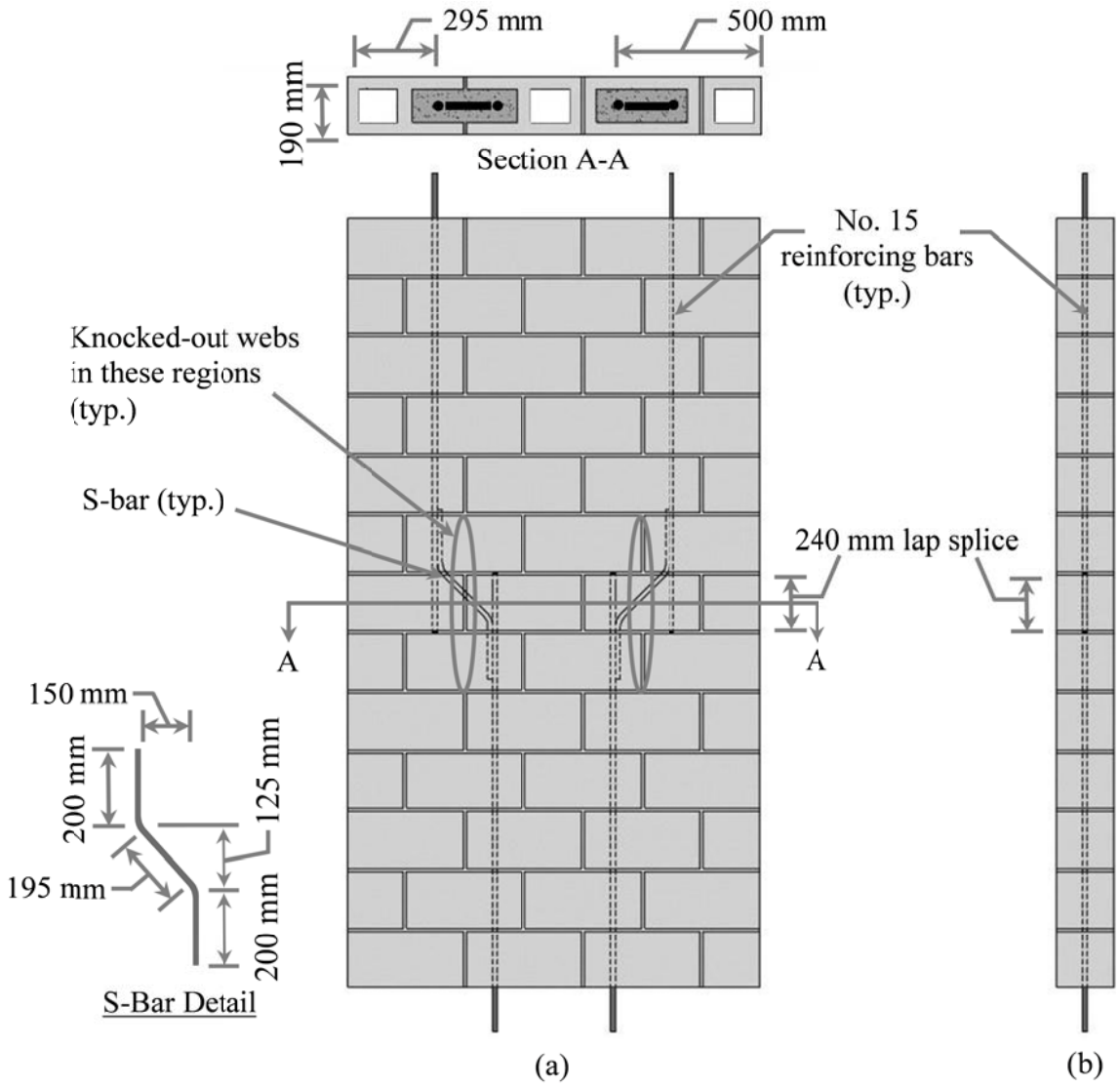

Figure 3A-4: Remedial Wall Splice Specimen with S-Shaped Splice Reinforcement and Un-Grouted Confinement Cells (UGC-SBAR): (a) Elevation Including a Section at Splice Level, and (b) Side Profile.

APPENDIX 3B: AGGREGATE GRADATIONS

This appendix presents the gradation for the two different aggregates used in the construction of the wall splice specimens. Table 3B-1 shows the gradation of the aggregate used in the mortar. Table 3B-2 to Table 3B-4 show the gradation of the aggregate used in the grout. The gradation of both aggregates was determined using the protocols specified in CSA A179-04 (CSA, 2004b). The required gradations, as specified by CSA A179-04 (CSA, 2004b), for both aggregate types are presented in the respective tables as a reference. The requirements for the aggregate gradations of are specified in CSA A179-04 (CSA, 2004b) and were met by the aggregate used in this study.

Table 3B-1: Gradation of Aggregate Used in the Mortar.

ISO Sieve Size	Cumulative % Passing						
	Phase 1			Phase 2			CSA A179-04 (2004b) Requirements
	Sample 1	Sample 2	Sample 3	Sample 1	Sample 2	Sample 3	
5 mm	100	100	100	100	100	100	100
2.5 mm	99	99	99	99	99	99	90-100
1.25 mm	97	97	97	97	97	97	85-100
630 µm	90	90	91	91	92	92	65-95
315 µm	53	63	64	46	55	55	15-80
160 µm	17	17	18	14	15	16	0-35

Table 3B-2: Gradation of Aggregate Used in the Grout for the Phase 1 Wall Splice Specimens.

ISO Sieve Size	Cumulative % Passing							
	Phase 1						CSA A179-04 (2004b) Requirements	
	Sample 1		Sample 2		Sample 3			
	Fine	Coarse	Fine	Coarse	Fine	Coarse	Fine	Coarse
14 mm	--	100	--	99	--	97	--	100
10 mm	--	69	--	78	--	71	--	85-100
5 mm	100	24	100	25	100	19	100	10-30
2.5 mm	100	12	100	13	100	10	90-100	0-10
1.25 mm	100	0	100	0	100	0	85-100	0-5
630 µm	73	--	60	--	54	--	65-95	--
315 µm	11	--	6	--	5	--	15-80	--
160 µm	2	--	1	--	1	--	0-35	--

Table 3B-3: Gradation of Aggregate Used in the Grout for the Phase 1a Wall Splice Specimens.

ISO Sieve Size	Cumulative % Passing							
	Phase 1a						CSA A179-04 (2004b) Requirements	
	Sample 1		Sample 2		Sample 3			
	Fine	Coarse	Fine	Coarse	Fine	Coarse	Fine	Coarse
14 mm	--	100	--	96	--	100	--	100
10 mm	--	81	--	71	--	75	--	85-100
5 mm	100	27	100	22	100	23	100	10-30
2.5 mm	100	14	100	12	100	11	90-100	0-10
1.25 mm	100	0	100	0	100	0	85-100	0-5
630 µm	79	--	78	--	78	--	65-95	--
315 µm	22	--	21	--	21	--	15-80	--
160 µm	3	--	3	--	3	--	0-35	--

Table 3B-4: Gradation of Aggregate Used in the Grout for the Phase 2 Wall Splice Specimens.

ISO Sieve Size	Cumulative % Passing							
	Phase 2						CSA A179-04 (2004b) Requirements	
	Sample 1		Sample 2		Sample 3			
	Fine	Coarse	Fine	Coarse	Fine	Coarse	Fine	Coarse
14 mm	--	88	--	80	--	85	--	100
10 mm	--	69	--	58	--	67	--	85-100
5 mm	100	36	100	29	100	30	100	10-30
2.5 mm	100	20	100	16	100	16	90-100	0-10
1.25 mm	100	0	100	0	100	0	85-100	0-5
630 µm	73	--	72	--	73	--	65-95	--
315 µm	16	--	16	--	16	--	15-80	--
160 µm	3	--	3	--	3	--	0-35	--

APPENDIX 4A: PHASE 1A EXPERIMENTAL RESULTS

The results of the Phase 1a wall splice specimens and the corresponding companion specimens are presented in this appendix. These specimens were unintentionally constructed with a 240 mm lap splice length instead of the 200 mm lap splice length used in the wall splice specimens constructed in Phases 1 and 2. The difference in the lap splice length did not allow for a direct comparison between the results for the Phase 1a specimens and the specimens constructed in Phases 1 and 2.

Companion Specimen Test Results

Table 4A-1 details the number of mortar cubes, grout tests, and masonry prisms evaluated in Phase 1a. The table also presents the mean maximum compressive stress for each specimen type and the coefficient of variation.

The mortar cube construction and testing procedures are detailed in Sections 3.6.2 and 3.7.3, respectively. One statistical outlier was identified at the 95% confidence level using the procedure detailed in ASTM E178-08 (ASTM, 2008). The possible explanation for this outlier is the same as the one given in Section 4.1.1 for the outliers identified in Phases 1 and 2. The result from the outlying mortar cube test was not included in the calculation of the mean maximum stress and the coefficient of variation for Phase 1a.

The construction and testing of both the non-absorptive grout cylinders and absorptive grout prisms are detailed in Sections 3.6.3 and 3.7.3, respectively. Four non-absorptive grout cylinders and one absorptive grout prism were identified as statistical outliers at the 95% confidence level using the procedure detailed in ASTM E178-08 (ASTM, 2008). The possible explanations for these outliers are the same as those given in Section 4.1.2 for the outliers identified in Phases 1 and 2. The results from these tests were not included in the calculation of the mean maximum stress and the coefficient of variation reported in Table 4A-1.

Six concrete blocks were selected at random during the construction of the Phase 1a wall splice specimens and set aside for compression testing. Table 4A-1 shows the mean ultimate compressive strength and coefficient of variation for the concrete blocks tested in Phase 1a. The detailed results from each block test are shown in Appendix 4B. All the blocks tested achieved,

as a minimum, the nominal compressive strength of 15 MPa and there were no outliers identified using the procedure detailed in ASTM E178-08 (ASTM, 2008) at the 95% confidence level.

The geometry and construction procedure of the three different prism geometries is discussed in Section 3.6.4, while the testing procedure is detailed in Section 3.7.3. The results from the three block-high, stack bond prisms are discussed in this appendix as only their results were used to quantify the material properties of their representative wall splice specimens. Table 4A-1 shows the mean maximum compressive strength and coefficient of variation for the three block-high, stack bond masonry prisms. The results from each individual prism are presented in Appendix 4C.

The steel reinforcing bars used in the Phase 1a wall splice specimens originated from the same heat batch as the reinforcement used in the Phase 1 specimens. Table 4.3 presents a summary of the tensile properties of the steel reinforcing bars while the individual tensile test results are shown in Appendix 4B.

Tensile Capacity of the Spliced Reinforcement

The tensile resistance of the lapped reinforcement was calculated using the ultimate moments, reported in Table 4A-2, and the moment-curvature analysis detailed in Section 4.4.1. Table 4A-2 shows that the mean tensile resistance of the pair of lapped bars in the TBAR and SBAR-1a wall splice specimens was 131 kN (COV 8.38%) and 141 kN (COV 6.47%), respectively. This equated to a 7% increase in the average tensile capacity of the lap splices and a 30% decrease in the coefficient of variation between the two lap splice details. The reduction in the coefficient of variation was likely due to the increased number of knock-out webs installed between the lapped longitudinal bars in the SBAR-1a specimens. The increased number of knock-out webs reduced the likely hood of the diagonal compressive struts being intercepted by the grout-block interface and thus increased the capacity of their tensile resistance. Large longitudinal cracks were present between the lapped reinforcing bars on the compression face of the SBAR-1a specimens, similar to those shown in Figure 4.11. The likely cause of these cracks is the same as what was explained in Section 4.2 for the specimens with s-shaped splice reinforcement in Phase 2. A post-test investigation of the TBAR specimens did not reveal evidence of longitudinal cracks between the

lapped reinforcement which indicated that the transverse reinforcement provided some confinement within the splice region.

Table 4A-2 also shows that the mean tensile resistance of the pair of lapped bars in the UGCC and UGC-SBAR wall splice specimens was 120 kN (COV 5.57%) and 177 kN (COV 0.53%), respectively. This equated to a 32% increase in the average tensile capacity of the lapped reinforcement and a 950% decrease in the coefficient of variation between the two lap splice details. These performance increases are directly attributed to the installation of the three courses of knock-out webs and the s-shaped splice reinforcement. Large longitudinal cracks were also present between the lapped reinforcing bars on the compression face of the UGC-SBAR specimens, similar to SBAR-1a specimens.

The results of the Phase 1a wall splice specimens were used to refine the specimen designs tested in Phase 2. The transverse reinforcement in the TBAR specimens was deemed to not have a large enough impact on the tensile capacity compared to the s-shaped reinforcement in the SBAR-1a specimen to be rebuilt in Phase 2 with the correct, 200 mm, lap splice length. The transverse reinforcement was used in conjunction with the s-shaped reinforcement in the CT-SBAR specimens constructed in Phase 2. This was done in an effort to increase the confinement in the splice region to reduce the longitudinal cracks found in the SBAR-1a and UGC-SBAR specimens and to increase the tensile resistance of the lapped reinforcement. The use of ungrouted cells was also abandoned in Phase 2 since the effective depth of the reinforcing steel between partially and fully grouted wall splice specimens is different and thus does not allow for the direct comparison of the results between these two types of specimens.

The refinements that were made to the Phase 2 specimens from the knowledge that was acquired in the Phase 1a tests likely resulted in greater increases in the tensile resistance of the lapped reinforcement and reduced crack propagation in the specimens with s-shaped reinforcement.

Table 4A-1: Cementitious Companion Specimen Summary – Phase 1a.

Companion Test	Number of Specimens Used for Analysis	Mean Maximum Stress [MPa]	COV
Masonry Block	6	21.2	16.3%
Mortar Cubes	83*	18.6*	12.6%*
Absorbent Grout Prisms	21*	16.7*	10.9%*
Non-Absorbent Grout Cylinders	62*	13.5*	10.7%*
3-High, Stack Bond Masonry Prism	11**	13.1**	9.62%**

* Excludes statistical outliers identified at the 95% confidence interval using the procedure detailed in ASTM E178 (ASTM, 2008).

** Excludes the SBAR-1a#3 prism because it was constructed out of plumb.

Table 4A-2: Resulting Wall Data - Phase 1a.

Wall Set	Wall Number	Age @ Test [days]	Cracking Load [kN]	Max Applied Load [kN]	Max Midspan Moment [kNm]	Midspan Displacement @ Max Load [mm]	Curvature @ Max Load [1/m]	Tension in Spliced Reinforcing Bars [kN]	f'_m [MPa]	E_m [MPa]
TBAR	1	56	2.70	21.9	11.7	18.1	0.0240	127	14.3	9350
	2	55	3.00	20.8	11.3	21.0	0.0274	146	15.2	9170
	3	53	4.85	27.6	14.0	16.8	0.0224	120	15.2	9590
	Average		3.52	23.4	12.3	18.6	0.0246	131	14.9	9370
	COV [%]		27.0	12.8	9.65	9.42	8.48	8.39	2.85	1.84
SBAR-1a	1	48	3.40	27.6	13.8	17.9	0.0248	128	12.3	6560
	2	43	3.80	32.9	16.1	21.2	0.0284	145	12.3	6600
	3	46	3.80	35.2	17.0	29.4	0.0292	149	12.3	8610
	Average		3.67	31.9	15.6	22.8	0.0275	141	12.3	7270
	COV [%]		5.14	10.0	8.62	21.2	6.97	6.47	0.04	13.2
UGCC	1	35	2.90	27.1	13.8	15.6	0.0213	118	13.2	5880
	2	41	3.00	25.2	13.1	16.9	0.0234	129	12.9	6610
	3	38	3.40	20.6	11.2	14.6	0.0204	113	13.1	7520
	Average		3.10	24.3	12.7	15.7	0.0217	120	13.1	6670
	COV [%]		6.97	11.2	8.65	6.00	5.79	5.57	0.95	10.1
UGC-SBAR	1	33	3.10	39.3	18.7	26.4	0.0367	178	11.7	17600
	2	28	2.70	37.0	17.8	23.0	0.0331	176	11.0	8690
	3	32	2.90	37.3	17.9	26.9	0.0377	178	13.3	7920
	Average		2.90	37.9	18.1	25.4	0.0358	177	12.0	11400
	COV [%]		5.63	2.68	2.30	6.81	5.51	0.53	8.02	38.5

APPENDIX 4B: MASONRY BLOCK, MORTAR, GROUT, AND REINFORCING STEEL COMPANION TEST RESULTS

This appendix includes the individual test results for the masonry block, mortar, grout, and reinforcing steel properties for the materials prepared in conjunction with the three phases of construction. Table 4B-1 to Table 4B-3 present the compressive strengths of the mortar cubes tested in conjunction with the wall splice specimens of the same construction phase. The first number in the naming scheme of the mortar cubes corresponds to the batch number while the second number refers to the specimen number. Additional mortar cubes were also cast for tempered batches and were denoted with a "T" following the batch number. Table 4B-4 to Table 4B-6 report the compressive strength of the absorbent grout prisms tested in conjunction with the wall splice specimens of the same construction phase. The naming scheme for these specimens includes a number which represents the batch number the grout originated from and the term "abs" which signifies that it was an absorbent grout prism. Table 4B-7 to Table 4B-9 report the compressive strength of the non-absorbent grout cylinders tested in conjunction with the wall splice specimens of the same construction phase. The first number in the naming scheme of the grout cylinders corresponds to the batch number while the second number refers to the specimen number. Table 4B-10 reports the compressive strengths of the concrete block tests from each phase of construction. The first number in the naming scheme of the masonry block tests corresponds to the phase the block was tested in while the second number refers to the specimen number. Table 4B-11 shows the material properties from each reinforcing steel tension test.

The results from the masonry prism testing are not included in this appendix. Instead, the results from the each prism test are presented in Appendix 4C along with a comparative analysis of the three different prism geometries.

Table 4B-1: Mortar Cube Tests Performed in Conjunction with the Phase 1 Wall Splice Specimens.

Specimen ID	Compressive Strength [MPa]	Specimen ID	Compressive Strength [MPa]	Specimen ID	Compressive Strength [MPa]
1-1	15.1	5-6	16.4	9T-2	12.9
1-2	15.2	6-1	19.9	9T-3	13.1
1-3	12.7	6-2	21.0	10-1	22.5
1-4	13.9	6-3	18.0	10-2	22.5
1-5	15.1	6-4	18.8	10-3	19.3
1-6	17.1	6-5	19.9	10-4	22.7*
1T-1	11.8	6-6	17.8	10-5	21.6
1T-2	13.9	7-1	20.4	10-6	19.5
1T-3	14.8	7-2	19.0	10T-1	18.0
2-1	16.9	7-3	16.0	10T-2	18.0
2-2	15.6	7-4	22.3	10T-3	15.9
2-3	20.4	7-5	21.6	11-1	19.0
2-4	17.3	7-6	19.6	11-2	19.7
2-5	20.3	7T-1	15.3	11-3	17.8
2-6	19.1	7T-2	14.0	11-4	16.7
3-1	13.6	7T-3	12.5	11-5	19.9
3-2	15.7	8-1	18.3	11-6	17.5
3-3	15.4	8-2	19.8	11T-1	12.9
3-4	12.7	8-3	18.5	11T-2	14.5
3-5	15.6	8-4	16.2	11T-3	14.2
3-6	15.5	8-5	20.4	12-1	18.4
4-1	13.2	8-6	16.4	12-2	15.5
4-2	15.3	8T-1	13.2	12-3	15.3
4-3	16.1	8T-2	13.3	12-4	15.7
4-4	13.4	8T-3	12.9	12-5	17.1
4-5	15.5	9-1	21.1	12-6	20.2
4-6	17.4	9-2	21.4	13-1	14.6
5-1	18.7	9-3	18.9	13-2	15.1
5-2	16.4	9-4	21.8	13-3	14.1
5-3	15.6	9-5	21.3	13-4	14.6
5-4	17.4	9-6	18.1	13-5	15.9
5-5	17.4	9T-1	9.50*	13-6	15.4
				Mean Compressive Strength:	17.0 MPa
				COV:	16.2 %

*Denotes statistical outliers identified at the 95% confidence interval using the procedure detailed in ASTM E178-08 (ASTM, 2008) and were excluded from the computation of the mean material properties.

Table 4B-2: Mortar Cube Tests Performed in Conjunction with the Phase 1a Wall Splice Specimens.

Specimen ID	Compressive Strength [MPa]	Specimen ID	Compressive Strength [MPa]	Specimen ID	Compressive Strength [MPa]
1-1	14.6	4-5	18.6	4-5	18.6
1-2	15.9	4-6	19.2	4-6	19.2
1-3	14.1	4T-1	20.8	4T-1	20.8
1-4	14.9	4T-2	19.5	4T-2	19.5
1-5	16.7	4T-3	19.0	4T-3	19.0
1-6	17.3	5-1	15.1	5-1	15.1
1T-1	16.6	5-2	19.7	5-2	19.7
1T-2	16.8	5-3	17.5	5-3	17.5
1T-3	16.2	5-4	20.4	5-4	20.4
2-1	19.8	5-5	20.5	5-5	20.5
2-2	19.8	5-6	19.9	5-6	19.9
2-3	19.1	6-1	20.9	6-1	20.9
2-4	20.5	6-2	20.9	6-2	20.9
2-5	21.3	6-3	21.9	6-3	21.9
2-6	18.7	6-4	21.1	6-4	21.1
3-1	19.5	6-5	21.8	6-5	21.8
3-2	21.9	6-6	20.2	6-6	20.2
3-3	18.6	6T-1	10.2*	6T-1	10.2
3-4	20.0	6T-2	16.1	6T-2	16.1
3-5	21.2	6T-3	16.7	6T-3	16.7
3-6	17.5	7-1	17.5	7-1	17.5
3T-1	17.9	7-2	16.6	7-2	16.6
3T-2	18.4	7-3	17.0	7-3	17.0
3T-3	16.8	7-4	18.2	7-4	18.2
4-1	22.0	7-5	18.0	7-5	18.0
4-2	24.0	7-6	18.2	7-6	18.2
4-3	21.1	7T-1	14.5	7T-1	14.5
4-4	19.5	7T-2	16.5	7T-2	16.5
				Mean Compressive Strength:	18.6 MPa
				COV:	12.6 %

*Denotes statistical outliers identified at the 95% confidence interval using the procedure detailed in ASTM E178-08 (ASTM, 2008) and were excluded from the computation of the mean material properties.

Table 4B-3: Mortar Cube Tests Performed in Conjunction with the Phase 2 Wall Splice Specimens.

Specimen ID	Compressive Strength [MPa]	Specimen ID	Compressive Strength [MPa]	Specimen ID	Compressive Strength [MPa]
1-1	14.0	3-5	18.3	5T-3	13.3
1-2	15.9	3-6	17.1	6-1	15.4
1-3	15.0	4-1	18.7	6-2	14.6
1-4	17.0	4-2	19.1	6-3	15.3
1-5	16.6	4-3	18.8	6-4	16.7
1-6	17.0	4-4	13.0	6-5	15.9
1T-1	11.9*	4-5	13.6	6-6	15.6
1T-2	17.2	4-6	12.8	7-1	18.6
1T-3	15.9	4T-1	15.1	7-2	19.9
2-1	18.5	4T-2	15.1	7-3	18.4
2-2	18.4	4T-3	14.5	7-4	17.7
2-3	18.2	5-1	17.4	7-5	17.3
2-4	16.4	5-2	17.3	7-6	17.7
2-5	17.5	5-3	16.7	8-1	20.2
2-6	17.3	5-4	19.0	8-2	18.7
3-1	15.9	5-5	18.7	8-3	18.3
3-2	15.5	5-6	19.1	8-4	17.7
3-3	14.7	5T-1	14.1	8-5	16.5
3-4	18.2	5T-2	14.5	8-6	15.1
				Mean Compressive Strength:	16.7 MPa
				COV:	10.9 %

*Denotes statistical outliers identified at the 95% confidence interval using the procedure detailed in ASTM E178-08 (ASTM, 2008) and were excluded from the computation of the mean material properties.

Table 4B-4: Absorbent Grout Prism Tests Performed in Conjunction with the Phase 1 Wall Splice Specimens.

Specimen ID	Compressive Strength [MPa]	Specimen ID	Compressive Strength [MPa]	Specimen ID	Compressive Strength [MPa]
1_abs	17.6	12_abs	20.0*	23_abs	13.1
2_abs	13.5	13_abs	14.9	24_abs	14.8
3_abs	15.9	14_abs	13.1	25_abs	14.8
4_abs	13.2	15_abs	16.6	26_abs	14.6
5_abs	15.7	16_abs	13.5	27_abs	12.6
6_abs	15.3	17_abs	14.6	28_abs	12.1
7_abs	14.4	18_abs	12.6	29_abs	14.3
8_abs	15.8	19_abs	11.0	30_abs	12.4
9_abs	15.8	20_abs	10.5	31_abs	15.2
10_abs	16.7	21_abs	12.4	32_abs	10.9
11_abs	13.3	22_abs	15.8		
				Mean Compressive Strength:	14.1 MPa
				COV:	12.5 %

*Denotes statistical outliers identified at the 95% confidence interval using the procedure detailed in ASTM E178-08 (ASTM, 2008) and were excluded from the computation of the mean material properties.

Table 4B-5: Absorbent Grout Prism Tests Performed in Conjunction with the Phase 1a Wall Splice Specimens.

Specimen ID	Compressive Strength [MPa]	Specimen ID	Compressive Strength [MPa]	Specimen ID	Compressive Strength [MPa]
1_abs	13.1	9_abs	14.1	17_abs	15.2
2_abs	15.3	10_abs	13.1	18_abs	11.9
3_abs	12.7	11_abs	14.2	19_abs	12.1
4_abs	13.0	12_abs	10.9*	20_abs	13.0
5_abs	14.1	13_abs	14.5	21_abs	15.7
6_abs	12.6	14_abs	16.0	22_abs	14.0
7_abs	12.3	15_abs	15.1		
8_abs	14.1	16_abs	13.9		
			Mean Compressive Strength:	13.8	MPa
			COV:	8.5	%

*Denotes statistical outliers identified at the 95% confidence interval using the procedure detailed in ASTM E178-08 (ASTM, 2008) and were excluded from the computation of the mean material properties.

Table 4B-6: Absorbent Grout Prism Tests Performed in Conjunction with the Phase 2 Wall Splice Specimens.

Specimen ID	Compressive Strength [MPa]	Specimen ID	Compressive Strength [MPa]	Specimen ID	Compressive Strength [MPa]
1_abs	19.2*	9_abs	16.3	17_abs	16.8
2_abs	15.5	10_abs	16.0	18_abs	13.6
3_abs	16.3	11_abs	13.1	19_abs	15.5
4_abs	16.9	12_abs	13.2	20_abs	15.5
5_abs	16.1	13_abs	13.4	21_abs	14.4
6_abs	17.2	14_abs	16.0	22_abs	16.4
7_abs	17.0	15_abs	15.8		
8_abs	16.2	16_abs	14.8		
			Mean Compressive Strength:	15.5	MPa
			COV:	8.08	%

*Denotes statistical outliers identified at the 95% confidence interval using the procedure detailed in ASTM E178-08 (ASTM, 2008) and were excluded from the computation of the mean material properties.

Table 4B-7: Non-Absorbent Grout Cylinder Tests Performed in Conjunction with the Phase 1 Wall Splice Specimens.

Specimen ID	Compressive Strength [MPa]	Specimen ID	Compressive Strength [MPa]	Specimen ID	Compressive Strength [MPa]
1-1	14.5	11-3	14.5	22-2	15.0
1-2	13.7	12-1	11.1	22-3	14.9
1-3	12.1	12-2	14.0	23-1	15.5
2-1	14.3	12-3	14.2	23-2	13.6
2-2	12.0	13-1	13.8	23-3	10.7
2-3	13.7	13-2	14.7	24-1	15.4
3-1	13.1	13-3	15.8	24-2	14.2
3-2	11.0	14-1	17.0	24-3	14.2
3-3	11.8	14-2	16.7	25-1	14.5
4-1	12.5	14-3	15.6	25-2	14.5
4-2	12.0	15-1	16.6	25-3	16.3
4-3	13.9	15-2	12.3	26-1	12.8
5-1	17.9	15-3	18.7	26-2	13.3
5-2	15.0	16-1	16.4	26-3	13.1
5-3	18.7*	16-2	17.6	27-1	13.8
6-1	12.7	16-3	18.2	27-2	13.7
6-2	17.2	17-1	15.2	27-3	11.6
6-3	16.6	17-2	12.1	28-1	14.0
7-1	14.2	17-3	18.0	28-2	7.60*
7-2	16.3	18-1	14.7	28-3	14.1
7-3	17.3	18-2	11.8	29-1	14.5
8-1	13.6	18-3	15.9	29-2	15.3
8-2	15.5	19-1	13.8	29-3	12.8
8-3	14.8	19-2	9.90	30-1	12.5
9-1	11.8	19-3	16.9	30-2	11.4
9-2	15.1	20-1	12.0	30-3	13.3
9-3	15.5	20-2	15.6	31-1	9.40*
10-1	11.7	20-3	13.5	31-2	11.6
10-2	15.5	21-1	15.6	31-3	11.6
10-3	12.2	21-2	14.8	32-1	12.2
11-1	14.0	21-3	12.9	32-2	13.6
11-2	15.2	22-1	15.2	32-3	7.20*
				Mean Compressive Strength:	14.2 MPa
				COV:	13.3 %

*Denotes statistical outliers identified at the 95% confidence interval using the procedure detailed in ASTM E178-08 (ASTM, 2008) and were excluded from the computation of the mean material properties.

Table 4B-8: Non-Absorbent Grout Cylinder Tests Performed in Conjunction with the Phase 1a Wall Splice Specimens.

Specimen ID	Compressive Strength [MPa]	Specimen ID	Compressive Strength [MPa]	Specimen ID	Compressive Strength [MPa]
1-1	13.6	8-2	13.8	15-3	15.1
1-2	15.3	8-3	13.0	16-1	14.9
1-3	13.9	9-1	13.1	16-2	12.7
2-1	11.5	9-2	14.9	16-3	14.2
2-2	13.4	9-3	13.8	17-1	13.9
2-3	12.3	10-1	14.2	17-2	9.60
3-1	13.7	10-2	13.7	17-3	13.6
3-2	11.3	10-3	12.0	18-1	11.8
3-3	13.7	11-1	11.2	18-2	12.7
4-1	11.3	11-2	13.8	18-3	13.6
4-2	11.2	11-3	7.80*	19-1	12.0
4-3	12.4	12-1	9.50	19-2	13.1
5-1	14.2	12-2	13.5	19-3	8.40*
5-2	13.9	12-3	13.6	20-1	11.6
5-3	14.2	13-1	15.7	20-2	14.1
6-1	8.20*	13-2	15.1	20-3	13.8
6-2	12.4	13-3	14.7	21-1	14.2
6-3	11.7	14-1	14.0	21-2	14.8
7-1	14.4	14-2	15.6	21-3	13.3
7-2	15.9	14-3	13.8	22-1	13.3
7-3	16.2	15-1	14.6	22-2	8.40*
8-1	15.4	15-2	15.9	22-3	12.3
				Mean Compressive Strength:	13.5 MPa
				COV:	10.7 %

*Denotes statistical outliers identified at the 95% confidence interval using the procedure detailed in ASTM E178-08 (ASTM, 2008) and were excluded from the computation of the mean material properties.

Table 4B-9: Non-Absorbent Grout Cylinder Tests Performed in Conjunction with the Phase 2 Wall Splice Specimens.

Specimen ID	Compressive Strength [MPa]	Specimen ID	Compressive Strength [MPa]	Specimen ID	Compressive Strength [MPa]
1-1	14.7	8-2	11.8	15-3	10.8
1-2	11.1	8-3	13.8	16-1	12.7
1-3	12.1	9-1	11.7	16-2	10.6
2-1	10.8	9-2	14.4	16-3	13.8
2-2	14.1	9-3	14.5	17-1	12.2
2-3	13.7	10-1	9.00*	17-2	11.7
3-1	12.1	10-2	14.3	17-3	11.1
3-2	14.3	10-3	10.3	18-1	12.5
3-3	16.0	11-1	11.9	18-2	11.6
4-1	12.2	11-2	10.5	18-3	13.1
4-2	14.8	11-3	13.8	19-1	13.8
4-3	10.0	12-1	13.1	19-2	12.6
5-1	15.3	12-2	12.7	19-3	12.3
5-2	13.6	12-3	14.4	20-1	10.7
5-3	11.9	13-1	16.2*	20-2	10.8
6-1	13.4	13-2	12.3	20-3	11.4
6-2	11.1	13-3	15.3	21-1	12.3
6-3	13.0	14-1	11.3	21-2	9.4
7-1	11.4	14-2	13.0	21-3	10.9
7-2	13.9	14-3	12.1	22-1	13.2
7-3	10.7	15-1	11.1	22-2	13.2
8-1	8.90*	15-2	13.7	22-3	12.5
				Mean Compressive Strength:	12.5 MPa
				COV:	11.7 %

*Denotes statistical outliers identified at the 95% confidence interval using the procedure detailed in ASTM E178-08 (ASTM, 2008) and were excluded from the computation of the mean material properties.

Table 4B-10: Compressive Strength of the Masonry Block.

Test Phase	Specimen ID	Compressive Stength [MPa]	Mean Compressive Stength [MPa]	COV [%]
1	1-1	23.0	19.7	10.5
	1-2	19.7		
	1-3	19.3		
	1-4	19.3		
	1-5	20.8		
	1-6	16.0		
1a	1a-1	20.8	21.2	16.3
	1a-2	21.9		
	1a-3	23.1		
	1a-4	16.4		
	1a-5	26.9		
	1a-6	17.8		
2	2-1	20.8	21.5	8.39
	2-2	22.2		
	2-3	23.7		
	2-4	18.2		
	2-5	23.1		
	2-6	21.0		

Table 4B-11: Tensile Test Results of the Reinforcing Bars.

Test Phase	Sample designation	Dynamic yield stress f_y [MPa]	Modulus of elasticity E_s [GPa]	Strain at the initiation of strain hardening ε_h	Slope at initiation of strain hardening E_{sh} [MPa]	Ultimate steel stress f_{ult} [MPa]
1*	1	441	170	0.0143	9280	666
	2	439	214	0.0191	5790	662
	3	441	168	0.0143	8230	668
	4	439	205	0.0140	6800	668
	5	440	168	0.0148	7680	666
	6	446	219	0.0146	6340	665
	7	444	185	0.0137	5920	670
	8	443	224	0.0127	6470	669
	9	448	176	0.0144	5970	663
	Average	442	192	0.0146	6942	666
	COV	0.65%	11.4%	11.4%	16.3%	0.38%
2	1	433	168	0.0116	2720	593
	2	438	150	0.0189	2510	593
	3	433	170	0.0175	2960	592
	4	440	217	0.0118	2950	594
	5	437	190	0.0136	3240	591
	6	434	232	0.0101	1940	591
	7	436	189	0.0106	2930	596
	8	431	120	0.0130	2470	600
	Average	435	180	0.0134	2715	594
	COV	0.64%	18.7%	22.5%	13.9%	0.46%

*This data also applies for the reinforcment used in specimens constructed during Phase 1a as all the reinforcment used in these two phases originated from a common batch

APPENDIX 4C: PRISM ANALYSIS

The results from the compressive tests of the masonry prisms are presented in this appendix. The compressive strengths of all three prism designs, detailed in Section 3.6.4, are also compared and individual stress versus strain diagrams from each prism test are presented. These results will supplement continuing research focused on masonry prism testing.

Table 4C-1 to Table 4C-3 present the results of the masonry prism compressive tests. The name of each prism refers to the wall splice specimen its material properties represent. Figure 4C-1 to Figure 4C-20 show the stress versus strain diagrams for each individual prism test. The construction and testing procedures associated with the masonry prisms are detailed in Sections 3.6.4 and 3.7.3, respectively. There were no statistical outliers identified at the 95% confidence level using the procedure detailed in ASTM E178-08 (ASTM, 2008).

The mean compressive strength of the three block-high stack bond and the four block-high running bond masonry prisms was 13.1 MPa (COV 13.3%) and 9.14 MPa (COV 14.3%), respectively. This equated to a 43% decrease in the mean compressive strength and a 7% increase in the coefficient of variation of the four block-high running bond masonry prism results compared to the three block-high stack bond prisms. This represents a statistically significant difference in the mean maximum compressive strength between the two prism designs.

The lower compressive strength and higher coefficient of variation of the four block-high prisms was likely due to the higher slenderness ratio, additional bed joint, and a reduction in the effectiveness of the confinement caused by the reactions at each end of the prism. The higher slenderness ratio of the four block-high prisms reduced the overall compressive strengths and increased the coefficient of variation since it lowered the buckling strength of the assemblage, making it a possible mode of failure. Mortar joints are typically the weakest component of a masonry assemblage and thus increasing the number of bed joints in a prism provides for more possible locations for compressive failures to originate. The head joints present in the four block-high running bond prisms likely did not have a noticeable effect on the compressive strength since crack propagation in these joints was not observed during the tests.

The mean compressive strength of the four block-high running bond masonry prisms with a knock-out web was 8.77 MPa (COV 17.0%). The difference between the mean compressive

strength of the two four block-high prism designs was 4%. This does not represent a statistically significant difference in the mean maximum compressive strength of the two prism designs. It also indicates that the installation of knock-out webs does not have a noticeable effect on the compressive strength of masonry assemblages.

The results from the testing of the three masonry prism designs indicate that the compressive strength of a masonry prism is likely dependent mainly on their height and not on the bond pattern and installation of knock-out web, however the test database is not extensive enough to make any conclusions.

Table 4C-1: Compressive Strength Test Results for Three Block-High Stack Bond Prisms.

Wall Splice Specimen Represented by Prism	Test Phase	Maximum Compressive Strength, f'_m [MPa]	Modulus of Elasticity, E'_m [MPa]	Wall Splice Specimen Represented by Prism	Test Phase	Maximum Compressive Strength, f'_m [MPa]	Modulus of Elasticity, E'_m [MPa]	
NCLS#1	1	12.9	8910	TBAR#1	1a	14.3	9350	
NCLS#2	1	13.5	8600	TBAR#2	1a	15.2	9170	
NCLS#3	1	11.9	10500	TBAR#3	1a	15.2	9590	
GCC#1	1	14.9	7770	SBAR-1a#1	1a	12.6	10100	
GCC#2	1	14.2	10100	SBAR-1a#2	1a	12.3	6600	
GCC#3	1	11.9	7450	SBAR-1a#3	1a	12.3	8600	
1KO#1	1	15.9	15000	UGC-SBAR#1	1a	11.7	17600	
1KO#2	1	11.7	11100	UGC-SBAR#2	1a	11.0	8690	
1KO#3	1	15.2	10900	UGC-SBAR#3	1a	13.3	7920	
3KO#1	1	12.9	7200	SBAR#1	2	15.6	8350	
3KO#2	1	14.4	10900	SBAR#2	2	13.8	8560	
3KO#3	1	11.5	9990	SBAR#3	2	13.9	8700	
CLS#1	1	12.5	10100	C-SBAR#1	2	13.4	8120	
CLS#2	1	12.5	6890	C-SBAR#2	2	12.7	7970	
CLS#3	1	14.9	8710	C-SBAR#3	2	8.75	6460	
UGCC#1	1a	13.2	5880	CT-SBAR#1	2	11.4	20180	
UGCC#2	1a	12.9	6610	CT-SBAR#2	2	7.91	9434	
UGCC#3	1a	13.1	7520	CT-SBAR#3	2	15.2	8420	
					Mean	13.1	9390	MPa
				Coefficient of Variation		13.3	30.5	%

Table 4C-2: Compressive Strength Test Results for Four Block-High Running Bond Prisms.

Wall Splice Specimen Represented by Prism	Test Phase	Maximum Compressive Strength, f'_m [MPa]	Modulus of Elasticity, E'_m [MPa]	Wall Splice Specimen Represented by Prism	Test Phase	Maximum Compressive Strength, f'_m [MPa]	Modulus of Elasticity, E'_m [MPa]	
NCLS#1	1	9.64	7080	TBAR#2	1a	11.8	16800	
GCC#2	1	Error*	Error*	SBAR-1a#3	1a	8.45	13000	
1KO#1	1	10.3	13700	UGC-SBAR#2	1a	7.24	9880	
3KO#2	1	10.0	13900	SBAR#1	2	8.92	7870	
CLS#1	1	9.47	14300	C-SBAR#2	2	8.36	8560	
UGCC#3	1a	9.39	20300	CT-SBAR#1	2	7	12000	
*Instrument malfunction					Mean	9.14	12500	MPa
				Coefficient of Variation		14.3	30.5	%

Table 4C-3: Compressive Strength Test Results for Four Block-High Running Bond Prisms.

Wall Splice Specimen Represented by Prism	Test Phase	Maximum Compressive Strength, f'_m [MPa]	Modulus of Elasticity, E'_m [MPa]	Wall Splice Specimen Represented by Prism	Test Phase	Maximum Compressive Strength, f'_m [MPa]	Modulus of Elasticity, E'_m [MPa]	
1KO#1	1	11.5	9520	UGC-SBAR#2	1a	7.45	9490	
3KO#2	1	9.43	15800	SBAR#1	2	7.94	6310	
TBAR#2	1a	10.1	11300	C-SBAR#2	2	7.44	5520	
SBAR-1a#3	1a	5.91*	11400*	CT-SBAR#1	2	7.5	6300	
					Mean	8.77	9180	MPa
				Coefficient of Variation		17.0	36.5	%

*Specimen constructed out of plumb, therefore data was excluded from analysis

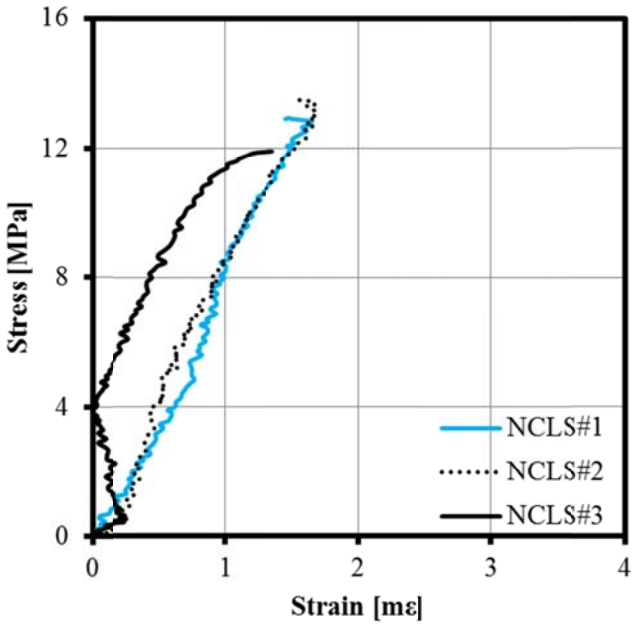

Figure 4C-1: Compressive Stress Versus Strain Diagram for the Three Block-High Masonry Prisms Corresponding to the NCLS#1, NCLS#2, and NCLS#3 Wall Splice Specimens.

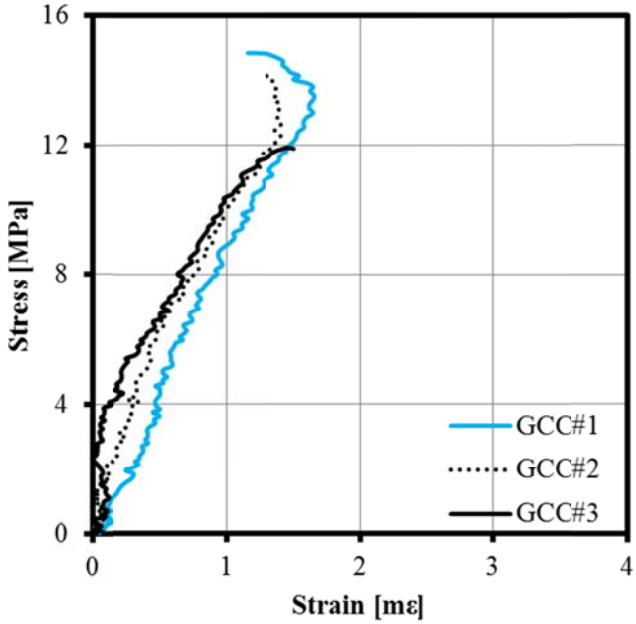

Figure 4C-2: Compressive Stress Versus Strain Diagram for the Three Block-High Masonry Prisms Corresponding to the GCC#1, GCC#2, and GCC#3 Wall Splice Specimens.

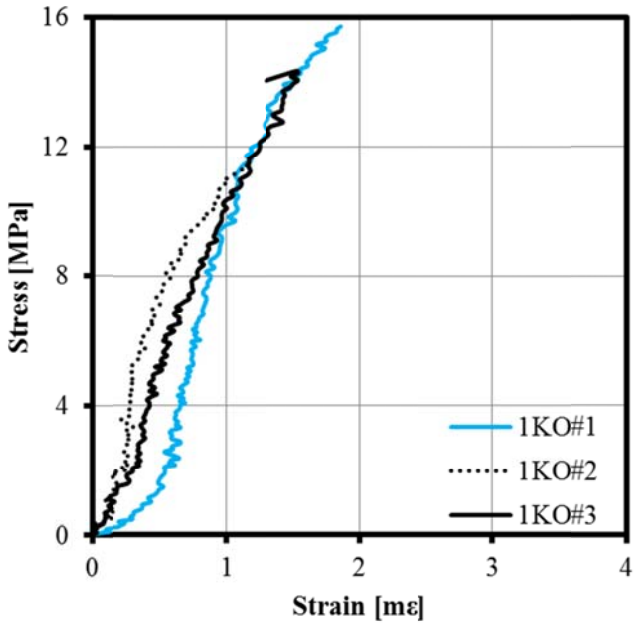

Figure 4C-3: Compressive Stress Versus Strain Diagram for the Three Block-High Masonry Prisms Corresponding to the 1KO#1, 1KO#2, and 1KO#3 Wall Splice Specimens.

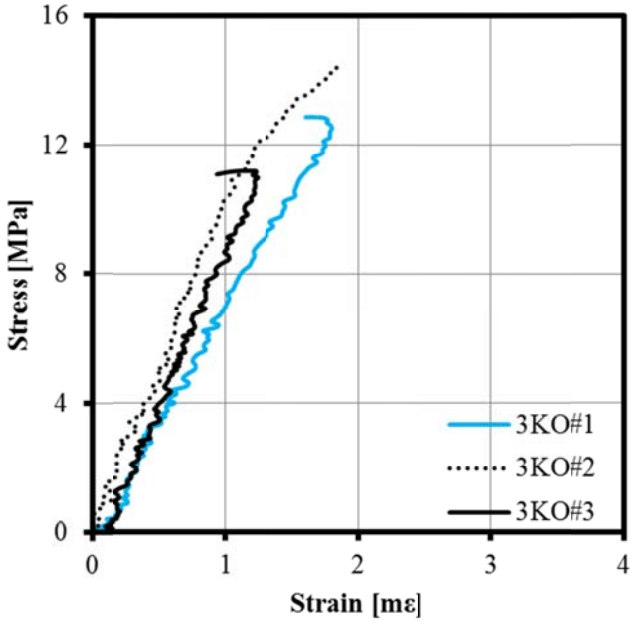

Figure 4C-4: Compressive Stress Versus Strain Diagram for the Three Block-High Masonry Prisms Corresponding to the 3KO#1, 3KO#2, and 3KO#3 Wall Splice Specimens.

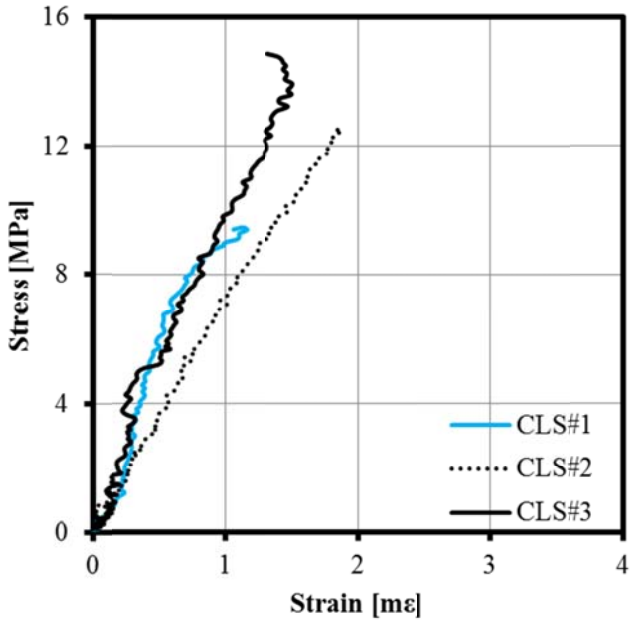

Figure 4C-5: Compressive Stress Versus Strain Diagram for the Three Block-High Masonry Prisms Corresponding to the CLS#1, CLS#2, and CLS#3 Wall Splice Specimens.

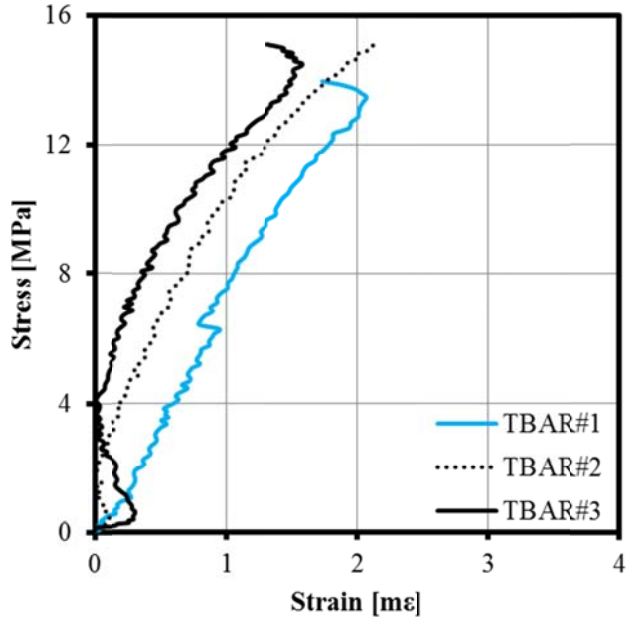

Figure 4C-6: Compressive Stress Versus Strain Diagram for the Three Block-High Masonry Prisms Corresponding to the TBAR#1, TBAR#2, and TBAR#3 Wall Splice Specimens.

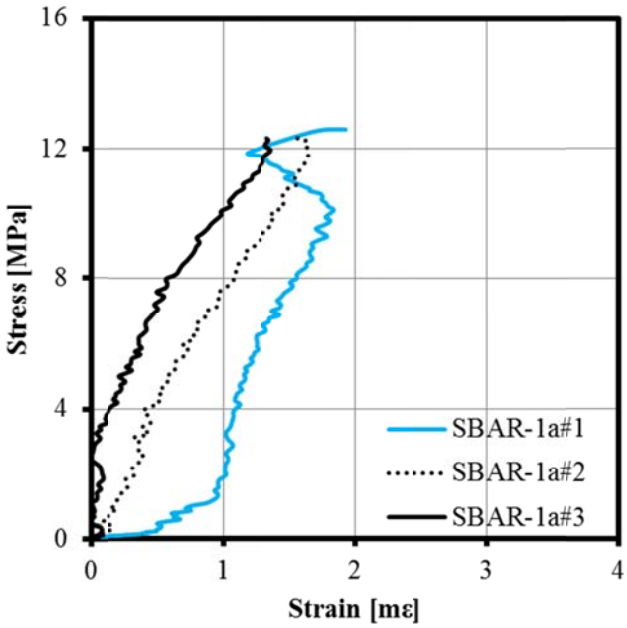

Figure 4C-7: Compressive Stress Versus Strain Diagram for the Three Block-High Masonry Prisms Corresponding to the SBAR-1a#1, SBAR-1a#2, and SBAR-1a#3 Wall Splice Specimens.

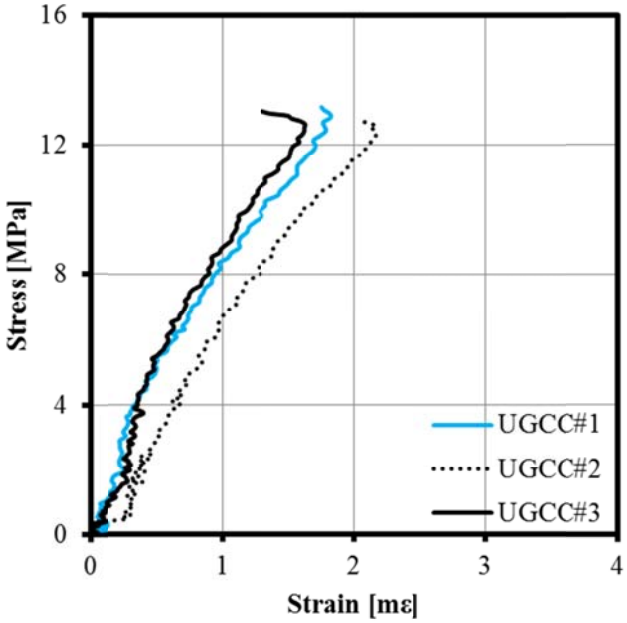

Figure 4C-8: Compressive Stress Versus Strain Diagram for the Three Block-High Masonry Prisms Corresponding to the UGCC#1, UGCC#2, and UGCC#3 Wall Splice Specimens.

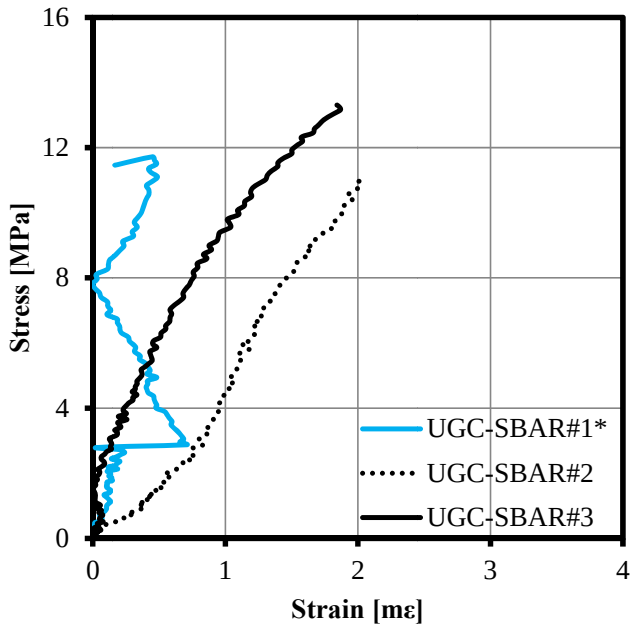

* LVDT slip occurred during test

Figure 4C-9: Compressive Stress Versus Strain Diagram for the Three Block-High Masonry Prisms Corresponding to the UGC-SBAR#1, UGC-SBAR#2, and UGC-SBAR#3 Wall Splice Specimens.

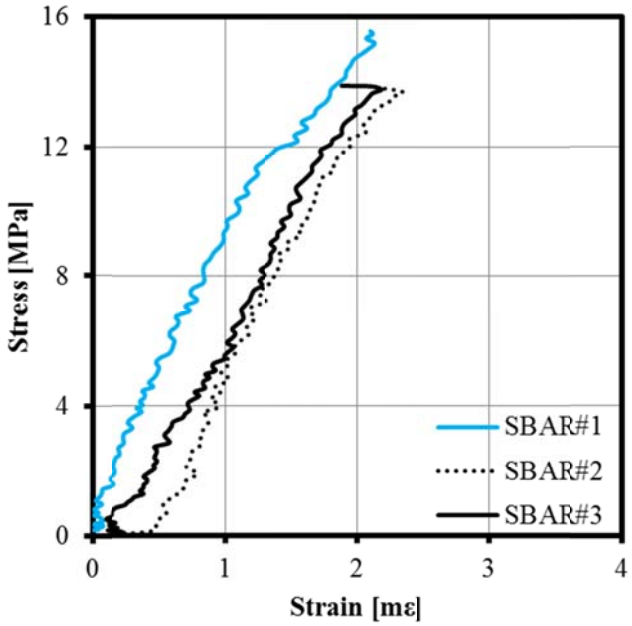

Figure 4C-10: Compressive Stress Versus Strain Diagram for the Three Block-High Masonry Prisms Corresponding to the SBAR#1, SBAR#2, and SBAR#3 Wall Splice Specimens.

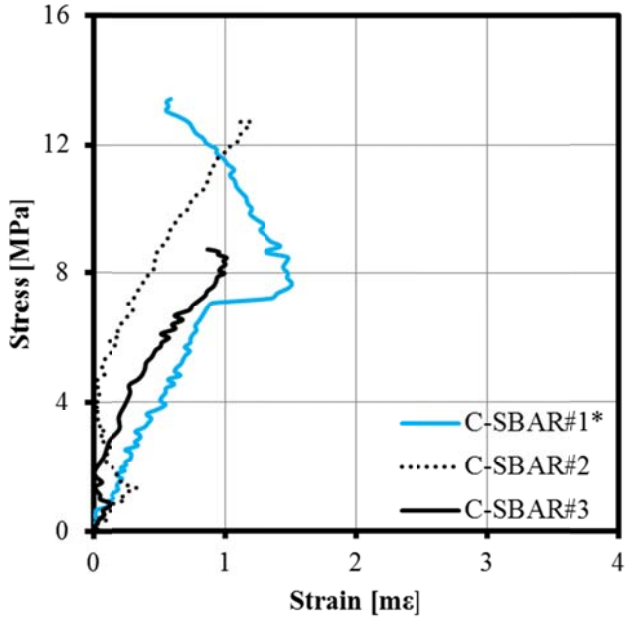

* LVDT slip occurred during test

Figure 4C-11: Compressive Stress Versus Strain Diagram for the Three Block-High Masonry Prisms Corresponding to the C-SBAR#1, C-SBAR#2, and C-SBAR#3 Wall Splice Specimens.

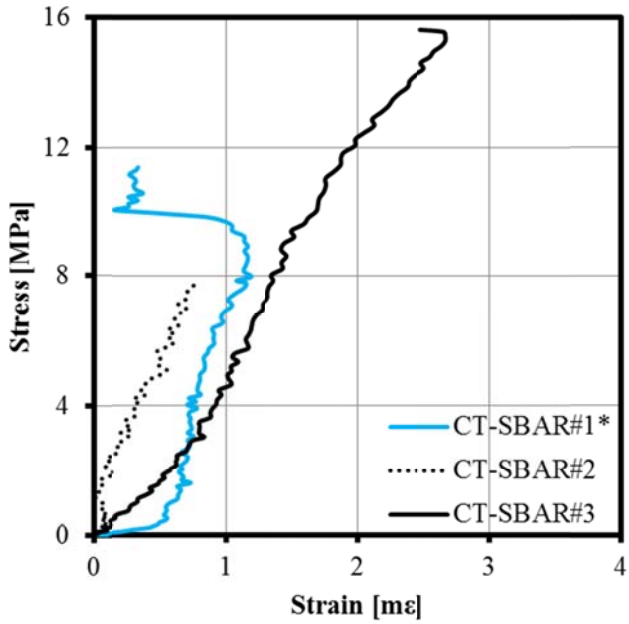

* LVDT slip occurred during test

Figure 4C-12: Compressive Stress Versus Strain Diagram for the Three Block-High Masonry Prisms Corresponding to the CT-SBAR#1, CT-SBAR#2, and CT-SBAR#3 Wall Splice Specimens.

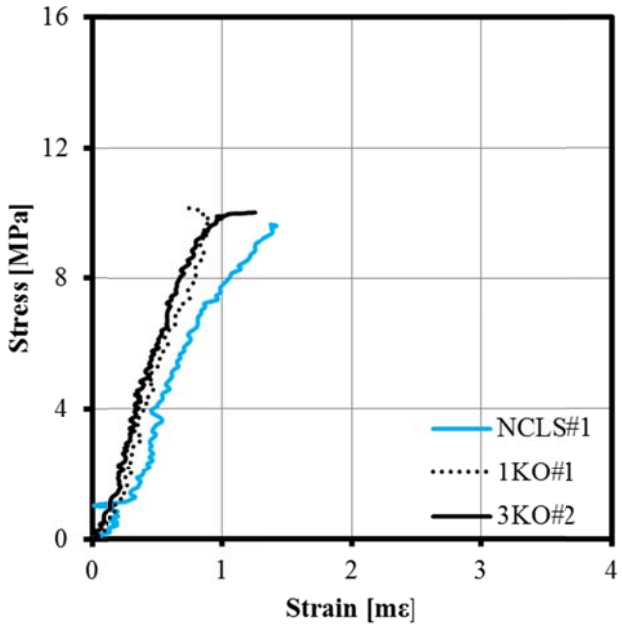

Figure 4C-13: Compressive Stress Versus Strain Diagram for the Four Block-High Masonry Prisms Corresponding to the NCLS#1, 1KO#1, and 3KO#2 Wall Splice Specimens.

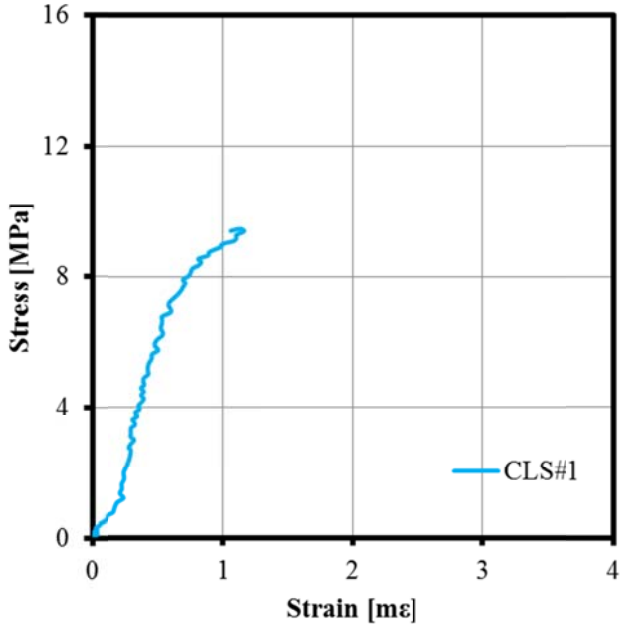

Figure 4C-14: Compressive Stress Versus Strain Diagram for the Four Block-High Masonry Prisms Corresponding to the CLS#1 Wall Splice Specimen.

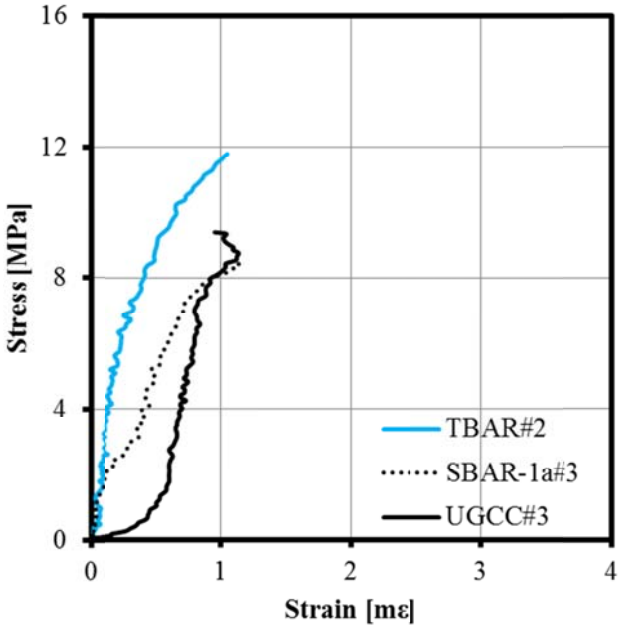

Figure 4C-15: Compressive Stress Versus Strain Diagram for the Four Block-High Masonry Prisms Corresponding to the TBAR#2, SBAR-1a#3, and UGCC#3 Wall Splice Specimens.

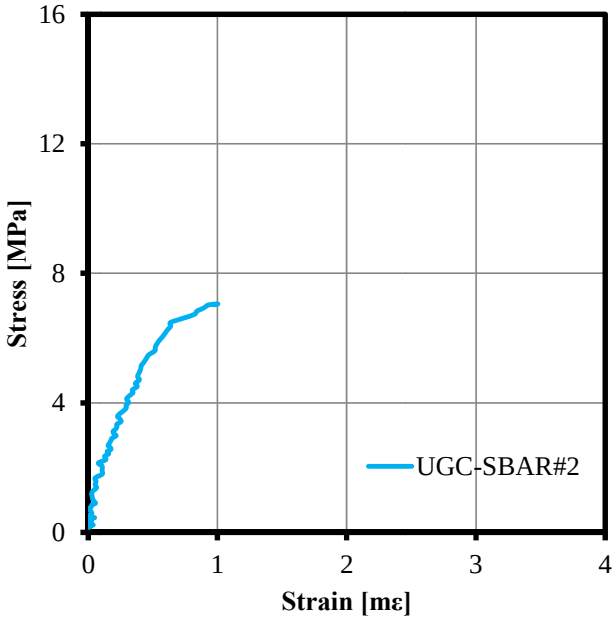

Figure 4C-16: Compressive Stress Versus Strain Diagram for the Four Block-High Masonry Prisms Corresponding to the UC-SBAR#2 Wall Splice Specimen.

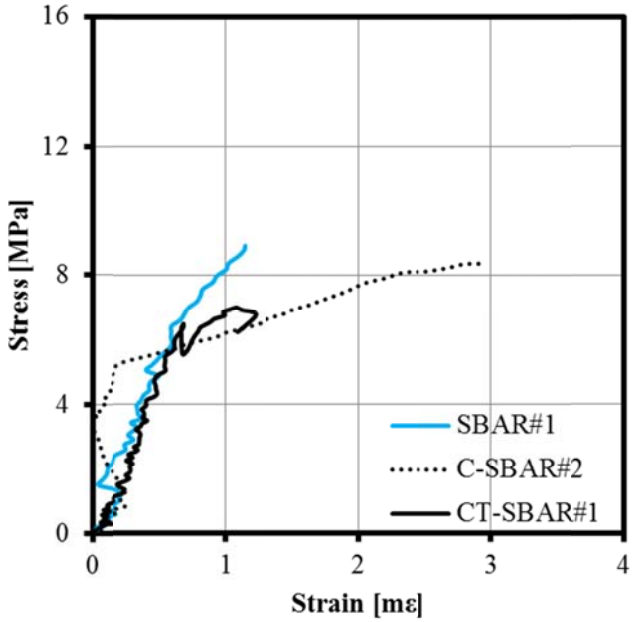

Figure 4C-17: Compressive Stress Versus Strain Diagram for the Four Block-High Masonry Prisms Corresponding to the SBAR#1, C-SBAR#2, and CT-SBAR#1 Wall Splice Specimens.

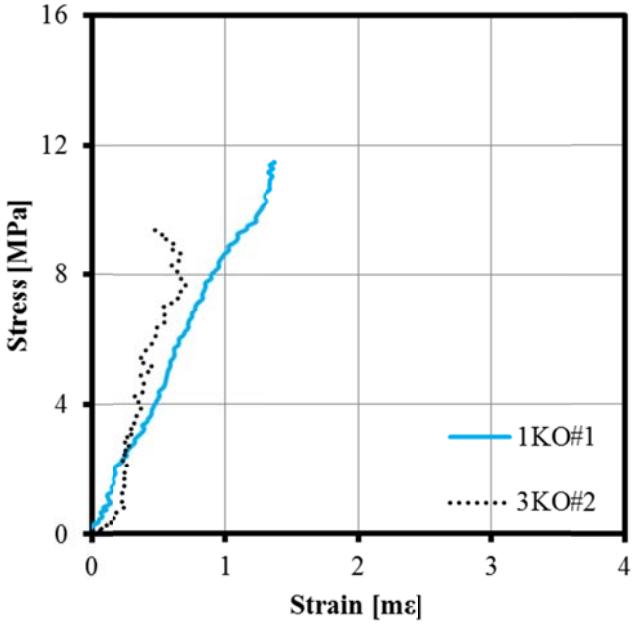

Figure 4C-18: Compressive Stress Versus Strain Diagram for the Four Block-High Masonry Prisms with Knock-Out Webs Corresponding to the 1KO#1 and 3KO#2 Wall Splice Specimens.

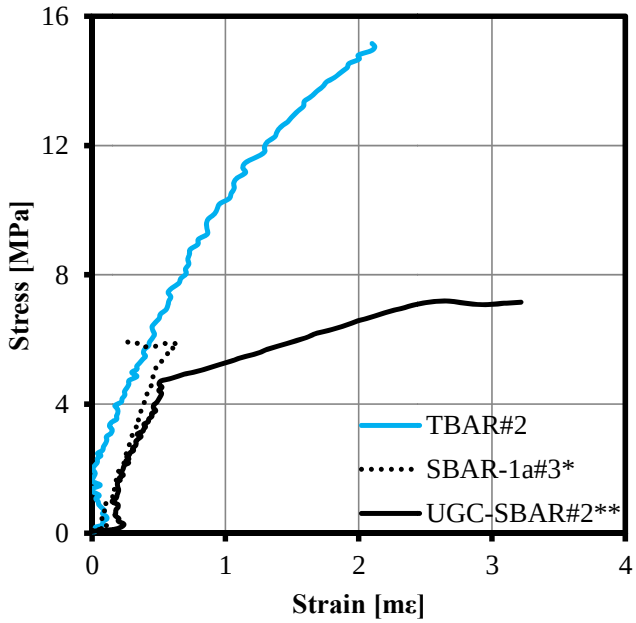

* LVDT slip occurred during test

** LVDT bracket malfunction

Figure 4C-19: Compressive Stress Versus Strain Diagram for the Four Block-High Masonry Prisms with Knock-Out Webs Corresponding to the TBAR#2, SBAR-1a#3, and UC-SBAR#2 Wall Splice Specimens.

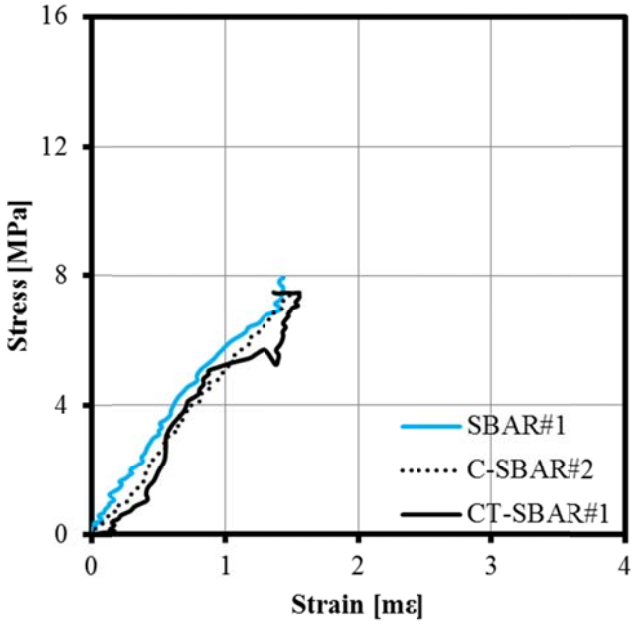

Figure 4C-20: Compressive Stress Versus Strain Diagram for the Four Block-High Masonry Prisms with Knock-Out Webs Corresponding to the SBAR#1, C-SBAR#2, and CT-SBAR#1 Wall Splice Specimens.

APPENDIX 4D: DEVELOPMENT OF THE THEORETICAL TENSILE STRESS-STRAIN CURVE FOR THE STEEL REINFORCEMENT

This appendix presents the mathematical expressions used in the derivation of the theoretical tensile stress versus strain response of the steel reinforcement used in the wall splice specimens. The curve was comprised of three segments: a linear elastic zone, yield plateau, followed by a strain hardening curve. The tensile stress in the steel reinforcement at any given strain, $f_s(\varepsilon_s)$, was determined by:

Linear Elastic Zone: ($\varepsilon_s \leq \varepsilon_y$)

$$f_s(\varepsilon_s) = E_s \cdot \varepsilon_s \qquad [4D\text{-}1]$$

Where: E_s= the modulus of elasticity of the steel reinforcement [MPa]

ε_s= the strain in the steel reinforcement

ε_y= the strain at the initiation of yield of the steel reinforcement

Yield Plateau: ($\varepsilon_y < \varepsilon_s \leq \varepsilon_{sh}$)

$$f_s(\varepsilon_s)=f_y \qquad [4D\text{-}2]$$

Where: ε_{sh}= the strain in the steel reinforcement at the initiation of strain hardening

f_y= the yield stress of the steel reinforcement

Strain Hardening Curve: ($\varepsilon_{sh} < \varepsilon_s \leq \varepsilon_u$)

The strain hardening region was represented by the cubic function:

$$f_s(\varepsilon_s)=A+B\varepsilon_s+C\varepsilon_s^2+D\varepsilon_s^3 \qquad [4D\text{-}3]$$

Where: ε_u= the strain in the steel reinforcement at the ultimate stress

The constants A, B, C, and D were derived from the boundary conditions:

$f_s(\varepsilon_{sh})=f_y$

$f_s(\varepsilon_u)=f_u$

$f_s'(\varepsilon_{sh})=E_{sh}$

$f_s'(\varepsilon_u)=0$

Where: f_u= the ultimate stress of the steel reinforcement

E_{sh}= the slope at the initiation of strain hardening of the steel reinforcement

The constants were solved using the matrix operation:

$$\begin{bmatrix} A \\ B \\ C \\ D \end{bmatrix} = \begin{bmatrix} 1 & \varepsilon_{sh} & \varepsilon_{sh}^2 & \varepsilon_{sh}^3 \\ 1 & \varepsilon_u & \varepsilon_u^2 & \varepsilon_u^3 \\ 0 & 1 & 2\varepsilon_{sh} & 3\varepsilon_{sh}^2 \\ 0 & 1 & 2\varepsilon_u & 3\varepsilon_u^2 \end{bmatrix}^{-1} \cdot \begin{bmatrix} f_y \\ f_u \\ E_{sh} \\ 0 \end{bmatrix}$$

The results from this analysis were then implemented into the moment-curvature analysis which was ultimately used to calculate the tension in the lapped reinforcing steel.

APPENDIX 4E: LOAD VERSUS DISPLACEMENT PLOTS FOR THE WALL SPLICE SPECIMENS

Figure 4E-1 to Figure 4E- 24 as included in this appendix show the load versus midspan deflection plots for the wall splice specimens tested in Phases 1 and 2. The experimental cracking load and the theoretical midspan displacement, based on the analysis discussed in Section 4.4.2, are shown on each plot. The "loops" shown in Figure 4E-13 to Figure 4E-15 are a result of the hydraulic actuator malfunction discussed in Section 4.3. The figures in appendix show that all the wall splice specimens with a 200 mm lap splice length failed in bond prior to the yielding of the reinforcement.

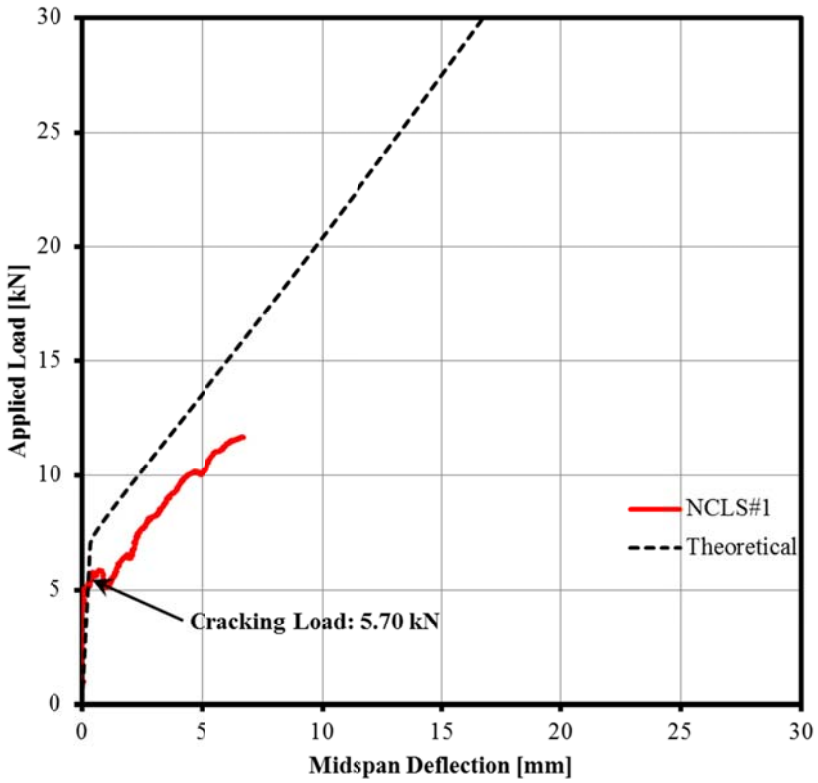

Figure 4E-1: Load Versus Deflection – NCLS#1

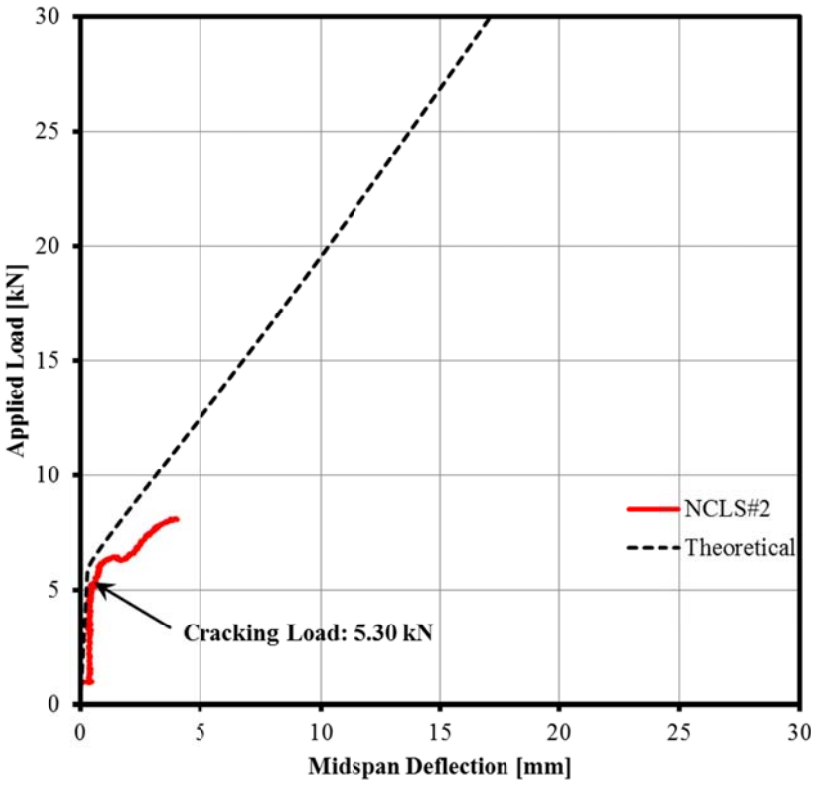

Figure 4E-2: Load Versus Deflection – NCLS#2

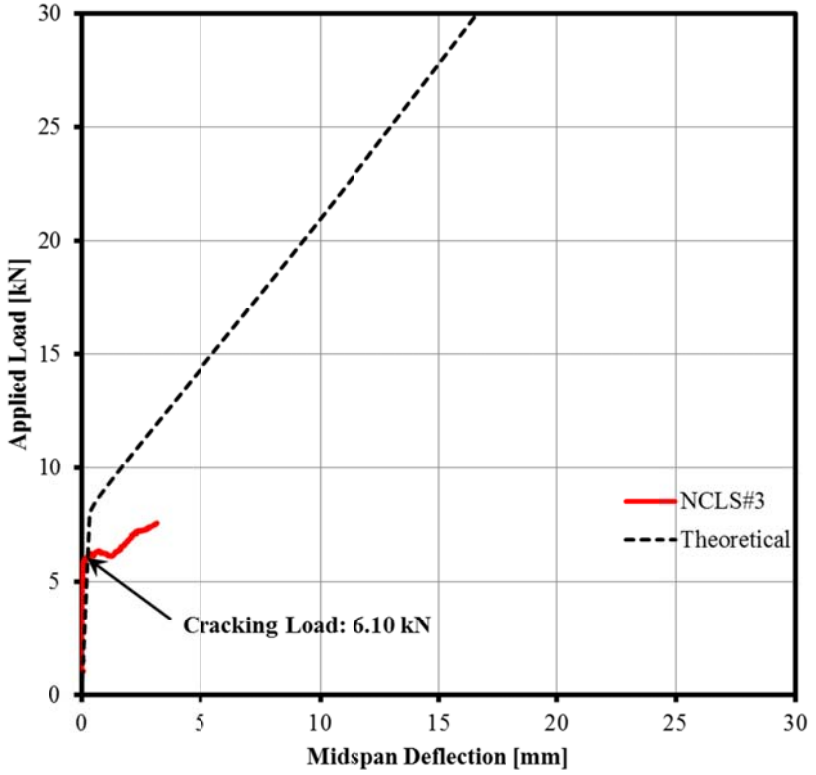

Figure 4E-3: Load Versus Deflection – NCLS#3

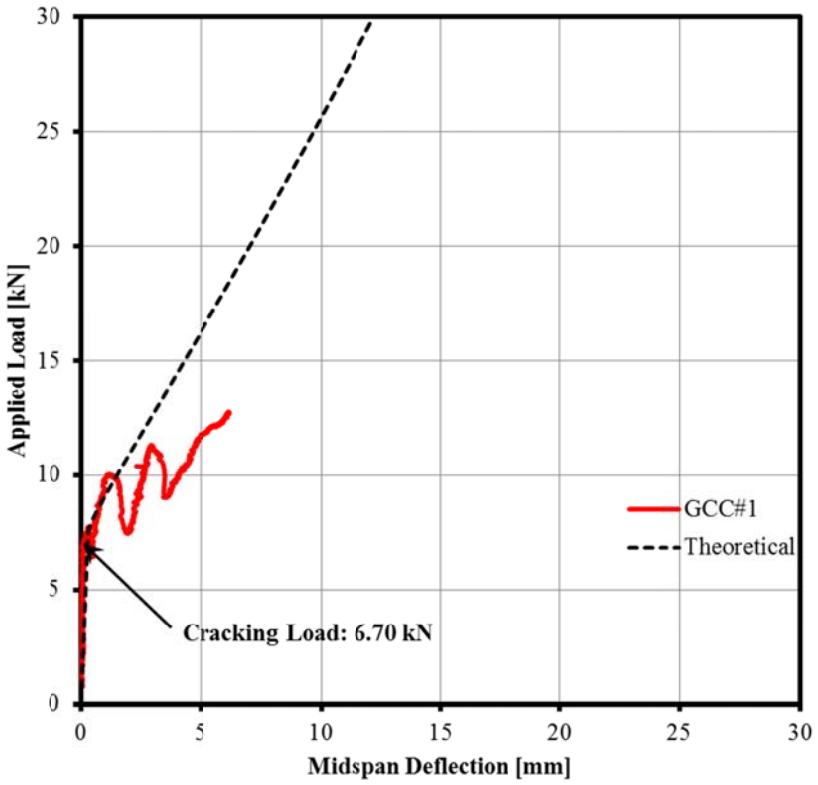

Figure 4E-4: Load Versus Deflection – GCC#1

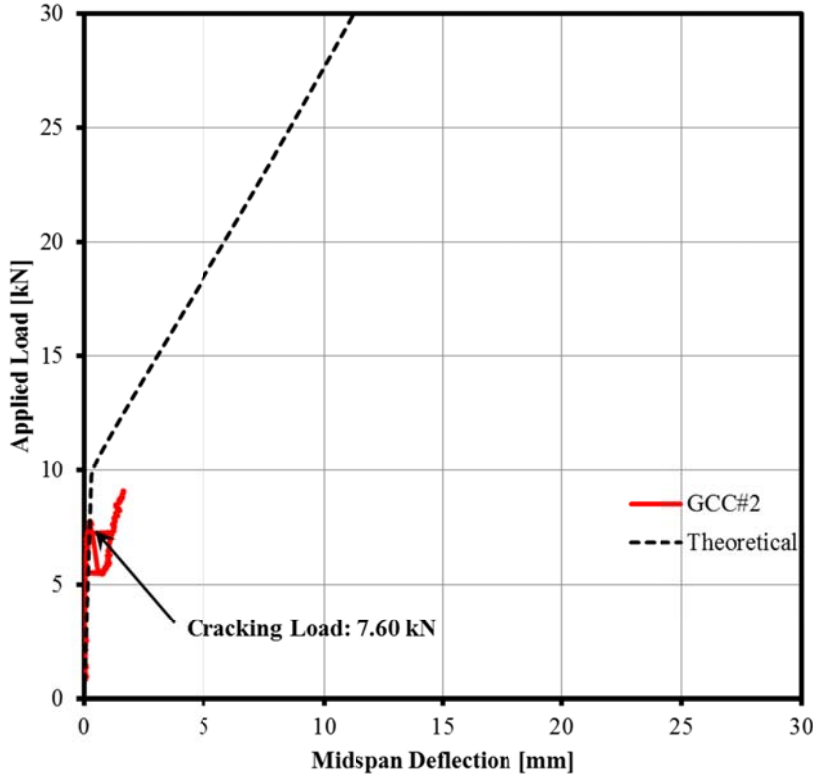

Figure 4E-5: Load Versus Deflection – GCC#2

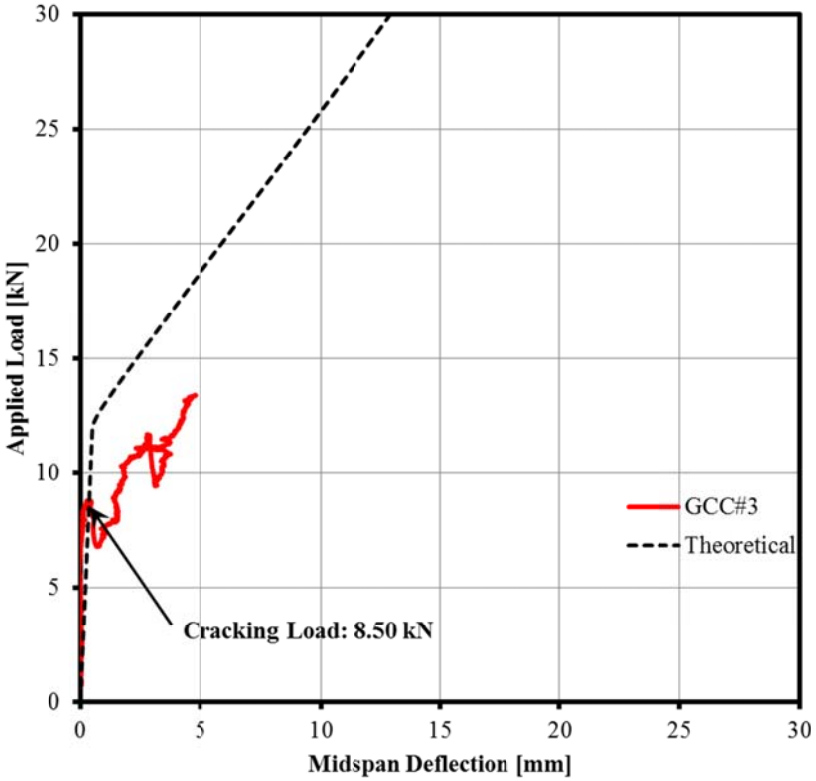

Figure 4E-6: Load Versus Deflection – GCC#3

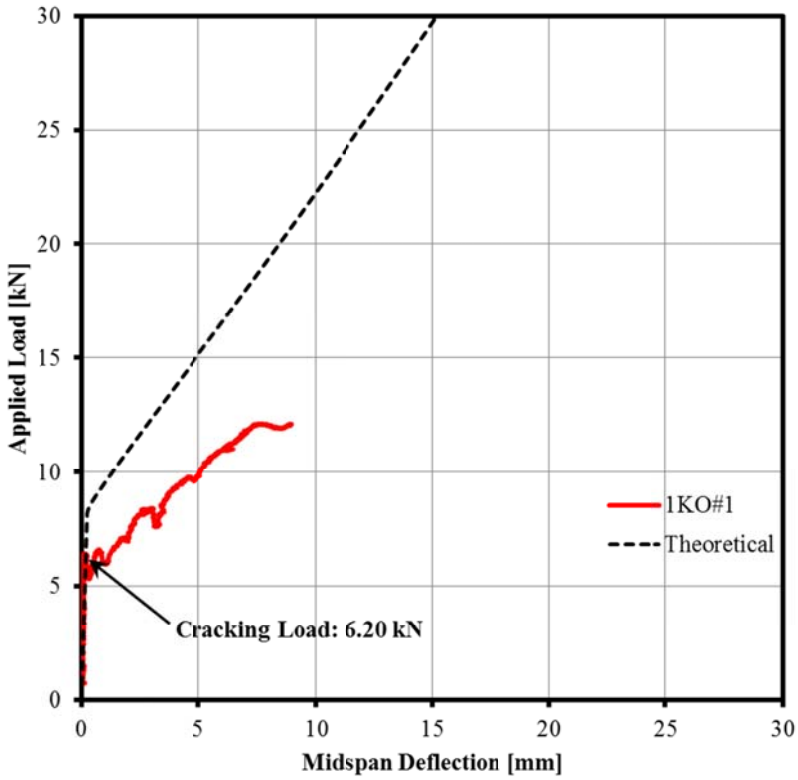

Figure 4E-7: Load Versus Deflection – 1KO#1

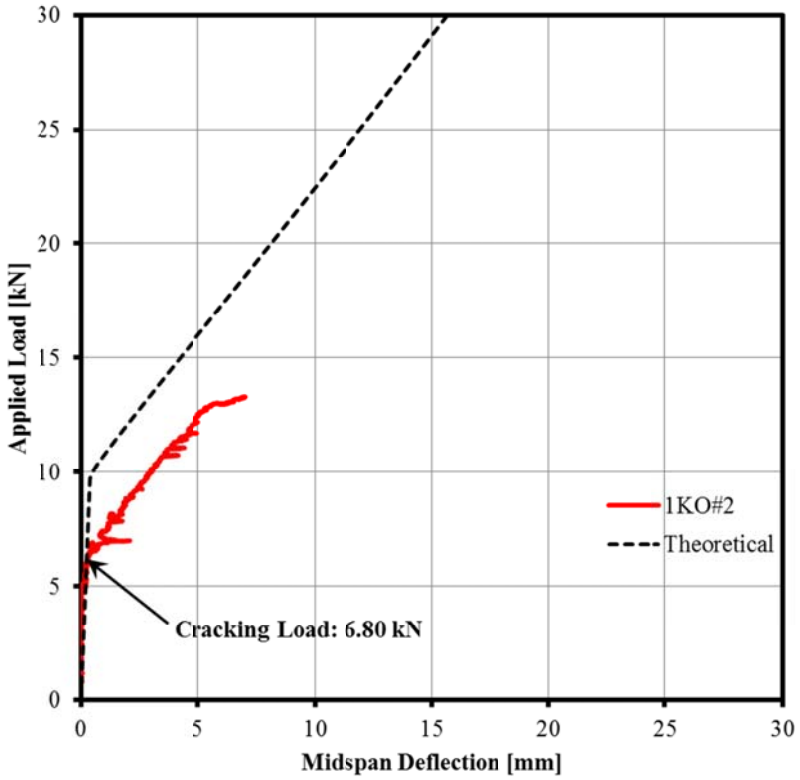

Figure 4E-8: Load Versus Deflection – 1KO#2

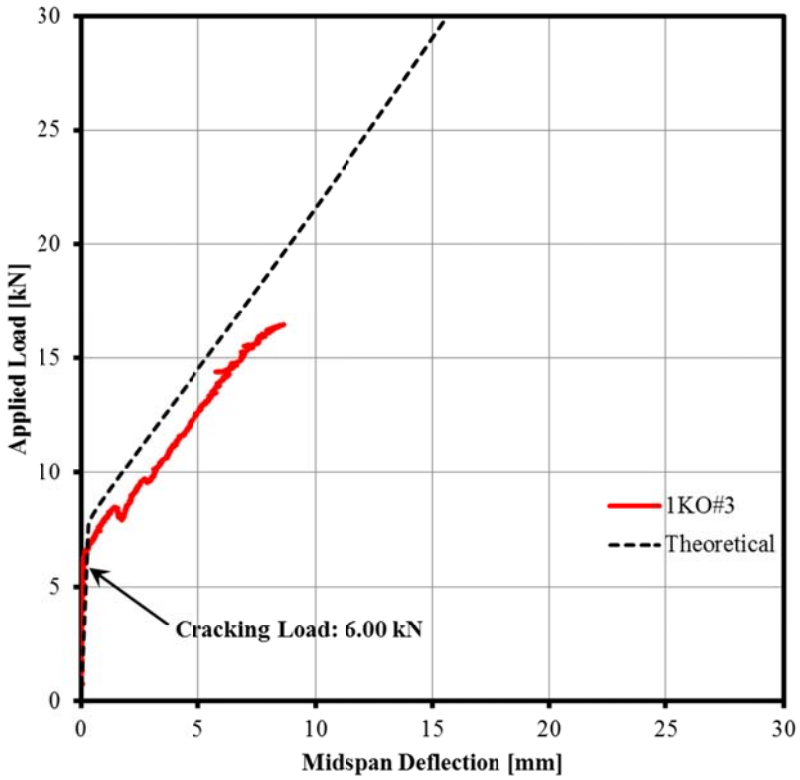

Figure 4E-9: Load Versus Deflection – 1KO#3

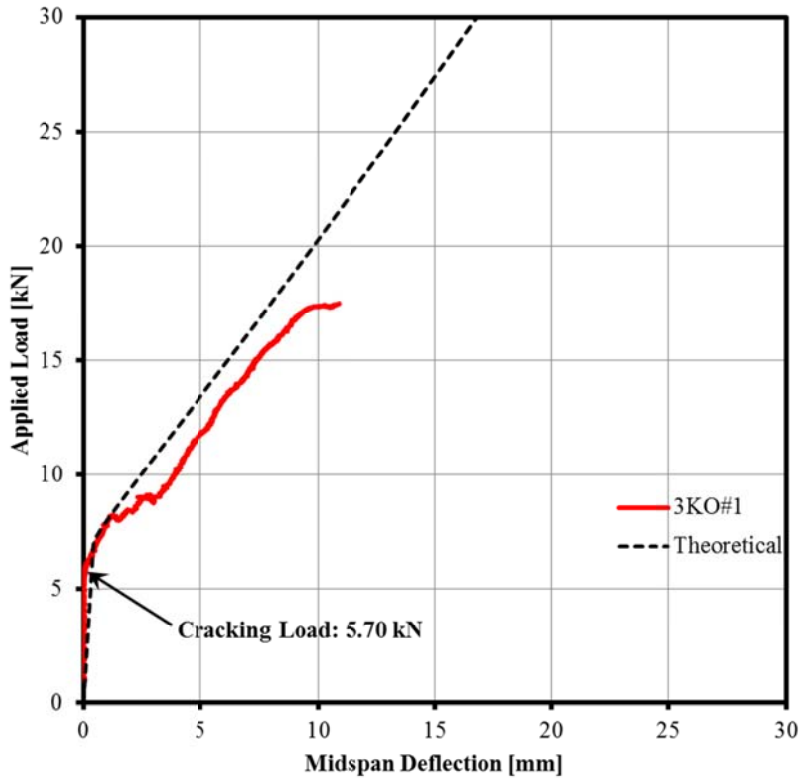

Figure 4E-10: Load Versus Deflection – 3KO#1

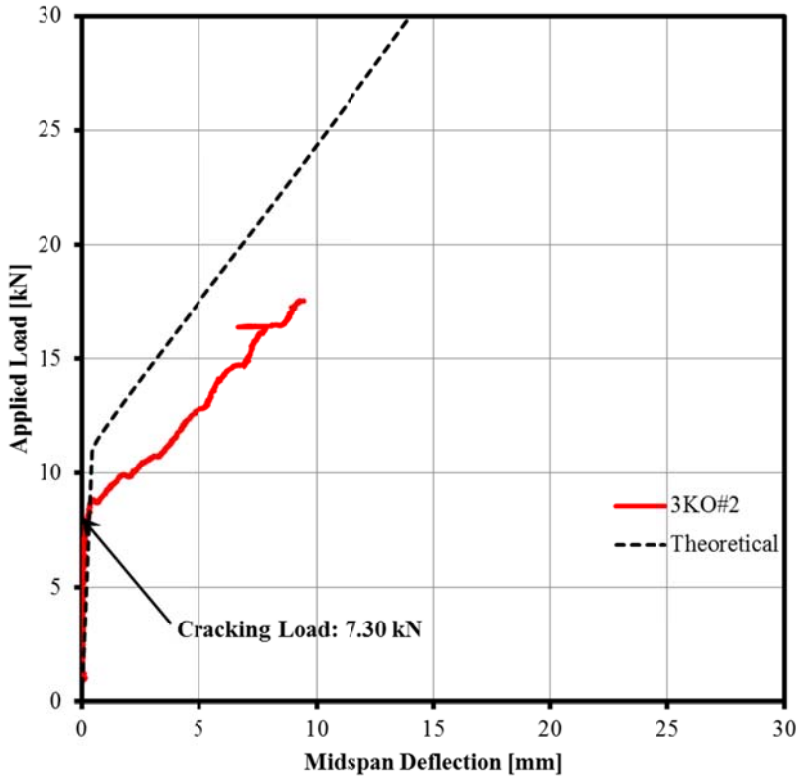

Figure 4E-11: Load Versus Deflection – 3KO#2

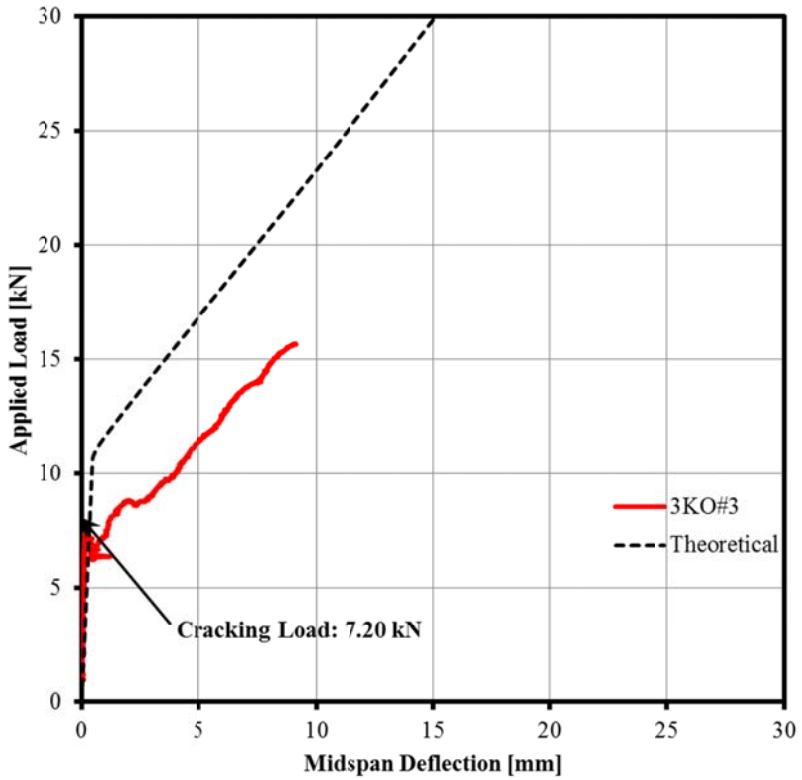

Figure 4E-12: Load Versus Deflection – 3KO#3

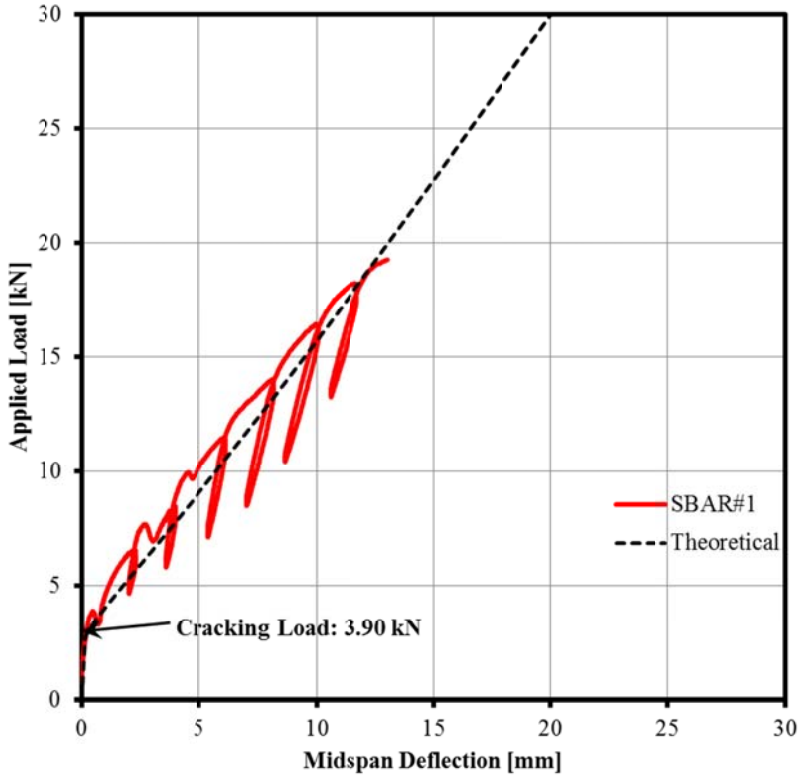

Figure 4E-13: Load Versus Deflection – SBAR#1

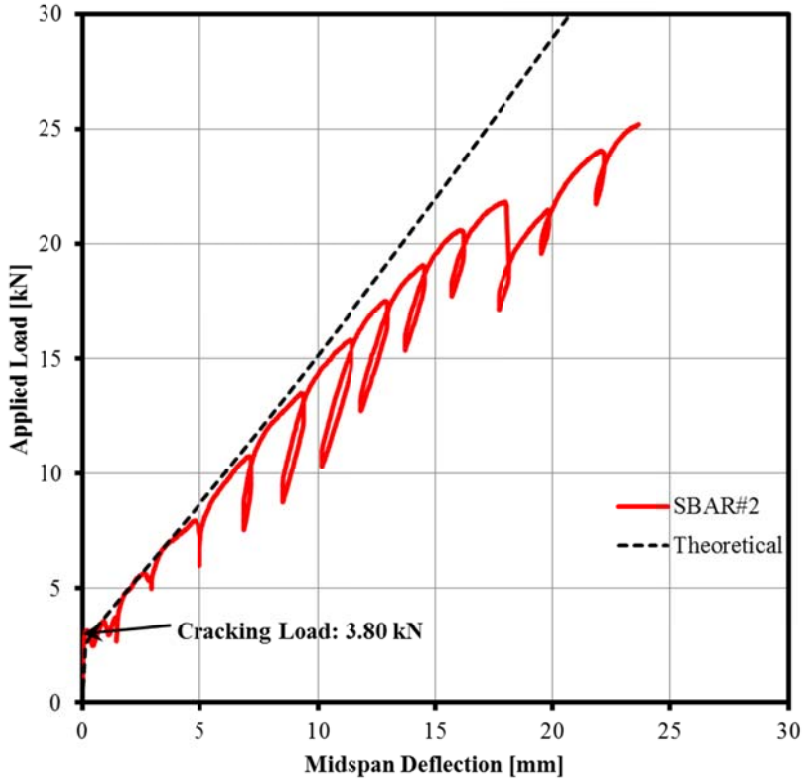

Figure 4E-14: Load Versus Deflection – SBAR#2

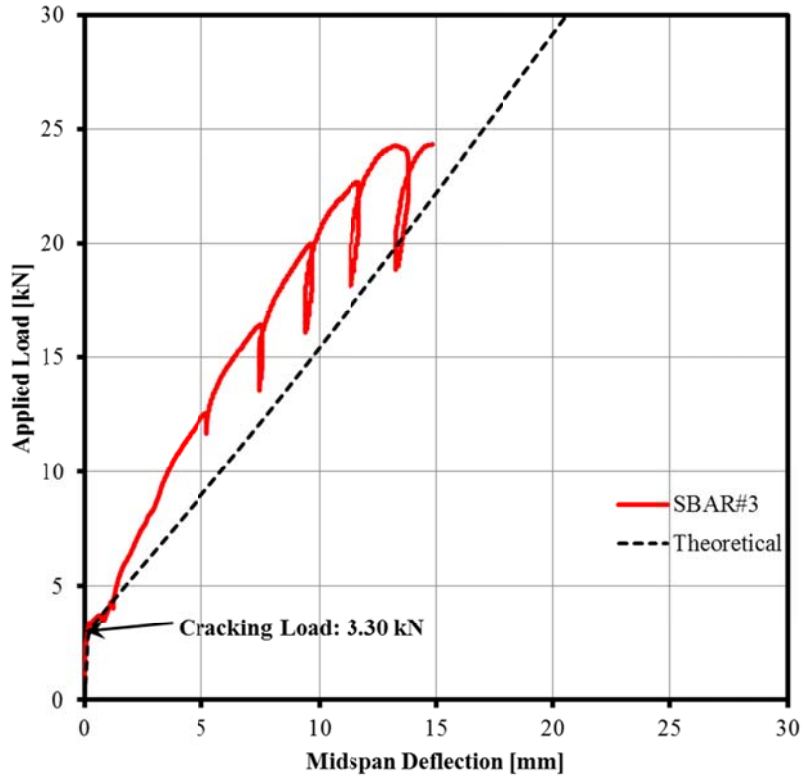

Figure 4E-15: Load Versus Deflection – SBAR#3

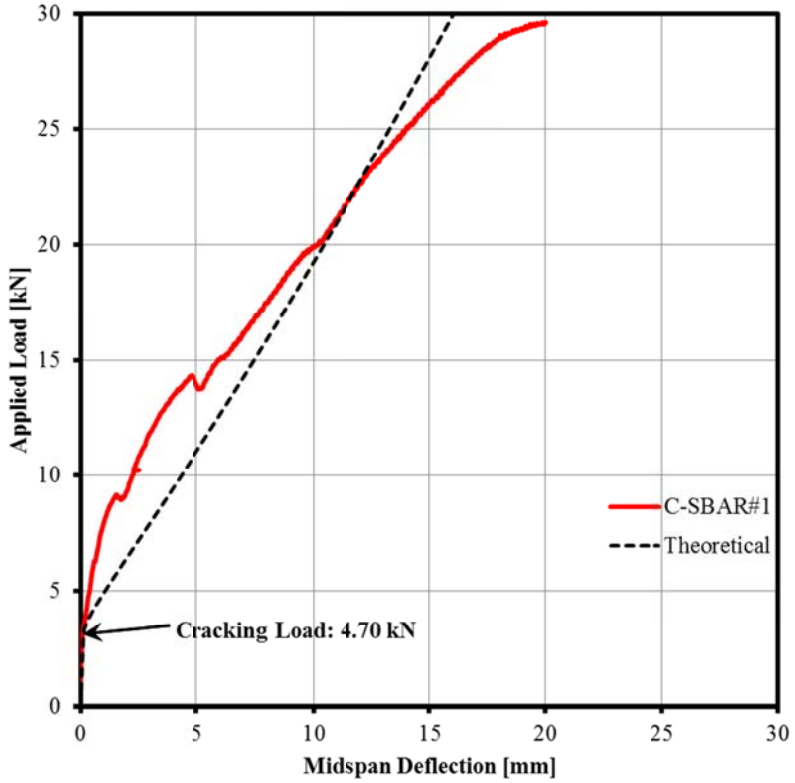

Figure 4E-16: Load Versus Deflection – C-SBAR#1

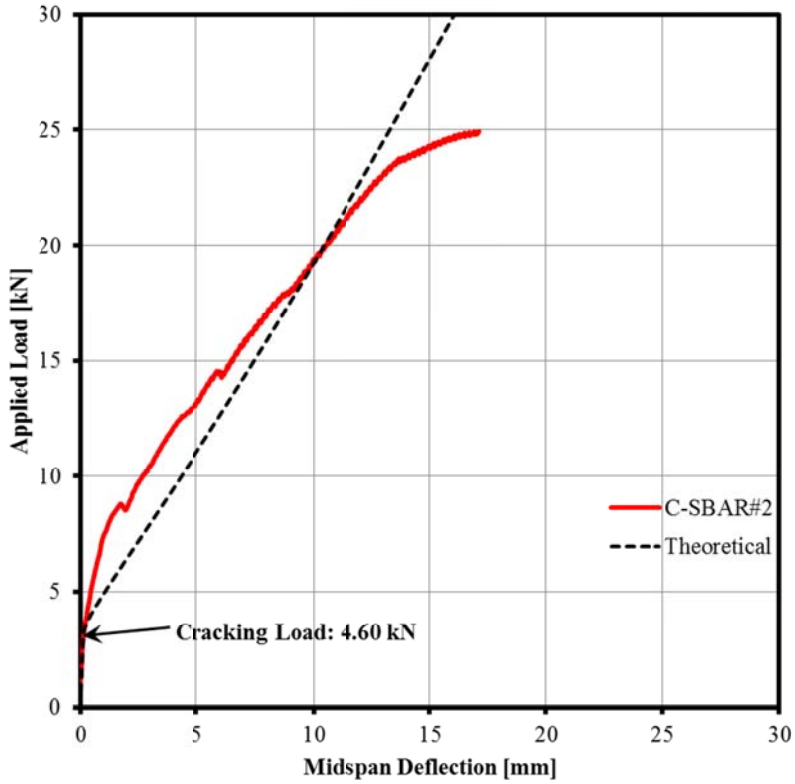

Figure 4E-17: Load Versus Deflection – C-SBAR#2

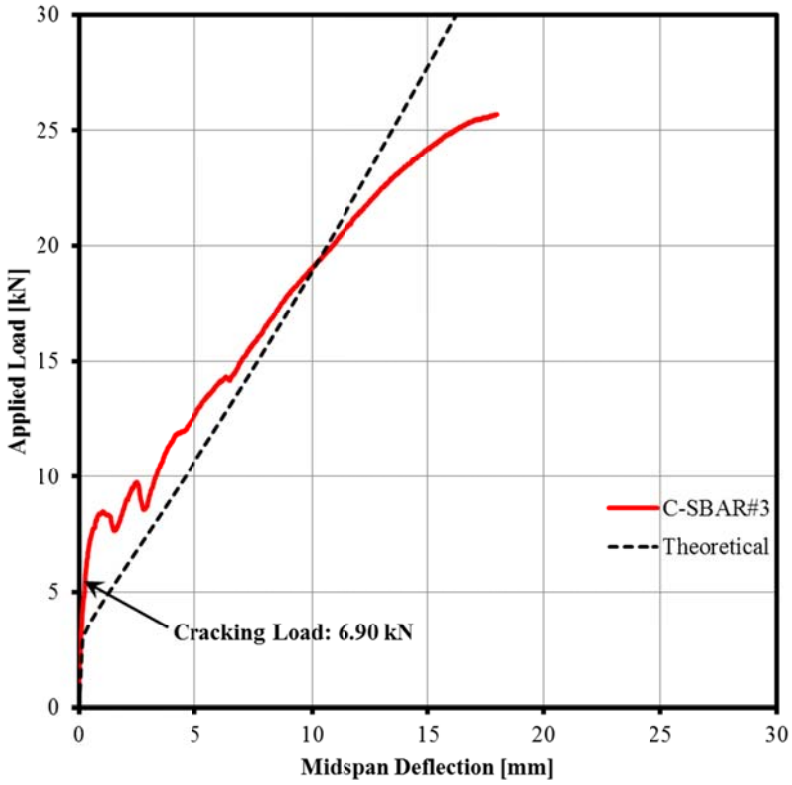

Figure 4E-18: Load Versus Deflection – C-SBAR#3

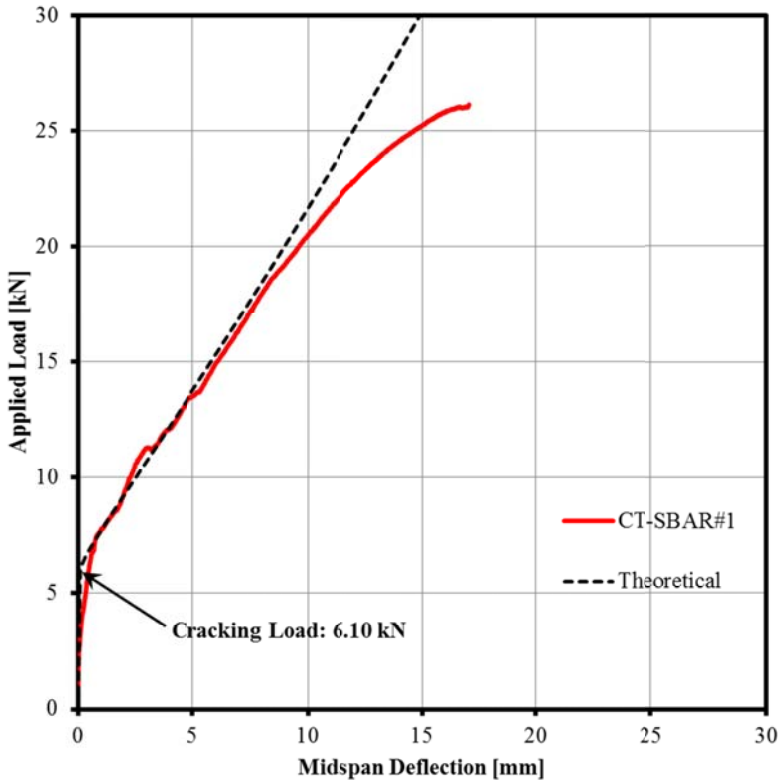

Figure 4E-19: Load Versus Deflection – CT-SBAR#1

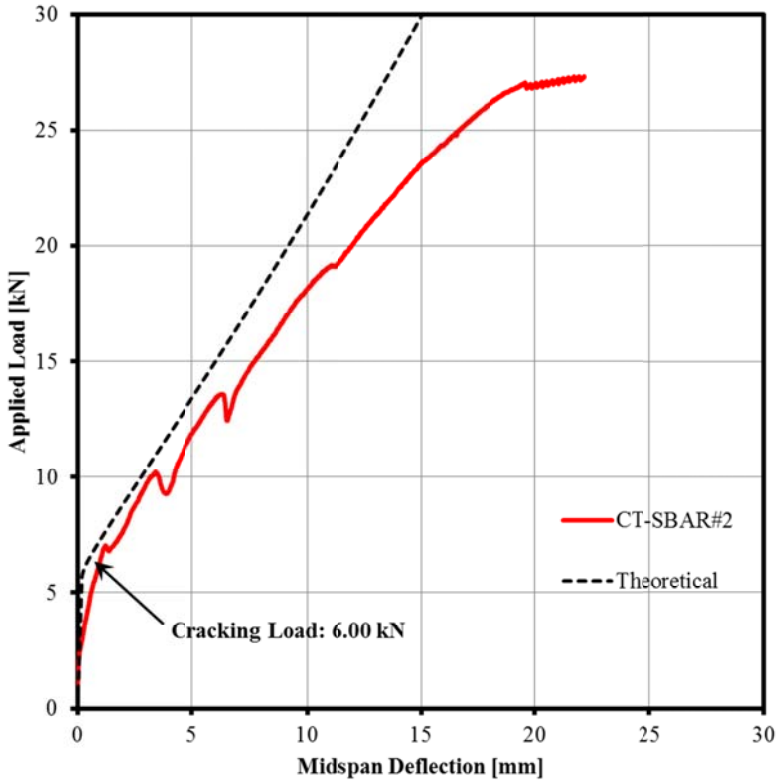

Figure 4E-20: Load Versus Deflection – CT-SBAR#2

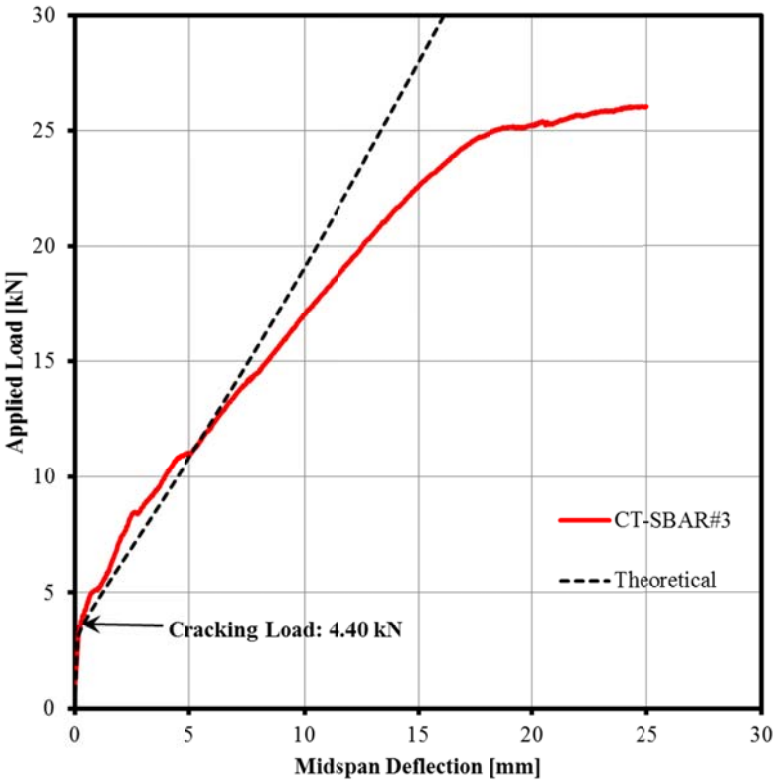

Figure 4E-21: Load Versus Deflection – CT-SBAR#3

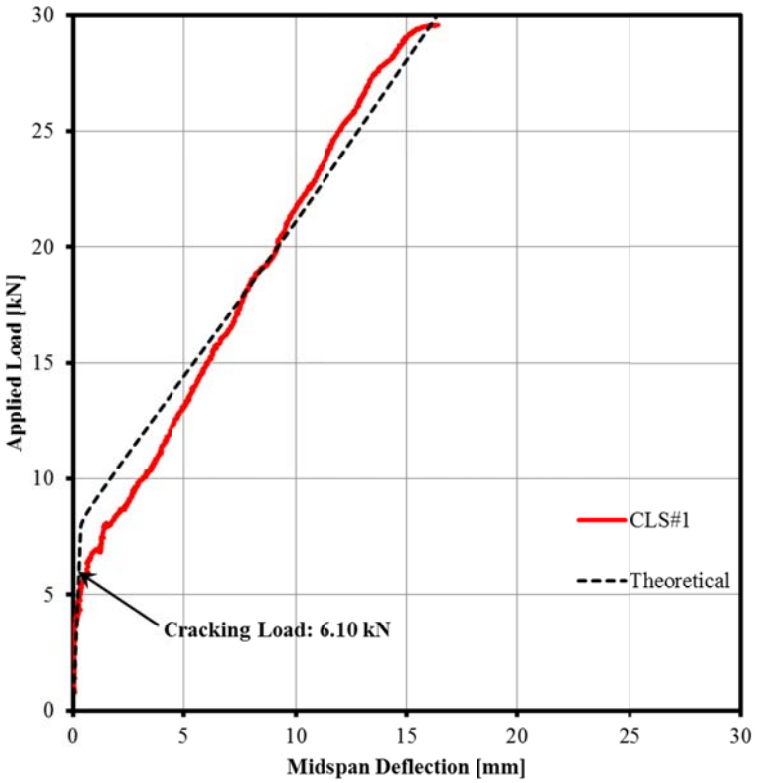

Figure 4E-22: Load Versus Deflection – CLS#1

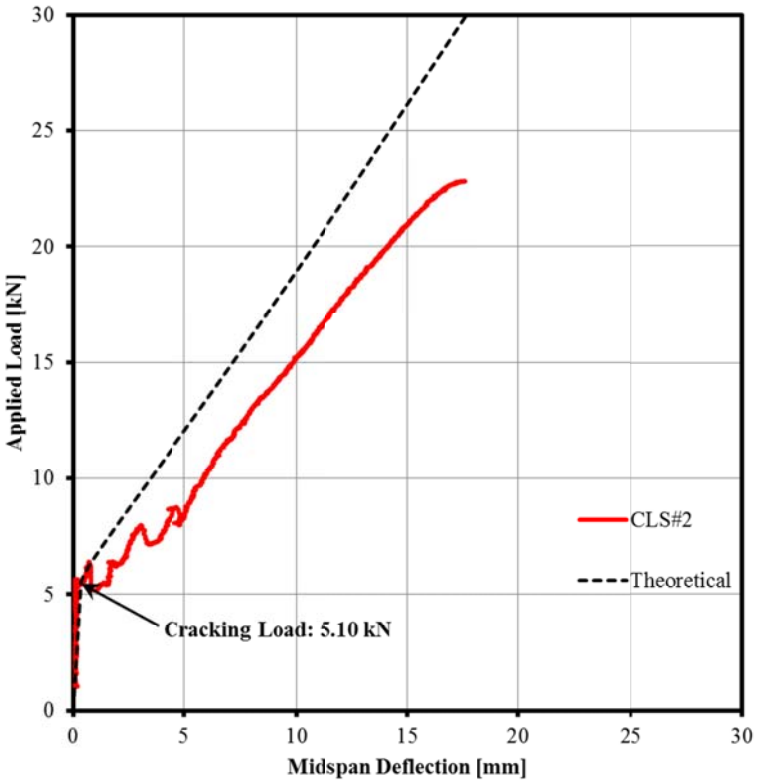

Figure 4E-23: Load Versus Deflection – CLS#2

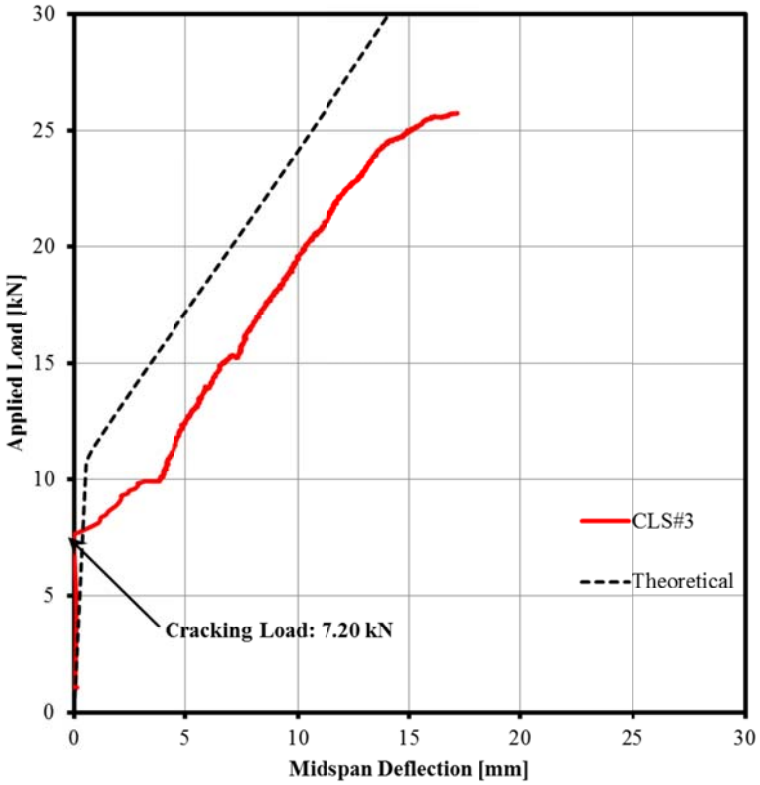

Figure 4E- 24: Load Versus Deflection – CLS#3

APPENDIX 4F: DEVELOPMENT OF THE THEORETICAL COMPRESSIVE STRESS-STRAIN CURVE FOR THE GROUTED MASONRY ASSEMBLAGE

This appendix presents the mathematical expressions used in the derivation of the theoretical compressive stress versus strain response of the grouted masonry assemblage. As discussed in Section 4.1.4, a modified Kent-Park curve (1971) was adopted to represent this stress versus strain response. The curve was comprised of two segments: a parabolic rising curve, followed by a linearly decreasing curve. The compressive stress in the masonry assemblage at any given strain, $f_m(\varepsilon_m)$, was determined by:

Rising Curve: ($\varepsilon_m \leq 0.002K$)

$$f_m(\varepsilon_m)=K\cdot f'_m\cdot\left[\left(\frac{2\varepsilon_m}{0.002K}\right)-\left(\frac{\varepsilon_m}{0.002K}\right)^2\right] \quad [4F\text{-}1]$$

Where: $$K=1+\rho_s\cdot\left(\frac{f_{yh}}{f'_m}\right) \quad [4F\text{-}2]$$

ε_m= the masonry prism compressive strain

f'_m= the unconfined masonry prism compressive strength [MPa]

f_{yh}= the yield strength of the confinement steel (equal to zero since the masonry prisms did not contain confining steel)

K= strength enhancement factor (equal to one for masonry which does not contain confining steel)

ρ_s= the volumetric ratio for the confining steel (equal to zero since the masonry prisms did not contain confining steel)

Falling Curve: ($0.002K < \varepsilon_m \leq 0.01$)

$$f_m(\varepsilon_m)=K\cdot f'_m\cdot[1-Z_m\cdot(\varepsilon_m-0.002K)] \quad [4F\text{-}3]$$

Where: $$Z_m=\frac{0.5}{\left(\frac{3MPa+0.29f'_m}{145f'_m-1000MPa}\right)-0.002K} \quad [4F\text{-}4]$$

The results from this analysis were then implemented into the moment-curvature analysis which was ultimately used to calculate the tension in the lapped steel reinforcing bars.

APPENDIX 4G: DEVELOPMENT OF THE THEORETICAL MOMENT-CURVATURE ANALYSIS

This appendix presents the mathematical expressions used in the development of the theoretical moment-curvature analysis and the resulting MathCAD code. A similar numerical analysis was also used to calculate the tension in the reinforcing steel from the curvature at the ultimate moment. The MathCAD code for this calculation is also shown in this appendix. The error associated with the selection of the number of segments used to calculate the compressive force in the cross section of the wall splice specimen is also presented.

Un-Cracked Moment-Curvature Analysis:

A linear moment-curvature relationship exists prior to the initial cracking of the wall splice specimen. This relationship is represented by:

$$\phi_{uc} = \frac{M_{cr}}{E'_m I_g} \qquad [4G\text{-}1]$$

Where: $E'_m = 850f'_m$: the modulus of elasticity of masonry, as calculated in accordance to CSA S304.1-04 (CSA, 2004) [MPa]

I_g= the gross moment of inertia for the wall splice specimen cross-section [mm^4]

M_{cr}= the cracking moment determined by the experimental values reported in Table 4.4 [kN·m]

Cracked Moment-Curvature Analysis:

The depth of the neutral axis, c, needed to be assumed to determine the curvature of the wall splice specimen following the initiation of cracking. The strain at the extreme compressive fibre, ε_{ex}, was then calculated using similar triangles from the linear strain diagram shown in Figure 4.20 (b):

$$\varepsilon_{ex} = c \cdot \phi \qquad [4G\text{-}2]$$

Where: ϕ= the curvature of the wall splice specimen

The distance from the compression face to the neutral axis, c, was then divided into 100 equal layers, each with a thickness of $\frac{c}{100}$. The calculation for the error associated with 100 equal layers is shown at the end of this appendix. The strain at the j^{th} layer, ε_j, was calculated using the linear strain profile shown in Figure 4.20 (b):

$$\varepsilon_j = d_j \cdot \frac{\varepsilon_{ex}}{c} \qquad [4G\text{-}3]$$

Where: d_j= the distance from the neutral axis to the centroid of the j^{th} layer [mm]

The compressive stress in the j^{th} layer, f_j, was then calculated using the equations for the compressive strain of the masonry assemblage, 4F-1 and 4F-3, shown in Appendix 4F.

$$f_j = f_m(\varepsilon_m) \qquad [4G\text{-}4]$$

Where: f_m = the function used to determine compressive stress in the masonry assemblage at a given strain

Assumption of the compressive stress in all layers then resulted in the total compressive force developed in the compressive zone:

$$C_{tot} = \sum_{n=1}^{100} f_{m_n} \cdot b \cdot \frac{c}{100} \qquad [4G\text{-}5]$$

Where: b= the width of the wall splice specimen [mm]

The strain in the reinforcement was also determined using similar triangles from the linear strain diagram shown in Figure 4.20 (b). This strain value was then used in the equations 4D-1, 4D-2, and 4D-3, shown in Appendix 4D, to calculate the stress in the reinforcing steel.

$$\sigma_s = f_s\left[\frac{\varepsilon_{ex}}{c} \cdot (d_{eff} - c)\right] \qquad [4G\text{-}6]$$

Where: f_s = the function used to determine tensile stress in the steel reinforcement at a given strain

d_{eff}= the effective depth to the reinforcing steel from the compressive face of the wall splice specimen [mm]

The tension in reinforcement, T, was then computed:

$$T = \sigma_s \cdot A_s \qquad [4G\text{-}7]$$

Where: A_s= the cross-sectional area of the longitudinal reinforcing steel in the wall splice specimen [mm^2]

An iterative MathCAD program, included as follows, was used to determine the depth of the neutral axis, c, such that equilibrium between the compressive and tensile forces ($C_{tot} = T$) was satisfied to a 0.5% tolerance. The total cross-sectional moment, M_{tot}, was calculated once the neutral axis depth was established:

$$M_{tot} = \sum_{n=1}^{100} f_{m_n} \cdot b \cdot d_n + [T \cdot (d_{eff} - c)] \qquad [4G\text{-}8]$$

Iterative MathCAD Program Code:

List of Symbols:

A_s Cross-sectional area of the lapped longitudinal reinforcement in a wall splice specimen [mm^2]

b Width of wall splice specimen [mm]

c Depth to neutral axis from the compression face [mm]

c_{guess} Assumed depth to neutral axis from the compression face [mm]

C_{tot} Total compressive force in the wall splice specimen cross-section [kN]

$curve_{tot}$ Complete moment-curvature function including un-cracked and cracked analyses

d_{eff} Depth to the centroid of the steel reinforcement from the compressive face [mm]

E_m Compressive modulus of elasticity of the masonry assemblage [MPa]

f_m Function used to determine compressive stress in the masonry assemblage

f_s Function used to determine tensile stress in the reinforcement

I_g Gross moment of inertia [mm^4]

M_c Moment due to compressive forces in the wall splice specimen cross-section [kN·m]

M_{tot} Total moment due to forces in the cross-section of the wall splice specimen [kN·m]

T Tensile force in the steel reinforcement [kN]

ε_{ex} Strain in the extreme compressive fibre for an assumed neutral axis depth, c_{guess}

$\varepsilon_{extreme}$ Strain in the compressive fibre for the calculated neutral axis depth, c

ε_s Strain at the level of the steel reinforcement

σ_s Stress in the lapped reinforcement

Moment Corresponding to a Given Curvature (Cracked Section):

$$
\begin{aligned}
&M_c(\phi) := \left|
\begin{array}{l}
\text{for } i \in 60, 59.9 .. 10 \\
\quad \left|
\begin{array}{l}
c_{guess} \leftarrow i \cdot mm \\
\varepsilon_{ex} \leftarrow c_{guess} \cdot \phi \\
\text{for } j \in 1 .. 100 \\
\quad \left|
\begin{array}{l}
d_j \leftarrow \dfrac{c_{guess}}{100} \cdot (j - 0.5) \\
\varepsilon_j \leftarrow \dfrac{\varepsilon_{ex}}{c_{guess}} \cdot d_j \\
f_j \leftarrow f_m(\varepsilon_j)
\end{array}
\right. \\
C_{tot} \leftarrow \left(\sum_{n=1}^{100} f_n \right) \cdot b \cdot \dfrac{c_{guess}}{100} \\
\sigma_{s.guess} \leftarrow f_s\left[\dfrac{\varepsilon_{ex}}{c_{guess}} \cdot (d_{eff} - c_{guess}) \right] \\
T \leftarrow \sigma_{s.guess} \cdot A_s \\
c \leftarrow c_{guess} \quad \text{if} \left| \dfrac{C_{tot} - T}{T} \right| \le 0.005
\end{array}
\right. \\
\varepsilon_{extreme} \leftarrow c \cdot \phi \\
\text{for } k \in 1 .. 100 \\
\quad \left|
\begin{array}{l}
d_k \leftarrow \dfrac{c}{100} \cdot (k - 0.5) \\
\varepsilon_k \leftarrow \dfrac{\varepsilon_{extreme}}{c} \cdot d_k \\
f_k \leftarrow f_m(\varepsilon_k) \\
M_{C_k} \leftarrow f_k \cdot b \cdot \dfrac{c}{100} \cdot d_k
\end{array}
\right. \\
\varepsilon_s \leftarrow \dfrac{\varepsilon_{extreme}}{c} \cdot (d_{eff} - c) \\
T \leftarrow A_s \cdot f_s(\varepsilon_s) \\
M_{total} \leftarrow \sum_{n=1}^{100} M_{C_n} + T \cdot (d_{eff} - c) \\
M_{total}
\end{array}
\right.
\end{aligned}
$$

Moment and Curvature Arrays (Cracked Section):

```
Moment := | mom_1 ← 0kN·m
          | for i ∈ 1..429
          |   momϕ ← i·0.001·1/m
          |   mom_(i+1) ← M_c(momϕ)
          |   trace(momϕ)
          |   trace(mom)
          | mom
```

```
Curvature := | for i ∈ 1..430
             |   curv_i ← (i − 1)·0.001·1/m
             | curv
```

Moment =

	1
1	0
2	0.466
3	0.932
4	1.396
5	1.859
6	2.321
7	2.782
8	3.242
9	3.701
10	...

·kN·m

Curvature =

	1
1	0
2	$1\cdot10^{-3}$
3	$2\cdot10^{-3}$
4	$3\cdot10^{-3}$
5	$4\cdot10^{-3}$
6	$5\cdot10^{-3}$
7	$6\cdot10^{-3}$
8	$7\cdot10^{-3}$
9	$8\cdot10^{-3}$
10	...

$\frac{1}{m}$

Curvature Corresponding to any Moment (Cracked Section):

```
curve(x) := | cur ← Curvature_1  if x = 0kN·m
            | for i ∈ 1..450                          if x ≠ 0kN·m
            |   if x < Moment_i
            |     C1 ← Curvature_i
            |     C2 ← Curvature_(i−1)
            |     M1 ← Moment_i
            |     M2 ← Moment_(i−1)
            |     cur ← C2 + [ ((x − M2)·C1 − (x − M2)·C2) / (M1 − M2) ]
            |     break
            | cur
```

Moment-Curvature Plot with Combined Un-Cracked and Cracked Sections:

Curvature corresponding to a given moment for both un-cracked and cracked sections:

$$\text{curve}_{tot}(m) := \begin{cases} k \leftarrow \dfrac{m}{E_m \cdot I_g} & \text{if } m \le M_{cr} \\ k \leftarrow \text{curve}(m) & \text{otherwise} \\ k \end{cases}$$

Representative Plot – CLS#3:

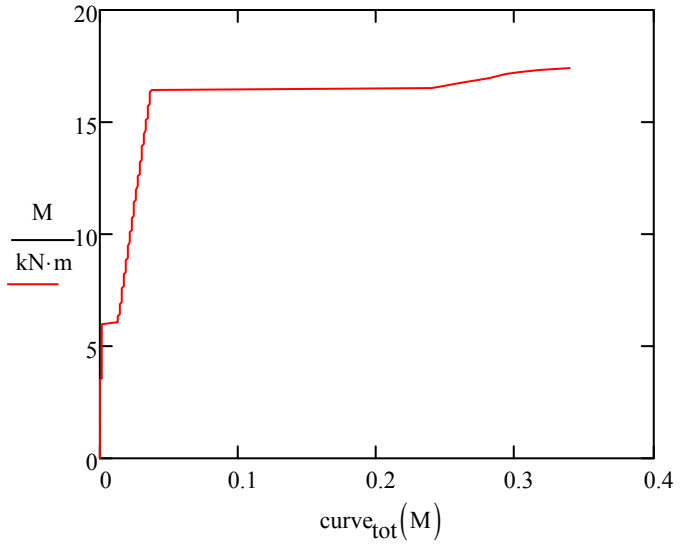

Tension in the Lapped Reinforcement Corresponding to a Given Curvature:

$$\text{Tension}(\phi) := \left| \begin{array}{l} \text{for } i \in 60, 59.9 .. 10 \\ \quad \left| \begin{array}{l} c_{guess} \leftarrow i \cdot mm \\ \varepsilon_{ex} \leftarrow c_{guess} \cdot \phi \\ \text{for } j \in 1 .. 100 \\ \quad \left| \begin{array}{l} d_j \leftarrow \dfrac{c_{guess}}{100} \cdot (j - 0.5) \\ \varepsilon_j \leftarrow \dfrac{\varepsilon_{ex}}{c_{guess}} \cdot d_j \\ f_j \leftarrow f_m(\varepsilon_j) \end{array} \right. \\ C_{tot} \leftarrow \left(\sum_{n=1}^{100} f_n \right) \cdot b \cdot \dfrac{c_{guess}}{100} \\ \sigma_{s.guess} \leftarrow f_s\left[\dfrac{\varepsilon_{ex}}{c_{guess}} \cdot (d_{eff} - c_{guess}) \right] \\ T \leftarrow \sigma_{s.guess} \cdot A_s \\ c \leftarrow c_{guess} \quad \text{if} \left| \dfrac{C_{tot} - T}{T} \right| \le 0.005 \end{array} \right. \\ \varepsilon_{extreme} \leftarrow c \cdot \phi \\ \varepsilon_s \leftarrow \dfrac{\varepsilon_{extreme}}{c} \cdot (d_{eff} - c) \\ T \leftarrow A_s \cdot f_s(\varepsilon_s) \\ T \end{array} \right.$$

Associated Error with the Selection of 100 Compressive Strips:

Figure 4G-1 shows the resulting moments corresponding to a fixed curvature of 0.025/m when the number of segments in the compression zone, n, was varied. The curvature value was selected such that it was located in the linear moment-curvature region prior to yielding of the reinforcement. The calculated moment values corresponding to n= 10, 25, 50, 100, 250, 500, and 1000 yielded the values: 10.180 kNm, 10.184 kNm, 10.185 kNm, 10.185 kNm, 10.185 kNm, 10.185 kNm, 10.185 kNm, respectively. Figure 4G-1 shows that the asymptote is located at approximately 10.185 kNm, therefore the resulting error associated with the selection of n=100 in the moment-curvature analysis is less than 0.1%.While this result corresponds to a specific value of curvature it is representative of the error of the whole data set and it also implies that there is little error associated with the chosen "n".

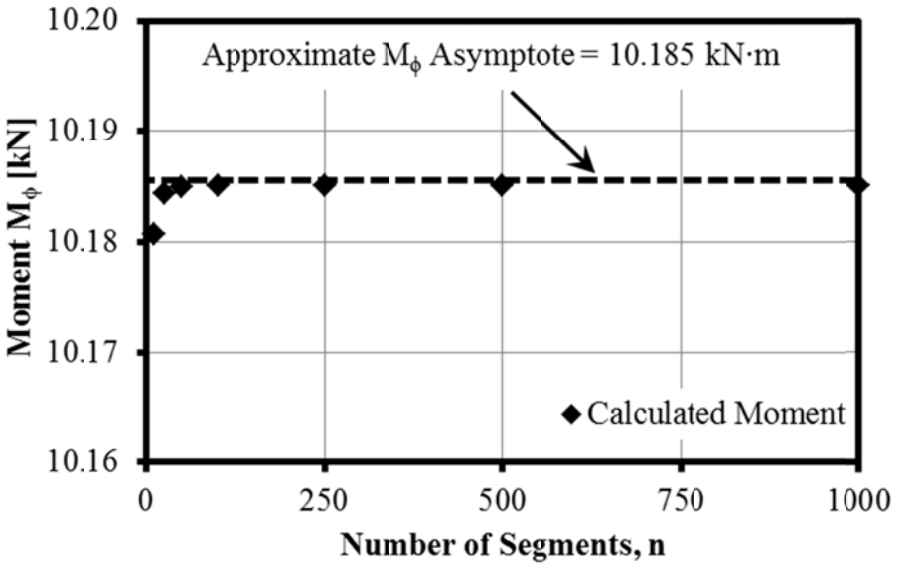

Figure 4G-1: Moment Corresponding to a Fixed Curvature of 0.025/m Versus the Number of Segments in the Compression Zone.

APPENDIX 4H: MOMENT-CURVATURE PLOTS FOR THE WALL SPLICE SPECIMENS

Figure 4H-1 to Figure 4H-24, as included in this appendix, show the moment-curvature plots for the wall splice specimens tested in Phases 1 and 2. The theoretical moment-curvature, based on the analysis discussed in Section 4.4.1 and provided in detail in Appendix 4G, is also shown on each plot. The "loops" shown in Figure 4H-13 to Figure 4H-15 are a result of the hydraulic actuator malfunction discussed in Section 4.3. All figures included herein show that all of the wall splice specimens failed in bond prior to the yielding of the reinforcement.

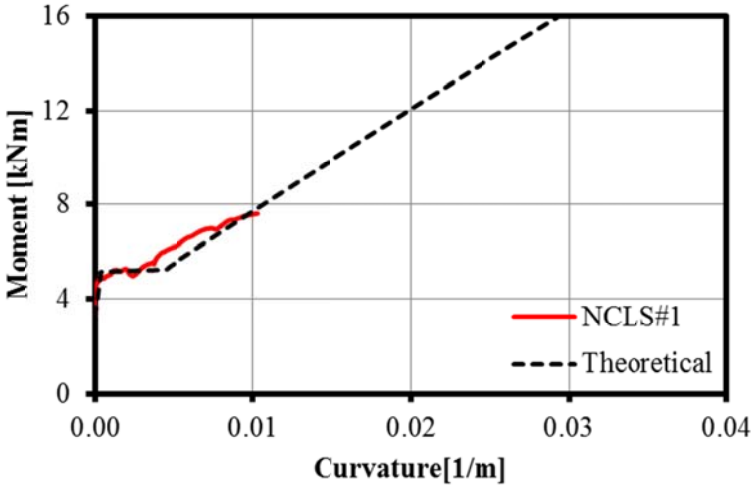

Figure 4H-1: Moment-Curvature Plot – NCLS#1

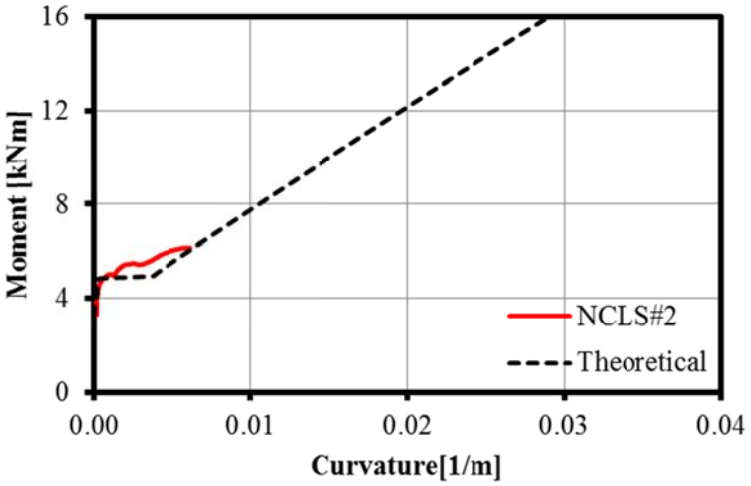

Figure 4H-2: Moment-Curvature Plot – NCLS#2

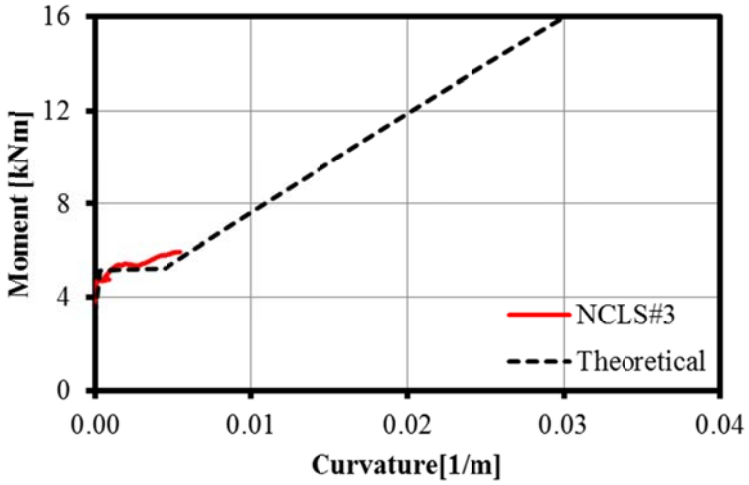

Figure 4H-3: Moment-Curvature Plot – NCLS#3

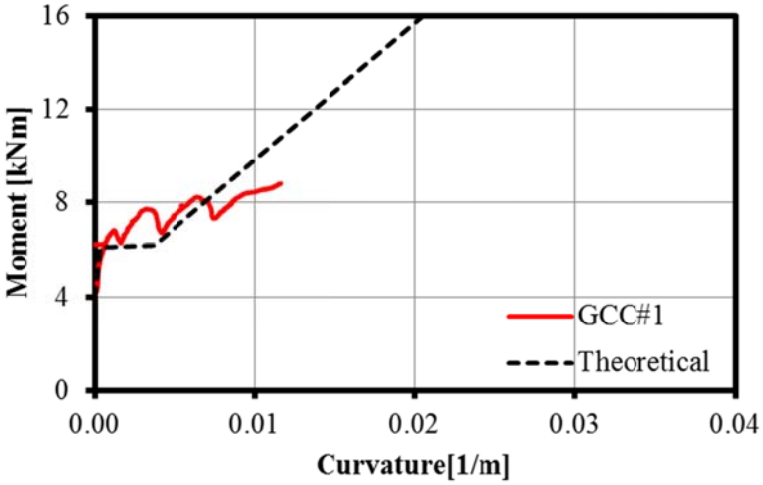

Figure 4H-4: Moment-Curvature Plot – GCC#1

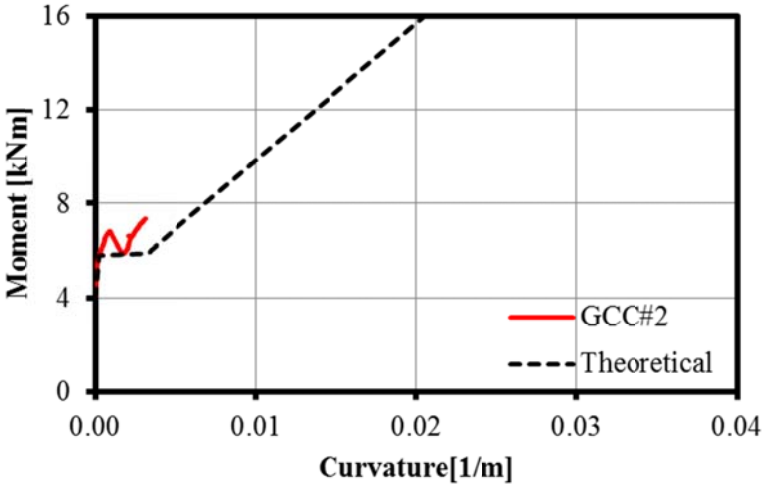

Figure 4H-5: Moment-Curvature Plot – GCC#2

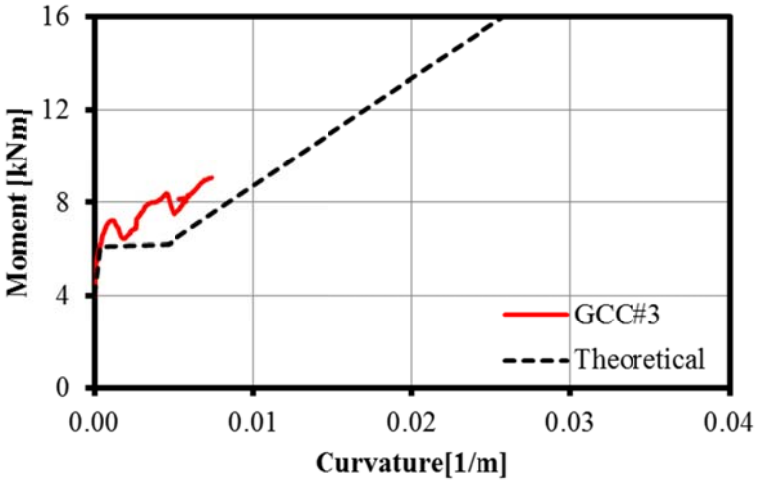

Figure 4H-6: Moment-Curvature Plot – GCC#3

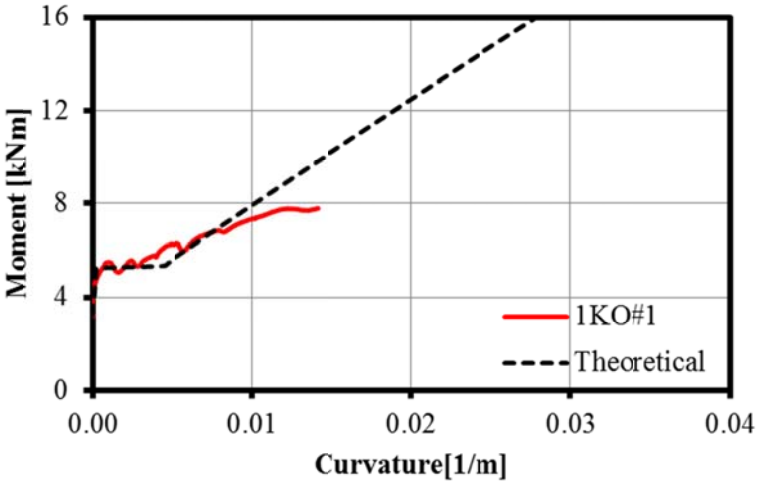

Figure 4H-7: Moment-Curvature Plot – 1KO#1

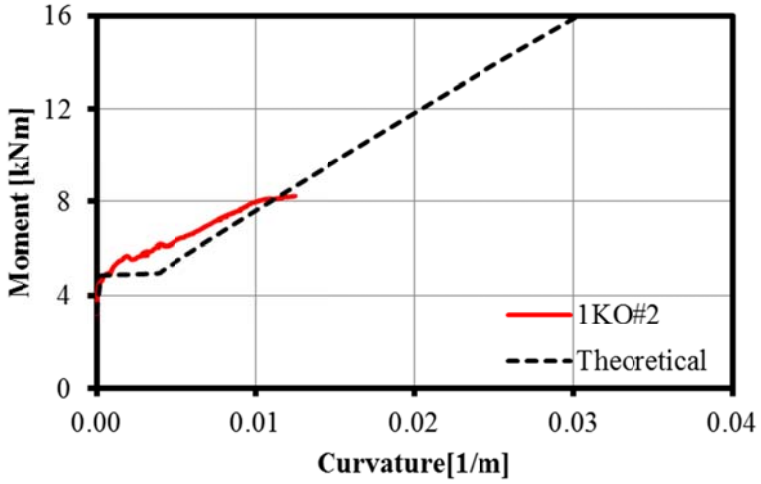

Figure 4H-8: Moment-Curvature Plot – 1KO#2

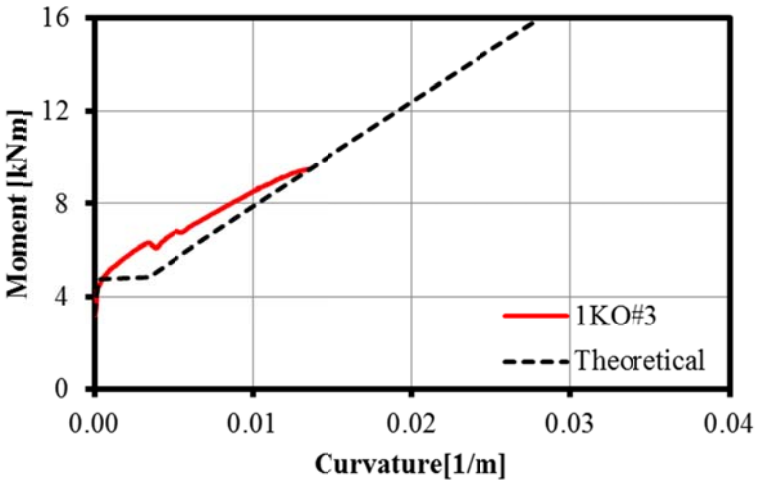

Figure 4H-9: Moment-Curvature Plot – 1KO#3

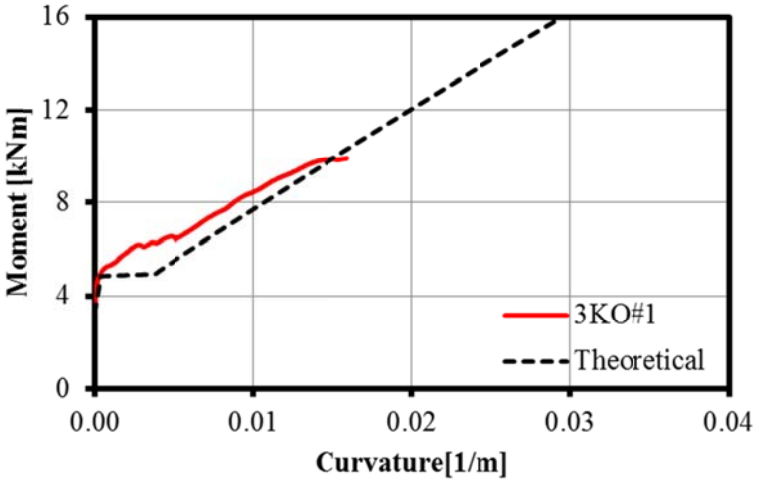

Figure 4H-10: Moment-Curvature Plot – 3KO#1

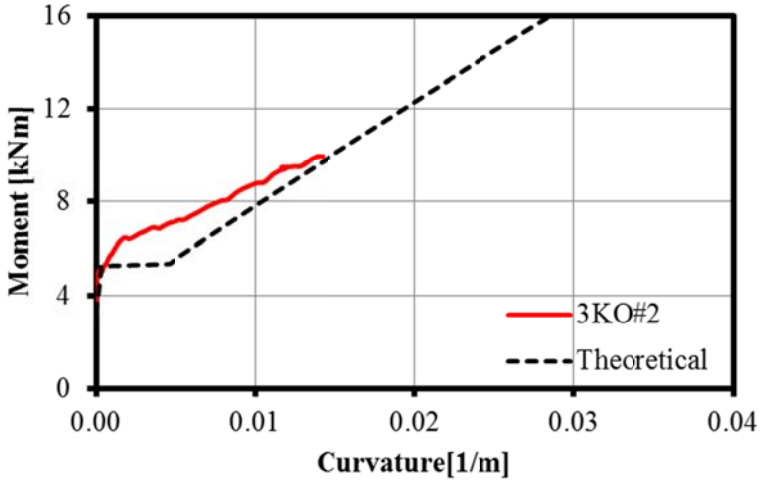

Figure 4H-11: Moment-Curvature Plot – 3KO#2

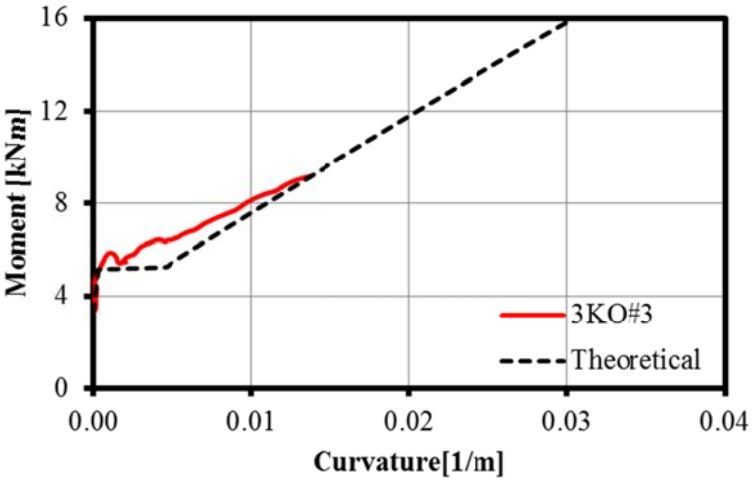

Figure 4H-12: Moment-Curvature Plot – 3KO#3

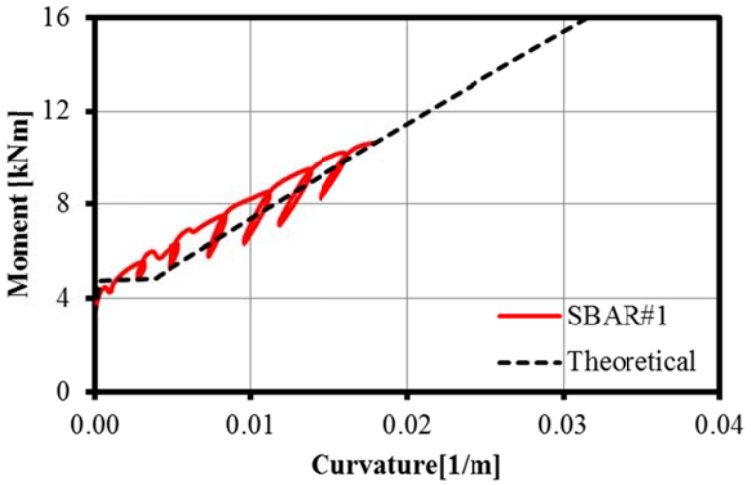

Figure 4H-13: Moment-Curvature Plot – SBAR#1

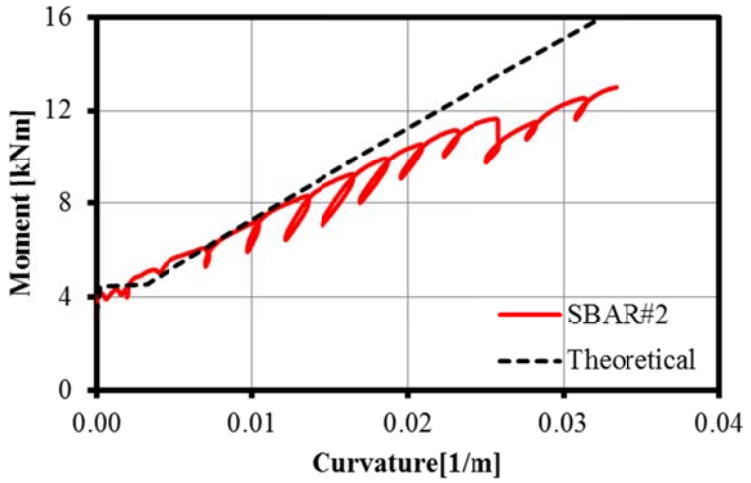

Figure 4H-14: Moment-Curvature Plot – SBAR#2

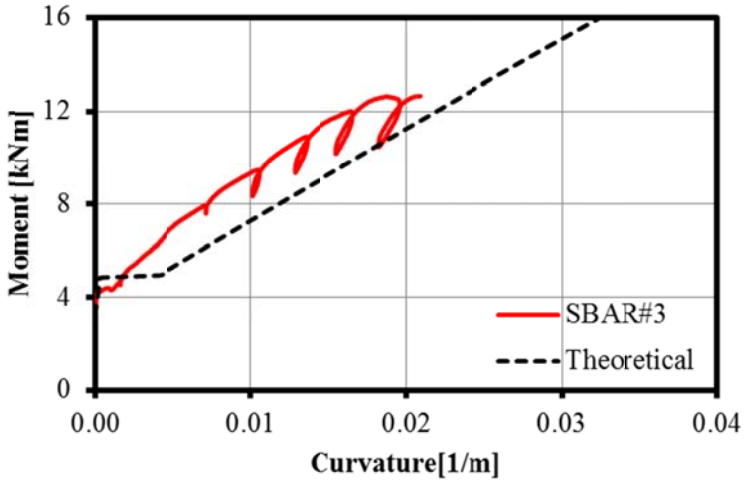

Figure 4H-15: Moment-Curvature Plot – SBAR#3

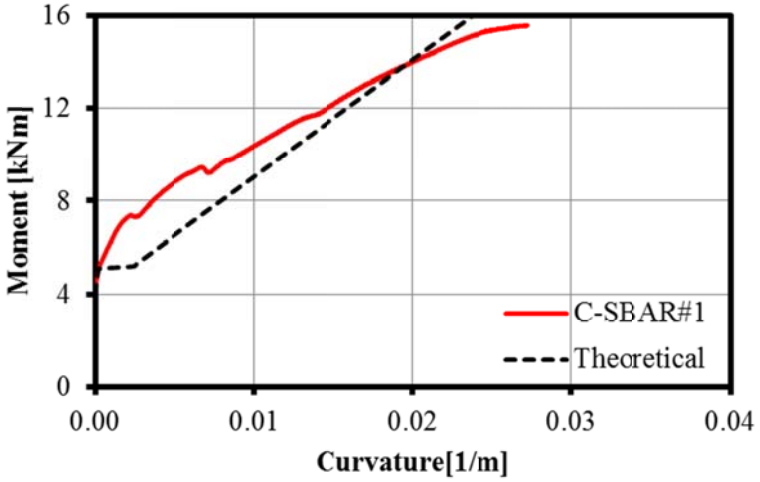

Figure 4H-16: Moment-Curvature Plot – C-SBAR#1

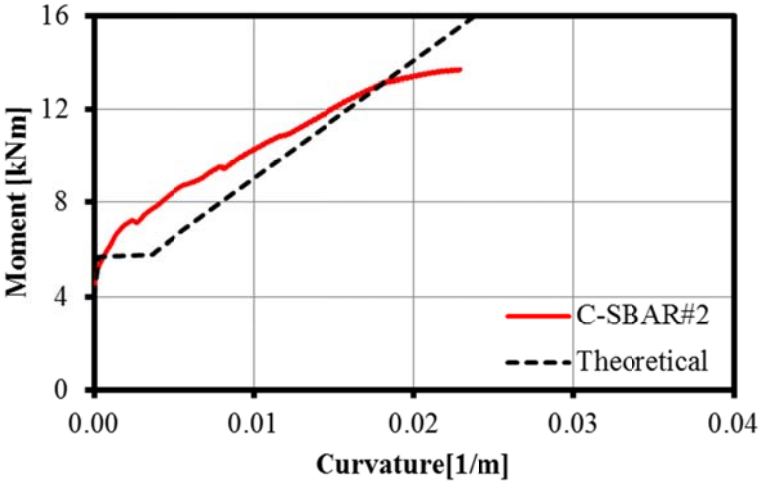

Figure 4H-17: Moment-Curvature Plot – C-SBAR#2

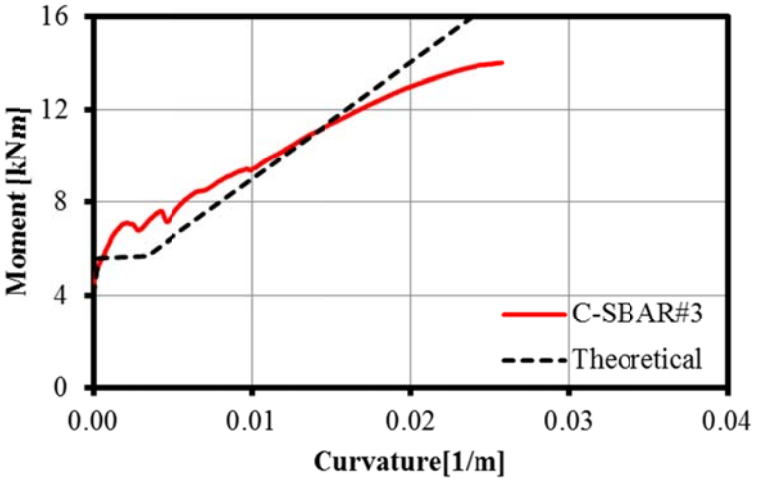

Figure 4H-18: Moment-Curvature Plot – C-SBAR#3

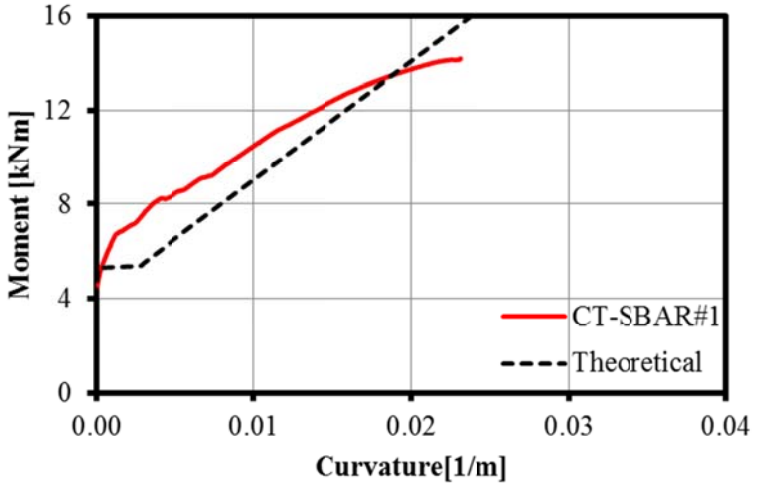

Figure 4H-19: Moment-Curvature Plot – CT-SBAR#1

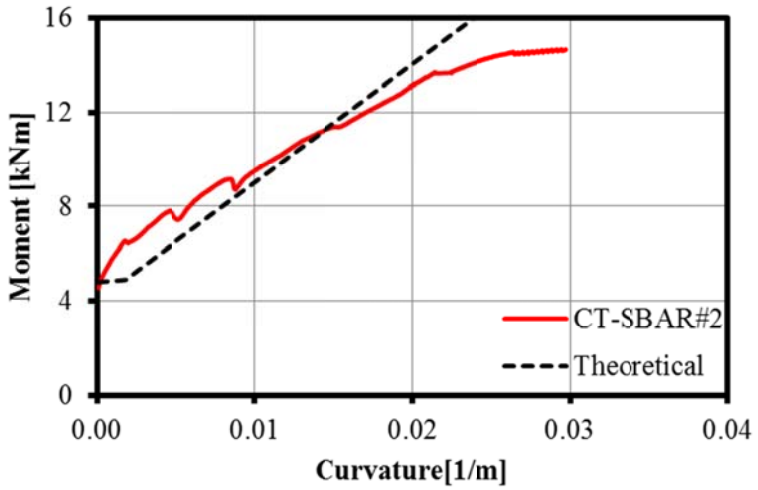

Figure 4H-20: Moment-Curvature Plot – CT-SBAR#2

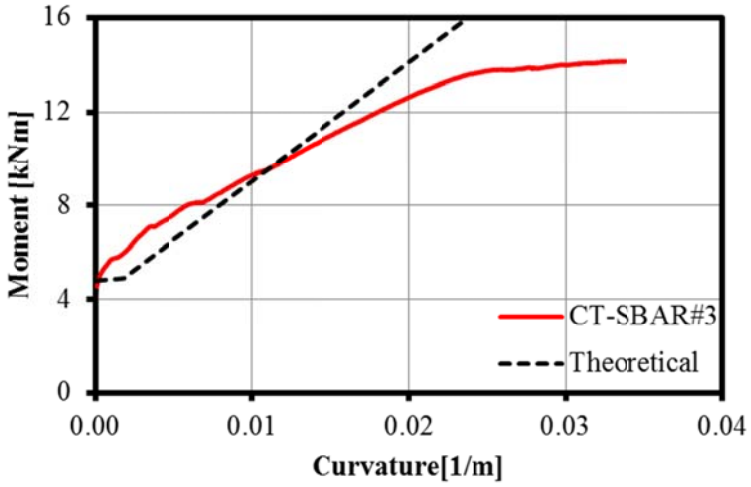

Figure 4H-21: Moment-Curvature Plot – CT-SBAR#3

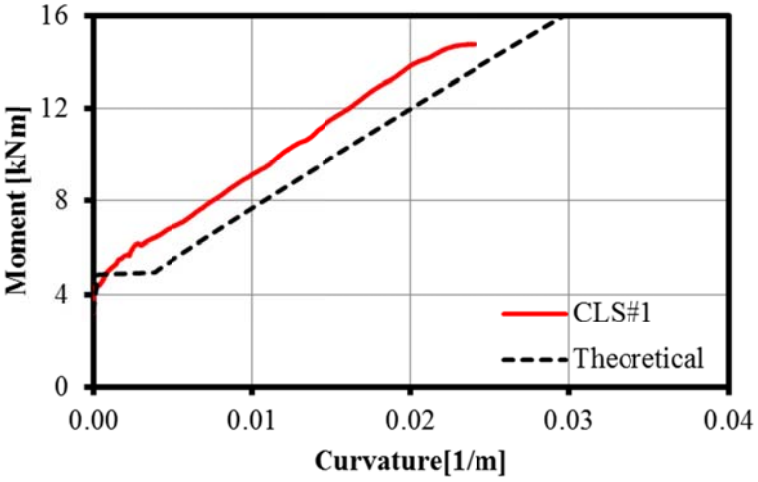

Figure 4H-22: Moment-Curvature Plot – CLS#1

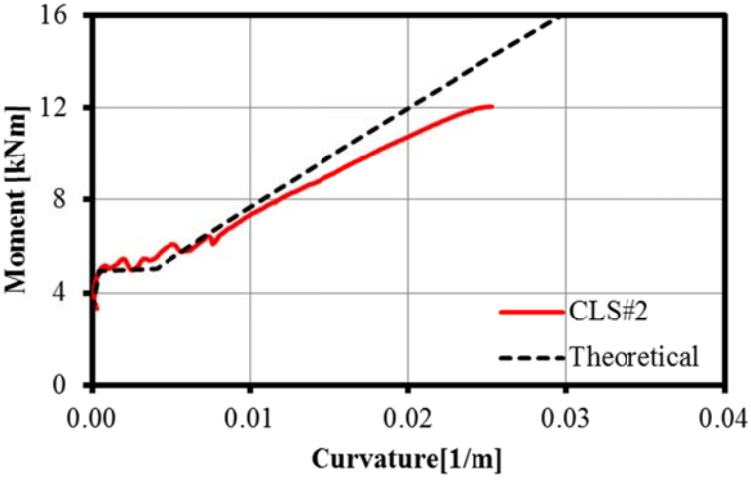

Figure 4H-23: Moment-Curvature Plot – CLS#2

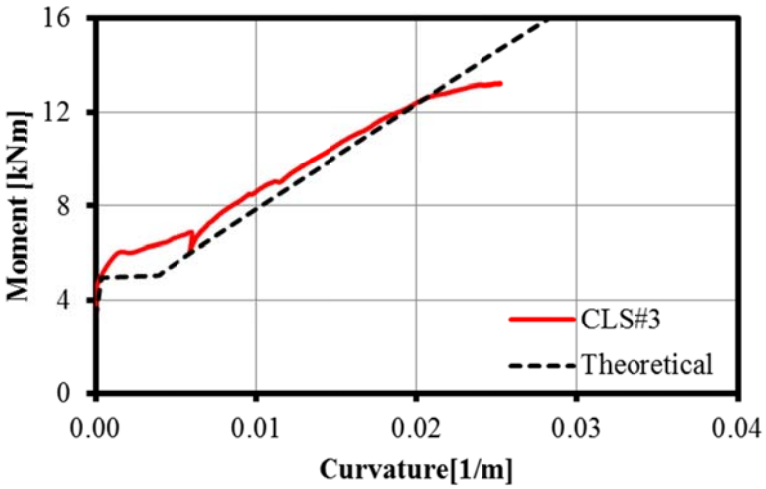

Figure 4H-24: Moment-Curvature Plot – CLS#3

APPENDIX 4I: DEVELOPMENT OF THE THEORETICAL LOAD VERSUS DEFLECTION ANALYSIS

The derivation of the midspan deflection for the wall splice specimens was completed using the conjugate beam method. The curvature therefore corresponded to the moment along the length of the wall splice specimen for any given load level and included the self-weight of the specimen. This allowed for the calculation of the theoretical midspan deflection using the numerical value of the midspan moment. This appendix presents the mathematical expressions used in the development of the theoretical load versus displacement analysis and the corresponding MathCAD code. The error associated with the selection of the number of segments used to calculate the midspan deflection is also presented.

An expression for effective curvature was derived using Bischoff's (2005) equation for the effective moment of inertia to consider the effects of the gradual transition from the un-cracked to cracked section properties of the wall splice specimens. This process is similar to that presented by Ahmed (2011).

$$I_e = \frac{I_{cr}}{1 - \left(1 - \frac{I_{cr}}{I_g}\right) \cdot \left(\frac{M_{cr}}{M_a}\right)^2} \qquad [4I\text{-}1]$$

Where: I_e= the effective moment of inertia [mm^4] (Bischoff, 2005)

I_{cr}= the moment of inertia for the cracked wall splice specimen cross-section [mm^4]

I_g= the gross moment of inertia for the wall splice specimen cross-section [mm^4]

M_a= the applied moment determined through the analysis of the experimental load data [kN·m]

M_{cr}= the cracking moment determined using the data presented in Table 4.4 [kN·m]

Expanding and re-arranging equation 4I-1:

$$I_e = \frac{I_{cr} I_g}{I_g - I_g \cdot \left(\frac{M_{cr}}{M_a}\right)^2 + I_{cr} \cdot \left(\frac{M_{cr}}{M_a}\right)^2} \qquad [4I\text{-}1a]$$

Inverting equation 4I-1a:

$$\frac{1}{I_e} = \frac{I_g - I_g \cdot \left(\frac{M_{cr}}{M_a}\right)^2 + I_{cr} \cdot \left(\frac{M_{cr}}{M_a}\right)^2}{I_{cr} I_g} \qquad [4I\text{-}1b]$$

Multiplying both sides of equation 4I-1b by $\frac{M_a}{E_m}$ and simplifying:

$$\frac{M_a}{E'_m I_e} = \frac{M_a I_g \cdot \left[1 - \left(\frac{M_{cr}}{M_a}\right)^2\right] + I_{cr} \cdot \left(\frac{M_{cr}}{M_a}\right)^2}{E'_m I_{cr} I_g} \qquad [4I\text{-}1c]$$

Where: $E'_m = 850 f'_m$: the modulus of elasticity of masonry, as calculated in accordance to CSA S304.1-04 (CSA, 2004) [MPa]

Observing that $\phi = \frac{M}{EI}$, equation 4I-1c becomes:

$$\phi_e = \phi_{cr} \cdot \left[1 - \left(\frac{M_{cr}}{M_a}\right)^2\right] + \phi_g \cdot \left(\frac{M_{cr}}{M_a}\right)^2 \qquad [4I\text{-}2]$$

Where: ϕ_{eff}= the effective curvature

ϕ_{cr}= the curvature of the cracked section as obtained from the analysis described in Appendix 4G

ϕ_g= the curvature of the gross (un-cracked) section

The length of the wall splice specimen, L, was divided into n segments, each having an equal length of L/n. The average moment at the midpoint of each segment was then determined using the distance from the left support and elementary mechanics. The effective curvature, ϕ_e, corresponding to the moment at the midpoint of the segment was calculated using equation 4I-2. The midspan deflection of the wall splice specimen, Δ_{mid}, was calculated by summing the

midpoint deflections of each individual segment from the left support to the midspan of the wall splice specimen with the equation:

$$\Delta_{mid}=\frac{L_{tot}}{n}\sum_{n=1}^{n}\left(\phi_{eff_n}L_n\right) \qquad [4I\text{-}3]$$

MathCAD Program Code:

List of Symbols:

$curve_{tot.sw}$ Complete moment-curvature function for the un-cracked and cracked analyses including the self-weight of the wall splice specimen

$def_{tot.sw}$ Midspan deflection function over the entire load spectrum including the self-weight of the wall splice specimen [mm]

$Ma_{sw}(x,P)$ Moment along the wall splice specimen at a distance of, x [mm] from the left support and at a given applied load [kN·m]

P Applied load [kN]

sw Self-weight of a wall splice specimen per unit length $\left[\frac{kN}{mm}\right]$

ϕ_i Effective curvature at the midpoint of the i^{th} segment along the length of the wall splice specimen

Moment Along the Length of the Wall Splice Specimen Corresponding to Any Load:

$$Ma_{sw}(x,p):=\begin{cases} ma\leftarrow\dfrac{sw\cdot(x)^2}{2}+\left[\left[\left(\dfrac{p}{2}+1200mm\,sw\right)-sw\cdot x\right]\cdot x\right] & \text{if } 0mm\le x<800mm \\ ma\leftarrow\dfrac{sw\cdot(x)^2}{2}+\left[(1200mm\,sw-sw\cdot x)\cdot x\right]+400mm\,p & \text{if } 800mm\le x\le 1600mm \\ ma\leftarrow\dfrac{sw\cdot(x)^2}{2}+1200mm\,p-\left(\dfrac{p}{2}\right)\cdot x+(1200mm\,sw-sw\cdot x)\cdot x & \text{if } 1600mm<x\le 2400mm \\ ma\leftarrow 0 & \text{otherwise} \end{cases}$$

Gross Section Curvature (Un-Cracked):

$$\text{curve}_{tot.sw}(M) := \begin{| k \leftarrow \frac{M}{E_m \cdot I_g} \quad \text{if } M \le M_{cr} \\ k \leftarrow \text{curve}(M) \quad \text{otherwise} \\ k \end{|$$

Deflection at the Midspan of the Wall Splice Specimen Over the Entire Load Spectrum:

$$\text{def}_{mid.sw}(x) := \begin{| \text{for } i \in 1..240 \\ \quad L_i \leftarrow i \cdot 10\text{mm} - 5\text{mm} \\ \quad \text{Mom} \leftarrow \text{Ma}_{sw}(L_i, x) \\ \quad \phi_i \leftarrow \frac{\text{Mom}}{E_m \cdot I_g} \quad \text{if Mom} \le M_{cr} \\ \quad \phi_i \leftarrow \text{curve(Mom)} \cdot \left[1 - \left(\frac{M_{cr}}{\text{Mom}}\right)^2\right] + \frac{\text{Mom}}{E_m \cdot I_g} \cdot \left(\frac{M_{cr}}{\text{Mom}}\right)^2 \quad \text{otherwise} \\ \text{def} \leftarrow 10\text{mm} \cdot \sum_{n=1}^{120} \left(\phi_n \cdot L_n\right) \\ \text{def} \end{|$$

Representative Plot – CLS#3:

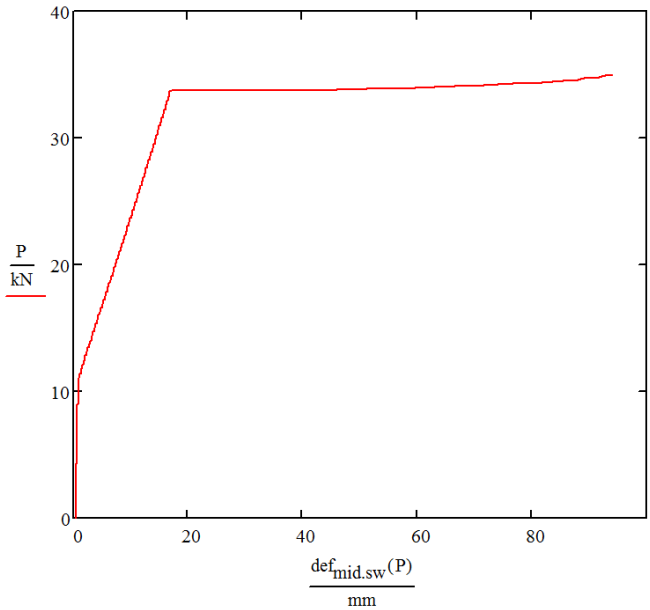

Associated Error with the Selection of 240 Segments:

Figure 4I-1 shows the resulting midspan displacements when the number of segments along the length of the wall splice specimen, n, was varied in equation 4I-3. The calculated moment values corresponding to n= 24, 50, 120, 240, 480, and 1200 yielded the values: 9.305 mm, 9.329 mm, 9.328 mm, 9.328 mm, 9.328 mm, 9.328 mm, respectively. Figure 4I-1 shows that the asymptote is located at approximately 9.328 mm, therefore the resulting error associated with the selection of n=120 in the calculation of the theoretical deflection is less than 0.01%.

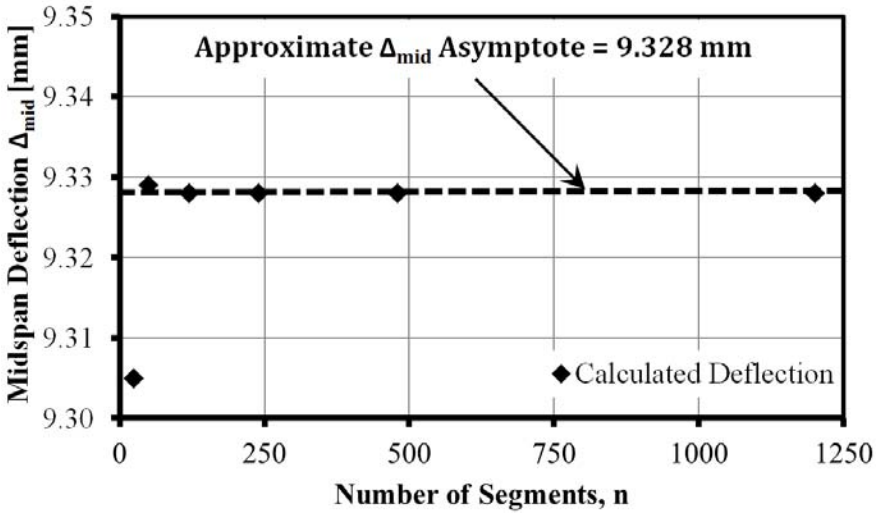

Figure 4I-1: Calculated Deflection Versus the Number of Segments Along the Length of the Wall Splice Specimen.